STRUCTURAL AND FUNCTIONAL CHARACTERIZATION OF HADITOXIN, A NOVEL NEUROTOXIN ISOLATED FROM THE VENOM OF OPHIOPHAGUS HANNAH (KING COBRA)

AMRITA ROY
M. Pharm.
Pharmaceutical Technology

A THESIS SUBMITTED

FOR THE DEGREE OF DOCTOR OF PHILOSOPHY

DEPARTMENT OF BIOLOGICAL SCIENCES
FACULTY OF SCIENCE
NATIONAL UNIVERSITY OF SINGAPORE

AUGUST, 2011

Dedication

This thesis is dedicated to my parents

Mrs. Subhra Roy

and

Mr. Haridas Roy

who taught me the value of education

PREFACE

This dissertation would not have been possible without the guidance and the help of several individuals who in one way or another contributed and extended their valuable assistance in the preparation and completion of this study.

First and foremost, I would like to thank my supervisor Professor R. Manjunatha Kini for his constant encouragement, critical comments and enlightening ideas throughout this study. I feel fortunate to be supervised by Prof. Kini, who not only taught me most of what I know about protein chemistry, but also about how to think and work independently. The best thing I have enjoyed in his lab is the freedom of thinking and designing my own experiments, which contributed a lot to develop my skills to become an independent researcher over the past few years.

I owe a great debt of gratitude to Dr. Selvanayagam Nirthanan (Niru) for his valuable suggestions and constant motivation. He has been a kind, humble and patient person who helped me whenever it was needed. His useful suggestions during the manuscript preparation are not only reflected in the published article but will also influence the way I write in future. Undoubtedly, his direction and encouragement have played a significant role in many aspects of my research.

I would like to thank the graduate program run by the National University of Singapore for their financial support for the past four years. Additionally, I thank the Biomedical Research Council (BMRC) of Singapore, for providing a generous grant to Prof. Kini which funded my work described in this thesis.

All this work would not have been possible without the support of our able collaborators. I would like to thank Assoc. Professor J. Sivaraman, for helping me out structural characterization part of my project. I am extremely thankful to Professor Daniel Bertrand for helping me out with all the electrophysiology experiments. His insightful suggestions have greatly improved the contents of this thesis and well as my research publications. My hearty thanks to Professor Palmer

Taylor and all his lab members who has kindly allowed me to work in their lab for a few days to perform the experiments with the binding protein. My sincere thank goes to Assoc. Professor Anders Asbjørn Jensen for helping me with the experiments related to $5HT_3$ receptors.

I would like to thank all the teachers who made a difference in my life by their contributions. I would like to thank Professor Tuhinadri Sen, Professor Dwijen Sarkar, Dr. V. Rajan, Dr. Samir Samanta, Paul Sir, Mr. Goutam Banerjee for their support and inspiration.

Thanks to all the people that make the Department run so smoothly. Thanks to Joanne, Reena, Mrs Chan and Priscilla. Special thanks go to Annie for helping us to design the beautiful cover page illustration for the Journal of Biological Chemistry, March 2010 issue.

I would like to thank all the past and present lab mates for making my stay fun and entertaining. Thanks to Dr. Rajagopalan Nandakishore, for the initial guidance during my first semester in the lab and for all the valuable discussions. Thanks to Dr. Cho Yeow for teaching me HPLC and Dr. Raghurama Hegde, for helping me to draw and modify the structures of macromolecules, Dr. Robin Doley for teaching me the basic steps in molecular biology. I would also like to thank Dr. Ryan, Dr. Reza, Dr. Guna Shekhar, Dr. Pushpalatha, Dr. Alex, Shiyang, Tzer Fong, Ee Xuan, Ming Zhi, Bee Har, Maulana, Shifali, Sindhuja, Angie, Aldo, Nazir, Summer, Bidhan and Varuna for all the help they have done. I would like to thank Ms. Tay Bee Ling for maintaining the lab finances and making sure we get things on time. In addition, I would also like to thank all the members of the Structural Biology lab (S3-04) for their constant help. My thanks extend to Mrs. Ting, Department of Pharmacology, NUS who has always been helpful during my experiments in the pharmacology department. I would also like to thank my friends Pradipta and Tanay from the Department of Chemistry, NUS for their help in many of my experiments.

It has indeed been a pleasure to have had the acquaintance of Ms. Sheena (Shins, that's how I address her). She has not only helped me with the pharmacological studies but also the long never-ending discussions with her have significantly contributed towards my understanding of *in vivo* and *in vitro* pharmacology. I would also like to thank Ms. Angelina who is an IT expert to me. She has always shared a hand for all my editing business. She is also the one planning for all our outings for a change of our routine lab work. I will definitely miss the exciting lunch and dinner dates with the two of them.

My special thanks go to Bhaskar and Garvita who has always been a help in my difficult times. Thanks for spreading their infectious enthusiasm especially for the charming coffee sessions.

It would be futile to even attempt to thank my colleague and friend, Girish, Vivek and Jhinuk. They have been a pillar of support throughout my time in Singapore in my personal as well as academic life. I truly thank the Almighty for providing me such unforgettable friends.

I am grateful to my family for their support and believe on me. Thanks to my grandmother Mrs. Amita Chatterjee, my father Mr. Haridas Roy and my mother Mrs. Subhra Roy, my in-laws Mr. Pratap Sarkar and Mrs. Namita Sarkar, my sisters Ms. Adrita Roy, Jyotsna di, Ms. Sudipta Sarkar, my brother Mr. Jit Chatterjee, Mr. Daipayan De, my uncle Late Mr. Paramananda Roy who saw me through difficult times and will now rejoice with me on achieving this academic milestone.

Above all, I am extremely thankful to my husband, Mr Debraj Sarkar for being my pillar of strength and support. I would not have come so far without his motivation and also my apologies for releasing my frustration on him which he endured quite patiently.

And there are plenty of other friends and colleagues too numerous to mention who have helped me in some way or the other. I greatly appreciate all of them!

Finally, I am grateful to God, who has moved in mysterious ways, but always with my best interests at heart.

Last but not the least, I would like to thank the king cobra, who has supplied the venom for my research in the Kentucky Reptile Zoo, USA and Mr. Kristen for sending me that venom. I would also like to thank all the chicks and rats who had sacrificed their life for the sake of pharmacology experiments related to this thesis.

Amrita Roy

August, 2011

TABLE OF CONTENTS

SUMMARY

Snake venoms are a rich source of pharmacologically active proteins and polypeptides, targeting a variety of receptors, which includes several potent and lethal neurotoxins. This family contains several types of neurotoxins that interact with different subtypes of nicotinic and muscarinic receptors involved in central and peripheral cholinergic transmission. They are being potentially used by the researchers as molecular probes to characterize different subtypes of cholinergic receptors.

In this study, we report the purification, structural and functional characterization of a novel non-covalent homodimeric neurotoxin, haditoxin, from the venom of *Ophiophagus hannah* (king cobra). This protein was first identified in a cDNA library from the venom gland mRNA of *O. hannah*. Haditoxin was purified to homogeneity from the venom using a two-step chromatography approach. The protein consists of 65 amino acid residues with four intramolecular disulfide bonds. From the cysteine scaffold it was concluded that this protein belong to the three-finger toxin family of snake venom proteins.

Haditoxin produced a potent postsynaptic neuromuscular blockade on avian and mammalian muscle preparations and the reversibility of the blockade was species-specific. In the elctrophysiological studies with expressed human nicotinic receptors haditoxin exhibited novel pharmacology with antagonism towards muscle ($\alpha\beta\gamma\delta$) and neuronal (α_7, $\alpha_3\beta_2$ and $\alpha_4\beta_2$) nicotinic acetylcholine receptors (nAChRs), with highest affinity for α_7-nAChRs. The high resolution (1.55 Å)

crystal structure revealed haditoxin as a non-covalent dimer with two identical subunits in a three-finger protein fold, which correlates well with the biophysical studies. Each of the monomer adapted a structure similar to the short-chain α-neurotoxins, with four intramolecular disulfide bridges, such as- erabutoxin, which interacts specifically with muscle (αβγδ) nAChRs. However, the quaternary structure is similar to that of κ-neurotoxins such as κ-bungarotoxin, which interact specifically with neuronal ($\alpha_3\beta_2$ and $\alpha_4\beta_2$) nAChRs. Clearly haditoxin shows unique structural and functional profiles. Haditoxin is the first dimeric neurotoxin to interact with the muscle nAChR as well as the first short-chain α-neurotoxin to interact with neuronal α_7-nAChR with nanomolar affinity. Interestingly however, haditoxin lacked the helix-like segment cyclized by the fifth disulfide bridge at the tip of loop II of long-chain α-neurotoxins, hitherto considered critical for binding to neuronal α_7-receptors. It is therefore likely that haditoxin, which shares a common tertiary fold with α-neurotoxins and κ-neurotoxins may have other functional determinants for recognizing neuronal α_7-receptors.

Finally, we have successfully expressed recombinant haditoxin which had also exhibited potent neuromuscular blockade. Further structure-function relationship studies are in progress. Delineating the structure-function relationship of this protein will help us to understand in great detail how a dimeric neurotoxin interacts with muscle nicotinic receptors as well as to identify the novel structural elements responsible for binding of a neurotoxin with neuronal nicotinic receptors. Thus, the novel ligand, haditoxin can lead to opening of new avenues for future studies that

can contribute to greater understanding of the biology of the nicotinic acetylcholine receptors.

RESEARCH COLLABORATIONS

The following laboratories provided invaluable experimental data which is discussed in this thesis. Their contribution is gratefully acknowledged.

Electrophysiology studies on haditoxin

Professor Daniel Bertrand and Dr. Dieter D'hoedt.
Department of Physiology, Centre Medical Universitáire, University of Geneva,
1 Rue Michel Servet, 1211 Geneva 4, Switzerland.

Crystallographic studies on haditoxin

Associate Professor Jayaraman Shivaraman and Dr. Xingding Zhou.
Structural Biology Laboratory 5, S3-04,
Department of Biological Sciences, National University of Singapore.
Singapore.

Radioligand binding studies of haditoxin with AChBP

Professor Palmer Taylor, Dr Todd Talley, Dr. Zoran Radic, Mr. Akos Nemecz and Ms Joannie Ho.
Skaggs School of Pharmacy and Pharmaceutical Sciences,
University of California, San Diego,
9500 Gilman Drive, La Jolla, California 92093, USA.

Interaction studies of haditoxin with 5-HT_3 receptors

Associate Professor Anders Asbjørn Jensen.
Faculty of Pharmaceutical sciences, University of Copenhagen,
Universitetsparken 2, 2100 Copenhagen, Denmark.

PUBLICATIONS

RESEARCH ARTICLES

(1) Mani Senthil Kumar KT, Gorain B, Roy DK, Zothanpuia, Samanta SK, Pal M, Biswas P, **Roy A**, Adhikari D, Karmakar S and Sen T. Anti-inflammatory activity of *Acanthus ilicifolius*. J Ethnopharmacol. 2008 Oct 30;120(1):7-12.

(2) Samanta SK, Kumar KT, **Roy A**, Karmakar S, Lahiri S, Palit G, Vedasiromoni JR and Sen T., An insight on the neuropharmacological activity of *Telescopium telescopium*--a mollusc from the Sunderban mangrove. Fundam Clin Pharmacol. 2008 Dec;22(6):683-91.

(3) **Roy A**, Zhou X, Chong MZ, D'hoedt D, Foo CS, Rajagopalan N, Nirthanan S, Bertrand D, Sivaraman J and Kini RM., Structural and functional characterization of a novel homodimeric three-finger neurotoxin from the venom of *Ophiophagus hannah* (king cobra). J Biol Chem. 2010 Mar 12;285(11):8302-15. (Selected as "**Paper of the Week**" and for the **cover page illustration** for the March 12, 2010 issue of the JBC)

(4) **Roy A**, Rajagopalan N, and Kini RM. Identification and characterization of a α-helical molten globule intermediate of β-cardiotoxin, an all β-sheet protein isolated from the venom of *Ophiophagus hannah* (king cobra). *Manuscript under preparation.*

(5) **Roy A**, Sivaraman J, and Kini RM. Structural and functional characterization of a novel weak neurotoxin from the venom of Ophiophagus hannah (king cobra). *Manuscript under preparation.*

INTERNATIONAL CONFERENCE PRESENTATIONS & SYMPOSIUMS

(1) Structural and Functional Characterization of a Novel Homodimeric Three-finger Neurotoxin from the Venom of *Ophiophagus hannah* (King Cobra). (Poster presentation) **Amrita Roy**, Xingding Zhou, D'hoedt Dieter, Ming Zhi Chong, Chun Shin Foo, Nandhakishore Rajagopalan, Selvanayagam Nirthanan, Daniel Bertrand, J Sivaraman, R. Manjunatha Kini ; 6th International Conference on Structural Biology & Functional Genomics. Singapore, December 6 - 8, 2010. Received the **Best Poster award**.

(2) Structural and Functional Characterization of a Novel Homodimeric Three-finger Neurotoxin from the Venom of *Ophiophagus hannah* (King Cobra). (Poster presentation) **Amrita Roy**, Xingding Zhou, D'hoedt Dieter, Ming Zhi Chong, Chun Shin Foo, Nandhakishore Rajagopalan, Selvanayagam Nirthanan, Daniel Bertrand, J Sivaraman, R. Manjunatha Kini ; The 24th Annual Symposium of the Protein Society. San Diego, USA, August 1 - 5, 2010.

(3) Structural and functional characterization of a novel homodimeric three-finger neurotoxin from the venom of Ophiophagus hannah (King cobra). (Oral presentation) **Roy A**, Zhou X, Chong MZ, D'hoedt D, Foo CS, Rajagopalan N, Nirthanan S, Bertrand D, Sivaraman J and Kini RM.; 14th Biological Sciences Graduate Congress. Bangkok, Thailand, December 10 - 12, 2009.

(4) Attended the IUPAB sponsored workshop on "NMR and its applications in Biological systems" at Tata Institute of Fundamental Research, Mumbai, India, November 23 – 30, 2009.

(5) Isolation and characterization of a novel neurotoxic protein from the venom of *Ophiophagus hannah.* (Poster presentation) **Roy A**, Chong MZ, Rajagopalan N and Kini R M.; Joint 5th Structural Biology and Functional Genomics and 1st Biological Physics International Conference. Singapore, December 9 - 11, 2008.

(6) Isolation and characterization of a novel neurotoxic protein from the venom of *Ophiophagus hannah*. (Poster presentation) **Roy A**, Chong MZ, Rajagopalan N and Kini R M.; 13th Biological Sciences Graduate Congress. Singapore, December 15 - 17, 2008.

(7) Biochemical studies on telescopium telescopium – a marine mollusk from the coastal regions of west Bengal. (Poster presentation) Samir K. Samanta, Aniruddha Roy, Arnab Datta, **Amrita Roy**, K.T. Manisenthil Kumar, J.R. Vedasiromani, Dwijen Sarkar and Tuhinadri Sen.; IMBC 2007 - 8th International Marine Biotechnology Conference. Eilat, Israel, March 11 - 16, 2007.

LIST OF FIGURES

Chapter one

Chapter two

Chapter three

Chapter four

Chapter five

LIST OF TABLES

Chapter one

Chapter three

Chapter four

Chapter five

ABBREVIATIONS

Single letter and three letter abbreviations of amino acid residues were followed as per the recommendations of the IUPAC-IUBMB Joint Commission on Biochemical Nomenclature.

Chemicals and reagents

ACh	Acetylcholine
ACN	Acetonitrile
Amp	Ampicillin
BS3	Bis(sulfosuccinimidyl) suberate
$CaCl_2$	Calcium chloride
CCh	Carbamylcholine (carbachol)
$Ca(NO_3)_2$	Calcium Nitrate
dTC	d-tubocurarine
EDTA	Ethylenediaminetetraacetic acid
EFS	Electric field stimulation
HCl	Hydrochloric acid
HEPES	4-(2-hydroxyethyl)-1-piperazineethanesulfonic acid
IPTG	Isopropyl β-D-thiogalactopyranoside
KCl	Potassium chloride
KH	Krebs-Henselsit
KH_2PO_4	Monopotassium phosphate
LB	Luria-bertani
$MgSO_4$	Magnesium sulfate
NaCl	Sodium chloride
$NaHCO_3$	Sodium bicarbonate
NaOH	Sodium hydroxide
PEG	Polyethylene glycol
PTH	Phenylthiohydantion
SDS	Sodium dodecyl sulfate
TFA	Trifluoroacetic acid

X-gal	5-bromo-4-chloro-3-indolyl-β-D-galactopyranoside

Units and measurements

°C	Degree Celcius
µg	Micro gram
µl	Micro liter
µM	Micro molar
Å	Angstrom
amu	Atomic mass units
cm	Centi meter
CPS	Counts per second
D	Dose
Da	Daltons
FU	Fluorescence units
g	Grams
h	Hour
Hz	Hertz
K	Kelvin
kb	Kilo base
kg	Kilo gram
K_{On}	Association constant
K_{Off}	Dissociation constant
L	Liter
LVDEP	Left ventricle diastolic end pressure
M	Molar
mg	Milli gram
min	Minute
ml	Milli liter
mM	Milli molar
Mr	Relative molecular weight
ms	Millisecond
MW	Molecular weight

m/z	Mass-to-charge ratio
n	Number of experiments
nH	Hill coefficient
nM	Nano molar
nm	Nano meter
rmsd	Root mean square deviation
rpm	Revolutions per minute
RT	Room temperature
s	Second
SEM	Standard error of mean
T	Survival time
t_{50}	Time required to produce 50% twitch blockade
t_{90}	Time required to produce 90% twitch blockade
V	Volt

Others

5-HT_3	5-hydroxytriptamine type 3 receptors
3FTX	Three-finger toxin
AChBP	Acetylcholine-binding protein
AChE	Acetylcholinesterase
BLAST	Basic local alignment search tool
cAMP	Cyclic monophosphate
Ca^{2+}	Calcium ion
CBCM	Chick biventer cervicis muscle
CD	Circular dichroism
cDNA	Complementary DNA
CNS	Central nervous system
CO_2	Carbon dioxide
C-terminal	Carboxy terminal
DNA	Deoxyribonucleic acid
EBI	European bioinformatics institute
ESI-MS	Electrospray ionization-mass spectrometry

G Proteins	GTP binding proteins
GPCR	G protein-coupled receptor
HPLC	High performance liquid chromatography
i.p.	intra peritoneal
IC_{50}	Dose which causes 50 % inhibitory effect
K^+	Potassium ion
LC/MS	Liquid chromatography/mass spectrometry
LC/MS/MS	Liquid chromatography/mass spectrometry/mass spectrometry
LD_{50}	Lethal dose causing death of 50 % of animals tested
LNTX	Long neurotoxin
mAChR	Muscarinic acetylcholine receptor
MT	Muscarinic toxin
MTLP	Muscarinic toxin like protein
nAChR	Nicotinic acetylcholine receptor
NCBI	National center for biotechnology information
NMR	Nuclear magnetic resonance
N-terminal	Amino terminal
PCR	Polymerase chain reaction
PLA_2	Phospholipase A_2
RAM	Rat anococcygeus muscle
RGD	Arg-Gly-Asp- tripeptide
RHD	Rat hemidiaphragm
RP-HPLC	Reverse phase-high performance chromatography
SD	Sprague-Dawley
SDS-PAGE	Sodium dodecyl sulfate polyacrylamide gel electrophoresis
TEVC	Two-electrode voltage-clamp
TM	Transmembrane
UV	Ultra violet
WTX	Weak toxin
α	Alpha
β	Beta
γ	Gamma

κ	Kappa
ε	Epsilon

Chapter One

Introduction

CHAPTER ONE

Introduction

1.1 Poisons to potions

Poisonous or venomous organisms are usually associated with fascination, fear and myths for mankind throughout history. These organisms are widely spread throughout the animal kingdom, comprising more than 100,000 species distributed among all major phyla, such as chordates (reptiles, fishes, amphibians, mammals), echinoderms (starfishes, sea urchins), mollusks (cone snails, octopi), annelids (leeches), nemertines, arthropods (arachnids, insects, myriapods) and cnidarians (sea anemones, jellyfish, corals) (Calvete *et al*, 2009). To survive in a competitive environment nature herself has provided some solutions by way of evolutionary peptide engineering in venom glands of these animals. Poisons or venoms have evolved with the main purpose, to help the venomous animals to subdue, immobilize and kill their prey or to defend themselves through chemical means. Thus, venom represents an adaptive trait and an example of convergent evolution (Fry *et al*, 2006, Fry *et al*, 2008; Fry *et al*, 2009). Venoms are a deadly mixture of proteins and peptide originated by natural selection process. These proteins and polypeptides aim a wide range of physiological targets in the prey affecting the major organ systems and thereby death. Hence, venoms are a rich and abundant source of pharmacologically active proteins and peptides which are also known as toxins. Therefore, the chances of finding bioactive components are extremely high in venoms compared to any other tissue or organ where the proteins are evolved to maintain the identity and function of each type of cells and not to

secrete out and exert the function somewhere else (Kini, 2010). Although primary research on venoms and toxins have focused mainly to find ways and means to neutralize the toxicity and adverse effects of envenomation, but the medicinal value of venoms and toxins are well documented since ancient times (Harvey *et al*, 1998; Koh *et al*, 2006). However, extensive research on venom toxins has only been performed for the last few decades with an aim to develop therapeutic agents and molecular probes. This was motivated after the isolation of a bradykinin-potentiating peptide from the venom of the Brazilian viper *Bothrops jararaca* (this was further developed to the antihypertensive drug captopril) in 1950's (Rocha e Silva *et al*, 1949; Fernandez *et al*, 2004) as well as in the early 1960's the discovery of the curaremimetic neurotoxin α-bungarotoxin from the venom of the banded krait (Bungarus multicinctus) (Chang and Lee, 1963), which pioneered the identification and isolation of the nicotinic acetylcholine receptor, the first and most well characterized receptors till today (Langley, 1907 Katz and Thesleff , 1957; Changeux, 1990). Hereafter, research on venoms and toxins has also been carried out to determine the mode and mechanism of action of the toxins, to develop specific research tools that are useful in understanding normal physiological processes at both cellular and molecular levels as well as to develop prototypes of pharmaceutical agents based on the structure-function relationship of the toxins.

Venoms represent an enormous and unexplored pool of pharmacologically active components. This reservoir is spread among the 700 or so known species of Conus, the roughly 725 species of venomous snakes, the around 1500 species of scorpions, or the

ca. 37,000 known species of spiders, from which one can have a knowledge of the huge cornucopia of the bioactive molecules accumulated by nature (Calvete *et al*, 2009). Because of the high selectivity and affinity of venom peptides towards the molecular targets modulating various physiological processes they form ideal candidates as lead molecules for drug design and development. There are many success stories where deadly toxins have been fashioned into lifesaving drugs (Harvey *et al*. 1998; Ménez, 2002; Ménez *et al*, 2006). Starting from the antihypertensive drug captopril, an angiotensin converting enzyme (ACE) inhibitor (from the Brazilian pit viper, *Bothrops jararaca*) to the recently developed, potent analgesic ziconotide (from the marine cone snail *Conus magus*), several drugs have had humble origins from the pharmacopoeia present in animal venoms. Moreover, these naturally occurring biomolecules have provided useful probes in deciphering the molecular details of normal physiological processes and hence contributed to several aspects of life. Furthermore, they have also provided excellent insight into the evolution of different families of venom proteins and protein-protein interactions in general, which open up yet other appealing and important fields of study. Clearly, rather than the intended offensive and defensive purposes of the toxins, they go a long way for the benefit of science and medicine. This becomes a dramatic turning point of the villains to heroes!

Thus the contributions of toxins deserve much more credit than we give them!

Kini RM, 2010

1.2 The enigmatic serpents: Snakes

Snakes and their venom have been of great interest historically representing love and hatred, good and evil, life and death, medicine and poison. According to the modern taxonomic system, snakes belong to the class Reptilia, order Squamata and sub-order Serpentes. They have evolved from either burrowing or aquatic lizards probably during the Cretaceous age (100 to 120 million years ago) (Mc Dowell, 1972; Harris, 1991; Durand, 2004). During the Miocene period (less than 30 million years ago) in response to the rapid shift in prevailing environmental conditions snakes evolved the strategy of rapid locomotion and passive immobilization (Savitzky, 1980). The first venom producing apparatus known as, Duvernoy's gland was evolved during this period. Subsequently, during the course of evolution these glands were converted to the specialized and advanced venom glands associated with the venom delivery apparatus like the fangs in the venomous snakes. Living snakes are found on every continent except for Antarctica and few islands such as Ireland, Iceland, and New Zealand (Conant and Collins, 1991). Fifteen families are currently recognized, comprising 456 genera and over 2,900 species (Serpentes, ITIS, 2008; TIGR Reptile Database, 2008), of which 1300 species are known to be venomous (Phelps, 1981; Hider *et al*, 1991; Gold *et al*, 2002). All of the venomous snakes belong to the superfamily Colubroidea (Lawson *et al*, 2005; Pyron *et al*, 2011). These venomous colubroids are responsible for approximately 20,000–94,000 human fatalities every year (Kasturiratne *et al*, 2008). The superfamily Colubroidea consists of seven families, which are- Colubridae, Elapidae, Homalopsidae, Lamprophiidae, Pareatidae, Viperidae, and Xenodermatidae (Lawson *et al*, 2005; Vidal *et* al, 2007; Zaher *et* al,

2009; Pyron *et al*, 2011). The Colubridae includes the rat snakes, garter snakes, and other common snakes. Members of this family can be found in all parts of the world (Savitzky, 1980). Colubrids produce small volumes of venom and their venom delivery apparatus is poorly developed (White, 1998; Cogger, 2000; O'Shea, 2005). The Elapidae includes two subfamilies- the Elapinae (cobras, mambas, kraits, coral snakes) and the Hydrophiinae (sea snakes). Elapids are well represented in parts of Asia, Africa, America, Australia, Indian and Pacific oceans (Shine, 1998). They possess short, fixed fangs in the front of the mouth (Fairley, 1929a,b; O'Shea, 2005). The Viperidae includes three subfamilies- Azemiopinae (which include only the Fea's viper), Crotalinae (rattlesnakes, cottonmouths, mostly New World vipers), and Viperinae (which includes most of the Old World vipers). Species belonging to the Viperidae family can be found in parts of Africa, Europe, Asia, North America and South America (Harris, 1991). The venom delivery apparatus of the viperids is very advanced with retractable fangs (Fairley, 1929a; O'Shea, 2005).

1.2.1 *Ophiophagus hannah*: King of the serpents

This study involves the characterization of novel proteins isolated from the venom of *Ophiophagus hannah*, an elapid snake. It is also known as king cobra because of its size, it is the longest venomous snake in the world, growing to a maximum length of 18 feet (**Figure 1.1 A** and **B**). King cobra has a relatively long average lifespan of up to 25 years (Veto *et al*, 2007). These snakes are widely distributed in the dense rain forests and mangrove swamps in parts of Southeast Asia, South China and India

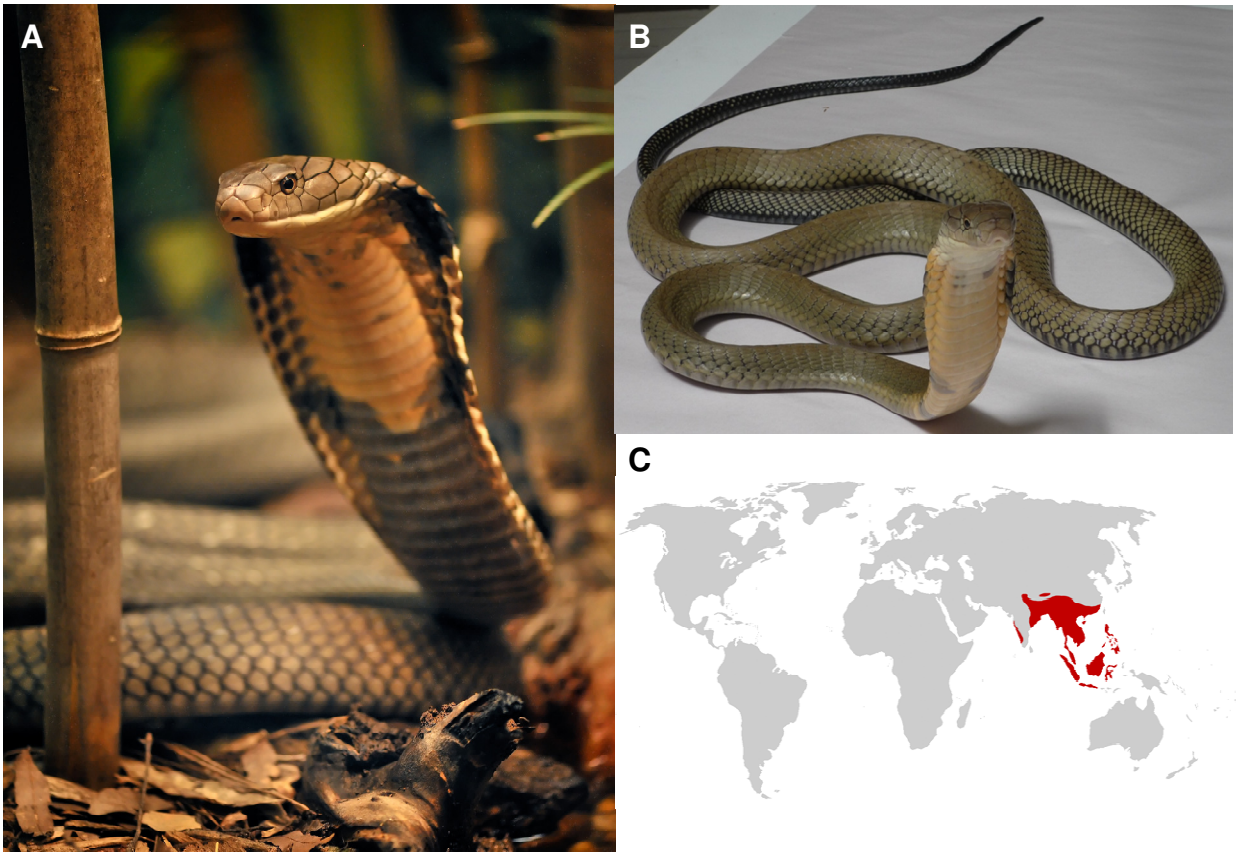

Figure 1.1: *Ophiophagus hannah* (king cobra) and its geographical distribution.

(A) An adult king cobra showing its hood, photo provided by Michael D. Kern (www.thegardensofeden.org), CA, USA, (B) A juvenile king cobra, photo provided by Mr. Peter Mirtschin, Venom Supplies Pty. Ltd., Australia. (C) Map showing the geographical distribution of the king Cobra in red (http://en.wikipedia.org/wiki/File:Distribution_O._hannah.png).

(Tan and Saifuddin, 1989) (**Fig 1.1 C**). The snake preferentially feeds on other venomous and non-venomous snakes, hence it is named as *Ophiophagus* (in Latin, 'Ophis' meaning 'snake' and 'phagein' meaning 'eat') (Coborn, 1991).

King cobra is regarded as one of the deadliest snakes in the world. It can deliver a large quantity of venom in one bite (420 mg dry weight per milking) (Ganthavorn, 1969). The LD_{50} of the crude venom of *O. hannah* in mice is 1.5 to 2.18 mg/kg via subcutaneous injection (Broad *et al*, 1979) and 1.28 mg/kg via intravenous injection (Ganthavorn, 1969). The lethality of *O. hannah* venom is relatively low when compared to some of the other elapids (0.025 to 1.2 mg/kg) and sea snakes (0.09 to 0.71 mg/kg) (Ganthavorn, 1969; Broad *et al*, 1979) which is compensated by the large volume. However, in a recent toxicology study the LD_{50} of Chinese king cobra venom was found to be 0.34 mg/kg (Gopalakrishnakone and Chou, 1990).

The king cobra can be highly aggressive if provoked. There have been several well reported *O. hannah* envenomation cases (Ganthavorn, 1971; Wetzel and Christy, 1989; Pe *et al*, 1995; Gold and Pyle, 1998; Veto *et al*., 2007). One third of the reported 35 cases of *O. hannah* envenomation have been fatal (Gold and Pyle, 1998). The venom of the king cobra consists of neurotoxins primarily, but it also contains cytotoxic compounds. The initial symptoms observed upon envenomation are drowsiness, nausea, headache, abdominal pain, hypotension and occasionally shock followed by massive swelling of bite areas and extensive tissue necrosis is observed (Gold and Pyle, 1998).

1.3 Snake venom: The complex mixture

Snake venom is highly modified saliva that is secreted from the venom glands of snakes. It is a complex mixture of pharmacologically active proteins and polypeptides. Peptides and proteins constitute over 90% of the dry weight of venom. Apart from proteins, snake venoms also contain non-protein low molecular weight compounds which include metal ions, lipids, nucleic acids, amino acids, carbohydrates and biological amines (Hider *et al*, 1991). The most common metal ions found in snake venoms are magnesium, calcium and zinc, while copper has been detected in certain venoms (Friederich and Tu, 1971). These metal ions are mainly associated with the proteins components and probably they serve the role of enzyme cofactors. Additionally, some venom, like that of the mamba contains high levels of bioactive amines like- acetylcholine and 5-hydroxytrypamine, which most likely play a defensive role as a potent algesic agent (Welsh, 1967). Another important non-protein constituent of several snake venoms is citrate, presumably serving a self-protective role by inhibiting the deleterious activity of venom enzymes within the venom gland (Freitas *et al*, 1992; Odell *et al*, 1999). Although the functional role of non-protein venom constituents should not be neglected; however, from the perspective of a venom scientist, the protein components are of major interest. They constitute of a highly evolved and organized arsenal of proteins acting on diverse molecular targets involving the vital processes of a normal physiological systems. Venom proteins mainly exert cytotoxic, neurotoxic or hemotoxic effects. Moreover, these proteins bind to their targets with high selectivity and affinity. Therefore, snake venom acts as a naturally occurring gold mine of bioactive prototypes for therapeutic and scientific

interests (Dufton, 1993; Harvey, 2002; Pal *et al*, 2002; Lewis and Garcia, 2003; Bogin, 2005; Koh *et al*, 2006; Calvete *et al*, 2009; Kini, 2010). Single snake venoms may contain more than hundred of different proteins. However, most of the proteins belong to a small number of structural superfamilies (Menez 1998; Kordis and Gubensek, 2000). A superfamily is defined as a collection of proteins, in which all members have a similar three-dimensional structure, but may differ from each other with respect to their physiological targets and pharmacological effects. In a broader spectrum snake venom protein families are divided into enzymatic (**Table 1.1** and **Fig. 1.2**) and non-enzymatic (**Table 1.2** and **Fig. 1.3**) superfamilies. Snake venoms are rich in enzymatic proteins. More than 20 different enzymes are known to be present in snake venoms. Venoms of the viperids and crotalids are primarily enzymatic (80-95%) whereas, elapids contain relatively lower amounts (25-70%) followed by hydrophid venoms with lowest amounts of enzymatic proteins (~20%) (Hider *et al*, 1991). The pharmacological effects of these enzymes are listed in Table 1.1. The major components of the enzymatic venom proteins are: phospholipases A2 (PLA2s), L-amino acid oxidase (LAO), serine proteases, snake venom metalloproteases (SVMPs), acetylcholinesterases (AChEs), Venom factors (VFs) and phosphodiesterases (PDEs) (for reviews, see Iwanaga and Suzuki, 1979; Bailey, 1998). The non-enzymatic venom proteins are relatively smaller in size than the enzymatic ones. The predominant non-enzymatic venom proteins include- three-finger toxins (3FTXs), C-type lectin-related proteins (CLPs), serine proteinase inhibitors (SPIs), disintegrins, helveprins/CRISPs, sarafotoxins, waprins, vespryns, nerve growth factors (NGFs), bradykinin-potentiating

Table 1.1: Enzymatic proteins from snake venoms

Family	Distribution	Description
Phospholipase A_2 (PLA_2)	Abundant in elapidae, hydrophidae, viperidae and crotalidae venoms	Esterolytic enzymes hydrolyzing 3-sn-phosphoglycerides. They are composed of ~130 amino acid residues with 7 disulfide bridges. Unlike mammalian PLA_2, snake PLA_2 enzymes induce various pharmacological effects like pre- and postsynaptic neurotoxicity, myotoxicity, cardiotoxicity, hemolytic activity, anticoagulant activity, antiplatelet activity, hypotension, hemorrhage and edema.
L-amino acid oxidase (LAO)	Found widely in elapidae, viperidae and crotalidae venoms	Flavo enzymes catalyzing the conversion of L-amino acid substrates to α-keto acids. LAOs from snake venoms also induce pharmacological effects like induction or inhibition of platelet aggregation, association with mammalian epithelial cells and induction of apoptosis and anti bacterial activity. They are composed of ~500 residues with 2 subunits.
Serine Proteinases	Found widely in elapidae and viperidae venoms	Snake venom serine proteinases, in addition to their contribution to the digestion of prey, affect various physiological functions. They affect platelet aggregation, blood coagulation, fibrinolysis, the complement system, blood pressure and the nervous system. They are made up of 240 amino acid residues with 6 disulfide bridges.
Metalloproteinases	Found widely in elapidae and viperidae venoms	Snake venom metalloproteinases are endoproteolytic enzymes. Their catalytic activity is dependent on Zn2+ ions. In addition to their role in the digestion of prey, they exhibit several biological effects, including haemorrhagic, pro-coagulant, anticoagulant and antiplatelet effects. They consists of ~200 residues with 3-4 disulfide bridges.
Acetylcholinesterases	Primarily in elapidae venoms	The venoms of most Elapidae snakes contain large amounts of a highly active non-amphiphilic monomeric AChE. They regulate the cholinergic transmission in the prey. They are made up of ~550 residues and 5 disulfide bridges, they can exist as monomer, dimer or tetramer.
Venom factors	Primarily in elapidae venoms	Venom factors activates the complement system . They consist of three polypeptide chains each with 1200 residues and 13 disulfide bridges.
Phosphodiesterases	Ubiquitously present in all venoms	Snake venom phosphodiesterase shares a number of mechanistic features in common with the nucleotidyl transferases. All of these enzymes contain zinc, are activated by magnesium, and catalyze α-β phosphoryl bond cleavage.

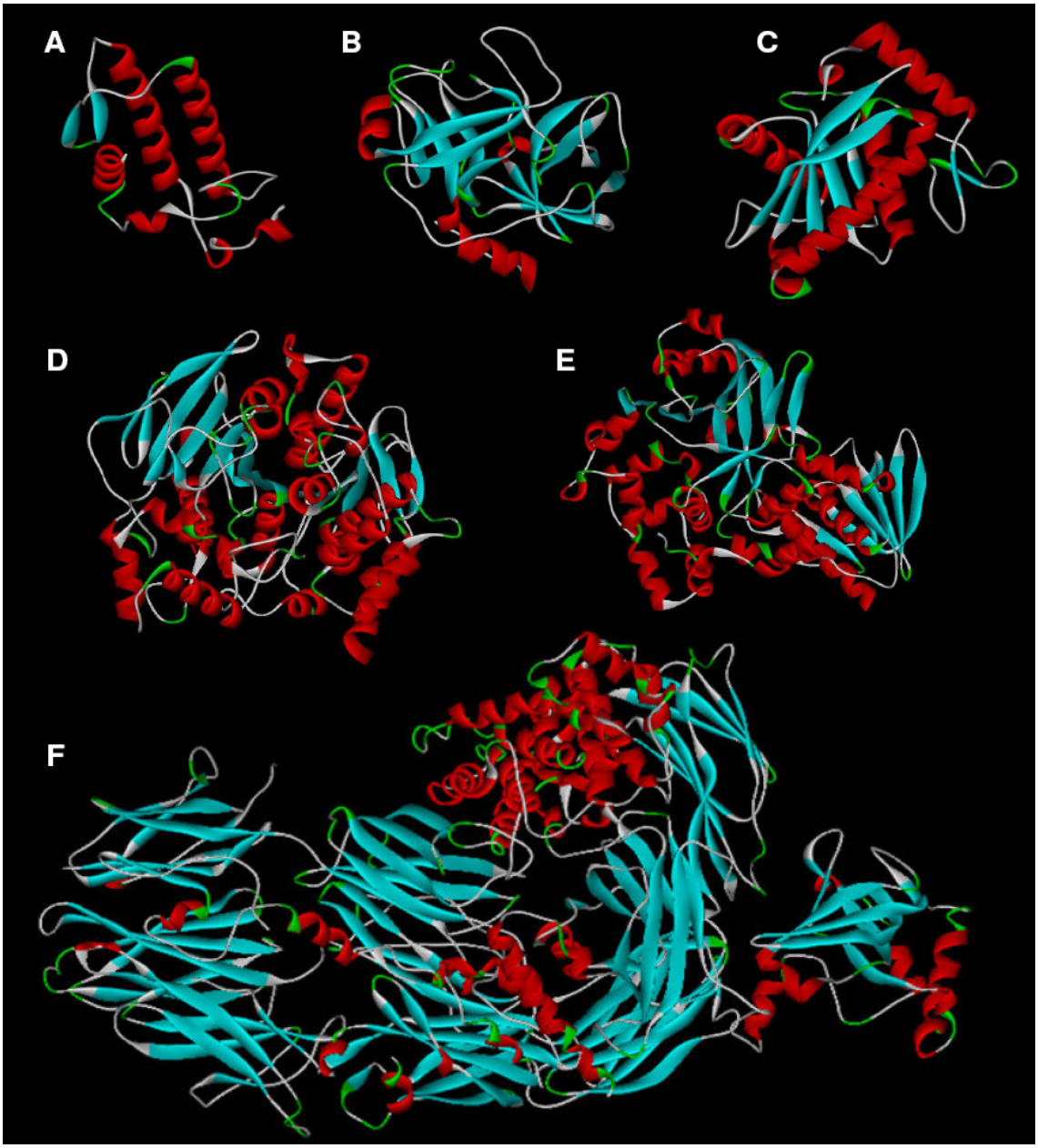

Figure 1.2: Representative examples of major families of enzymatic snake venom proteins.

(A) phospholipase A2: notexin (1AE7), (B) serine proteinase: TSV-PA (1BQY), (C) metalloproteinase: atrolysin (1ATL), (D) model of acetylcholinesterase from Bungarus candidus (Q92035) built based on acetylcholinesterase from Torpedo californica (2ACE), (E) model of L-amino oxidase from Notechis scutatus (AAY89681), (F) model of Austrelaps superbus venom factor (AY903291) built base on human complement component C3 (2A73). The protein data bank and/or GenBank accession numbers are given in parentheses. The structures are α-carbon solid ribbon representation and presented with the aid of DS ViewerPro50.

Table 1.2: Non-enzymatic proteins from snake venoms

Family	Distribution	Description
Three-finger toxins (3FTXs)	Abundant in elapidae and hydrophidae venoms	Members show similar molecular scaffold but varying functions like neurotoxicity, cardiotoxicity, anticoagulant activity and antiplatelet aggregation activity. Similar structures are found in a wide range of species from plants to mammals.
C-type Lectin-related proteins	Mostly found in viperidae and crotalidae venoms	These anticoagulant proteins inhibit prothrombin activation by non-enzymatic mechanisms.
Serine proteinase inhibitors	Distributed widely in many snake venoms	They range in size from ~ 5000 Da to ~ 6000 Da and has three disulphide bridges, and belong to the Kunitz pancreatic trypsin-inhibitor family. As all the proteinases in blood coagulation and fibrinolysis are serine proteinases, these group polypeptides are thought to be potential anticoagulants.
Disintegrins	Abundant in viperidae venoms	Bind to integrins through the RGD motif and prevent platelet aggregation.
Helveprins/CRISP	Identified in all families of snake venoms	Cyeteine-rich secretory proteins (CRISPs) or helothermine-related venom proteins are proteins with 16 conserved Cys residues. They are known to modulate the activity of various ion channels.
Waprins	Isolated from elapidae snakes Oxyuranus microlepidotus and Naja nigricollis	Whey acidic proteins related proteins (waprins) have 8 conserved Cys residues forming 4 disulfide bonds. Omwaprin shows anti-bacterial activity.
Vespryns	First identified from Ophiophagus hannah venom. Also found in other elapidae and viperidae venoms	Ohanin shows potent hypolocomotion and hyperalgesia in animals.
Bradykinin-potentiating peptides	Reported from viperidae and crotalidae venoms only	They are 9 to 13 residues long which are rich in Pro residues. They induce hypotension by acting on smooth muscles.
Natriuretic peptides	Reported from the venoms of Dendroaspis angusticeps, Micrurus corallinus, Pseudechis australis and Trimeresurus gramineus	Potent hypotensive and vasorelaxant properties.
Sarafotoxins	Isolated from the venom of Atractaspis engaddensis	These isopeptides are structurally and functionally related to mammalian endothelins. They are potent vacoconstrictors acting on cardiac muscles and brain.
Nerve growth factors (NGF)	First identified from the venom of Agkistrodon piscivorus (cottonmouth, water moccasin). Later isolated from venoms of viperidae, crotalidae and elapidae.	Divided into four groups, they range in size from ~ 25,000 Da to ~ 35,000 Da and may exist as homodimer and contain carbohydrate moiety. The exact role of these molecules in venoms is unknown. However, some suggest that they may act as carriers of other molecules like neurotoxins to the CNS.

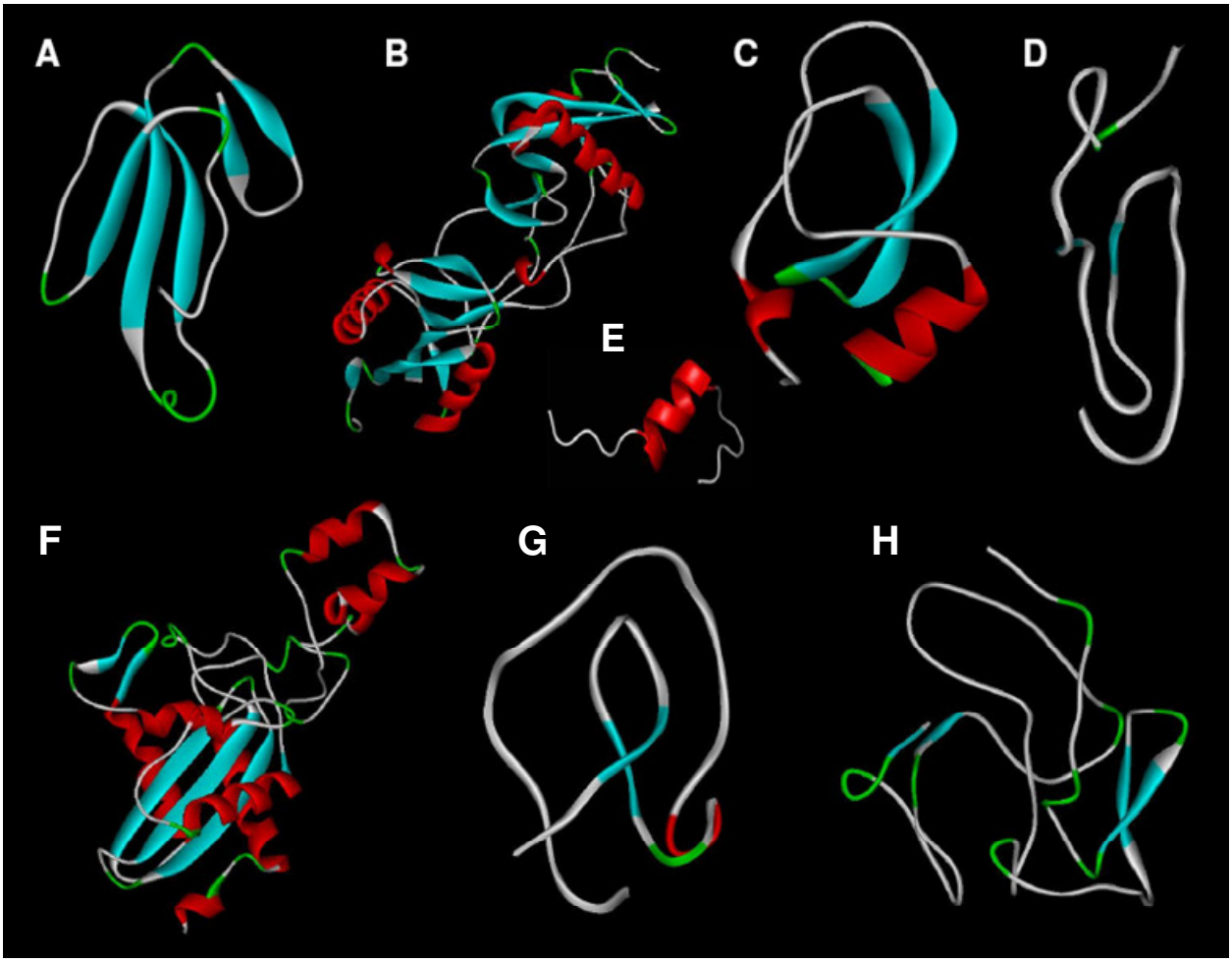

Figure 1.3: Representative examples of major families of non-enzymatic snake venom proteins.

(A) 3FTXs: α-cobratoxin (2CTX), (B) C-type lectin related proteins: factor IX binding protein (1IOD), (C) serine-proteinase inhibitors: dendrotoxins (1DTX), (D) disintegrins: echistatin (2ECH), (E) Sarafotoxins: SRTX-b (1SRB), (F) helveprins / CRISPs: triflin (1WVR), (G) waprins: nawaprin (1UDK), (H) vespryns: model of ohanin built base on PRY/SPRY domain (2FBE) . The protein data bank accession numbers are given in parentheses. The structures are α-carbon solid ribbon representation and presented with the aid of DS ViewerPro50.

peptides (BPPs) and natriuretic peptides (NPs) (Harvey, 1991; Kini, 2002; Torres *et al*, 2003). A brief description of these venom protein superfamilies is compiled in the Table 1.2. The scope of this thesis limits this review to just a description of the three-finger toxin family, because the protein being characterized belongs to this family.

1.4 Three-finger toxin (3FTX) family

Three-finger toxins (3FTXs) are the largest group of non-enzymatic snake venom proteins (Dufton and Hider, 1988; Harvey, 1991; Kini, 2002; Kini and Doley, 2010). These proteins consist of 60-75 amino acids residues (Tsetlin, 1999). They are most commonly and abundantly found in the venoms of elapid and hydrophiid snakes. Recently, our laboratory has also demonstrated the presence of 3FTXs in colubrid venoms (Pawlak *et al*, 2006; Pawlak *et al*, 2009) and 3FTX transcripts have also been found in the venom gland transcriptome of viperid snakes (Pahari *et al*, 2007; Junqueira-de-Azevedo *et al*, 2006; Jiang *et al*, 1987). The proteins in this family of toxins share a common structural scaffold of three β-sheeted loops emerging from a central core (**Fig. 1.4**) (Kini, 2002; Nirthanan and Gwee, 2004; Tsetlin, 1999; Kini and Doley, 2010). Because of this appearance, they resembles the three outstretched fingers of the hand hence, this family of proteins is referred as the three-finger toxin family. There are no α-helical segments in three-finger toxins and a multistranded β-structure is the predominant feature of these molecules (Tsetlin, 1999). Each toxin is essentially a flat "leaf-like" molecule with a slight concavity, the plane being determined by the extensive β-sheet (Tsetlin, 1999; Servent; Menez, 2001).

Despite the overall similarity in structure, these proteins have diverse functional properties (**Fig. 1.5**). Members of this family include neurotoxins targeting the cholinergic system (Changeux,

1990; Grant and Chiappinelli, 1985; Jerusalinsky and Harvey, 1994; Tsetlin, 1999) cytotoxins/cardiotoxins interacting with the cell membranes (Louw and Visser, 1978; Kumar *et al*, 1997; Bilwes *et al*, 1994), calciseptine and related toxins that block the L-type Ca^{2+} channels (de Weille *et al*, 1991; Albrand *et al*, 1995), dendroaspins, which are antagonists of various cell-adhesion processes (McDowell *et al*, 1992), fasciculins that inhibit the enzyme, acetylcholinesterase (Cervenansky *et al*, 1991), and β-cardiotoxin antagonizing the β-adrenoceptors (Rajagopalan *et al*, 2007). The subtle variations in their structures, such as the presence of extra disulfide bonds, number of β-sheets present, differences in size and overall conformation (twists and turns) of the loops and longer C-terminal and/or N-terminal extensions (Ricciardi *et al*, 2000), may contribute to the observed functional diversity as well as specificity of these toxins (Ohno *et al*, 1998).

However, there are a number of "orphan groups" of 3FTXs whose molecular target in the victim and hence their functional roles in the snake venoms are not yet known (Fry *et al*, 2003). Hence, every new 3FTX isolated from the snake venom should be considered as a new challenge, as it might show unique pharmacological properties associated with a new molecular target.

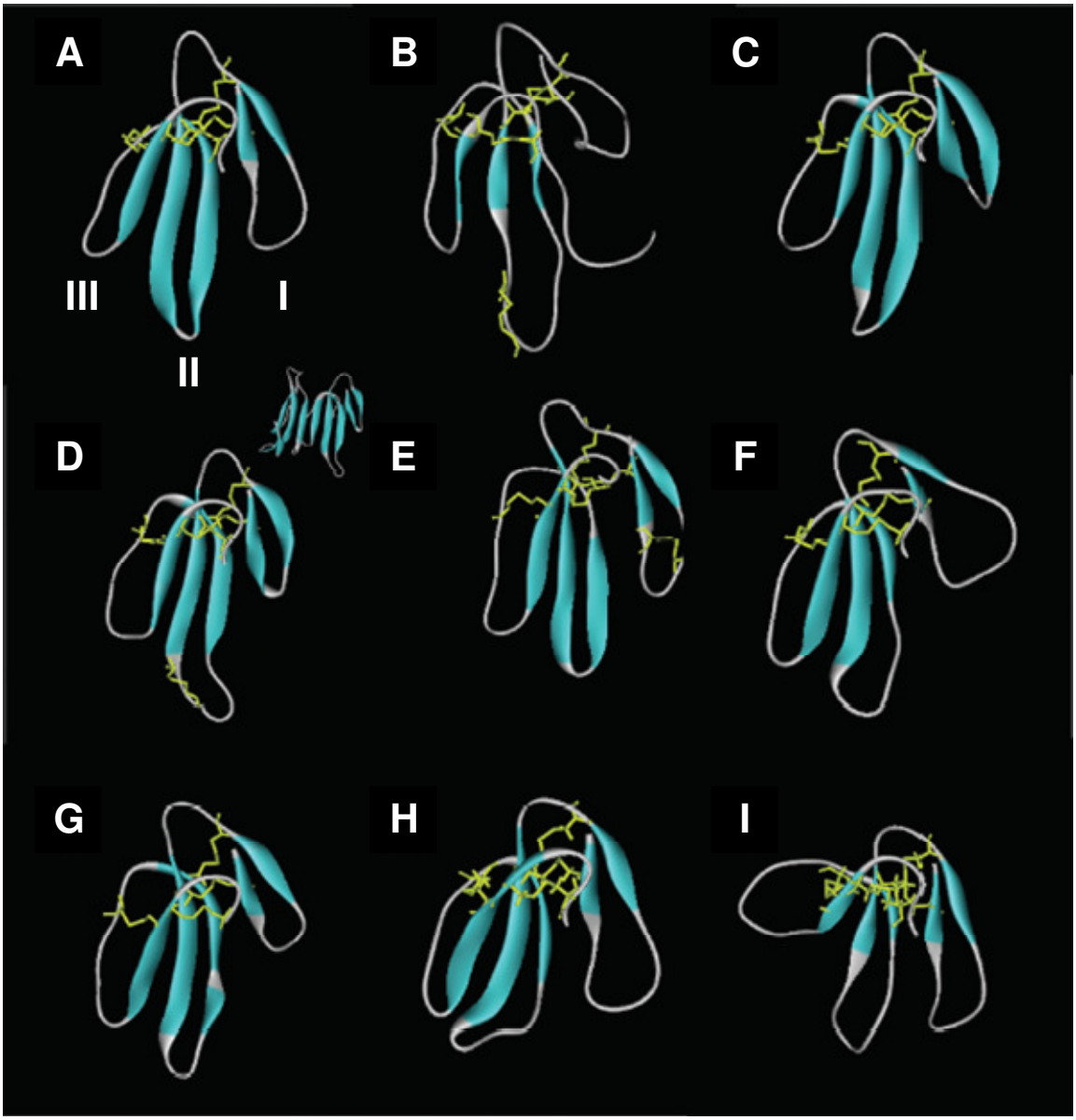

Figure 1.4: Three-dimensional structural similarity among 3FTXs from snake venoms.

(A) Erabutoxin a (1QKD), (B) α-bungarotoxin (2ABX), (C) cardiotoxin V4 (1CDT), (D) κ-bungarotoxin (1KBA), inset, dimer, (E) candoxin (1JGK), (F) fasciculin 2 (1FAS), (G) muscarinic toxin MT-2 (1FF4), (H) FS2 toxin (1TFS), (I) dendroaspin (1DRS). The protein data bank codes are stated in parentheses. All 3FTXs share a common fold: three finger-like loops emerging from the core at the top of the molecules, which contains four conserved disulphide bridges (shown in yellow). Some toxins, such as α-bungarotoxin (B) and κ-bungarotoxin (D) have the fifth disulphide bridge in loop II. In contrast candoxin (E) has the fifth disulphide bridge in loop I. Three β-sheeted loops numbered right to left as loop I, II and III respectively. The β-sheet structure is shown in blue. Figures were adapted from Kini, 2002 and modified accordingly.

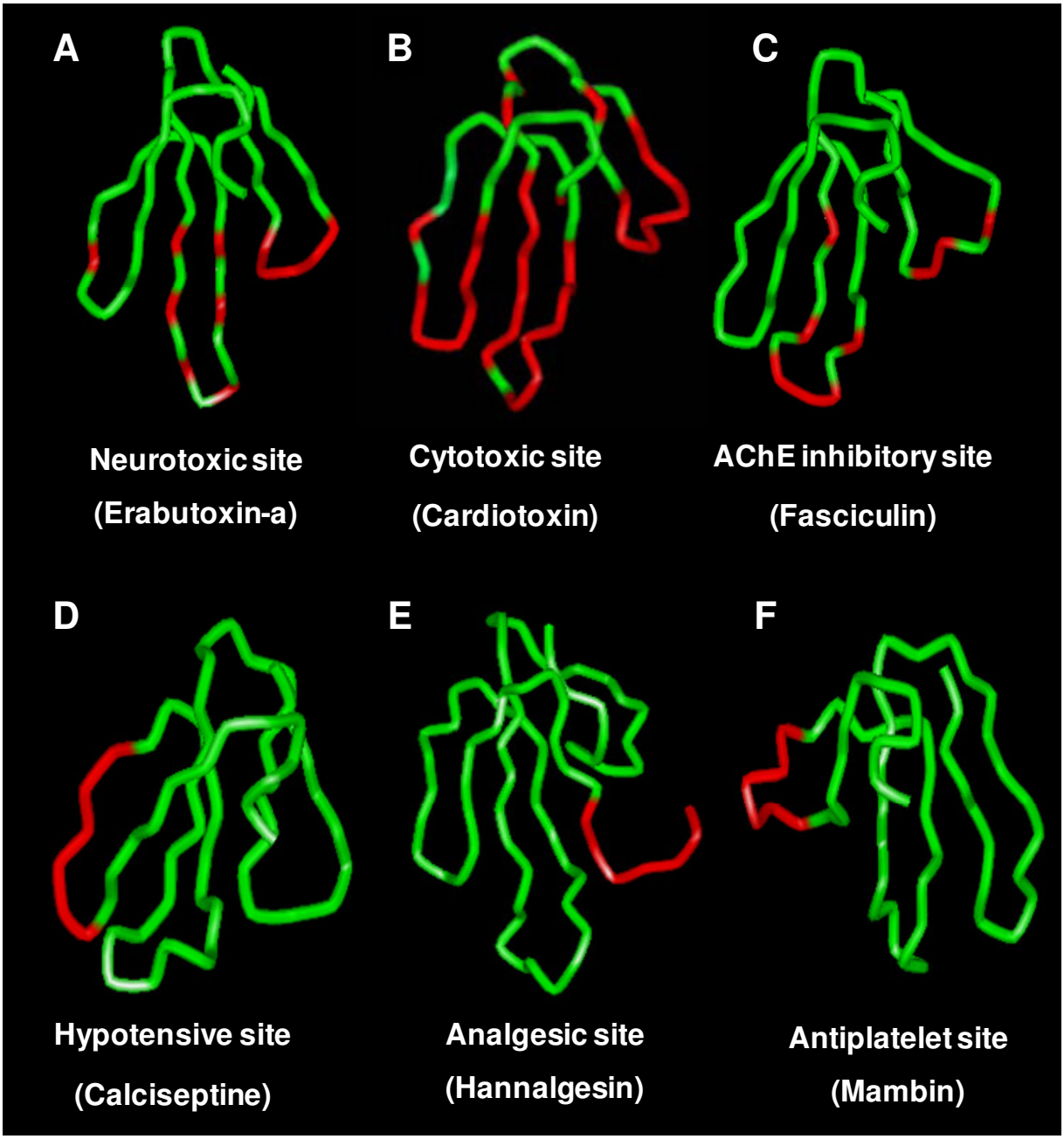

Figure 1.5: Functional diversity of three-finger toxins.

Six different functional sites elaborated on a common three-finger motif of three-finger toxins: (A) neurotoxic site of erabutoxin-a; (B) cytolytic site of cardiotoxin; (C) acetylcholine esterase (AChE) inhibitory site of fasciculin; (D) hypotensive site of calciseptine; (E) analgesic site of hannalgesin; (F) antiplatelet site of mambin. The functional site(s) are shown in red on the green α-carbon back structure of the respective toxins. All structures are shown in the α-carbon-line representation. Figures were adapted from Kini, 2002 and modified accordingly.

1.5 The ubiquitous three-finger fold

Interestingly, the three-finger fold is not only restricted with snake venom toxins. This fold has been associated with protein from mammalian and non-mammalian organisms. It is observed that many non-toxic proteins have adopted this three-finger fold like- mammalian Ly-6 family of cell-surface accessory proteins expressed in immune system cells (Fleming *et al*, 1993; Kieffer *et al*, 1994; Gumley *et al*, 1995). This fold has also been utilized by the extracellular domain of the human complement regulatory protein CD59 (Fletcher *et al*, 1994), a domain of the receptor for the urokinase-type plasminogen activator (Ploug and Ellis 1994; Llinas *et al*, 2005), epidermal neuromodulators SLURP-1 & SLURP-2 (Chimienti *et al*, 2003; Arredondo *et al*, 2006), bone morphogenetic protein IA (Kirsch *et al*, 2000), type II activin receptor (Greenwald *et al*, 1999), xenoxins from frog (Xenopus laevis) skin secretions (Kolbe *et al*, 1993) pheromones like Plethodontid Modulating Factor (PMF) in salamander (Palmer *et al*, 2007), plasma protein like trout toxin 1 in rainbow trout (Gumley *et al*, 1995) and HEP21 from hen egg white (Nau *et al*, 2003). A few plant lectins like wheat germ agglutinin (Drenth *et al*, 1980) and hevein (Gidrol *et al*, 1994) is also known to possess the unique three-finger fold. Interestingly, lynx1 (Miwa *et al*, 1999 and Ibanez-Tallon *et al*, 2002) and lynx2 genes (Dessaud *et al*, 2006) encodes for two non-toxic three-finger proteins, which are highly expressed in murine nervous system. They have been found to act as novel modulators of neuronal nicotinic acetylcholine receptors *in vitro* (Miwa *et al*, 1999). The protein lynx1 was found to co-localize with both, $\alpha_4\beta_2$- and α_7-subtypes of nicotinic receptors. Further, it was also found to increase the effective concentration of acetylcholine required for activation of these receptors as well as slow their recovery from desensitization (Ibañez-Tallon *et al*, 2002). Of particular interest, this is the first instance of a three-finger protein from a non-venom source that is directly associated with

nicotinic receptor function. Moreover, these proteins as well as the Ly-6 family of proteins share the common structural patters (with respect to the cysteine bonding) with the non-conventional three-finger toxins. Furthermore, all these family of proteins share a common gene organization, which raises the possibility of their evolutionary relationship. An ancestral gene encoding for the three-finger fold proteins might have been duplicated during evolution and recruited to the venom gland (Fry, 2005). Further the descendents of this gene has undergone accelerated evolution via extensive gene duplications in the protein-coding regions (Nakashima *et al*, 1993; Nakashima *et al*, 1995; Nobuhisa *et al*, 1996; Kini and Chan 1999; Fujimi *et* al, 2003; Doley *et* al, 2009; Kini and Doley, 2010), leaving only parts essential for the integrity of the three-finger fold, at the same time manipulating the functional residues.

1.6 Three-finger toxins interacting with the cholinergic systems

Snake venoms are rich in toxins that are well known to interfere with cholinergic transmission (Chang and Lee, 1963; Karlsson 1966; Lee, 1972; Chang, 1979; Karlsson, 1979) in the central and peripheral nervous systems. Snake venom toxins targeting the cholinergic system can be subdivided into three major classes- Muscarinic toxins, Fasciculins and Neurotoxins.

1.6.1 Muscarinic toxins

Muscarinic toxins were originally isolated from African mamba snake, *Dendroaspis angusticeps* (Adem *et al*, 1988) and are predominantly found in mamba venoms (Bradley, 2000; Servent and Fruchart-Gaillard, 2009). They are the first protein ligands to interact with the muscarinic acetylcholine receptors (mAChRs). Hence, they were named as muscarinic toxins (MTs). Muscarinic ACh receptors (mAChRs) belong to the G-protein coupled receptor (GPCR)

superfamily, which comprises of seven transmembrane helices with extra- and intra-cellular loops. As the name suggests, GPCRs act through GTP binding proteins (G proteins) to stimulate or inhibit intracellular effector systems (Segalas *et al*, 1995, Karlsson *et al*, 2000; Jerusalinsky and Harvey, 1994). There are five subtypes of mAChRs (M1 to M5), depending on their different G protein coupling properties (Caulfield and Birdsall 1998), which control a large number of physiological processes (Segalas *et al*., 1995; Karlsson *et al*., 2000). mAChRs have been implicated as important drug targets in disorders like schizophrenia, depression, drug addiction, Parkinson's and Alzheimer's diseases (Segalas *et al*, 1995; Bradley, 2000; Scarr and Dean 2008; Langmead *et al*, 2008). Although currently there are many conventional small molecular ligands available for these receptors, but all of these bind non-specifically with more than one subtype of mAChR (Bradley, 2000; Lee *et al*, 2001). As a result of this, it was difficult to assess the functional role of the individual subtypes of mAChRs in different tissues as more than one subtype of the receptor may exist simultaneously in many organs (Jerusalinsky and Harvey, 1994, Karlsson *et al*., 2000; Adem and Karlsson, 1997) as well as to develop specific drugs against a disease involving a particular subtype of mAChRs without affecting the normal activity of the others. The only ligands to show subtype specificity for these receptors are the naturally occurring snake venom muscarinic toxins (**Fig. 1.6**).

MTs belong to the snake venom three-finger toxin family. About 10 different MTs have been isolated from the venom of either *Dendroaspis angusticeps* or *Dendroaspis polylepis*. The sequence of the MTs vary in length, each containing 65–66 residues, eight cysteine residues forming four disulfide linkages and showing a sequence identity of ~50%.

A

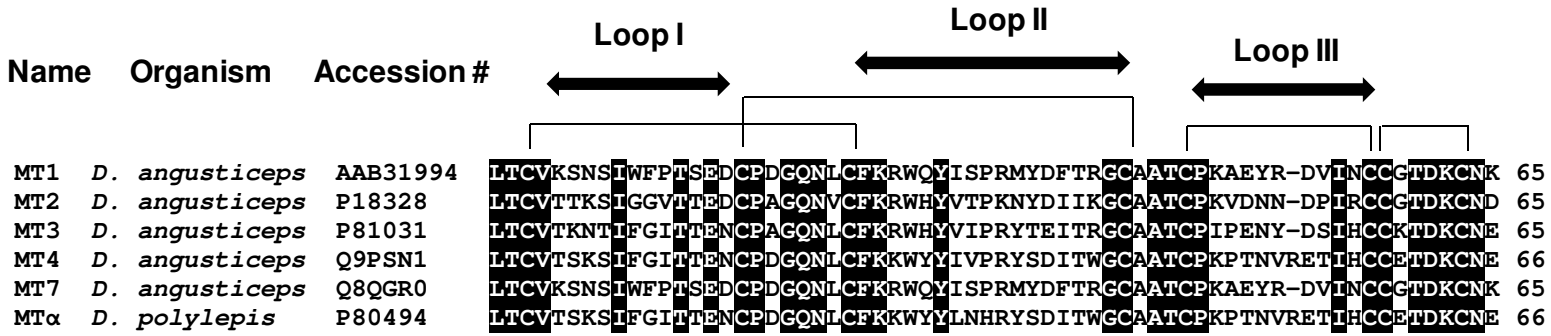

Consensus sequence

LTCV----I---T-E-CP-GQN-CFK---Y----------GC-ATCP-------I-CC-TDKCN-

B

Figure 1.6: Muscarinic toxins from mamba venom.

(A) Muscarinic toxins from *Dendroaspis angusticeps* (green mamba) and *D. Polylepis* (black mamba) venoms. The consensus sequences are highlighted in black, the disulfide bridges are shown in black lines and the loop regions are indicated by black solid arrows. (B) Structure of muscarinic toxin 2 (MT2) isolated from *Dendroaspis angusticeps* (1FF4). The conserved disulfide bridges are represented in sticks.

The three dimensional structure of MTs along with the highly conserved sequences are shown in figure 1.6. Despite of the similarity in their primary and tertiary structures, MTs exhibit clear functional differences and display distinct interaction profiles with the different subtypes of muscarinic receptors (Karlsson *et al*., 2000). Moreover, MTs have a variety of functional characteristics, with the competitive antagonistic effect, they can also act as allosteric modulator or agonist (Servent; Fruchart-Gaillard, 2009). This has made them invaluable scientific tools for therapeutic applications.

1.6.2 Fasciculins

Fasciculins do not interact with any cholinergic receptors but they inhibit the enzyme, acetylcholine esterase (AChE). Like MTs, fasciculins were also isolated from the venom of mambas. The first one was isolated from the venom of *Dendroaspis angus*ticeps (Viljoen and Botes, 1973; Karlsson *et al*, 1984) which was followed by other closely related proteins from *Dendroaspis polylepis* and *Dendroaspis viridis* (le Du *et al*, 1996). Fasciculins are composed of about 61 amino acid residues with four disulfide bridges and similar to other 3FTXs composed of predominantly β-sheet structure (**Fig. 1.7 A**). Fasciculins are potent inhibitors of the enzyme acetylcholinesterase (AChE) and they bind with a 1:1 stoichiometry to the peripheral anionic site of the enzyme (le Du *et al*, 1996). AChE is a synaptic enzyme whose principal role is the termination of impulse transmission at cholinergic synapses by the rapid hydrolysis of the neurotransmitter acetylcholine. By inhibiting this enzyme, fasciculins cause severe, generalized and long-lasting fasciculation of skeletal muscles due to the accumulation of acetylcholine in the synaptic cleft (Harel *et al*, 1995). The crystal structure of a complex between AChE from

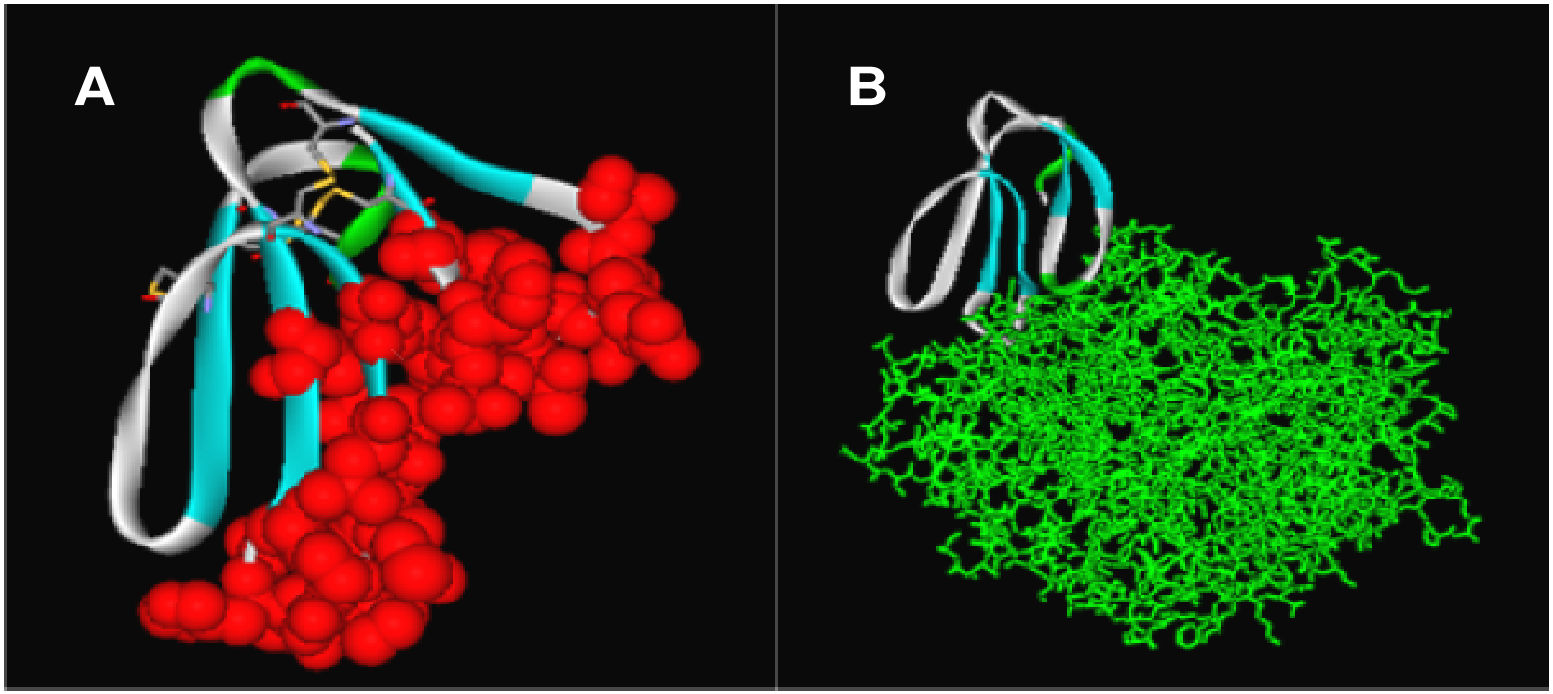

Figure 1.7: Fasciculins from snake venom

(A) Structure of Fasciculin 1 from the green mamba *Dendroaspis angusticeps* (1FAS). The important residues involved in interactions with the target molecule (AChE) are shown in red (CPK representation) and the conserved cysteines are represented in as sticks (B) Structure of Fasciculin II (*Dendroaspis angusticeps*) in complex with AChE (represented as green sticks) enzyme (1FSS).

Torpedo californica (Pacific electric ray) and fasciculin-II (FAS-II) from *D. angusticeps* (eastern green mamba) shows a stoichiometric complex with one molecule of FAS-II bound to each AChE subunit (**Fig. 1.7 B**). FAS-II binds to the peripheral anionic site of the enzyme and seals the narrow gorge leading to the active site. The structures of the two partners in the complex appear similar to their monomeric structures showing that there are no conformational changes associated with complex formation. The high affinity of FAS-II for AChE (K_i ~ 0.1 nM) is due to a remarkable surface complementarity involving a large contact area (~ 2000 $Å^2$) (Harel *et al*, 1995). Most of the residues involved in important contacts with the target enzyme are located on the first and second loops of the toxin (**Fig. 1.7 A**).

1.6.3 Neurotoxins

Neurotoxins are extremely important components of snake venom as they are useful in the effective capture of prey. They cause rapid paralysis of the voluntary muscles and, hence, inhibit movement and respiration followed by death. Depending on the site of action snake neurotoxins are generally classified as either postsynaptic or presynaptic. The three-finger neurotoxins are mainly postsynaptic toxins. They are widely referred to as 'curare-mimetic toxins' due to their similarity in action to the arrow poison curare which is a competitive nicotinic acetylcholine receptor (nAChR) antagonist (Endo & Tamiya, 1991). These neurotoxins bind with high affinity and specificity to acetylcholine binding sites on skeletal muscle nicotinic receptors (Changeux *et al*, 1970). Over the years, more than 100 α-neurotoxins have been isolated from snake venom which contributed significantly to isolation and characterization of nAChRs.

Depending on the target receptors as well as primary structures, these neurotoxins can be broadly divided into various groups such as- Curaremimetic or α-neurotoxins, κ-neurotoxins and non-conventional or weak toxins. The α-neurotoxins can be subdivided into short-chain and long-chain α-neurotoxins depending on the primary structural features (amino acid residues and number of disulfide bridges). Short-chain α-neurotoxins are composed of 60-62 amino acid residues with four conserved disulfide bonds (**Fig. 1.8 A**) and long-chain α-neurotoxins are composed of 66-74 amino acid residues and four conserved disulfide bonds with an additional disulfide bond in the tip of loop II (**Fig. 1.8 B** and **C**) (Endo and Tamiya, 1991; Servent and Menez, 2001). Both short-chain and long-chain α-neurotoxins target muscle ($\alpha\beta\gamma\delta$ or α_1 subtype) nAChRs (Nirthanan and Gwee, 2004; Tsetlin, 1999; Changeux, 1990). Functional difference lies in the kinetics of association and dissociation between the two types of α-neurotoxins with the skeletal muscle nicotinic receptor (Tsetlin, 1999). It was shown that short-chain neurotoxins tend to associate about 6-7 folds faster with the receptor and dissociate 5-9 fold faster than long-chain neurotoxins (Chicheportiche *et al,* 1975). In addition, long-chain neurotoxins, but not short-chain neurotoxins, also target neuronal α_7-nAChRs associated with neurotransmission in the brain (Servent *et al*, 1997; Servent *et al*, 2000). While lacking the extra disulfide bridge, *Laticauda colubrina* toxins (Lc-a and Lc-b) is considered to be a long-chain neurotoxin based on high sequence homology with other long-chain aneurotoxins (Endo & Tamiya, 1991; Servent *et al*, 1997). However, functionally they behave as short-chain neurotoxins, showing high affinity towards muscle receptors and poor affinity towards neuronal receptors (Servent *et al*, 1997). Therefore, they are referred as atypical long-chain neurotoxins.

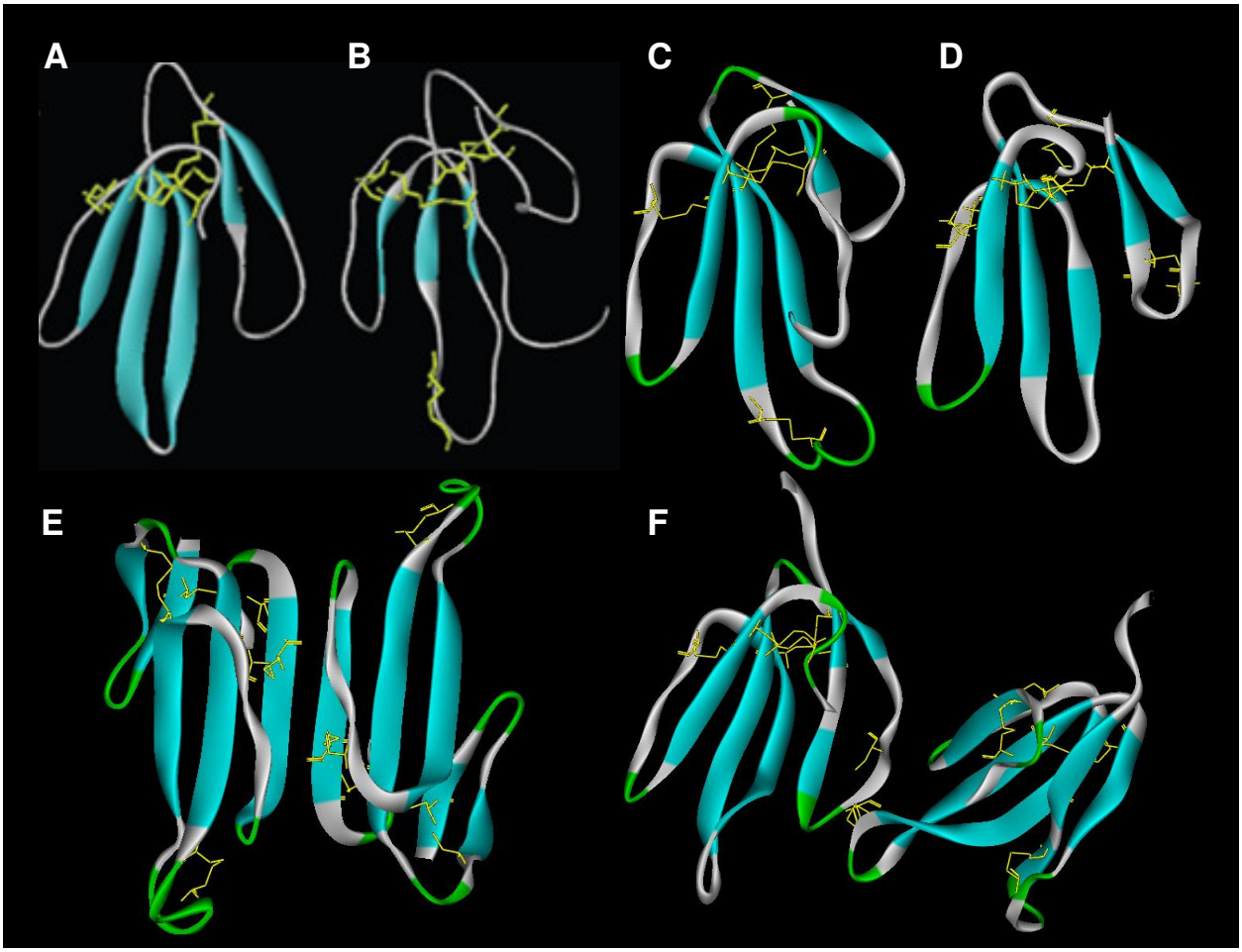

Figure 1.8: Snake toxins that interact with nicotinic acetylcholine receptors.

Representative examples of: (A) erabutoxin-a (5EBX): short-chain α-neurotoxin (monomer); (B) α-bungarotoxin (1IDI): long-chain α-neurotoxin (monomer); (C) α-cobratoxin (2CTX): long-chain α-neurotoxin (monomer); (D) candoxin (1JGK): non-conventional toxin from elapid snake (monomer); (E) κ-bungarotoxin (1KBA): κ-neurotoxin (non-covalent homodimer), (F) irditoxin (2H7Z): non-conventional toxin from colubrid snake (covalent heterodimer). The protein data bank accession codes are stated in parenthesis. All toxins share a common three-finger scaffold that includes a core region cross-linked by four conserved disulfide bridges (shown in yellow). β-sheets are shown in cyan. The structures are α-carbon solid ribbon representation and presented with the aid of DS ViewerPro50.

κ-Neurotoxins are first 3FTX reported to exist as a homodimeric complex (**Fig. 1.8 E**) (Dewan *et al*, 1994). These molecules are structurally similar to long-chain α-neurotoxins with five disulfide bonds (the additional one is in the tip of loop II). However, they have a shorter C-terminal tail like the short α-neurotoxins, and intermediate number of (66) amino acid residues (Grant and Chiappinelli 1985; Fiordalisi *et al*, 1994). The κ-neurotoxins, such as κ-bungarotoxin (*Bungarus multicinctus*), show specificity for other neuronal subtypes, $\alpha_3\beta_2$- and $\alpha_4\beta_2$-nAChRs (Grant and Chiappinelli, 1985; Wolf *et al*, 1988).

Non-conventional toxins are not so well characterized class of 3FTXs. They consist of 62-68 amino acid residues and five disulfide linkages. However, unlike the long-chain α-neurotoxins and κ-neurotoxins, the fifth disulfide linkage is present in the loop 1 (**Fig. 1.8 D**). The non-conventional toxins showed low lethality (LD50 ~ 5–80 mg/kg) compared to the highly lethal α-neurotoxins (LD50 ~0.04–0.3 mg/kg). Thus, this group of toxins has also been referred to as 'weak toxins' (Utkin *et al*. 2001). However, this convention does not hold true for a few cases like γ-bungarotoxin and candoxin isolated from the venom of *Bungarus multicinctus* (Antil *et al*, 1999; Nirthanan *et al*, 2002). Candoxin produced a potent neuromuscular blockade, but unlike α-neurotoxins this blockade was readily reversible. Additionally, candoxin also interacted with α_7-nAChRs and the affinity is in nanomolar range (Nirthanan *et al*, 2002).

All neurotoxins characterized to date exist as monomers with the exception of κ-neurotoxins from *Bungarus sp.* (Chiappinelli and Lee, 1985; Chiappinelli and Wolf, 1989), which are non-covalently linked homodimers that binds neuronal ($\alpha_3\beta_2$ and $\alpha_4\beta_2$), but not muscle ($\alpha\beta\gamma\delta$) nAChRs. More recently, an article was published which was the first report of a covalent heterodimeric neurotoxin, irditoxin (**Fig. 1.8 F**) from the venom of *Boiga irregularis*, which was a unique irreversible inhibitor of muscle ($\alpha\beta\gamma\delta$) nAChRs (Pawlak *et al*, 2009). The current

study is the first to report the existence of a novel homodimeric short neurotoxin that interacts with nAChRs.

1.7 Nicotinic Acetylcholine Receptors

Nicotinic acetylcholine receptors (nAChRs) are member of the pentameric "Cys-loop" superfamily of Ligand-Gated Ion Channels (LGICs), also referred to as ionotropic receptors. These receptors are a group of intrinsic transmembrane ion channels which open in response to binding of a chemical messenger, referred as ligands. LGICs are divided into three superfamilies based on their structural organization (**Fig. 1.9**) (Le Novere and Changeux, 1999)- trimeric - made up with 3 homologous subunits, each with 2 transmembrane segments (eg. ATP gated channels); tetrameric - made up with 4 homologous subunits, each with 3 transmembrane segments (eg. glutamate activated cationic channels such as- NMDA receptors) and pentameric - made up with 5 homologous subunits, each with 4 transmembrane segments (eg. Cys loop superfamily such as- nAChRs, 5-HT_3 receptors, $GABA_A$ receptors, glycine receptors).

Nicotinic receptors are transmembrane, allosteric glycoproteins of molecular weight ~290 kDa, involved in fast ionic responses to acetylcholine (Grutter and Changeux, 2001; Karlin, 2002). They are composed of 5 homologous subunits arranged symmetrically around the ion channel perpendicular to the membrane (**Fig 1.10** and **1.11**). These subunits can be divided into α and non-α types. The principal component of the ligand binding site is formed by α-subunits. The non-α subunits constitute the complementary component of binding site or sometimes they provide structural integrity (Changeux and Edelstein, 1998; Corringer, *et al*, 2000; Itier and Bertrand, 2001) (**Fig. 1.10 B**). Each subunit can be divided into four domains: a large N-terminal extracellular domain which contains the ligand binding pocket, a membrane-

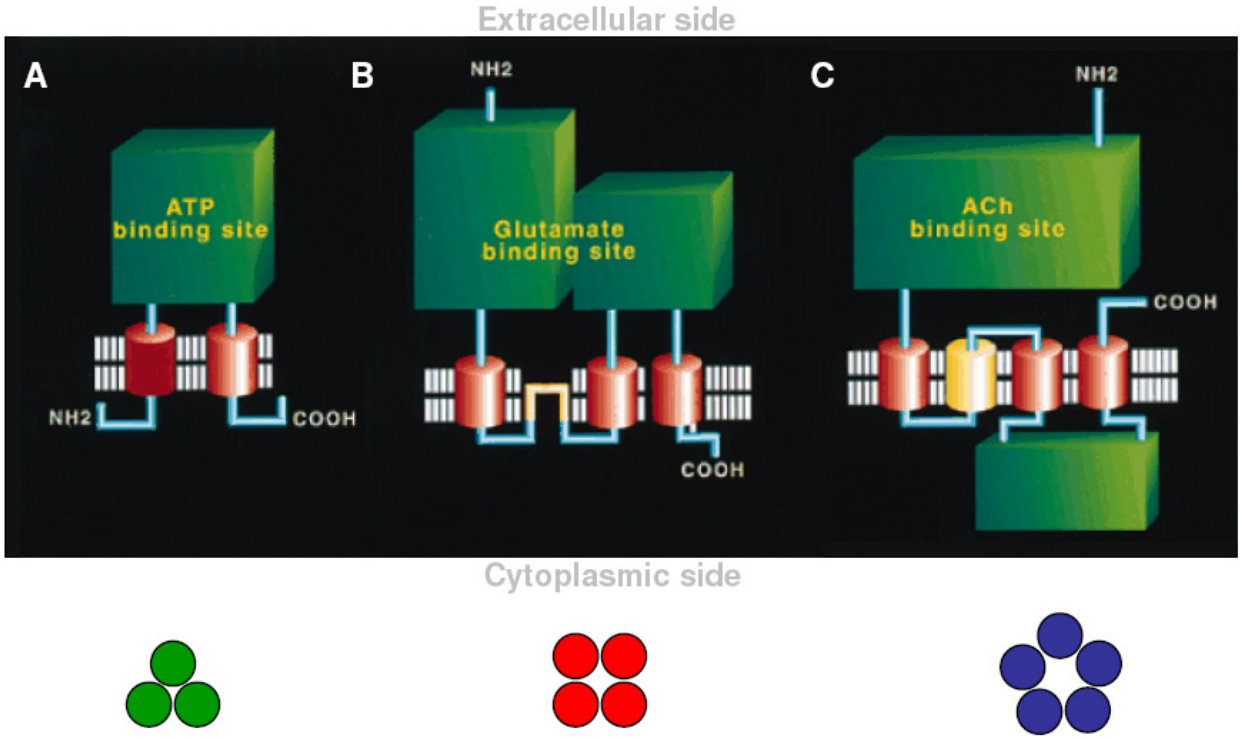

Figure 1.9: Schematic representation of superfamilies of ligand-gated ion channels.

A) trimeric receptors - ATP gated channels superfamily B) tetrameric - glutamate activated cationic channels superfamily C) Cys-loop superfamily. Figure adopted from (Le Novere and Changeux, 1999).

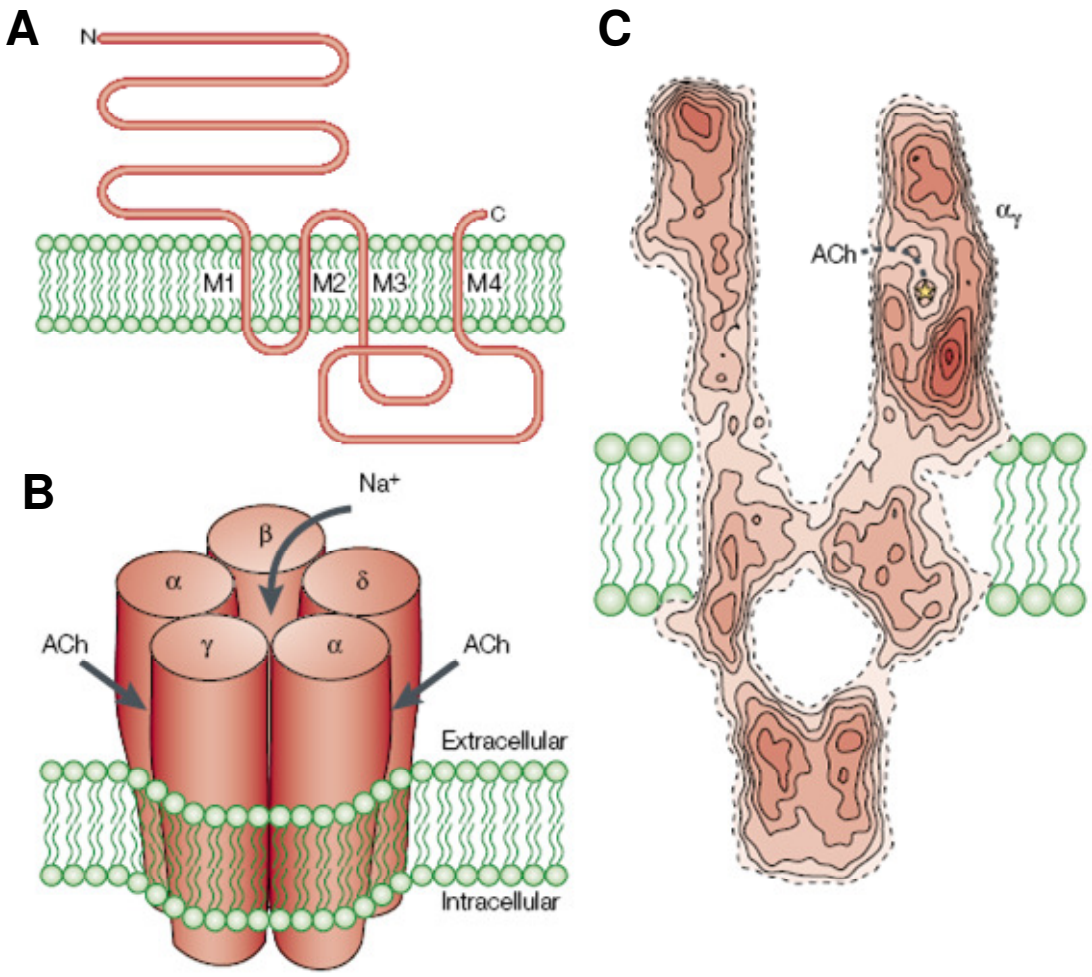

Figure 1.10: Structure of the nicotinic acetylcholine receptors.

(A) Schematic representation of the threading pattern of receptor subunits through the cell membrane. (B) A schematic representation of the quaternary structure, showing the arrangement of the subunits in the muscle-type receptor, the location of the two acetylcholine binding sites (between an α- and a γ-subunit, and an α- and a δ- subunit), and the axial cation-conducting channel. (C) A cross-section through the 4.6 Å structure of the receptor determined by electron microscopy of tubular crystals of Torpedo membrane embedded in ice. Dashed line indicates proposed path to binding site. Figure was adapted from Karlin, 2002 and Miyazawa *et al*, 1999 and modified accordingly.

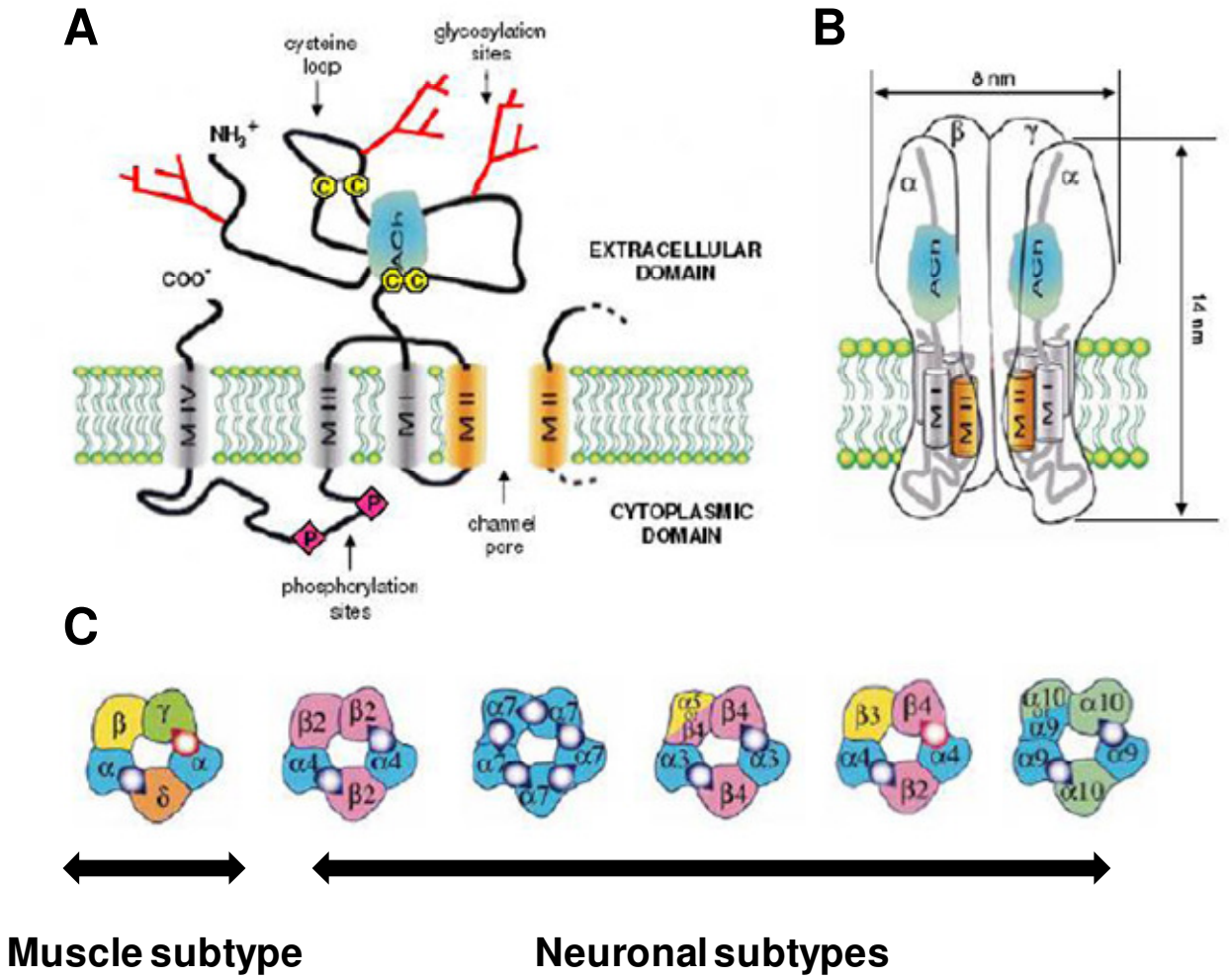

Figure 1.11 Schematic representations of nicotinic receptor and its subtypes.

A) Drawing of the single α-subunit of nAChR. The glycosylation sites are represented in red and the intracellular phosphorylation sites are represented by pink diamond with P letter. The four transmembrane domains are named MI to M IV. The MII domains of all five subunits line the ionic pore. ACh symbol represents the biding site for the ligand acetylcholine B) nAChR, composed of 5 homologous subunits. The model represents muscle receptor with the stoichiometry (α1)2βγδ, but for clarity δ subunit is not shown. The ACh binding site is localized at the interface between two subunits. C) The subunit composition of various subtypes of nAChRs and respective ACh binding sites. Starting from left: 1) muscle or electric organ nAChR 2) heteropentameric neuronal nAChR with two types of subunits (α2, α3, α4, α6 and β2, β4) 3) neuronal homopentameric nAChR (α7, α8, α9) 4) ganglionic receptor 5) neuronal heteropentameric (four types of subunits) β3 can be replaced by α5 6) hair cells (α9, α10). Figure adopted from Tassonyi *et al*, (2002).

spanning pore composed of four trans-membrane helices (MI, MII, MIII, MIV), a large cytoplasmic loop between MIII and MIV and a smaller extracellular C-terminal domain, giving it a total length of about 160 Å normal to the membrane plane (**Fig. 1.10 A** and **1.11 A**). The N-terminal domain is composed of 210-220 amino acid residues, which contains the characteristic "Cys-loop" consisting of 13 residues between Cys128-Cys141 (all numbering is according to Torpedo muscular receptor). This domain contains ligand binding site as well as glycosylation sites important for expression and secretion of the receptor (Ramanathan and Hall, 1999). In some species (e.g. mongoose (Barchan *et al*, 1992)) the glycosylation also offers resistance to α-neurotoxins (Kreienkamp *et al*, 1994). The transmembrane domain is composed of 70 residues long hydrophobic region divided into 3 transmembrane segments of 19-27 amino acid residues called: MI, MII and MIII. MI segment is required for the assembling of subunits and a heterodimeric ligand-binding site formation (Wang *et al*, 1996). The ion channel pore is formed by the contribution of MII domains of all five subunits. The pore has a diameter of ~6.5 Å in the narrowest part and is ~3-6 Å long. It possesses 3 rings (extracellular, intermediate and intracellular) of negatively charged residues and one central ring of polar residues. These rings attract cations into the channel and also act as selectivity filers for them (**Fig. 1.15 B**) (Ashcroft, 2000). The cytoplasmic domain contains phosphorylation sites. They are key mechanism in complex regulation of ion channel activity. It has been shown that a balance between kinases and phosphatases regulates tyrosine phosphorylation of the receptors at the cell surface in order to control the opening and closing of the channel (Voitenko *et al*, 2000).

1.8 Subtypes of nAChRs

In vertebrates, huge variety of alpha and non-alpha subunit subtypes and combinatorial assembly of homo- and heteropentamers generates a wide diversity of receptor types (**Fig. 1.11 C**). Very broadly, nicotinic receptors can be divided into two main families: the muscle and neuronal nAChRs (Corringer *et al*, 2000).

1.8.1 Muscular type of nAChR

The muscle type nicotinic receptor is well-characterized. It was discovered in Torpedo and Electrophorus in 1970 (**Fig. 1.12**). α-Bungarotoxin enabled purification of the receptor and its characterization further (Chang and Lee, 1963; Changeux *et al*, 1970). Muscle nAChR consists of a combination of α, β, δ and γ or ε subunits in the stoichiometry of (α)2βγδ or (α)2βεδ in the embryonic or adult receptor, respectively (**Fig. 1.12**) (Mishina *et al*, 1986). Muscle nAChRs are densely distributed on the postsynaptic membrane of the neuromuscular junction and they are involved in the neuromuscular transmission (**Fig. 1.13**). The muscle-type with stoichiometry (α)2βγδ is also found in abundance in the electric organ of the electric ray *Torpedo sp*.

Neurotransmission in neuromuscular junction

The neuromuscular junction is the well-studied synapse (reviewed in Durant, 1984; Pollard, 1994; Feldman, 1996; Naguib *et al*, 2002). It is referred as the point of contact between the axon terminal of a motor nerve fibre and the associated skeletal muscle fibre. The presynaptic membrane of the nerve terminal and postsynaptic membrane of the muscle is separated by a

synaptic cleft of ~20-30 nm (**Fig. 1.13**). The transmission of an electrical impulse involves a series of events involving the neurotransmitter ACh, leading to the ultimate muscle contraction. ACh is synthesized in the cytoplasm of the presynaptic bouton of nerve terminal (**Fig. 1.13**). During an action potential induced membrane depolarization, there is a sharp increase in the intracellular calcium concentration. This increase in calcium level triggers the fusion of the synaptic vesicle containing ACh is fused with the presynaptic membrane followed by ACh released to synaptic cleft (**Fig. 1.13**). A single nerve impulse may release between 100 – 300 vesicles of ACh. The postsynaptic membrane contains densely populated nAChRs. Binding of ACh to the receptors causes the opening of the cation channel and provoke the entrance of sodium ions on the muscle fiber. This ion influx leads to local depolarization of the postsynaptic membrane (from the resting value of -50 mV to +10 mV) and finally muscle contraction. The action of acetylcholine is terminated as a result of hydrolysis into choline and acetate by the enzyme, acetylcholinesterase.

1.8.2 Neuronal type of nAChRs

Neuronal nAChRs are localized in the central and peripheral nervous system. Neuronal nAChRs are pentamers consisting of subunits alpha and beta (**Fig. 1.14**).

Till date, 12 subunits including nine α (α2-α10) and four β (β2-β5) have been cloned (McGehee and Role, 1995). Different combinations of those subunits give rise to a great diversification of neuronal nAChRs accompanied by different pharmacological profiles and physiological properties. The most common heteropentameric arrangement consists of two identical α-subunits and three identical β-subunits. Subunits α2, α3, α4 and α6 can form functional heteropentameric receptors, when they are co-expressed with β2 or β4 in Xenopus oocytes.

Functional heteropentamers can also be created by subunits α7/α8 and α9/α10. Homopentamers can be assembled by α7, α8 and α9 subunits (McGehee and Role, 1995). The different subunit organizational patterns lead to different functional effects of neuronal nicotinic receptors (**Fig 1.11 C**).

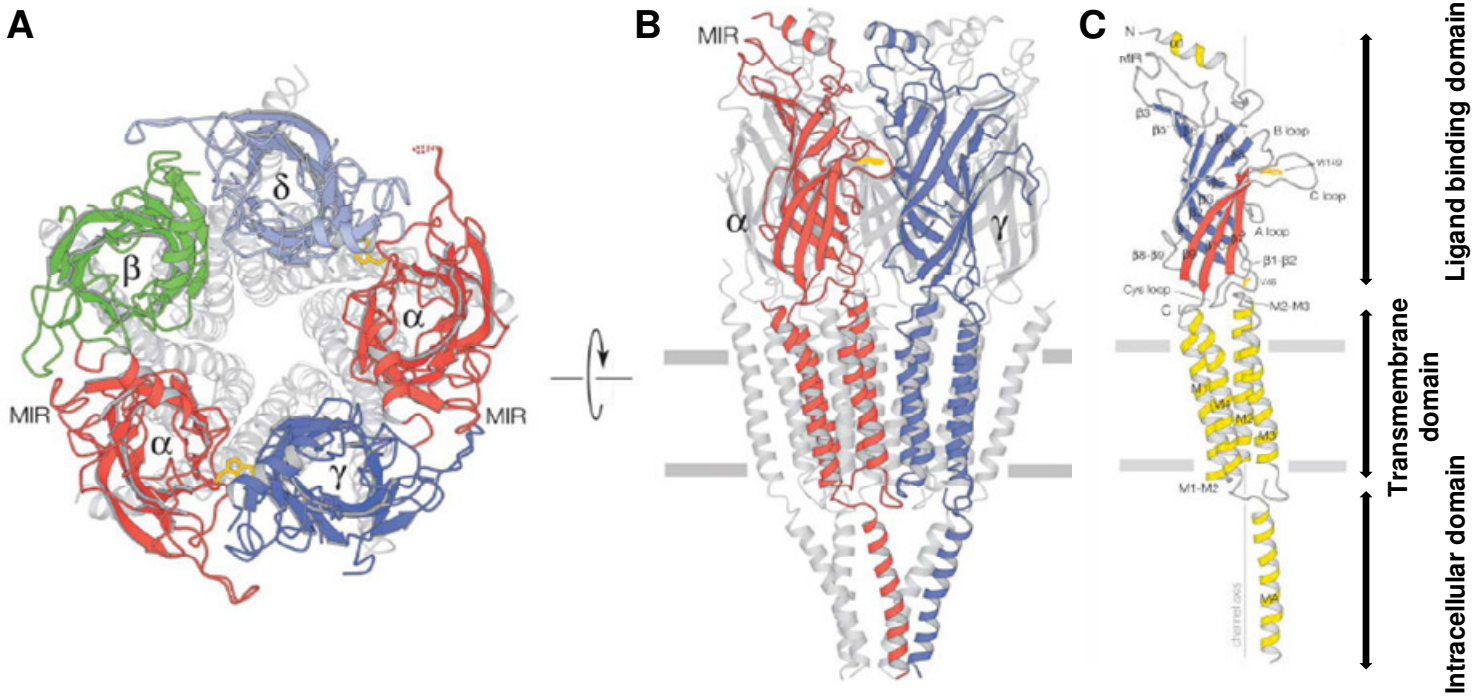

Figure 1.12: Structure of Torpedo marmorata (marbled electric ray) nAChR at 4 Å obtained by cryo-electron microscopy (2BG9) (Unwin, 2005).

(A) Ribbon diagrams of the whole receptor, as viewed from the synaptic cleft. For clarity, only the ligand-binding domain is highlighted. Subunits are shown in colors: α, red; β, green; γ, blue; δ, light blue. B) Ribbon diagrams of the whole receptor, viewed parallel with the membrane plane. For clarity only the front two subunits are highlighted. Also shown are the locations of Trp149 (yellow), the main immunogenic region (MIR), the membrane (horizontal grey bars)and the ligand binding or extracellular, transmembrane and intracellular domain by solid black arrows. C) Ribbon diagrams of a single subunit viewed parallel with the membrane plane, in orientations such that the central axis of the pentamer (vertical line) is at the back. The α-helices are in yellow; the β-strands composing the β-sandwich are in blue (inner) and red (outer). Locations of the N and C termini, Trp149, Val46, the Cys loop disulphide bridge and the membrane (horizontal bars) are indicated. Part of the M3 - M4 loop (connecting MA to M3) is missing.

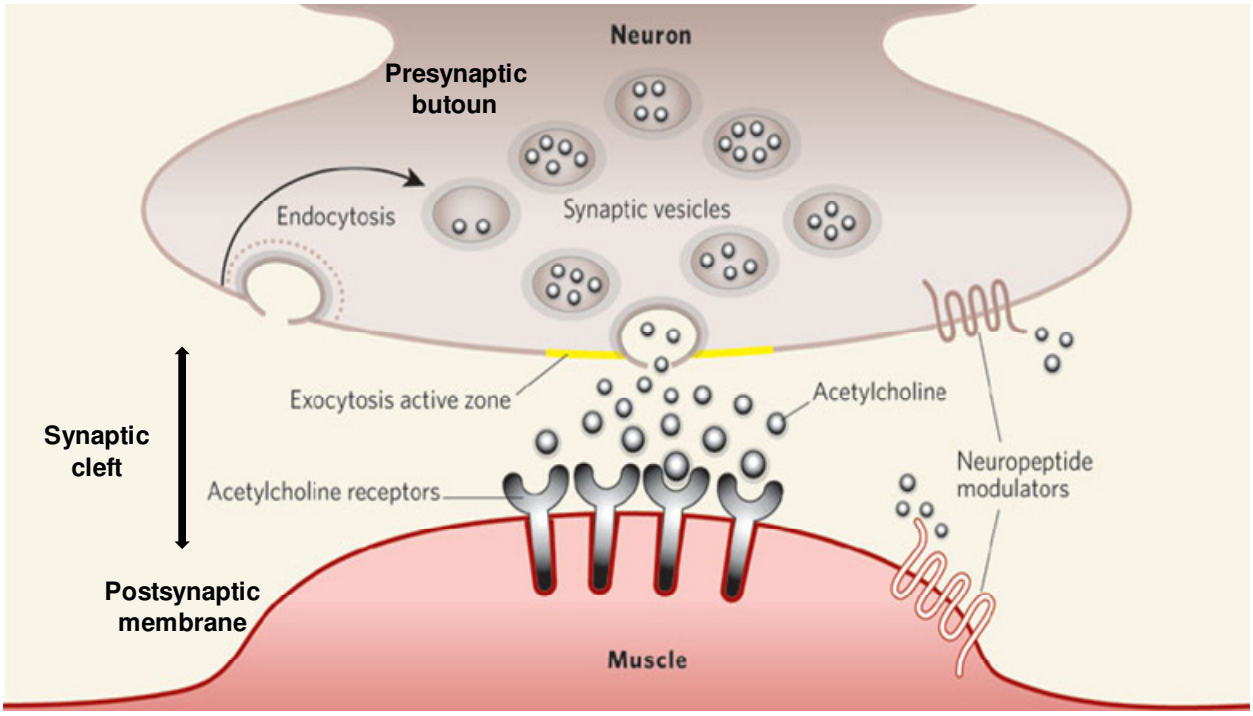

Figure 1.13: Signal transmission at the neuromuscular junction (the synapse).

A schematic diagram representing the structure of the mammalian neuromuscular junction. The presynaptic membrane of the nerve terminus is separated from the postsynaptic membrane of the skeletal muscle by the synaptic cleft (30-50 nm), shown by black solid arrow. The postsynaptic membrane is characterized by numerous junctional folds and is densely populated with muscle-type nicotinic acetylcholine receptors. These receptors are congregated specially at region of the junctional folds. Acetylcholine containing synaptic vesicles are present in large numbers in the nerve terminal, specifically at the active zones that face the openings of the junctional folds of the postsynaptic membrane. The figure was adapted from Bargmann, 2005 and modified accordingly.

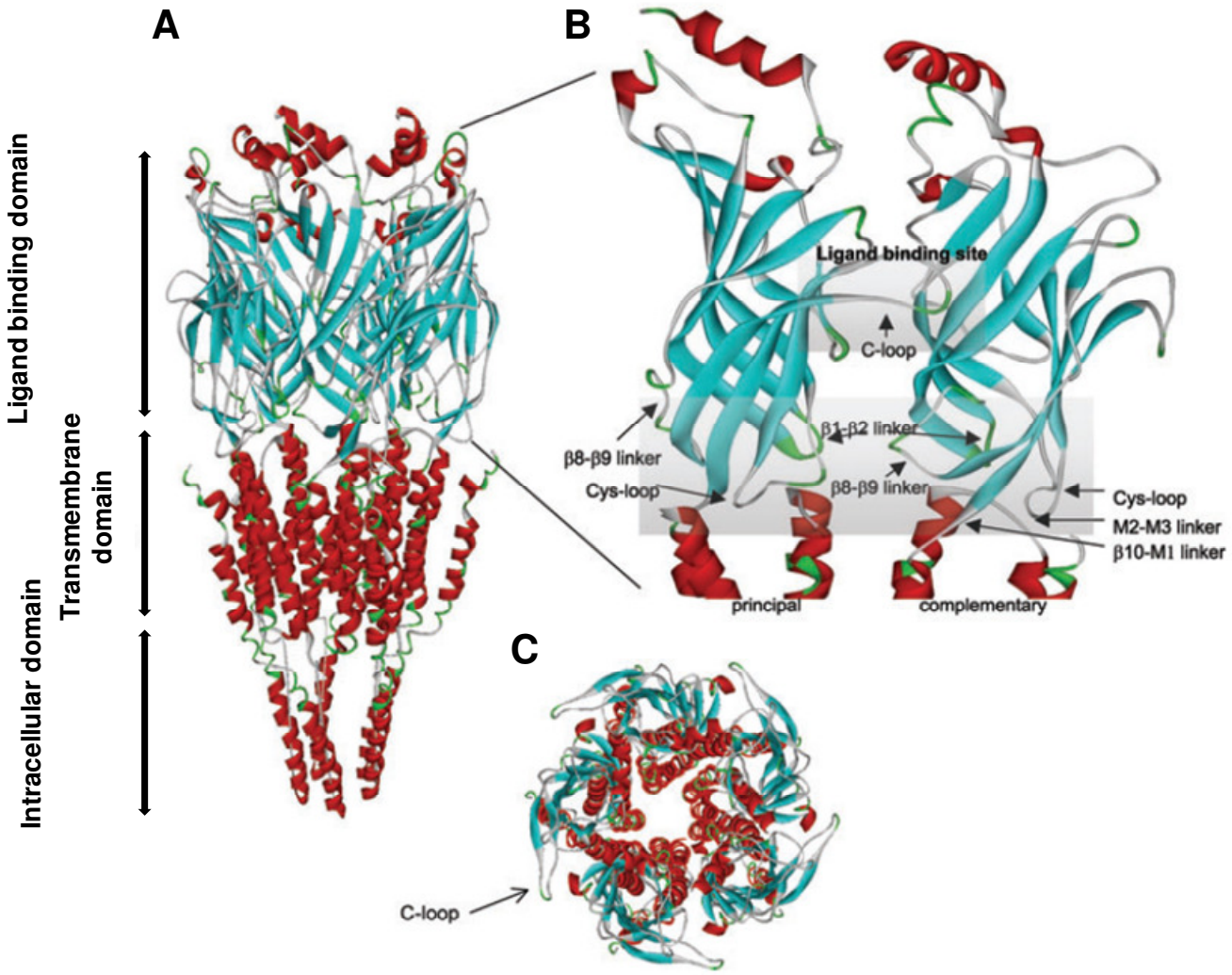

Figure 1.14: Molecular model of mammalian (rat) α7 nicotinic receptor

The model was developed based on sequence alignment with the cryoelectron microscopy structure of the *T. marmorata* nAChR as indicated in Gay *et al.* (2007). The α-helices are shown in red and the β-strands in blue, (A) a side view of the pentameric *α*7 receptor model, the ligand binding or extracellular, transmembrane and intracellular domain are indicated by solid black arrows. (C) a top-down view of the α7 receptor model. (B) The extracellular ligand binding domain is shown close up in. The ligand binding site is composed of a cluster of aromatic residues from both the principal and complementary subunits and is capped by the C-loop. The transition domain consists of several loops including: Cys-loop, β1-β2 linker, β8-β9 linker, β10-M1 linker and the M2-M3 linker. Figure was adapted from Yakel, 2010 and modified accordingly

The anatomical distribution of the variety of neuronal receptors is less well understood. In the rat brain, a wide distribution of the α7 subunit as well as α4 and α2 subunits suggested that α7 and α4β2 nAChRs represent the major subtypes present in the vertebrate brain (Seguela *et al*, 1993; McGehee and Role, 1995). Minimal cognitive deficits was observed with knockout mice lacking α4 and α2 subunits implying that brain nAChRs may not be crucial for the survival of the animal, but may play a more subtle role in brain functions such as learning, memory and attention (Picciotto *et al*, 1995). The α9 homopentamaric receptor is expressed in vertebrate cochlear hair cells as part of a cholinergic efferent innervation (Chen and Patrick, 1997). nAChRs affects both excitatory and inhibitory nerve activity. At the cellular level, neuronal these receptors have been shown to modulate the release of several neurotransmitters and to depolarize and generate action potentials in various types of neuronal cells (Wonnacott, 1997). Neuronal nAChRs are known to be involved in nicotine addiction in smokers as well as the positive effects of nicotine on cognition, memory and attention are also mediated by them. They are also known to be involved in several pathological conditions including schizophrenia, Alzheimer's disease, Parkinson's disease and certain forms of epilepsy (Lindstrom, 1997; Lena and Changeux, 1997; Paterson and Nordberg, 2000). Another major central function in which nicotinic transmission appears to be involved is pain processing and nociception (Pan *et al*, 1999). Many nicotinic receptor agonists (e.g. epibatidine) are reported to exert potent antinociceptive action (Meyer *et al*, 2000) probably by a selective action at α4β2 receptors (Tassonyi *et al*, 2002).

In the autonomic ganglia of peripheral nervous system, α3β4 receptors, represent the main receptor type at postsynaptic sties and are responsible for fast synaptic transmission. Knockout mice lacking α3 and β4 subunits present significant physiological deficits indicating the critical

role of this receptor in autonomic ganglia (Xu *et al*, 1999a; 1999b). Nicotinic autoreceptors, presumably of the α3β2 and α7 subtypes, have been described in the membranes of motor nerve terminals (Tsuneki *et al*, 1995) and postulated to be involved in process of transmitter release in response to rapid nerve stimulation.

1.9 The ligand-binding domain of nAChRs

The extracellular N-terminal domains of nAChRs are 210-220 amino acid residues long and contain binding site for ligands (agonists and competitive antagonists). The ligand binding site is located at the interface between two subunits with contributions from both counterparts (**Fig. 1.15 A**) (Corringer *et al*, 2000; Arias, 2000; Yakel, 2010). Affinity labelling of the ACh-binding site led to the first identification of a receptor subunit, the electrocyte ACh receptor α-subunit (Reiter *et al*, 1972). The affinity-labelled residues were a pair of adjacent cysteines, αCys192 (bp187) and αCys193 (bp188) (Kao *et al*, 1984), (numbers of the residues correspond to the mature Torpedo α-subunit and are followed by the numbers of the aligned residues in acetylcholine binding protein (AChBP), preceded by 'bp', for details on AChBP see below section 1.10), which are characteristic of all ACh receptor α-subunits. Subsequently, four widely spaced aromatic residues in the α-subunit such as- αTyr93 (bpTyr89), αTrp149 (bpTrp143), αTyr190 (bpTyr185) and αTyr198 (bpTyr192), were also found to be affinity labeled (Galzi *et al*, 1990; Middleton and Cohen, 1991). Alike the cysteines, these aromatic residues are also conserved in all ACh receptor α-subunits (except in neuronal α5, Tyr190 is replaced by Asp190). The involvement of the cysteines pair and the aromatic residues in ligand binding was also proven by further mutagenesis studies (for a review see, Karlin, 2002). Labelling and cross-linking studies have provided evidence that the ACh-binding sites are located in the interface

between subunits. In an experiment using dTC the aligned pairs γTrp53 (bpTrp53) and δTrp55, and γTyr111 (bpVal106) and δArg113, as well as γTyr117 (bpLeu112) were specifically photolabelled. Using another inhibitor, benzoylbenzoylcholine, the aligned pairs γLeu109 (bpArg104) and δLeu111 were also found to be photolabelled (Wang *et al*, 2000). Therefore, from all these experiments it was inferred that the principal component of the binding pocket is formed by the α-subunit and the complementary component of the binding pocket is formed by the non α-subunits. Amino acid residues from the α-subunit contributes to the formation of loops A, B and C, which are the principle components, whereas the neighbouring subunit (δ, γ or ε in muscle and α or β subtypes in neuronal receptors) residues contribute to loops D, E and F that form the complementary component of the binding pocket (**Fig. 1.15**) (Changeux and Edelstein, 1998; Corringer *et al*, 2000; Arias, 2000; Itier and Bertrand, 2001). Thus, the muscle nAChR contains two different ligand binding sites (α/δ and α/γ) with distinct affinities for nicotinic antagonists (Corringer *et al*, 2000), whereas the homopentameric α7 receptor offers five identical ligand binding sites (**Fig. 1.14**) (Palma *et al*, 1996; Itier and Bertrand, 2001; Yakel, 2010).

1.10 Acetylcholine binding protein (AChBP)

The isolation and characterization of an acetylcholine binding protein (AChBP) from the marine and fresh water snails *Lymnaea stagnalis* and Aplysia californica (Smit *et al*, 2001; Brejc *et al*, 2001; Hansen *et al*, 2004) has provided an excellent insight into the structure-function relationship of nAChRs. AChBP is a homopentameric, soluble protein that is secreted by snail glial cells into cholinergic synapses, where it interacts with acetylcholine to modulate cholinergic transmission (Smit *et al*, 2001). Mature AChBP forms a stable homopentamer, in

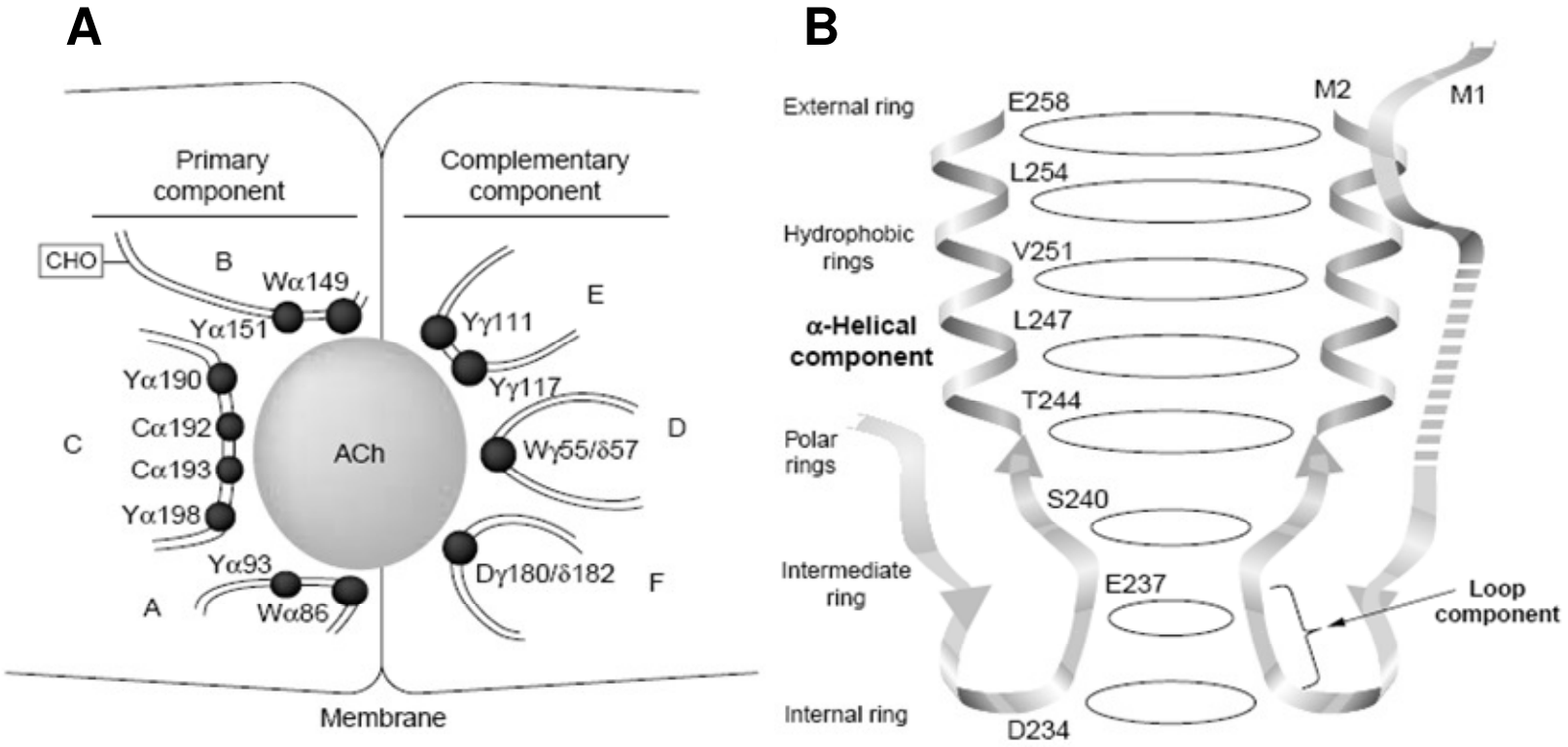

Figure 1.15: Representation of the ligand binding site and the ion channel of the nicotinic receptors

(A) The ligand binding site of nAChRs, as viewed from the exterior of the receptor along the plane of the membrane. Residues identified by affinity labeling and site-directed mutagenesis are indicated in the primary site present on α-type subunits and the complementary site present on γ or δ subunits of muscle receptor, or on α subunits of homopentameric neuronal receptors or β subunits of heteromeric neuronal receptors (B) The ion channel of nAChRs. Residues from M2 and the cytoplasmic loop component implicated in the selectivity filter are presented. Figure was adapted from Corringer *et al*, (2000); Changeux and Edelstein, 2001 and modified accordingly.

which each subunit consists of 210 amino acid residues (**Fig. 1.16**). It binds to the agonists and competitive antagonists of the nicotinic ACh receptor, including the small molecular ligands such as- ACh, nicotine, epibatidine, (+)-tubocurarine as well as protein ligands such as- conotoxins and snake venom α-neurotoxins. The spectrum of binding affinities resembles that of homomeric neuronal nicotinic receptors that are composed of α7- or α9-subunits. This soluble protein is a homologue of the N-terminal ligand binding domain of nAChRs, particularly α-subunits, but it lacks the transmembrane and intracellular domains. The amino acid sequence of AChBP and the N-terminal domain for nAChR are highly conserved, including those that are relevant for ligand binding (discussed above in section 1.9). The sequence identity of AChBP to the human α7 subunit is about 26% (Smit *et al*, 2001) and this value reaches up to ~ 60% when considering only the functional loop (A-F) regions (Fruchart-Gaillard *et al*, 2002). The high resolution crystal structure of AChBP (**Fig. 1.16**) revealed the predominantly β-sheeted structure, which correlates well with the structure of Torpedo nAChR (**Fig. 1.12**) predicted by cryo-electron microscopy (Miyazawa *et al*, 1999; Unwin 2005). As for the AChBP, nearly all the residues of the agonist-binding site of the α7 receptor that were previously identified by photoaffinity labeling and mutagenesis experiments (reviewed in Grutter and Changeux, 2001; Karlin, 2002), are located in a small cavity of about 10-12 Å diameter. This cavity is primarily formed by aromatic residues that are contributed by both, the principle and complementary sides of two adjacent subunits. All ligands of the ACh receptor have at least one quaternary ammonium group or a protonated tertiary ammonium group. The aromatic side chains present in the principle and complementary binding sides are proposed to make cationic- π interactions (a non-covalent interaction between a cation and the face of an aromatic ring) with the ammonium group of agonists (Grutter and Changeux, 2001). Moreover,

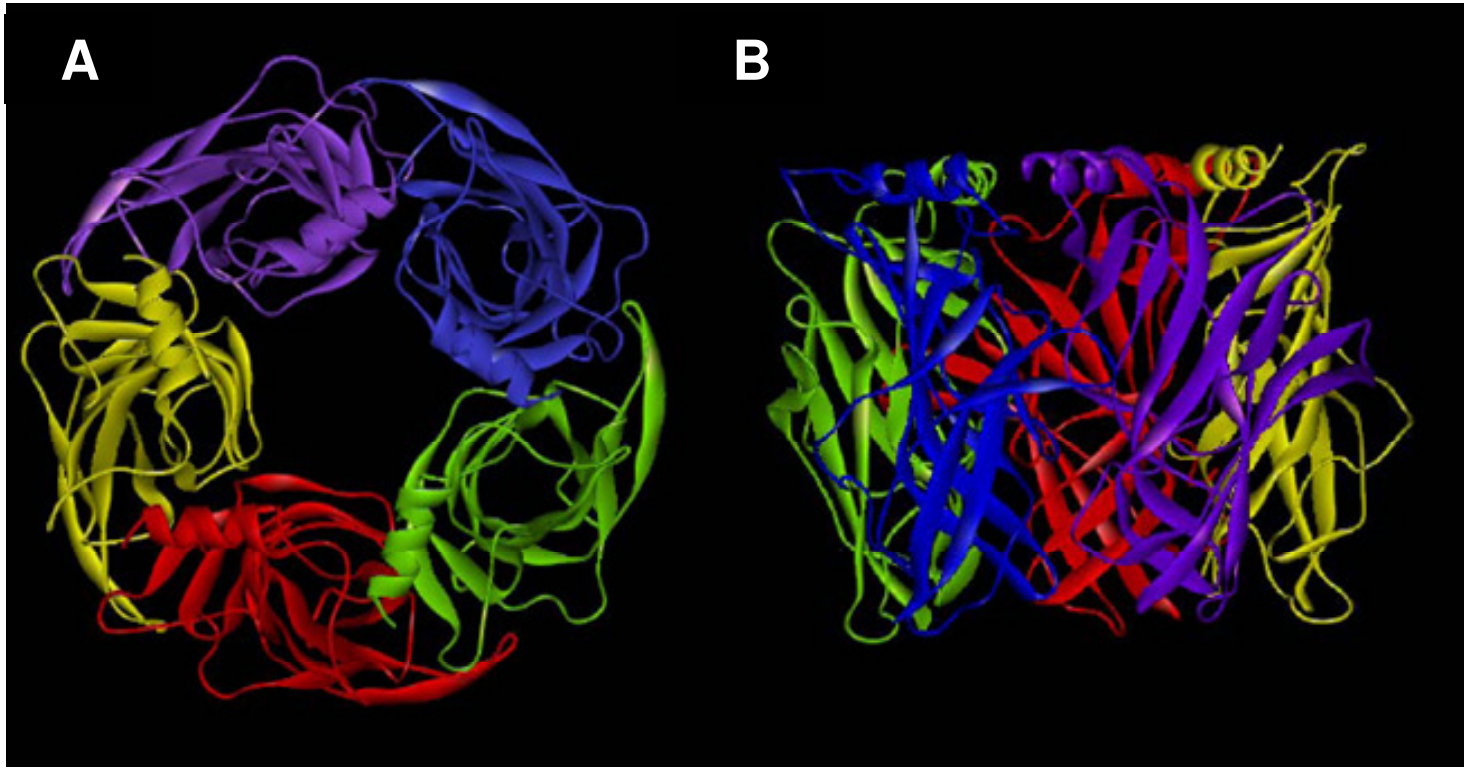

Figure 1.16: The acetylcholine binding protein (119B) from *Lymnaea stagnalis*.
(A) Top view of the 2.7 Å resolution crystal structure of the acetylcholine binding protein (AChBP) homopentamer from *Lymnaea stagnalis* glial cells (Brejc *et al*, 2001). The AChBP coloured to show the five subunits constituting the pentameric structure. Each AChBP subunit is a single domain protein. With the exception of the amino-terminal region of each subunit which consists of a short α-helix segment, β-sheet sandwich structure predominates (shown in ribbon diagram). The five equivalent dimer interfaces serve as the only links between the subunits. The interface buries a large surface area of 2,700 $Å^2$. The cavity/pocket at each interface between the subunits are lined by residues which were biochemically shown to be involved in ligand binding in nicotinic acetylcholine receptors and therefore likely constitute the ligand binding site. (B) The AChBP viewed perpendicular to the five-fold axis. It forms a 62 Å-high cylinder with a diameter of 80 Å. The N- and C- termini are located at 'top' and 'bottom' of the pentamer, respectively. The ligand-binding pockets are roughly equatorially positioned, about 30 Å away from the C termini conforming to the expected location of the *Torpedo* receptor ligand-binding site.

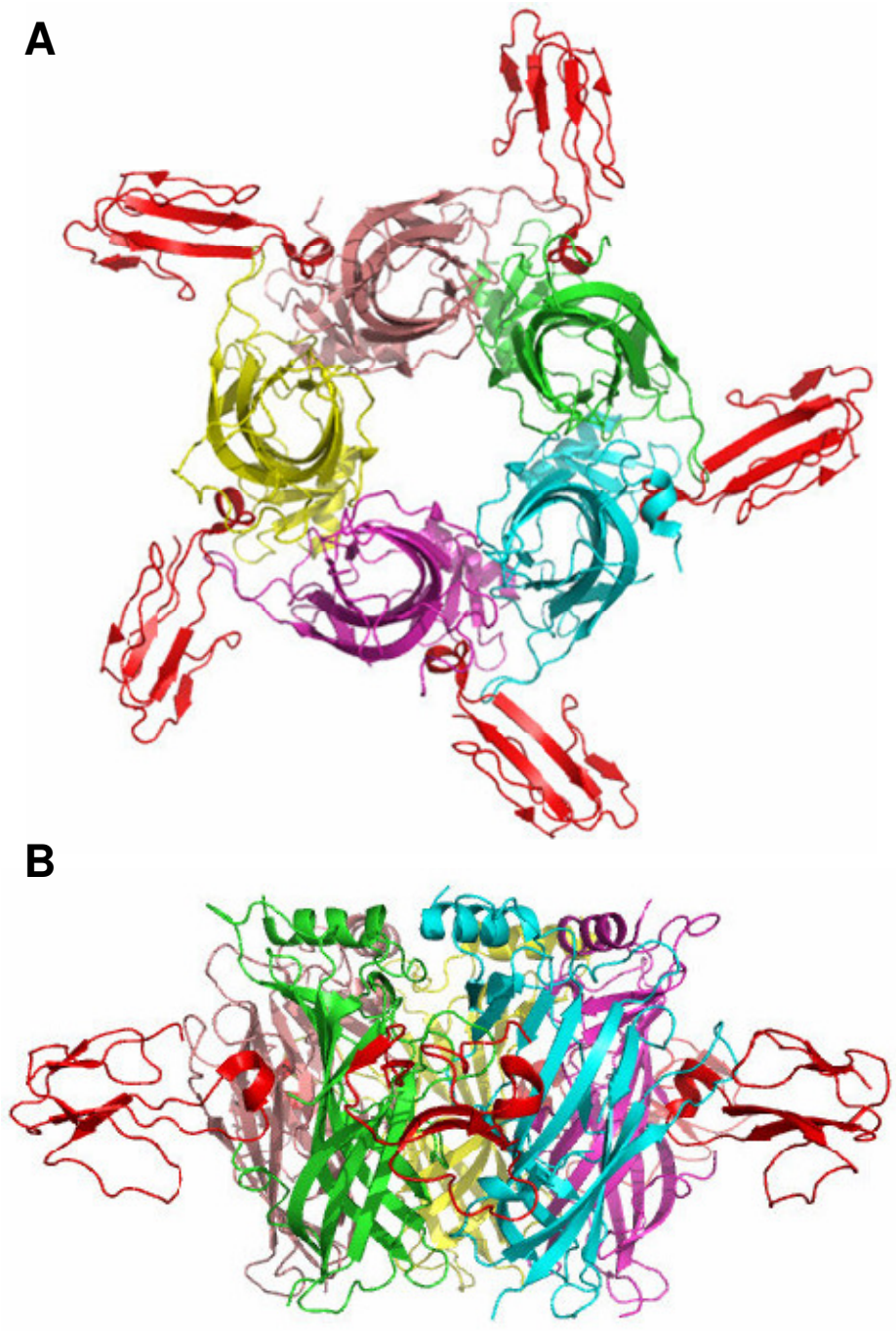

Figure 1.17: Three dimensional structure of the α-cobratoxin (Cbtx)-AChBP complex.

The 4.2 Å crystal structure of AChBP from *Lymnaea stagnalis* (1YI5) colored to show five subunits complex with Cbtx. The Cbtx molecule bound at this subunit interface is shown in red. The pentameric complex is viewed (A) along and (B) perpendicular to the AChBP five-fold axis. Figure was adapted from Bourne *et al*, (2005) and modified accordingly.

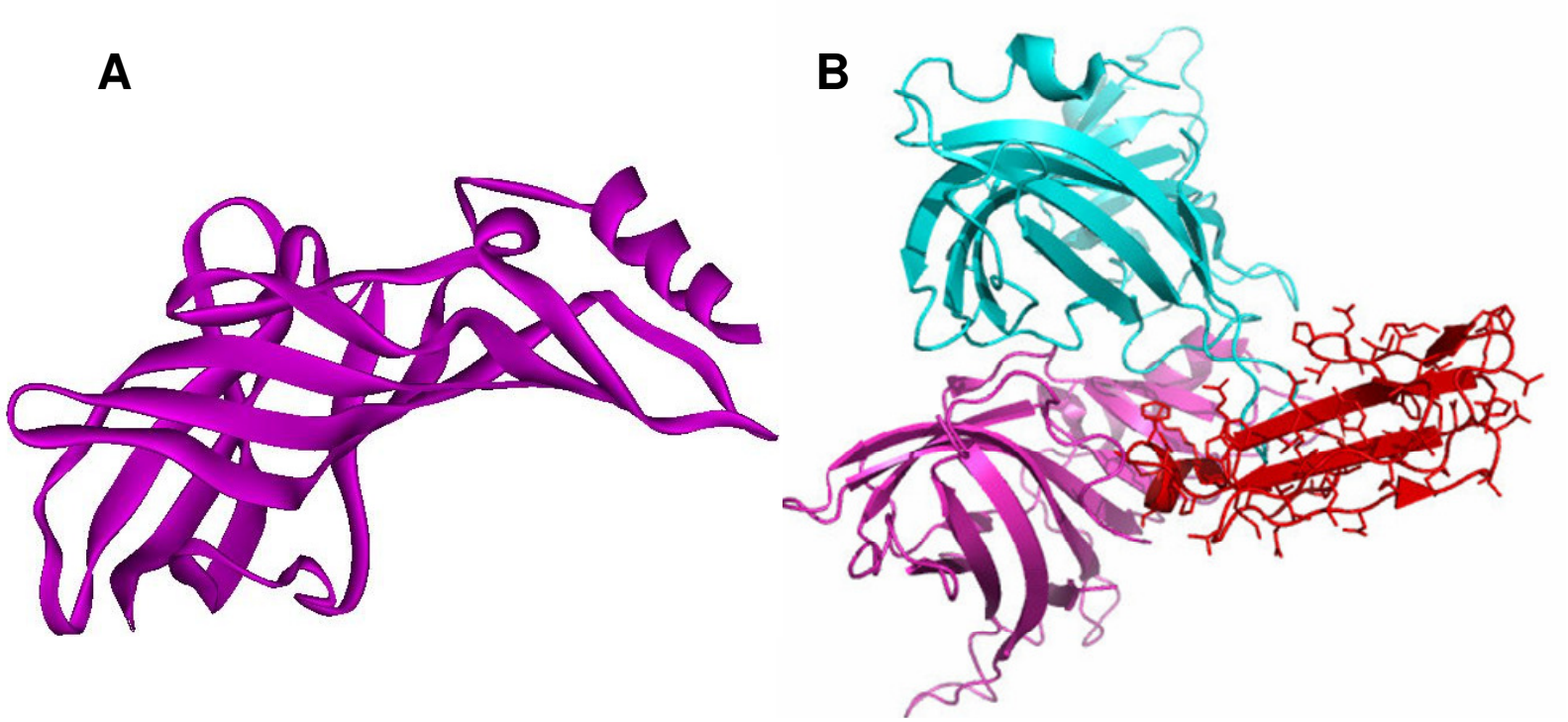

Figure 1.18: Close up view of a single AChBP subunit and the Cbtx molecule bound at this subunit interface (1YI5).

(A) A single subunit of AChBP (shown in magenta). The structural elements are predominantly β-sheet, except a small α-helical segment at the N-terminal, (B) AChBP subunits B (cyan) and C (magenta), which respectively contribute to the principal and the complementary faces of the interface and Cbtx molecule (red) bound at subunits interface. The residues involved in the complex formation for both the proteins are listed in Table 1.3.

Table 1.3: Intermolecular interactions between α-cobratoxin and AChBP (Bourne *et al*, 2005)

Cbtx[b]	AChBP subunit interface	
	Principal face (subunit A)	Complementary face (subunit B)
Loop I		
Thr6	**Thr184**	
Pro7 (Ala7)	Ser182, **Thr184**, Glu190, Ala191	
Ile9	Glu190	
Loop II		
Trp25		**Glu163**
Cys26–Cys30		Glu157, **Asp160**
Asp27	**Tyr185**	
Ala28		Lys34, Tyr164
Phe29	**Tyr185**, **Tyr192**	**Trp53**
Ser31		Gln55, Thr155
Ile32 (Ser35)		Gln55, Leu112, Met114
Arg33	Thr144, Cys187, **Tyr192**	Arg104
Gly34	Ser186	
Lys35	Ser186	
Arg36 (Val39)	**Tyr185**	
Val37	**Thr184**, Ser186	
C-terminus		
Phe65 (His68)	**Thr184**, Cys187, Pro189	
Arg68 (Gln71)	Ser186	

[a]Within a 4.5 Å distance between atoms from each partner in the complex.
[b]Residue substitutions in Bgtx are indicated in parentheses.
[c]Indicated in bold are those residues in Cbtx and in the α7 receptor (AChBP numbering) whose mutations cause an affinity decrease of more than five- and seven-fold, respectively (Fruchart-Gaillard *et al*, 2002).

the crystal structure of AChBP complexed with α-cobratoxin (Bourne *et al*, 2005) both beautiful and enlightening. It revealed that the toxin/ligand binding site is located in a cleft at a subunit interface (**Fig. 1.17** and **1.18**), formed by the series of loops from the principal face of one subunit (loops A, B and C) and another series of loops from the complementary face of an adjacent subunit (loops D, E and F). The residues involved in the interaction for both cobratoxin and AChBP is listed in table 1.3. The AChBP-toxin complex structure correlates well with affinity labelling and mutational binding studies to nAChRs (Fruchart- Gaillard *et al*. 2002; Karlin, 2002). Recently, many structures of AChBP complexes with various ligands and α-conotoxins have been solved (Celie *et al*, 2004; Hansen *et al*, 2005; Ulens *et al*, 2006), which are greatly contributing to the understanding of nAChR-ligand interactions.

1.11 Nicotinic acetylcholine receptors: Allosteric properties

Acetylcholine receptors are allosteric, in that they are oligomeric, contain multiple agonist-binding sites, and gates that interact at a distance (away from the ligand binging sites) through changes in the quaternary structure of the receptor (Karlin, 2002). Specifically, the binding of an agonist to the ligand-binding site of the receptor induces allosteric interactions between subunits, resulting numerous conformational transitions which lead to the rapid opening of the transmembrane cation channel and ultimate membrane depolarization followed by muscle contraction (reviewed in Changeux and Edelstein, 1998; 2001; Karlin, 2002). Three functional states have been described for nicotinic receptors, basal or resting (closed), active (open), or desensitized (closed) (Changeux and Edelstein, 1998). The resting state is the most stable state in the absence of agonist. The equilibrium between the various conformational states of nAChRs is affected by the presence of nicotinic ligands, which includes agonists, competitive

antagonists, and also the noncompetitive allosteric modulators. Indeed, the ligands will stabilize the states for which they display the highest affinity. In particular, agonists exhibit a higher affinity for the active (open) than for the basal (closed) state, therefore causing the opening of the channel. The continued presence of an agonist leads to receptor desensitization and ion channel closure. In the desensitized state, the receptor is refractory to activation although it displays higher affinity for agonist binding. In contrast, snake toxins block the receptor by stabilizing the basal (closed) state (Fruchart-Gaillard *et al*, 2002). Other competitive antagonists such as dTC also preferentially stabilize the receptor in the closed state, either the basal or desensitized configuration (Changeux and Edelstein, 1998).

1.12 The scope for nicotinic acetylcholine receptor ligands

Despite the growing library of the nicotinic ligands, there is still a lack of subtype-specific ligands, agonists and antagonists, especially directed towards the less abundant neuronal nicotinic receptor subtypes. Several ligands with this degree of specificity have been isolated from natural sources, animal venoms in particular. Starting from α-bungarotoxin which played a pivotal role in the early characterization of the acetylcholine receptor, till the wide variety of conotoxins with specificity for different interfaces of the receptor, venom peptides have provided some of the most useful molecular probes known to date. The discovery or design of more subtype-specific ligands will greatly facilitate the elucidation of the physiological and pathological roles of the different neuronal subtypes and thereby discovering the therapeutic potential of individual neuronal receptors. Moreover, the venom peptides possess immense potential to provide the structural insights of the ligand binding domain of nicotinic receptors as provided by the cobratoxin-AChBP complex. Considering the enormous significance and

influence of nicotinic receptors on central and peripheral nervous system activities, the target-oriented search for venom peptides will no doubt continue.

1.13 Aim and scope of the thesis

Snake venoms have been a natural source of bioactive proteins. These molecules have long been useful in research as molecular probes to identify novel targets and in drug discovery as lead compounds to develop therapeutic molecules. Till date, many of the highly abundant venom proteins have been well-characterized, but the minor venom components are poorly understood. The usefulness of these molecules are not only restricted to their unique pharmacological properties, but also on the structural and functional characterization of these molecules. Understanding the structure-function relationship of these proteins will help us to explore its scientific potential in the pharmaceutical industry.

In search for novel toxins Rajagopalan *et al* (2007) has constructed a cDNA library from the venom gland of *O. hannah*. Few novel sequences were identified in the cDNA library, among them one, β-cardiotoxin, has been characterized (Rajagopalan *et al*, 2007) with novel β-adrenergic receptor blocking activity. The current study was aimed to isolate and characterize another novel protein from cDNA library of the venom gland of *O. hannah*. Specifically, the objectives of the study were:

1. To isolate and purify to homogeneity the protein of interest from the crude venom of *O. hannah*, confirm the identity and compare the homology of its primary structure to other three-finger toxins.

2. To carry out a detailed pharmacological characterization of the protein of interest in several isolated smooth muscle and skeletal muscle preparations

3. To investigate the effects of the protein on acetylcholine currents in oocyte expressed muscle ($\alpha\beta\gamma\delta$) and neuronal (α_7, $\alpha_3\beta_2$ and $\alpha_4\beta_2$) nicotinic acetylcholine receptors using electrophysiological techniques.

4. To investigate the existence of oligomeric species for the protein of interest in solution.

5. To solve the three-dimensional structure of the protein and to carry out a detailed structure-function analysis with respect to the homologous proteins from the same family.

6. To understand the structure-function relationship of the protein by co-crystallization and mutagenesis studies.

Chapter Two

Isolation and purification of haditoxin

CHAPTER TWO

Isolation and purification of haditoxin

2.1 INTRODUCTION

Snake venoms are a blend of bioactive proteins and polypeptides. More than 90% of the venom's dry weight constitutes of proteins. The venom from each snake is a complex mixture showing up to 200 different proteins and polypeptides (Harvey, 1991; Birrell *et* al, 2007) and this composition can vary depending on the evolutionary diversities. Approximately 20% of the total snake population in the world is venomous and their venoms form a goldmine of proteins and polypeptides for researchers. The venom components must achieve their effects at very low concentrations because of the minute amount of venom reaching the bloodstream during envenomation. Thus purification of these proteins to homogeneity from the crude snake venom is a redoubtable challenge for scientists. In the past, most research have focused on the isolation and characterization of the highly abundant or/and highly toxic proteins from venoms, but recently with more advanced and sophisticated proteomics tools, it is possible now to identify low-abundance venom proteins present in minute amounts (Kini, 2002; Rajagopalan *et al*, 2007; Omprova *et al*, 2010; Chatrath *et al*, 2011).

This chapter details the isolation and purification of haditoxin. Haditoxin was first identified as MTLP-3 homolog in the cDNA library of the venom gland tissue of *O. hannah* along with four other novel proteins (Rajagopalan *et al*, 2007). Liquid chromatography/mass spectrometry (LC/MS) studies of *O. hannah* venom done

previously in our lab (Pung *et al*, 2005) showed the presence of four (DQ902574, DQ902575, DQ902576 and AY354198) out of the five newly identified proteins in the venom. We describe a two step chromatographic approach for the isolation of these proteins from the crude venom of *O. hannah*. The procedure involved size exclusion chromatography as the initial step and reverse phase-high performance liquid chromatography (RP-HPLC) as the second step. Size exclusion chromatography which is also known as gel filtration chromatography separates the protein based on their molecular size. The porous gel matrix acts as a molecular sieve which allows different degrees of access to the analyte molecules (smaller molecules have greater access and larger molecules less). This method is widely used as an initial step for venom protein purification because of its simple and mild nature. As this method offers group separation that is the components of a sample are separated into two/more major groups according to the size, so it is generally combined with other chromatographic techniques. For example, in the case of several elapid venoms gel filtration offers a separation of three major groups, >40 kDa (mainly enzymes), 11-25 kDa (phospholipases, ohanin etc.) and 6-8 kDa (three-finger toxins, proteinase inhibitors, etc.). Therefore, during the purification of haditoxin, we have used RP-HPLC as a second step of purification where the proteins are separated based on their hydrophobicity. RP-HPLC is not extensively used for protein purification because of the use of higher concentration of organic solvents in mobile phase which can cause protein denaturation with loss of activity. Fortunately, the robust disulfide-linked three-finger fold of the 3FTXs makes them fairly resistant to denaturation. Also, this highly robust fold allows the purification procedure to be carried out at

room temperature instead of 4 °C, because of the resistance of 3FTXs to thermal degradation due to proteolysis. Use of RP-HPLC as a final step also allows us to purify the protein in a desalted form, ready to be lyophilized.

The lyophilized purified protein was subjected to N-terminal sequencing by Edman degradation to confirm its identity. It is also vital to ensure that the purified protein does not contain any contaminants that could mask and/or interfere in its biological activity. Therefore, the homogeneity of the purified protein was confirmed by capillary electrophoresis where separation is based on the size to charge ratio of the analytes. Capillary electrophoresis offers an accurate estimation of the homogeneity because of its high sensitivity and resolution. Circular dichroism (CD) was used to determine the secondary structure of the purified protein. CD spectroscopy measures differences in the absorption of left-handed polarized light versus right-handed polarized light which arise due to structural asymmetry such as- α-helix or β-sheet in proteins.

2.2 MATERIALS AND METHODS

2.2.1 Materials

Lyophilized *O. hannah* venom was obtained from PT Venom Indo Persada (Jakarta, Indonesia) and Kentucky Reptile Zoo (Slade, KY, USA). Reagents for N-terminal sequencing by Edman degradation are from Applied Biosystems (Foster City, CA, USA). Acetonitrile (ACN) and trifluoroacetic acid (TFA) were from Merck KGaA, Darmstadt, Germany. Superdex 30 Hiload (16/60) column and Jupiter C18 (5 µ, 300 Å, 4.6 mm x 250 mm) were purchased from GE Healthcare Life Sciences (Piscataway, NJ, USA) and Phenomenex (Torrance, CA, USA) respectively. All the reagents were of the highest purity grade. Water was purified using a MilliQ system (Millipore, Billerica, MA, USA).

2.2.2 Sequence Analysis

Sequence analysis was carried out using the BLAST program against the non-redundant database of NCBI (www.ncbi.nlm.nih.gov) and ExPASy proteomics tools (www.expasy.ch). Sequence alignments were carried out using the online server ClustalW (www.ebi.ac.uk) followed by manual adjustments to obtain the best possible alignment.

2.2.3 Protein purification from crude venom

Haditoxin was purified from the venom of *O. hannah* crude venom using a two-step chromatographic approach. Crude venom (100 mg) was dissolved in 1 ml of deionized water, centrifuged at 14,000 rpm for 15 min and the supernantant was filtered through a 0.45 µm syringe filter. The filtrate was loaded onto a Superdex

30 (1.6 x 60 cm) gel filtration column, equilibrated with 50 mM Tris-hydrochloride (HCl) buffer; pH 7.4 and eluted with the same buffer at a flow rate of 1 ml/min using an ÄKTA purifier system (GE Healthcare Life Sciences, Piscataway, NJ, USA) and fractions of 2 ml were collected. Pooled fractions containing the toxin of interest were further sub-fractionated by reverse phase-high performance liquid chromatography (RP-HPLC) using a Jupiter C18 column, equilibrated with 0.1% (v/v) TFA and eluted with a linear gradient of 80% (v/v) ACN in 0.1% (v/v) TFA at 1 ml/min flow rate. Elution was monitored at 280 and 215 nm. Fractions were directly injected into an API-300 LC/MS/MS system (PerkinElmer Life Sciences, Wellesley, MA, USA) to determine the mass and homogeneity of the protein. Fractions showing the expected molecular mass were pooled and lyophilized.

2.2.4 Molecular mass determination

The mass and homogeneity of the novel proteins were determined by electrospray ionization mass spectrometry (ESI-MS) using an API-300 liquid chromatography/tandem mass spectrometry system (PerkinElmer Life Sciences,Wellesley, MA, USA). RP-HPLC fractions were directly used for the analysis. Ion spray, orifice, and ring voltages were set at 4600, 50, and 350 V, respectively. Nitrogen was used as the nebulizer and curtain gas. A Shimadzu LC-10AD pump was used for solvent delivery (50% acetonitrile in 0.1% formic acid) at a flow rate of 40 µl/min. Data was acquired in a positive ion mode. Nitrogen was used as curtain gas with a flow rate of 0.6 L/min and as nebulizer gas with a pressure setting of 100 psi. Full scan data were acquired over the ion range from

1000 to 2000 m/z with step size of 0.1 Da. Analyte software (PerkinElmer Life Sciences, Wellesley, MA, USA) was used to analyze and deconvolute the raw mass data.

2.2.5 N-terminal sequencing

N-terminal sequencing of the native protein was performed by automated Edman degradation using a Procise 494 pulsed-liquid-phase protein sequencer (Applied Biosystems, Foster City, CA, USA) with an on-line 785A phenylthiohydantion (PTH)-derivative analyzer. The PTH amino acids were sequentially identified by mapping the respective separation profiles with the standard chromatogram.

2.2.6 Capillary electrophoresis

Capillary electrophoresis was performed on a BioFocus3000 system (Bio-Rad, Hercules, CA, USA) to determine the homogeneity of the protein after RP-HPLC. The native protein (1 µg/µl) was injected to a 25 µm x 17 cm coated capillary using a pressure mode (5 p.s.i./s) and run in 0.1 M phosphate buffer (pH 2.5) under 18 kV at 20 °C for 20 min. The migration was monitored at 200 nm.

2.2.7 CD spectroscopy

Far-UV CD spectra (260 - 190 nm) were recorded using a Jasco J-810 spectropolarimeter (Jasco Corporation, Tokyo, Japan). All measurements were carried out at room temperature using a 0.1 cm path length capped cuvette. The instrument optics and cuvette chamber were continuously flushed with 10 L of nitrogen/min before and during the recording of the spectra to provide an oxygen-

free environment. The spectra were recorded using a scanning speed of 50 nm/min, a resolution of 0.1 nm and a bandwidth of 1 nm. A total of three scans were recorded and averaged for each spectrum, and the baseline was subtracted with the blank. All samples were dissolved in deionized water.

2.3 RESULTS

2.3.1 Isolation and purification of haditoxin

The LC/MS profile of *O. hannah* venom (Pung *et al*, 2005) showed the presence of a 7,535.67 ± 0.60 Da protein (Appendix figure), similar to the calculated molecular weight of MTLP-3 homolog identified in the cDNA library of the venom gland tissue of *O. hannah*. Following this calculated mass the protein was purified from the crude snake venom using different chromatographic techniques. We used a two-step chromatographic approach, where the first step comprised of separating the venom components based on their sizes into five peaks using gel filtration chromatography (**Fig. 2.1**). Based on the calibration curve most of the 6-8 kDa protein elutes out in peak 3. Thus, we fractionated peak 3 using RP-HPLC and analyzed the mass of each fraction using ESI-MS. Unfortunately, we were unable to find a mass matching to that of the observed one in LC/MS profile. Subsequently, each peak of gel filtration chromatography was fractionated by RP-HPLC. The fractions were analyzed by ESI-MS to determine the mass and hence the tentative identification of the protein. One of the RP-HPLC fractions of peak 2 (marked by a black bar in **Fig. 2.1**) showed a molecular weight similar to that of the LC/MS profile. Further, the fractions containing peak 2 were pooled and separated by RP-HPLC (**Fig. 2.2**). The mass spectra of fraction 2a (indicated by a black arrow in **Fig. 2.2**) showed a molecular weight of 7535.88 ± 0.64 Da. It was observed that this protein eluted earlier in gel filtration chromatography compared to other 3FTXs (**Fig. 2.1**, most of the 3FTXs elutes in peak 3). This led us to investigate the oligomeric states of this protein and it was found to be a homodimer

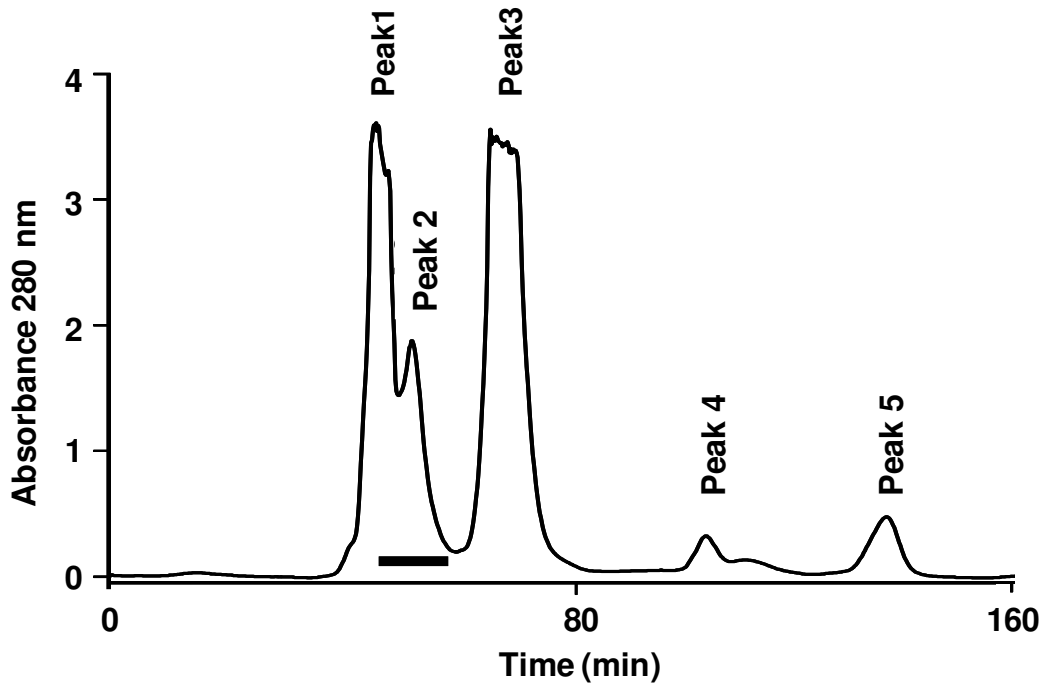

Figure 2.1: Gel filtration chromatogram of *O. hannah* crude venom.

Crude venom (100 mg/ml) was fractionated using a Superdex 30 Hiload (16/60) column. Column was pre-equilibrated with 50 mM Tris-HCl buffer (pH 7.4). Proteins were eluted at a flow rate of 1 ml/min using the same buffer. A black bar at peak 2 indicates the fractions containing haditoxin which were pooled and further subjected to RP-HPLC. The elution of the proteins was monitored at 280 nm.

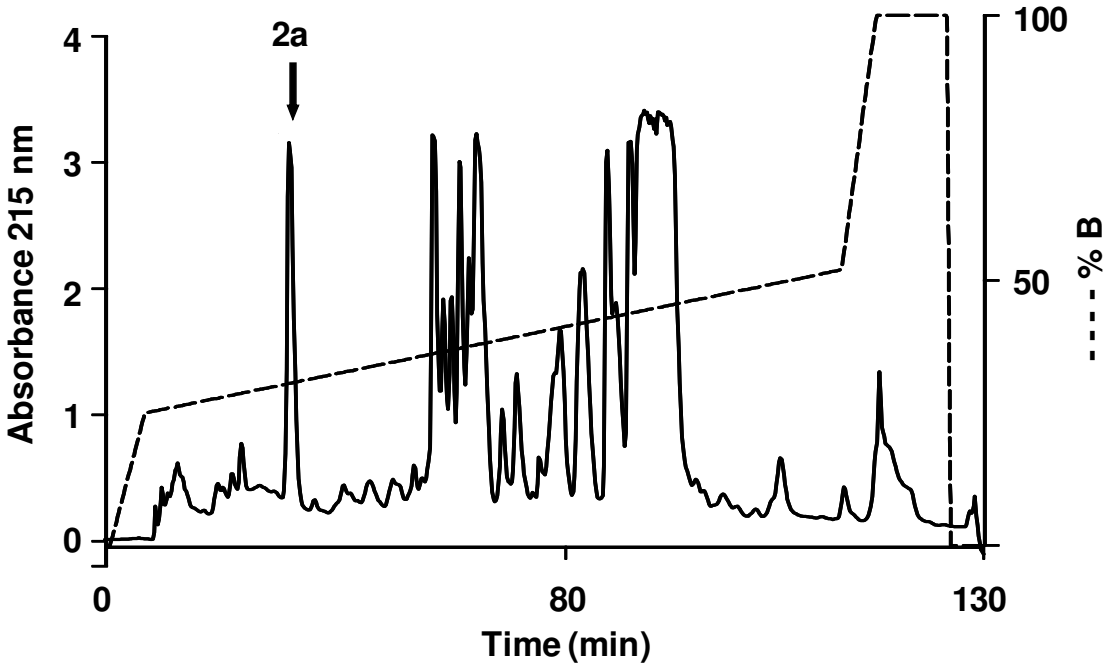

Figure 2.2: RP-HPLC profile of peak 2 from gel filtration chromatography. Fractions containing haditoxin of peak 2 from gel filtration chromatography was subjected to RP-HPLC using a Jupiter C18 (5 µ, 300 Å, 4.5 x 250 mm) analytical column was equilibrated with aqueous 0.1% (v/v) TFA (buffer A). Protein of interest was eluted from the column with a flow rate of 1 ml/min with a gradient of 23-49% (over a time period of about 90 minutes) buffer B (80% acetonitrile in 0.1% TFA). The dotted line (- - -) indicates the gradient of the buffer B. Downward arrow at peak 2a indicates fractions containing haditoxin. Elution of protein was monitored at 215 nm.

(discussed in chapter 4). Hence, the protein of interest was renamed as haditoxin (O. hannah dimeric toxin) following the nomenclature of dimeric 3FTXs (Pawlak *et al*, 2006; Pawlak *et al*, 2009).

2.3.2 Identification of haditoxin

The ESI-MS of fraction 2a (indicated by a black arrow in **Fig. 2.2**) showed three peaks with mass/charge (m/z) ratios ranging from +4 to +6 charges (**Fig. 2.3**), and the final reconstructed mass spectrum showed a molecular weight of 7535.67 ± 1.25 Da, which corresponds well with the calculated mass of 7534.42 Da (**Fig. 2.4**). The ESI-MS spectrum also revealed the purity of haditoxin (**Fig. 2.4**). N-terminal Edman degradation sequencing of the first 36 residues of the pure haditoxin matched with the cDNA sequence of MTLP-3 homolog (**Fig. 2.5**) thus confirming the identity of the protein.

2.3.3 Assessment of homogeneity of haditoxin

In order to ensure the uniformity haditoxin was subjected to capillary electrophoresis. Haditoxin eluted out as a single peak at about 13 min. The presence of a single peak in the electropherogram (**Fig. 2.6**) indicated the homogeneity of the protein, ensuring the absence of contaminants, especially other α-neurotoxin(s), cytotoxins and enzymatic proteins such as- phospholipases (because haditoxin eluted out in peak 2 in **Fig 2.1** together with phopholipases) present in the venom. This also confirmed the purity of the protein.

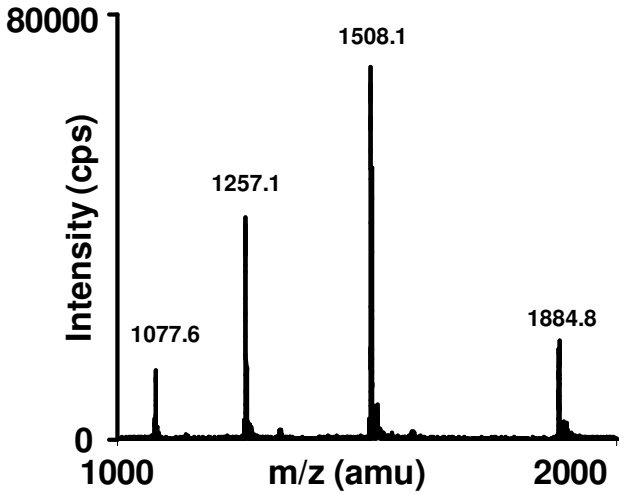

Figure 2.3: ESI-MS spectrum of the RP-HPLC fraction 2a.

RP-HPLC fraction containing haditoxin was subjected to ESI-MS using an API-300 liquid chromatography/tandem mass spectrometry system. The spectrum shows a series of multiply charged ions, corresponding to a single, homogenous peptide with a molecular weight of 7535.88 Da.

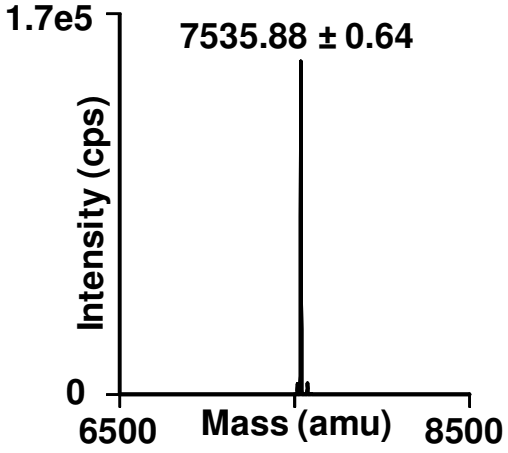

Figure 2.4: Reconstructed ESI-MS spectrum of haditoxin.

CPS = counts/s; amu = atomic mass units.

```
cDNA clone:     TKCYNHQSTTPETTEICPDSGYFCYKSSWIDGREGRIERGCTFTCPELTPNGKYVYCCRRDKCNQ   65
Pure haditoxin: TKXYNHQSTTPETTEIXPDSGYFXYKSSWIDGREGR----------------------------
```

Figure 2.5: N-terminal sequencing of haditoxin.

Purified haditoxin was subjected to N-terminal Edman degradation sequencing using a Procise 494 pulsed-liquid-phase protein sequencer. The first 36 residues of the purified protein matched with the sequence of the cDNA clone.

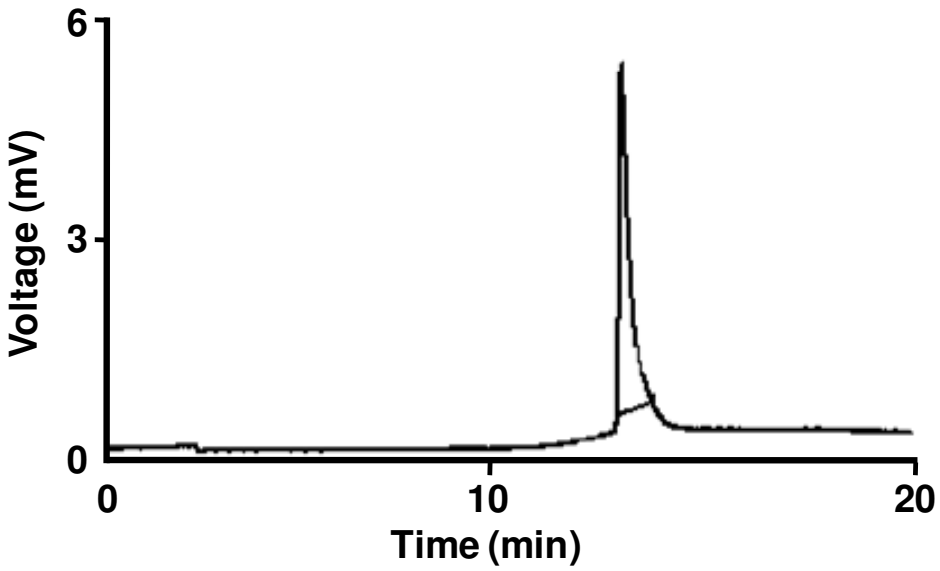

Figure 2.6: Capillary electropherogram of haditoxin.

Capillary electrophoresis of purified haditoxin was performed on a BioFocus3000 system. The sample was injected using pressure mode 5 p.s.i./s, and electrophoresis runs were carried out using a coated capillary (17 cm x 25 µm) at 18 kV, with 0.1 M phosphate buffer (pH 2.5) at 20 °C for 20 min. Migration was monitored at 200 nm.

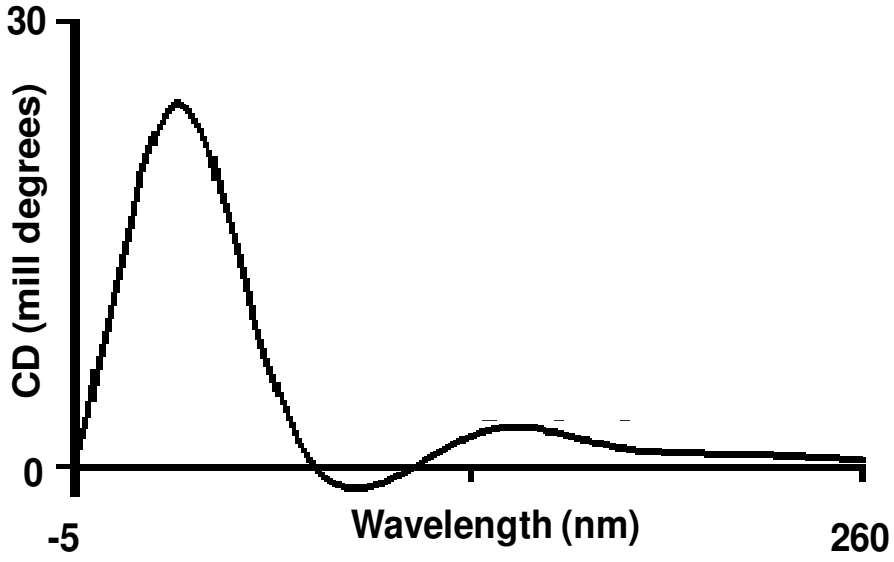

Figure 2.7: Circular dichroism spectrum of haditoxin.

Far-UV CD spectrum of purified haditoxin. The protein was dissolved in deionised water (0.5 mg/ml), and their CD spectra were recorded using a 0.1 cm path-length cuvette at room temperature in a Jasco J-810 spectropolarimeter.

2.3.4 Secondary structure analysis of haditoxin

The secondary structural elements of haditoxin were analyzed using far-UV CD spectroscopy. The spectrum shows maxima at 230 nm and 198-200 nm and a minimum at 215 nm (**Fig. 2.7**). Thus haditoxin was found to be composed of β-sheeted structure similar to all other 3FTXs (Harvey, 1991; de Weille *et al*, 1991; Servent *et al*, 2000).

2.4 DISCUSSION

Snake envenomation is a socio-medical problem of considerable magnitude. Annually about 2.5 million people are bitten by snakes, more than 100,000 fatally. However, although bites can be deadly, snake venom is a natural biological resource that contains several components of potential therapeutic value. Since ages, venom has been used in the treatment of a variety of pathophysiological condition in Ayurveda, homeopathy and folk medicine (Koh *et al*, 2006; Calvete, 2009). With the advancement of proteomics and genomics, the efficacy of such treatments has been substantiated by isolating and purifying components of venom and delineating their therapeutic properties for further applications in pharmaceuticals and basic research.

Five novel toxin sequences have been identified in the cDNA library from the venom gland tissue of *O. hannah* (Rajagopalan *et al*, 2007) (Appendix figure). The cysteine arrangement of all these novel sequences led us to the conclusion that all of them belong to the 3FTX family of snake venom non-enzymatic proteins. One of them, named β-cardiotoxin, has been characterized previously (Rajagopalan *et al*, 2007). Here, the purification and characterization of the second novel toxin, haditoxin, (identified previously as MTLP-3 homolog based on sequence homology (Rajagopalan *et al*, 2007) (**Fig. 2.9**) is described.

Haditoxin consists of a single polypeptide chain of 65 amino acids and four disulfide bridges. The disulfide scaffold of haditoxin as a result of cysteine pairing revealed that the protein belongs to the 3FTX family of snake venom proteins. Accordingly, it was found that haditoxin shares about 37-57% of similarity (**Fig. 2.8**) with other 3FTXs. The eight cysteines, forming the four conserved disulfide

bridges, common to all the 3FTXs contribute substantially (approximately 12%) to this homology. The loop regions in between the disulfide bridges are indicated by black lines. Haditoxin showed high similarity (80-83%) with muscarinic toxin like proteins (MTLP and MTLP-3) and neurotoxin homolog (NL1) (**Fig. 2.9**). All of the three proteins (MTLP, MTLP-3 and NL1) are known as muscarinic toxin homologs based on their sequence homology with muscarinic toxins. However, there is no available literature describing the molecular target and mechanism of action of these homologs. Since, we compared the sequence of haditoxin with that of the muscarinic toxins (MT-α, MT1 and MT3) and their homologs, (MTLP-1 and MTLP-2) (**Fig. 2.10**) for which the molecular target is known (Kukhtina *et al*, 2000; Servant and Fruchart-Gaillard, 2009), and haditoxin was found to share only about 51-54% similarity. Therefore, with an expectation to find out the novel characteristics of haditoxin we purified the protein from the crude venom of *O. hannah* and examined its pharmacological properties.

We have isolated and purified haditoxin using a two-step chromatographic approach from the crude venom of *O. hannah*. In gel filtration chromatography, haditoxin eluted in peak 2 (**Fig. 2.1**) together with higher molecular weight proteins like- phospholipases, ohanin and opharin (molecular weight range of ~ 11-25 kDa). This might be due to the existence of these molecules in multimeric states or the formation of complexes with any of the other larger molecules that elute in the same fraction which demands further investigation. Such interactions could be functionally important which led us to further characterize haditoxin structurally (discussed in chapter 4). The gel filtration fractions were further purified to homogeneity using reverse phase chromatography (**Fig. 2.2**).

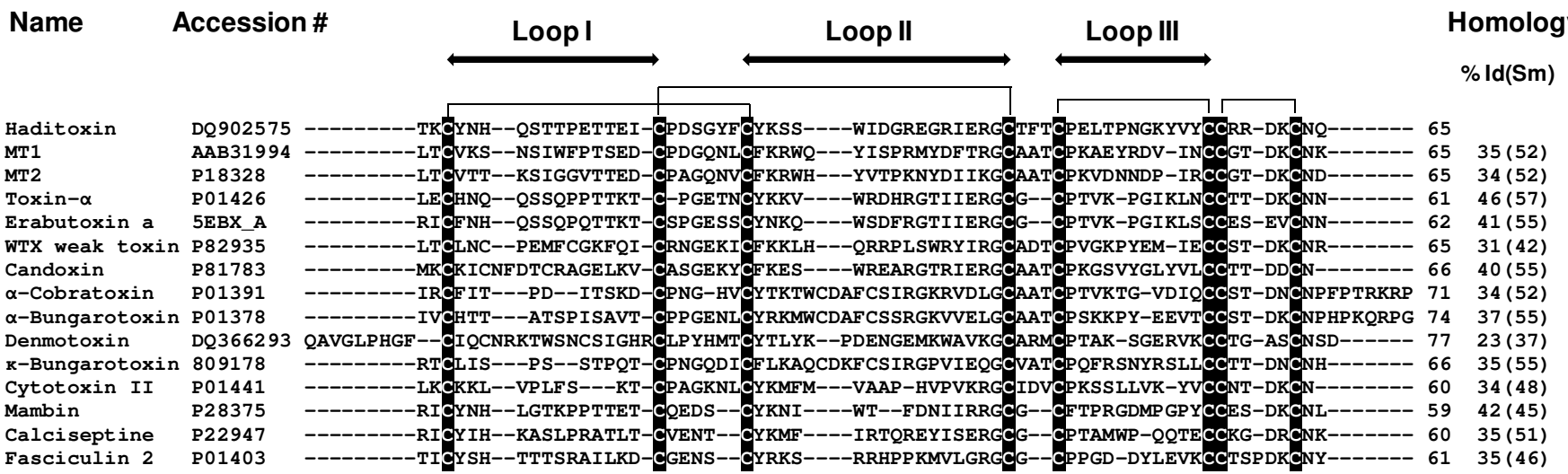

Figure 2.8: Comparison of the amino acid sequence of haditoxin with the sequences of other three-finger toxins.
The number of amino acid residues in each sequence is indicated at the end of the respective sequence. The homology of each of the sequence in (%Id) identity and homology or similarity (Sm) with the sequence of haditoxin is also mentioned. The conserved eight cysteine residues are highlighted in black and the disulfide linkages are shown by black lines. The black arrows indicate the segments contributing to the three loops. The accession number is also stated for each toxin. The source organisms for each of the toxin are as follows- Haditoxin (*Ophiophagus hannah*); MT 1, Muscarinic toxin 1 (*Dendroaspis angusticeps*); MT 2, Muscarinic toxin 2 (*Dendroaspis angusticeps*); Toxin-α (*Naja nigricollis*); Erabutoxin-α (); WTX weak toxin (*Naja kaouthia*); Candoxin (*Bungarus candidus*); α-Cobratoxin (*Naja kaouthia*); α-Bungarotoxin (*Bungarus multicinctus*); Denmotoxin (*Bioga dendrophila*); κ-Bungarotoxin (*Bungarus multicinctus*); Cytotoxin II (*Naja oxiana*); Mambin (*Dendroaspis jamesoni*); Calciseptine (*Dendroaspis polylepis*) and Fasciculin 2 (*Dendroaspis angusticeps*).

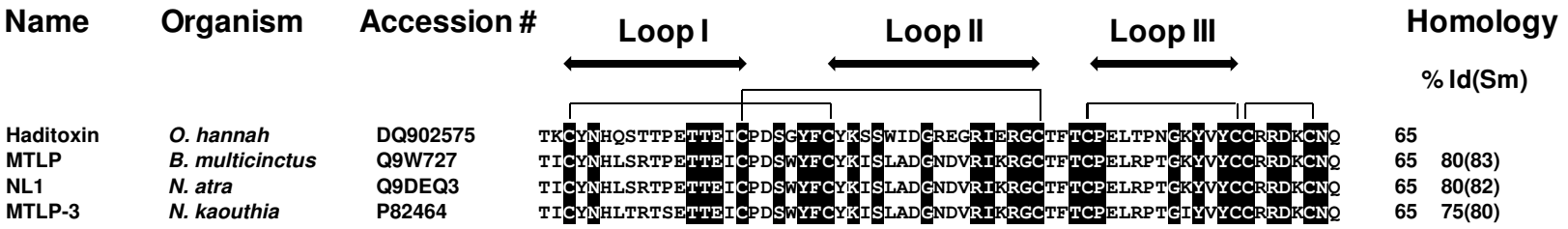

Figure 2.9: Sequence alignment of haditoxin with the most homologous sequences of other three-finger toxins.
The number of amino acid residues in each sequence is indicated at the end of the respective sequence. The homology of each of the sequence in (%Id) identity and homology or similarity (Sm) with the sequence of haditoxin is also mentioned. The conserved eight cysteine residues are highlighted in black and the disulfide linkages are shown by black lines. The black arrows indicate the segments contributing to the three loops. The identical residues among the sequences have been highlighted in black. The accession number and the source organism are also stated for each toxin. The names of the toxins are as follows- MTLP (Muscarinic toxin like protein), NL1 (Neurotoxin like protein 1) and MTLP-3 (Muscarinic toxin like protein-3).

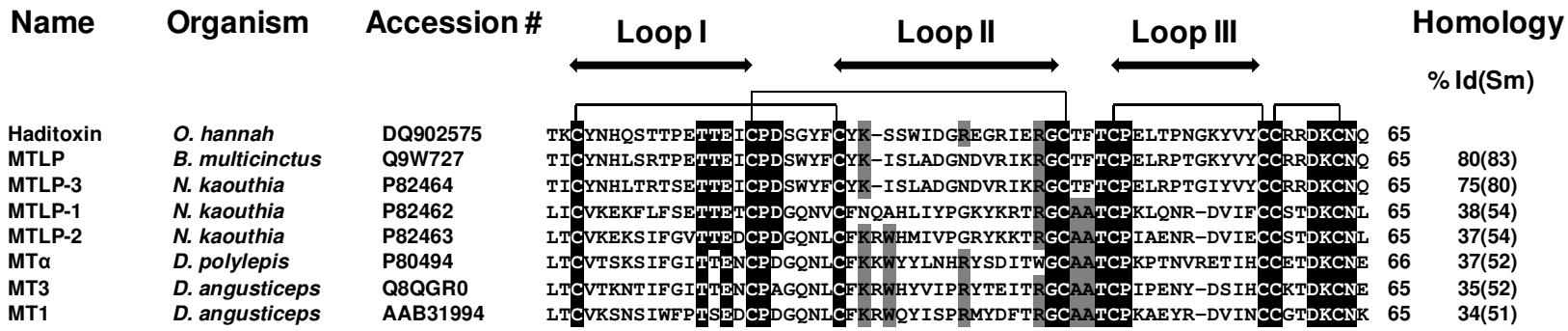

Figure 2.10: Sequence alignment of haditoxin with the sequences of muscarinic toxins and their homologs.
The number of amino acid residues in each sequence is indicated at the end of the respective sequence. The homology of each of the sequence in (%Id) identity and homology or similarity (Sm) with the sequence of haditoxin is also mentioned. The conserved eight cysteine residues are highlighted in black and the disulfide linkages are shown by black lines. The black arrows indicate the segments contributing to the three loops. The identical residues among the sequences have been highlighted in black and the homologous residues are highlighted in grey. The accession number and source organisms are also stated for each toxin. The names of the toxins are as follows- MTLP (Muscarinic toxin like protein), MTLP-3 (Muscarinic toxin like protein-3), MTLP-1 (Muscarinic toxin like protein-1), MTLP-2 (Muscarinic toxin like protein-2), MTα (Muscarinic toxin α), MT3 (Muscarinic toxin 3) and MT1 (Muscarinic toxin 1).

The homogeneity and purity of the isolated protein were confirmed using ESI-MS (**Fig. 2.3**) and capillary electrophoresis (**Fig. 2.6**). Further, the identity was confirmed by N-terminal Edman degradation sequencing (**Fig. 2.5**). The purified protein consists of predominantly β-sheeted secondary structure like all other 3FTXs.

To evaluate the muscarinic effects of haditoxin we examined its effect on *ex vivo* smooth muscle preparations, the rat ileum and rat anococcygeus muscle, pharmacologically characterized to represent mAChRs. As observed, in both preparations the protein had no effect (discussed in chapter 3). The highly conserved sequences among different mamba muscarinic toxins include eight cysteine residues, the LTCV and TDKCN N- and C-terminal motifs, and the GQN(L/V)CFK sequence in the region connecting loops I and II (for a review see, Servant and Fruchart-Gaillard, 2009). Haditoxin possesses all the eight cysteine residues together with the DKCN motif in the C-terminal but the N-terminal LTCV is replaced with TKCY and the inter-loop GQN(L/V)CFK is replaced by SGY(F)CYK (**Fig. 2.11**). Altogether, except for the eight cysteine residues (these are conserved for all 3FTXs) haditoxin reserves only the C-terminal motif of the conserved sequences of the muscarinic toxins. It also lacks the critical residues (Arg34, Met35, Tyr36 and Phe38) responsible for the interaction of toxins with the muscarinic receptors. Therefore, it is likely that the observed sequence similarity of haditoxin with muscarinic toxin homologs is probably coincidental due to either phylogeny or structure, including the presence of the core disulfide bridges, and not the function. This merits further investigation, hence we performed *in vivo* toxicity studies with the protein. Typical peripheral neurotoxic

symptoms were observed in the in vivo toxicity studies (discussed in chapter 3) which directed us to the sequence comparison of haditoxin with that of the snake venom α-neurotoxins.

Thus, a sequence comparison of haditoxin to other snake neurotoxins, including short-chain α-neurotoxin, long-chain α-neurotoxins and non-conventional neurotoxins, was conducted (**Fig**. **2.12-2.14**). The observed sequence similarity with short-chain neurotoxins was about 54-60% (**Fig. 2.12**), with long-chain neurotoxins was about 52-57% (**Fig. 2.13**) and with that of the non-conventional toxins was 42-55% (**Fig. 2.14**). Despite of the low sequence identity, it was observed that some of critical residues involved in the recognition of nicotinic acetylcholine receptor (nAChRs) by snake neurotoxins were conserved in haditoxin (Trp29, Asp31 and Arg33). This led us to the investigation of neuromuscular blockade properties of haditoxin on *ex vivo* organ-bath experiments using nerve-skeletal muscle preparations (rat hemidiaphragm muscle and chick biventer cervicis muscle). Potent neuromuscular blockade was observed with haditoxin which was partially reversible on chick muscle whereas irreversible on rat muscle (discussed in chapter 3). Therefore, we had also compared the sequence of haditoxin to the snake venom neurotoxin and neurotoxin homologs which is reported to produce either reversible or partially reversible neuromuscular blockade. These include neurotoxins such as- psedonajatoxin b (*Psedonaja textilis*), LSIII (*Laticauda semifasciata*) and fasciatoxin (*Bungarus fasciatus*) as well neurotoxin homologs, such as- CM10 and CM12 (*Naja haje annulifera*) and S5C10 (*Dendroaspis sp.*). However,

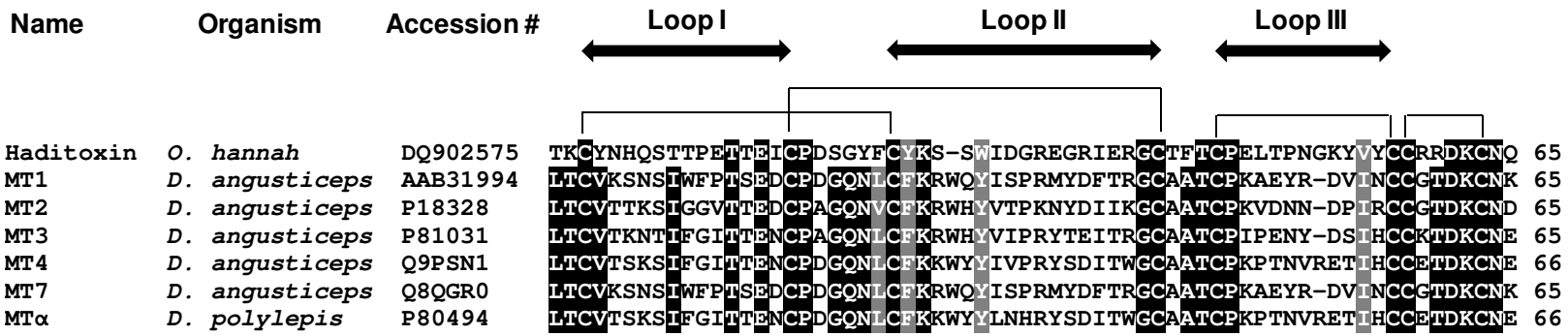

Consensus sequence

LTCV----I---T-E-CP-GQN-CFK---Y----------GC-ATCP-------I-CC-TDKCN-

Figure 2.11: Comparison of the amino acid sequence of haditoxin with the conserved sequences of muscarinic toxins.
The number of amino acid residues in each sequence is indicated at the end of the respective sequence. The highly conserved sequences (Consensus sequence) among different muscarinic toxins are highlighted in black (identical residues) and grey (homologous residues). The conserved eight cysteine residues are highlighted in black and the disulfide linkages are shown by black lines. The black arrows indicate the segments contributing to the three loops. The accession number and source organisms are also stated for each toxin. The names of the toxins are as follows- MT1 (Muscarinic toxin 1), MT2 (Muscarinic toxin 2), MT3 (Muscarinic toxin 3), MT4 (Muscarinic toxin 4), MT7 (Muscarinic toxin 7) and MTα (Muscarinic toxin α).

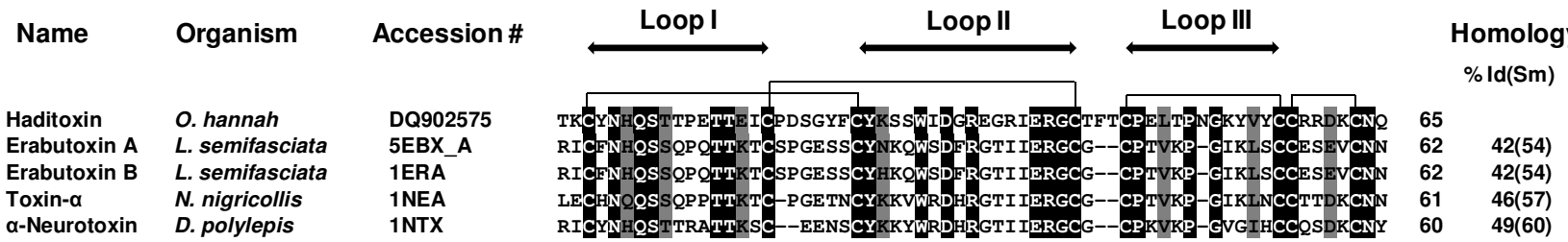

Figure 2.12: Sequence alignment of haditoxin with the sequences of short-chain α-neurotoxins.
The number of amino acid residues in each sequence is indicated at the end of the respective sequence. The homology of each of the sequence in (%Id) identity and homology or similarity (Sm) with the sequence of haditoxin is also mentioned. The conserved eight cysteine residues are highlighted in black and the disulfide linkages are shown by black lines. The black arrows indicate the segments contributing to the three loops. The identical residues among the sequences have been highlighted in black and the homologous residues are highlighted in grey. The accession number and source organisms are also stated for each toxin.

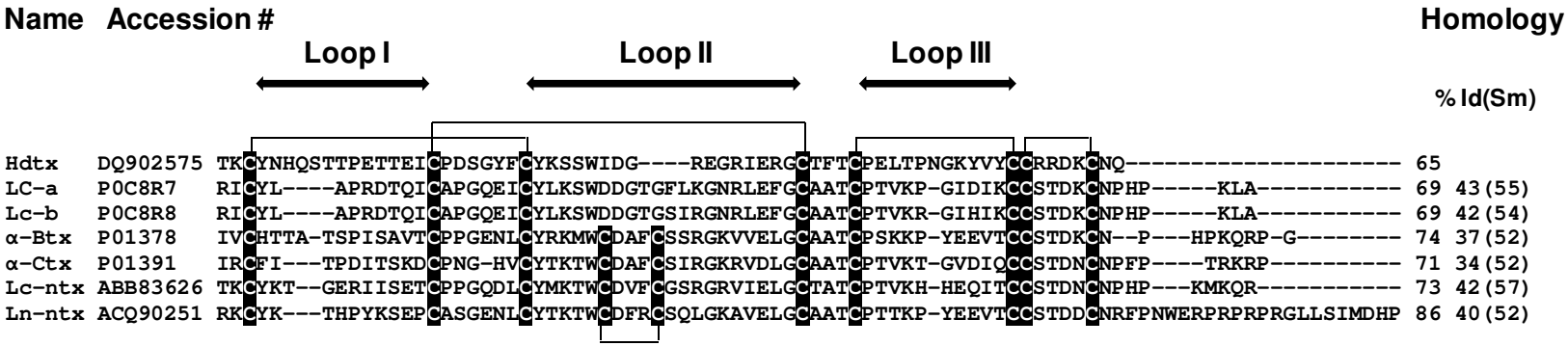

Figure 2.13: Sequence alignment of haditoxin with the sequences of long-chain α-neurotoxins.
The number of amino acid residues in each sequence is indicated at the end of the respective sequence. The homology of each of the sequence in (%Id) identity and homology or similarity (Sm) with the sequence of haditoxin is also mentioned. The conserved cysteine residues are highlighted in black and the disulfide linkages are shown by black lines. The black arrows indicate the segments contributing to the three loops. The accession number is also stated for each toxin. The source organisms for each of the toxin are as follows- Hdtx, Haditoxin (*Ophiophagus hannah*); Lc-a (*Laticauda colubrina*); Lc-b (*Laticauda colubrina*); α-Btx, α-Bungarotoxin (*Bungarus multicinctus*); α-Ctx, α-Cobratoxin (*Naja kaouthia*); Lc-ntx, Long-chain neurotoxin (*Ophiophagus hannah*) and Ln-ntx, Long neurotoxin (*Drysdalia coronoides*).

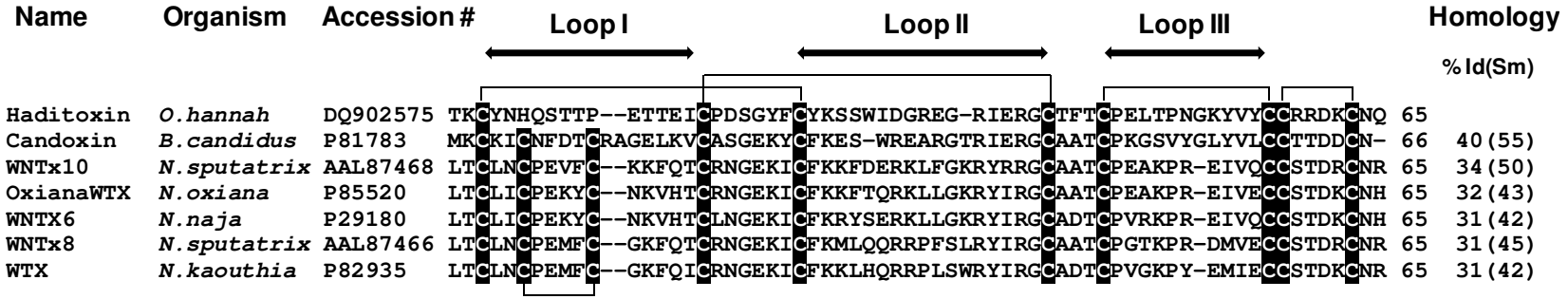

Figure 2.14: Sequence alignment of haditoxin with the sequences of non-conventional neurotoxins.
The number of amino acid residues in each sequence is indicated at the end of the respective sequence. The homology of each of the sequence in (%Id) identity and homology or similarity (Sm) with the sequence of haditoxin is also mentioned. The conserved cysteine residues are highlighted in black and the disulfide linkages are shown by black lines. The black arrows indicate the segments contributing to the three loops. The accession number and source organism are also stated for each toxin. The name of the toxins are as follows- Weak neurotoxin 10 (WNTx10), Oxiana weak toxin (OxianaWTx), Weak neurotoxin 6 (WNTx6), Weak neurotoxin 8 (WNTx8) and Weak toxin (WTX).

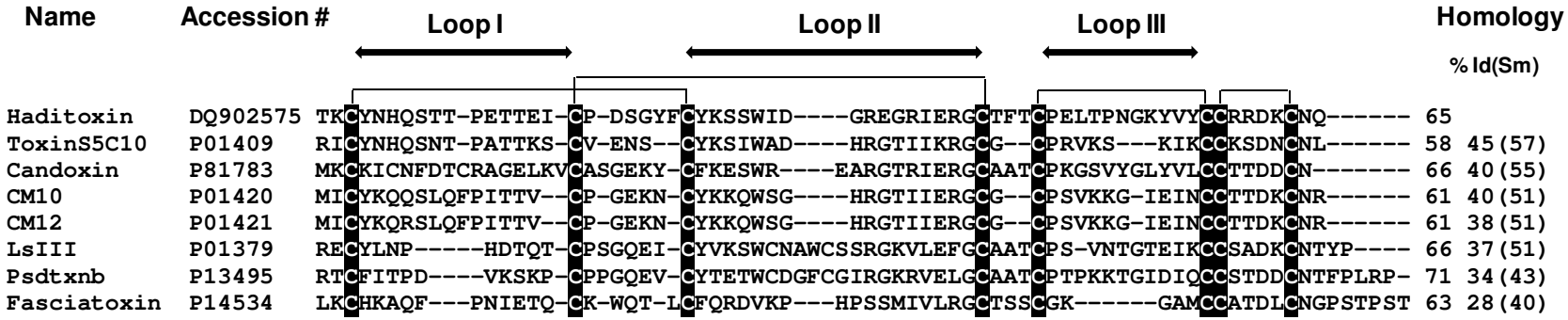

Figure 2.15: Sequence alignment of haditoxin with the sequences of reversible neurotoxins and neurotoxin homologs.
The number of amino acid residues in each sequence is indicated at the end of the respective sequence. The homology of each of the sequence in (%Id) identity and homology or similarity (Sm) with the sequence of haditoxin is also mentioned. The conserved cysteine residues are highlighted in black and the disulfide linkages are shown by black lines. The black arrows indicate the segments contributing to the three loops. The accession number is also stated for each toxin. The source organisms are as follows- Haditoxin (*Ophiophagus hannah*); ToxinS5C10 (*Dendroaspis jamesoni*); Candoxin (*Bungarus candidus*); CM10 and CM12 (*Naja haje annulifera*); LsIII (*Laticauda semifasciata*); Psdtxnb, Pseudonajatoxin b (*Pseudonaja textilis*) and Fasciatoxin (*bungarus fasciatus*).

haditoxin exhibited only 40-57% sequence similarity (**Fig. 2.15**) with these snake toxins.

As haditoxin eluted out earlier in gel filtration chromatography (peak 2 of **Fig. 2.1**) compared to the other 3FTXs (peak 3 of **Fig. 2.1**) indicating the existence of multimeric states of the molecule, therefore we compared the sequence of haditoxin with the existing snake venom dimeric 3FTXs. Among them there are κ-neurotoxins known to be composed of two identical monomers (homodimers) held together by non-covalent interactions such as- κ-bungarotoxin, κ2-bungarotoxin, κ-flavitoxin and others. Haditoxin bears about 52-57% of homology to κ-neurotoxins (**Fig. 2.16**). Further sequence comparison was also performed between haditoxin and covalently linked dimeric neurotoxins held together by a disulfide bridge. They are irditoxin (heterodimer of subunit A and B) isolated from a colubrid venom (*Boiga irregularis*) as well covalently (disulfide) linked homodimers of α-cobratoxin and heterodimers of α-cobratoxin in combination with a variety of three-finger cytotoxins all isolated from an elapid venom (*Naja kauothia*). Haditoxin possesses about 45% similarity with irditoxin subunit A and 46% with subunit B (**Fig. 2.17**). The sequence similarity of the protein of interest with that of α-cobratoxin was 52% and 48-49% (**Fig. 2.17**) to the elapid cytotoxins.

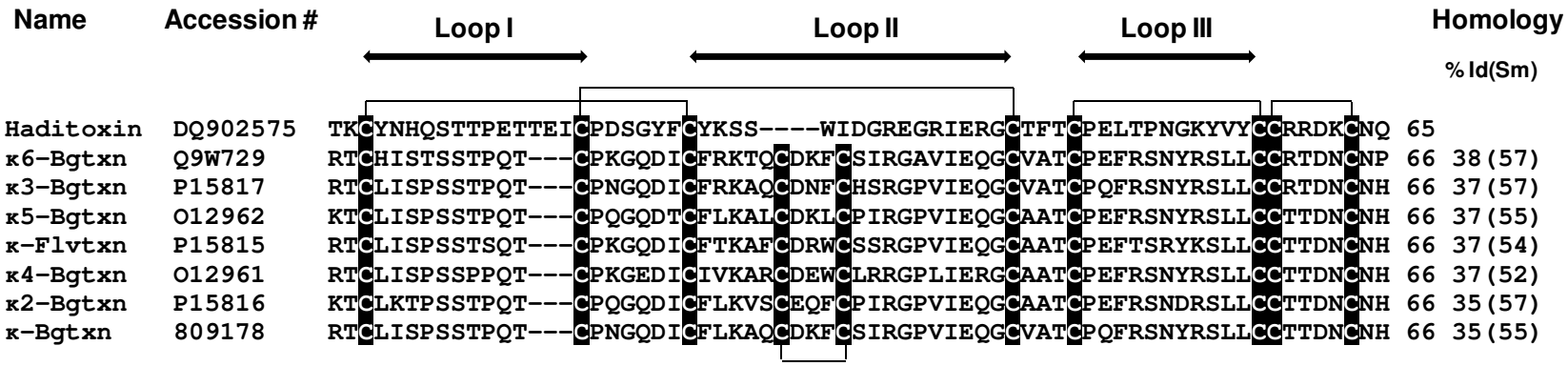

Figure 2.16: Sequence alignment of haditoxin with the sequences of κ-neurotoxins.
The number of amino acid residues in each sequence is indicated at the end of the respective sequence. The homology of each of the sequence in (%Id) identity and homology or similarity (Sm) with the sequence of haditoxin is also mentioned. The conserved cysteine residues are highlighted in black and the disulfide linkages are shown by black lines. The black arrows indicate the segments contributing to the three loops. The accession number is also stated for each toxin. The source organisms for each of the toxin are as follows- Hdtx, Haditoxin (*Ophiophagus hannah*); κ6-Bgtxn, κ6-bungarotoxin (*Bungarus multicinctus*); κ3-Bgtxn, κ3-bungarotoxin (*Bungarus multicinctus*); κ5-Bgtxn, κ5-bungarotoxin (*Bungarus multicinctus*); κ-Flvtxn, κ-flavitoxin (*Bungarus flaviceps flaviceps*); κ4-Bgtxn, κ4-bungarotoxin (*Bungarus multicinctus*); κ2-Bgtxn, κ2-bungarotoxin (*Bungarus multicinctus*) and κ-Bgtxn, κ-bungarotoxin (*Bungarus multicinctus*).

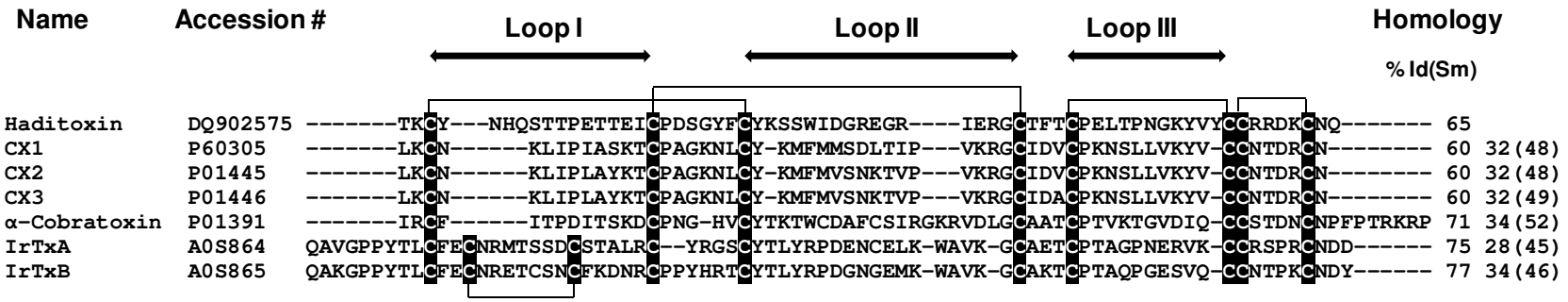

Figure 2.17: Sequence alignment of haditoxin with the sequences of covalent dimeric neurotoxins and cytotoxins.
The number of amino acid residues in each sequence is indicated at the end of the respective sequence. The homology of each of the sequence in (%Id) identity and homology or similarity (Sm) with the sequence of haditoxin is also mentioned. The conserved cysteine residues are highlighted in black and the disulfide linkages are shown by black lines. The black arrows indicate the segments contributing to the three loops. The accession number is also stated for each toxin. The source organisms are as follows- Haditoxin (*Ophiophagus hannah*); CX1, Cytotoxin 1 (*Naja kaouthia*); CX2, Cytotoxin 2 (*Naja kaouthia*); CX3, Cytotoxin 3 (*Naja kaouthia*); α-Cobratoxin (*Naja kaouthia*); IrTxA, Irditoxin subunit A (*Boiga irregularis*) and IrTxB, Irditoxin subunit B (*Boiga irregularis*).

2.5 CONCLUSIONS

In conclusion, a novel three-finger toxin, haditoxin was isolated and purified to homogeneity from the venom of an elapid, *O.* hannah. A detailed sequence analysis was carried out where haditoxin was compared with the different class of three-finger toxins. Although haditoxin showed high homology (> 80%) with muscarinic toxin homologs, it did not exhibit any muscarinic effect on isolated tissue. Moreover, a potent neuromuscular blockade was observed when haditoxin was applied to the mammalian and avian nerve-skeletal muscle preparation. Hence, haditoxin was subjected to a detailed pharmacological characterization using *in vivo* toxicity and *ex vivo* organ-bath studies as well as the effect of haditoxin was also observed on different subtypes of human nicotinic receptors using electrophysiological studies (discussed in chapter 3).

Chapter Three

Pharmacological characterization of haditoxin

CHAPTER THREE

Pharmacological characterization of haditoxin

3.1 INTRODUCTION

Pharmacology is one of the keystones of the drug discovery process. In drug discovery, in vivo, ex vivo and in vitro models using live animals, tissue/organ baths and electrophysiology/solid-phase binding studies lead to the development of novel, effective and selective molecules that can themselves be used as therapeutic agents or can be used to characterize different receptors and pathophysiological processes in the larger context of in vivo pharmacology. Although, pharmacology means 'the science of drugs' (Greek pharmakos, medicine or drug; and logos, study) but in the main tasks of pharmacologists involves 1) screening of molecules for desired activity, 2) determining their mode of action, and 3) quantifying drug activity (dose-response relationship).

For over one hundred years, isolated tissue and organ preparations have been used in regular practice by the pharmacologist (Tyrode, 1910; Krebs and Henseleit 1932; Krebs, 1950; Parascandola, 1986). Traditionally, tissue-organ baths are used to investigate the physiological and pharmacological response of a drug molecule on different tissue preparations (ring/vessel or strip) from various species (mice, chick, rat, guinea-pig, frog, rabbit, etc.) and finally to generate the dose-response relationship. Tissues or organs have been isolated for these studies include muscle (Smooth or Skeletal), arterial rings or strips, uterine tissue or Vas deferens, ileum, colon, atrial or ventricle and diaphragm. Typically, these experiments are performed in a temperature controlled environment and perfused

with an oxygenated physiological solution, which allows the study of evoked tissue responses to pharmacological drug/agents (Dose-response studies), electrical stimulation or both pharmacological and electrical stimulation (Kenakin, 2006). The recorded responses or biological activity usually are the contraction/relaxation of muscle in the tissue: Force (isometric), Displacement (isotonic). The type of transducers/probes (isometric or isotonic) used in organ bath setups will vary depending on the type of tissue and physiological parameters to be investigated. The advantages of this method include ease in preparation, minimal equipment requirements, reproducible concentration–effect curves can be obtained using either contractile or relaxant agents as well the independency of these preparations from the *in vivo* systemic influences (Furchgott, 1972).

Electrophysiology is a well established discipline to study the electrical properties of the living cells (for a review see, Scanziani and Häusser, 2009). It is defined as the study of endogenous electrical currents in cells and of the effects of applied electrical currents on cell function. The electrical activity in a cell is controlled by the movement of ions, such as- Na^+, K^+, Cl^- and Ca^{2+}, through ion channels. Therefore, molecules that affect the normal activity of the ion channels will alter the electrical properties of a cell and these effects can be visualized using different electrophysiological techniques. Many venom proteins are well-known to interact with the ion channel and thereby altering the electrical properties of the cells. Hence, electrophysiology is known to be a routine and reliable technique to understand the mechanism of action for different venom proteins as well as to elucidate their specificity for different subtypes of ion channels.

This chapter details the pharmacological characterization of haditoxin. The initial studies were done to find out the muscarinic effect of haditoxin, because of the observed high sequence similarity (discussed in chapter 1), using different isolated tissue preparations. Further we performed an *in vivo* toxicity study with haditoxin on mice to observe the biological effects of the protein on living organisms. Subsequently, action mechanism of haditoxin was elucidated using organ bath studies with different nerve-skeletal muscle preparations. The molecular target of this protein was finally identified by electrophysiological studies where two-electrode voltage-clamp (TEVC) experiments were performed using *Xenopus* oocytes expressing different subtypes of nicotinic receptors.

3.2 MATERIALS AND METHODS

3.2.1 Drugs and chemicals

All chemicals and reagents were purchased from Sigma (St. Louis, MO, USA). The drugs used in pharmacological studies: acetylcholine chloride, Carbamylcholine chloride (carbachol), atropine sulfate monohydrate, d-tubocurarine chloride, phentolamine methanesulfonate, neostigmine bromide and α-bungarotoxin were obtained from Sigma (St. Louis, MO, USA). Potassium chloride was obtained from Merck (Darmstadt, Germany). *O. hannah* venom in lyophilized form was obtained from PT Venom Indo Persada (Jakarta, Indonesia) and Kentucky Reptile Zoo (Slade, KY, USA). Haditoxin was purified from the venom as described in chapter 2 and lyophilized. The lyophilized powder was used to prepare the stock solution. The stock solutions of drugs and toxins were prepared fresh as and when required by dissolving them in deionized water. Further dilutions to required concentrations were made using either normal saline (0.89% NaCl) for the *in vivo* experiments or Krebs physiological salt solution (composition described below) for the *ex vivo* experiments.

3.2.2 Animals

Swiss albino male mice (3 weeks, 13 ± 2 g) were used for the *in vivo* toxicity study. Animals were acquired from the university Laboratory Animal Center and were acclimatized to the Animal Holding Unit surroundings for at least 3 days before the experiments. For *ex vivo* experiments male Sprague Dawely rats (250-350 g), 3 to 7-day-old domestic chicks (*Gallus domesticus*) (purchased from Chew's Agricultural Farm, Singapore) were used. Chicks were only received on

the day of experimentation. All other animals were kept under standard conditions with food and water available *ad libitum*. The animals were housed four per cage in a light controlled room (12 h light/dark cycle, light on 0700 h) at 23°C and 60% relative humidity. All animal experiments were conducted according to the protocol (021/07a) approved by the Institutional Animal Care and Use Committee of the National University of Singapore.

3.2.3 Methods of protein administration

The protein was dissolved in 200 µl of 0.89% NaCl (Braun, Malaysia) and administered through the intraperitoneal route for the *in vivo* toxicity study in mice. The various protein doses were dissolved in 200 µl of 0.89% NaCl solution and injected into the peritoneal cavity using a 27 G X [1⁄2]" needle (Becton-Dickinson, Franklin Lakes, NJ, USA) held at an angle of 45° to peritoneal cavity. The injection was made slowly and at a steady rate.

3.2.4 *In vivo* toxicity study

Native protein was injected intraperitoneally (*i.p.*) into the Swiss albino mice at doses of 5, 10 and 25 µg/g (n=2). The volume injected was 200 µl, and the protein was dissolved in 0.89 % NaCl. The animals were observed for the symptoms were observed and recorded to find out biological activity of haditoxin, and in the event of death, the times of death were noted. Control animals were injected 200 µl of 0.89 % NaCl. Postmortem examinations were conducted on the animals after their death.

3.2.5 Determination of LD_{50}

The method of Meier and Theakston (1986) for assessing the toxicity of venom and toxins was adapted to determine the lethal dose for 50% population (LD_{50}). As suggested by Aird and Kaiser (1985) additional guidelines were also taken into account. Male Swiss albino mice were given intraperitoneal injections of weight proportional doses (D) (5, 10 and 25 µg/g body weight) of the haditoxin. The toxin was dissolved in 0.89 % NaCl up to a volume of 200 µl prior to injection. Two animals were used for each dose. The time between injection and death (indicating the survival time) was recorded for each animal. The average survival time (T) was calculated for each dose of toxin. A plot of D/T (abscissa) versus D (ordinate) was constructed and the point where the regression line intersected the ordinate depicted the LD_{50}, defined by the method as the smallest dose of toxin responsible for killing of the 50% of experimental animals in an unlimited time.

3.2.6 *Ex vivo* organ bath studies

Isolated tissue experiments were performed using a conventional organ bath set-up. The Organ bath with a chamber volume of 6 ml was used for the different tissue preparations. Krebs physiological salt solution (118 mM NaCl, 4.8 mM KCl, 1.2 mM KH_2PO_4, 2.4 mM $MgSO_4$, 2.5 mM $CaCl_2$, 25 mM $NaHCO_3$, 11 mM D-(+) glucose, pH 7.4) was used for all the tissue-organ bath studies. Deionized water was used to prepare the fresh Krebs solution and it is continuously aerated with carbogen (5% carbon dioxide in oxygen) for all the isolated tissue experiments. The organ bath was maintained at physiological temperature (37 °C) for all the experiments. The resting tension of the isolated tissue was maintained

at 1-2 g unless specified otherwise. The preparations were allowed to equilibrate for about 30-45 min. Krebs solution was changed at intervals of 15 min during the equilibration period before the beginning the experiments and the tissue was left in contact with the toxin for a maximum of 3 h. Electrical field stimulation (EFS) was carried out through platinum ring electrodes using a Grass stimulator S88 (Grass Instruments, MA, USA). The magnitude of the contractile responses of the tissues was measured in gram (g) tension. Data was continuously recorded using a PowerLab/Chart 5 (AD Instruments, New South Wales, Australia) via a force displacement transducer (Model MLT0201, AD Instruments). A schematic representation of organ bath experimental setup is shown in figure 3.1. Neuromuscular blockade is expressed as a percentage of the original twitch height in the absence of toxin. Dose-response curves representing the percent blockade after 30 min of exposure to the respective toxins were plotted.

3.2.7 Reversal studies

To examine the reversibility of the neuromuscular blockade produced by haditoxin, the recovery of the toxin treated tissue was observed after the complete neuromuscular blockade or 80% blockade. The toxin was removed from the organ bath chamber by extensive washing (3 cycles of 30 sec on 30 sec off pulse with a flow rate of 20 ml/min) with fresh Krebs solution and it was continued at 30 min intervals over a period of 120 min. The effect of anticholinesterase neostigmine was observed on the reversal of the neuromuscular blockade produced by haditoxin either by the addition of single doses (3 and 5 µM) or by cumulatively adding (up to 10 µM) neostigmine to the tissue when it achieves 80% blockade.

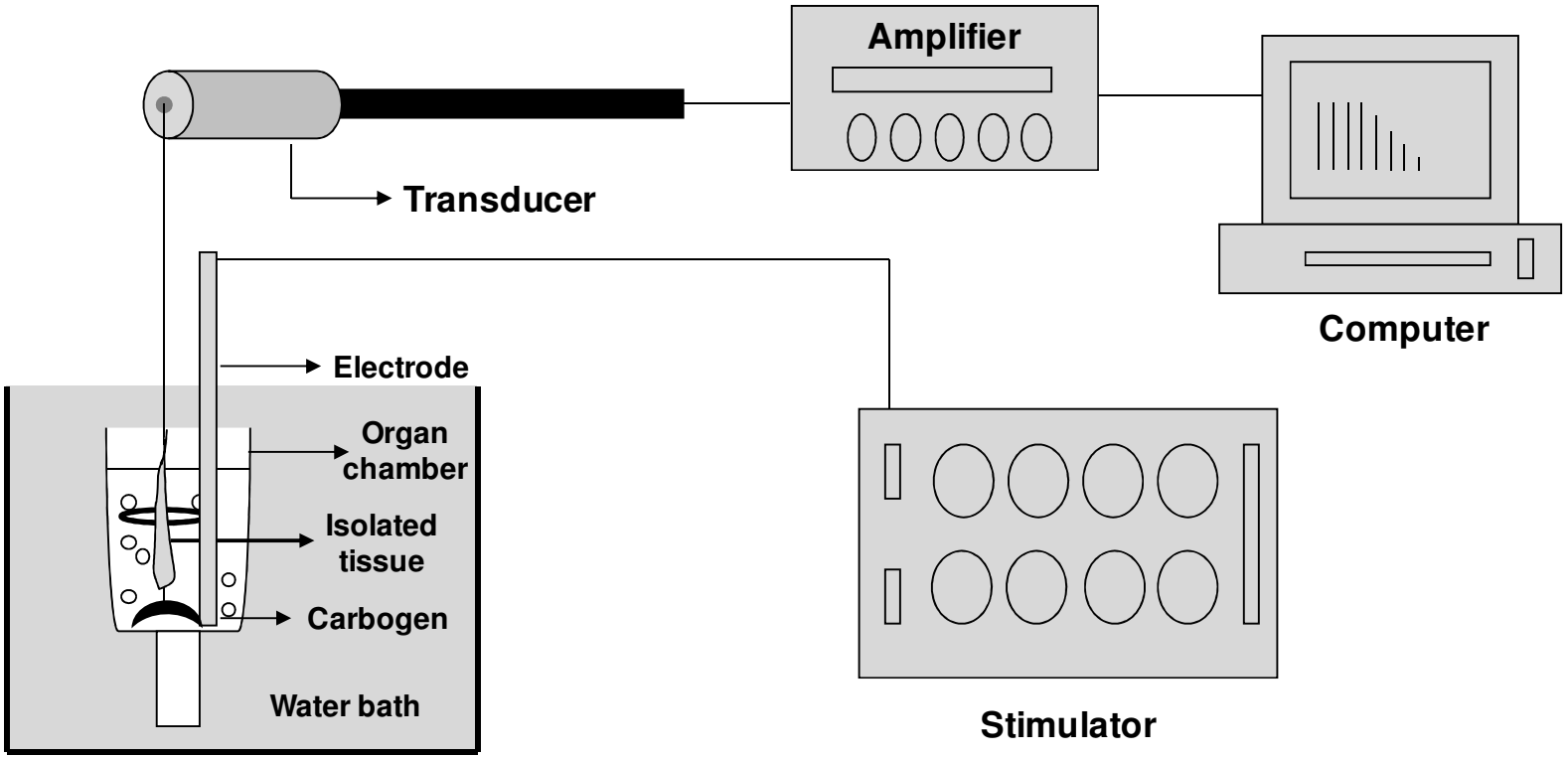

Figure 3.1: Schematic representation of the organ bath experimental setup used for studies of isolated tissues.
The water bath containing the organ bath chamber is maintained at 37 °C. The organ bath is continuously aerated with carbogan (95% O_2 and 5% CO_2) during the experiment. Fresh Krebs solution was supplied to the organ bath by controlled gravity-driven perfusion. The isolated tissue was mounted in the organ bath aligned to the platinum ring electrodes (the black ring attached to the electrode in the diagram) which is attached to the Grass stimulator S88 (Grass Instruments, MA, USA) through which the electrical field stimulation is applied when needed. The contractile response of the tissues was recorded using a computerized PowerLab/Chart 5 system (AD Instruments, New South Wales, Australia) via a force displacement transducer (Model MLT0201, AD Instruments

3.2.8 Rat ileum preparations

Intestinal smooth muscle activity is closely regulated by the parasympathetic nervous system. It is presumed, the muscarinic receptors principally reside within smooth muscle cells because of their synaptic contact with the cholinergic nerves (Buckley and Caulfield, 1992; Eglen *et al*, 1996). Like all other smooth muscles, rat ileum contains heterogeneous populations of muscarinic receptors (~70% M_2 and ~30% M_3 as determined by radioligand binding studies) (Ehlert and Tomas, 1995). The contracture of the smooth muscle in the gastrointestinal tract contains both M_2- and M_3-subtypes of muscarinic receptors. M_3 receptor mediates ileal contraction, whereas, the role for M_2 receptor, is relaxation which is driven by modulation of cAMP levels (Eglen *et al*, 1994; Eglen *et al*, 1996). The initial basis for this conclusion rests on the findings of several investigators who have shown that the potencies of subtype selective muscarinic antagonists for blocking contraction (see reviews by Eglen *et al*, 1996).

Healthy SD rats were euthanized by asphyxiation in an airtight chamber connected to a CO_2 gas tank. The lower abdomen was cut open with a midline incision and the ileum was isolated out. It was then flushed with warm Krebs solution and the intact ileum was stripped into approximately 2 cm segments. They were then suspended in the organ bath chamber using hooks. Contractile response was checked at intervals by adding 50 μM acetylcholine. The effect of haditoxin (1.5 μM, n=3) on the tissue was checked followed by acetylcholine (50 μM). If there was no blockade, atropine (1 μM), a non-selective muscarinic receptor antagonist, was added into the organ bath as a positive control.

3.2.9 Rat anococcygeus muscle preparations

The anococcygeus muscles are a pair of smooth muscles of the urogenital tract that originate in the upper coccygeal vertebrae and run around the terminal colon to the ventral surface (Gibson and McFadzean, 2001; Gillespie, 1972). The rat anococcygeus muscle (RAM) consists of a thin sheet of smooth muscle fibres, the autonomic innervations of which contains noradrenergic (motor excitatory), cholinergic (motor excitatory) and inhibitory (nitrergic) NANC components (Gillespie, 1972). As far as effects to exogenous cholinergic agents are concerned, the muscle responds to both muscarinic and nicotinic agonists. Muscarinic receptors located postjunctionally subserve contraction (Gillespie, 1972). A single type of muscarinic receptor, the M3 subtype, mediates the muscarinic contraction in RAM. Thus, the isolated RAM may serve as a novel and robust functional muscarinic M3 receptor model.

Healthy SD rats were euthanized by asphyxiation in an airtight chamber connected to a CO_2 gas tank. The pelvic region of the rat was cut open to expose the terminal colon in order to visualize the pair of anococcygeus muscles. The muscles were then tied with sutures on both ends and isolated and mounted in the organ baths. Motor responses of the muscle were then elicited by EFS of 20-30 V, 10 Hz, 1 ms pulse width every 2 min and the response was recorded. Haditoxin (1.5 μM, n=3) was added in the presence of EFS to find out its effect. If there was no blockade, phentolamine (an α-adrenergic antagonist) and atropine (a non-selective muscarinic receptor antagonist) were added into the bath as a positive control.

3.2.10 Rat phrenic nerve-hemidiaphragm muscle preparations

Pharmacological effect of a drug molecule on nAChRs can be evaluated by assessing the ability of the molecule to block the stimulation of the motor nerves innervating the skeletal muscle in isolated tissue preparations. The isolated phrenic nerve-diaphragm provides a simple preparation of mammalian muscle which can be easily stimulated by the phrenic nerve either directly or indirectly (Bulbring, 1946). It is a relatively straightforward system consisting of, 220 motoneurons and one muscle (Gottschall, 1981).

Healthy SD rats were euthanized by asphyxiation in an airtight chamber connected to a CO_2 gas tank. The hemidiaphragm muscle associated with phrenic nerve was isolated as described by Bulbring (1946). The isolated tissue is mounted in the organ bath. Indirect stimulation was performed at a frequency of 0.2 Hz in rectangular pulses of 0.2 ms duration at a supramaximal voltage of 7–10 V (Pawlak *et al*, 2009). Direct muscle stimulation was achieved by electrical stimulation (0.2 Hz, 2 ms, 20-30 V) in the presence of dTC (10 μM), which was used to abolish neuromuscular transmission. In control experiments, the effect of indirect or direct muscle stimulation of the rat phrenic nerve-hemidiaphragm muscle (RHD) was observed for a total duration of 90 min. The effects of various concentrations of haditoxin (0.15 to 15 μM; n=3), α-bungarotoxin (0.01 to 1.0 μM; n=3), or vehicle were investigated. The recovery of twitches was assessed by washing with Krebs solution, as described in the reversal studies (section 3.2.7 of this chapter).

3.2.11 Chick biventer cervicis muscle preparations

The chick biventer cervicis muscle (CBCM) is an avian nerve-skeletal muscle preparation commonly used to evaluate the effect of a drug on neuromuscular junction (Harvey *et al*, 1994 and Crachi *et al*, 1999). The biventer cervicis is innervated by nerves enclosed by the tendon attached to it. The chick muscle is multiply innervated, which means the muscle contains both fast and slow fibres. Stimulation of the nerves via electrodes in contact with the tendon results in a contraction of the muscle generating a twitch response via the fast fibres. The slow fibres do not have a propagated action potential, but can be stimulated to give a slow contracture by addition of an exogenous agonist such as ACh/CCh or KCl, which causes direct muscle stimulation, to the bath (Ginsborg and Warriner, 1960). Because of this advantage CBCM had been frequently used to assess the type of neurotoxicity and direct myotoxicity of the venom and toxins (Harvey *et al*, 1994).

There are several ways by which venom and toxins can affect the neuromuscular transmission. They can interact with the presynaptic membrane interfering with the release of neurotransmitter molecules during an action potential or they can bind to the postsynaptic nAChRs and thereby inhibiting the binding of ACh to these receptors. Additionally, the toxins can also exert their action by directly affecting the muscle producing myotoxicity. Using CBCM we can find out the mechanism of neurotoxicity (presynaptic, postsynaptic or myotoxic) for a venom component. A presynaptic toxin would abolish the nerve evoked twitch response without affecting the response to the exogenous agonist of the nicotinic receptors such as- ACh and/or CCh as well as the response to the direct muscle stimulation

elicited by KCl would also be restored. On the contrary, a postsynaptic toxin would abolish both the twitch response and the response to the exogenous agonists but the response to the direct muscle stimulation by KCl-induced depolarization will not be affected. In the case of myotoxic effect, the toxin initiates a contracture of the muscle which has a slow onset and irreversible nature. The twitch response of the muscle to the nerve stimulation as well the response to the exogenous cholinoceptor agonist would be blocked irreversibly. On top of this the muscle would not responds to the direct muscle stimulation either by exogenous KCl or by electrical stimulation (Rowan *et al*, 1989; Geh *et al*, 1992; Harvey *et al*, 1994; Geh *et al*, 1997). But the myotoxicity is subject to further investigation by histopathological studies.

Healthy chicks were euthanized by asphyxiation in an airtight chamber connected to a CO_2 gas tank. A midline incision was made down the back of the neck. The pairs of biventer cervicis muscles, which lie on either side of the midline, are removed and kept in warm Krebs solution. Each of the muscle is attached to a tissue holder with ring electrodes around the tendon and mounted in the organ bath (Ginsborg and Warriner, 1960). Maximal twitch responses of the muscle were elicited indirectly via stimulation of the motor nerve by applying an electrical field of 7–10 V potential difference at a frequency of 0.2 Hz in supramaximal rectangular pulses of 0.1 ms duration. For direct muscle stimulation, the electrodes were lowered from the tendon towards the belly of the muscle and twitch response was evoked by electric field stimulation (0.2 Hz, 1 ms, 20-30 V). To block the neuromuscular transmission during the direct muscle stimulation dTC was added at 10 μM concentration (Baraka, 1974). In control

experiments, the effect of indirect or direct muscle stimulation of the RHD was observed for a total duration of 180 min. The effects of various concentrations of haditoxin (0.15 to 15 μM; n=3) on the twitch response as well as direct muscle stimulation in the CBCM was investigated. The block response was expressed as a percentage of control twitch height in the absence of toxin. Additionally, the times taken to block the amplitude of the control twitch response by 50% (t_{50}) and 80% (t_{80}) were calculated in order to provide a quantitative measure of neurotoxicity. For comparison, the effect of α-bungarotoxin (0.01 to 1.0 μM; n=3) on the nerve evoked twitch response in CBCM was investigated. An individual tissue preparation was used for each dose of toxin. To study the reversibility of the neuromuscular blockade produced by haditoxin the recovery of nerve evoked twitch response was assessed by washing with Krebs solution, as described in the reversal studies (section 3.2.7 of this chapter).

At appropriate intervals, responses to exogenously applied 300 μM ACh, 10 μM CCh or 30 mM KCl were obtained in the absence of an electrical field stimulation. The magnitude of the response against these compounds varied from tissue to tissue but was reproducible with the same compound for the same tissue. After exposure to ACh, CCh or KCl the tissue was washed extensively with fresh Krebs solution. The electrical stimulation was then reestablished. In control experiments, the quantitative contractile response of the muscle to ACh, CCh or KCl before and after 180 min of uninterrupted nerve stimulation was obtained. The effects of various concentrations of haditoxin (0.15 to 15 μM; n=3) on the response of exogenous ACh, CCh or KCl on CBCM were investigated. Blockade

of the responses to ACh, CCh and KCl by haditoxin are expressed as a percentage of the respective control response prior to the addition of the toxin.

3.2.12 Statistical analysis

The data were expressed as mean ± standard error of mean (SEM) of at least 3-4 experiments. The experiments with higher dose of haditoxin (like- 5 and 15 µM) and α-bungarotoxin was done with n=3. The data was analyzed using SigmaPlot 10.0 software (Systat software Inc., San Jose, California, USA).

3.2.13 Electrophysiological characterization of haditoxin

Two-electrode voltage-clamp (TEVC) experiments were done using *Xenopus* oocytes to observe the effect of haditoxin on different human nicotinic receptor subtypes ($\alpha\beta\gamma\delta$, α_7, $\alpha_3\beta_2$ and $\alpha_4\beta_2$). The electrophysiological studies described below were carried out in the collaborating laboratory of Professor Daniel Bertrand, Department of Physiology, University of Geneva, 1 rue Michel Servet, 1211 Geneva 4, Switzerland.

3.2.14 Oocyte preparation and cDNA injection

The study of nAChRs reconstituted in *Xenopus* oocytes by expression of cloned cDNAs is an established method for the electrophysiological characterization of ligands that interact with nAChRs. *Xenopus* oocytes were isolated and prepared as previously described (Bertrand *et al*, 1991).

The oocytes were prepared and injected as described by Hogg *et al*, (Hogg *et al*, 2008). Oocytes were injected intra-nuclearly with expression vectors containing

the various cDNAs (2 ng) encoding for different nicotinic receptor subunits and incubated at 18 °C in Barth solution consisting of (in mM) 88 NaCl, 1 KCl, 2.4 $NaHCO_3$, 10 HEPES (4-(2-hydroxyethyl)-1-piperazineethanesulfonic acid), 0.82 $MgSO_4.7H_2O$, 0.33 $Ca(NO_3)_2.4H_2O$, 0.41 $CaCl_2.6H_2O$. Electrophysiological experiments were performed 2-3 days after the injection of the oocytes. The pH was adjusted to 7.4 with NaOH. All subunits were injected with equal concentrations. The medium was supplemented with 20 µg/ml of kanamycin, 100 units/ml of penicillin and 100 µg/ml of streptomycin to minimize contamination.

3.2.15 Electrophysiological recording

Electrophysiological recording were performed with a two-electrode voltage-clamp (GeneClamp amplifier, Axon instruments, Foster City, CA, USA) as previously described (Bertrand *et al*, 1992; Servent *et al*, 1997; Kasheverov *et al*, 2009). The oocytes were clamped at –100 mV and during recordings they were perfused with OR2 (oocyte Ringer) medium containing (in mM): 82.5 NaCl, 2.5 KCl, 1 $MgCl_2$, 2.5 Ca_2Cl_2, 5 HEPES, and 20 µg/ml BSA. The pH of the medium was adjusted to 7.4 prior to use. Atropine (0.5 µM) was added to all solutions to block activity of endogenous muscarinic receptors. Just before use, ACh and haditoxin were dissolved the OR2 solution and they were applied to the bath by gravity driven perfusion. The flow rate was approximately 6 ml/min and the chamber volume was less than 100 µl. Control responses were recorded before toxin exposure and toxin incubation was carried out in the recording chamber during 3–5 min with agitation. ACh concentration was close to the EC_{50} for receptor activation and toxin incubation time was determined by testing receptor

responses after increasing toxin incubation times. Equilibrium was assumed to be reached when no further inhibition of the response was seen. All recordings were performed with an automated TEVC robot.

3.2.16 Electrophysiological data analysis

Data were digitized and analyzed off-line using MATLAB (Mathworks, Natick, MA)**.** Dose-response curves for toxin inhibition were fit with the equation:

$$y = 1/(1 + ([toxin]/IC_{50})nH)$$

where, y is the normalized response, [toxin] is the toxin concentration, and nH is the Hill coefficient.

3.3 RESULTS

The isolated novel protein haditoxin showed high sequence similarity (80-83%) and identity (75-80%) to muscarinic toxin homologs (**Fig. 2.9** in chapter 2). The similarity observed with muscarinic toxins is about 51-54% (**Fig. 2.10** in chapter 2). Muscarinic toxins are especially found in mamba venoms and are known to interact with the muscarinic acetylcholine receptors (mAChRs), which belong to the GPCR superfamily (for review see, Servent and Fruchart-Gaillard, 2009; Jerusalinsky *et al*, 2000). Because of the observed sequence identity it was of interest to find out whether haditoxin exerts similar kind of effect as that of the muscarinic toxins.

3.3.1 Effect of haditoxin on the cholinergic transmission mediated by muscarinic receptors

To evaluate the effect of haditoxin on muscarinic receptors, we examined haditoxin on *ex vivo* smooth muscle preparations. Accordingly, different isolated muscle preparations are used for the study such as- the rat ileum and rat anococcygeus muscle.

Addition of haditoxin did not produce blockade of the contractile response to exogenously applied ACh, (**Fig 3.2**) of the ileum smooth muscle. As expected, the contractile response to exogenous ACh in the ileum was completely inhibited by the addition of atropine (a non-selective muscarinic receptor antagonist used as a positive control). This inferred that there is no interaction between haditoxin and the muscarinic receptors present in the smooth muscle of the ileum.

In order to further confirm the interaction of haditoxin with muscarinic receptors the protein was tested on the rat anococcygeus muscle. As observed in the anococcygeus muscle experiment, the contractions elicited by the EFS were unaffected after the addition of haditoxin (**Fig 3.3**) suggesting that the toxin did not block the cholinergic receptor mediated contractile responses of the muscle. Addition of phentolamine (α-adrenergic antagonist) and atropine (non-selective muscarinic receptor antagonist) as positive controls abolished the EFS contractile response. Hence, it can be concluded that haditoxin did not mediate any effect at the muscarinic receptors present in the smooth muscle of ileum and the anococcygeus muscle.

3.3.2 Biological activity of haditoxin in mice

Intraperitoneal injection of haditoxin in mice made them quite and sluggish. They also showed symptoms of flaccid paralysis particularly of the hind limbs and labored breathing which was followed by death presumably due to respiratory paralysis. Mice injected with 5, 10 and 25 µg/g dose died after 92, 35 and 19 min, respectively (n=2) **(Table 3.1)**. In control experiments, mice injected with equal volume of normal saline did not exhibit any symptoms of paralysis and survived. On post-mortem examination, no gross changes in the internal organs (heart, lungs, kidney, liver, intestine, stomach) notably hemorrhage, was observed.

3.3.3 Lethality of haditoxin in mice

The lethality of haditoxin was assessed on mice. To measure the acute toxicity of snake venom toxins determination of LD_{50} has gained wide acceptance. The

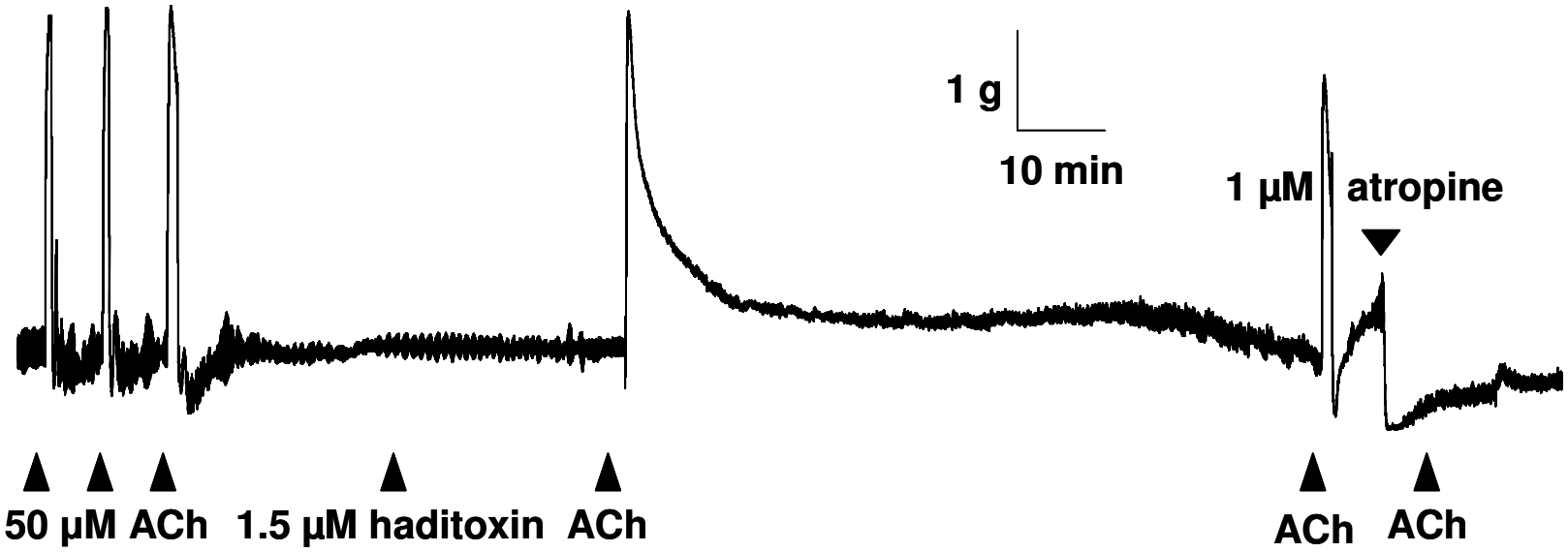

Figure 3.2: Effect of haditoxin on the cholinergic transmission in the smooth muscle of rat ileum.
A segment of tracing showing the effect of haditoxin (1.5 µM) on rat ilium muscle preparation. Intact and stripped ileum was isolated from male Sprague Dawely rats (250-350 g) and mounted in the organ bath. Contractile response was checked at intervals by adding 50 µM acetylcholine (ACh). The effect of the protein (1.5 µM, n=3) was observed followed by ACh (50 µM). Atropine (1 µM) (a non-selective muscarinic receptor antagonist) was added as a positive control.

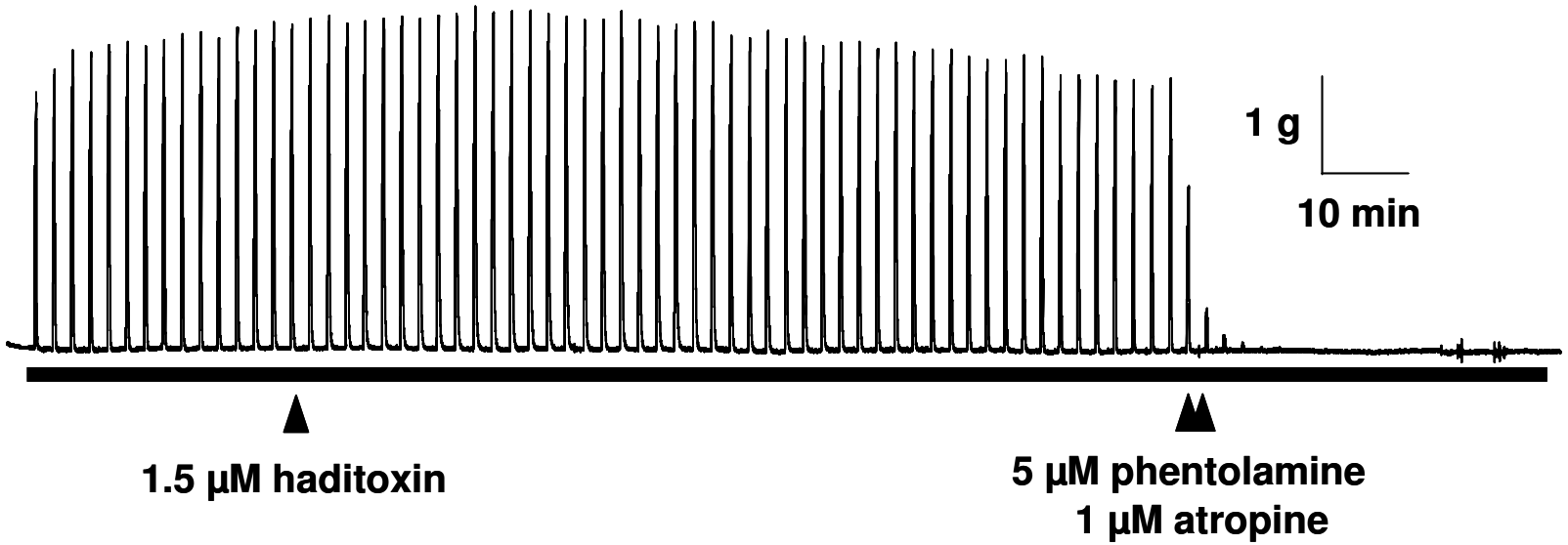

Figure 3.3: Effect of haditoxin on the cholinergic transmission in rat anococcygeus muscle.

A segment of tracing showing the effect of haditoxin (1.5 µM) on rat annococcygeus muscle preparation. The anococcygeus muscles from rats were isolated and mounted. Contractile response of the muscle was elicited by EFS of 20-30 V, 10 Hz for 10 s, 1 ms pulse width every 2 min and was recorded. The black bar indicates the electrical field stimulation (EFS). The effect of the protein of interest (1.5 µM, n=3) on EFS was observed. Phentolamine (5 µM) (an alpha-adrenergic antagonist) and atropine (1 µM) were added as a positive control.

Table 3.1: Effects of haditoxin injected intraperitoneally into Swiss albino mice

Dose (µg/g)	Paralysis	Hemorrhage	Avg. time of death (min)	Number of animals (n)
Control	-	-	-	1
5	+	-	20	2
10	++	-	32.5	2
25	+++	-	94	2

method of Meier and Theakston (1986) was followed to determine the LD_{50} of haditoxin. The time of death was recorded for each animal, with the average calculated to be 94, 32.5 and 20 min, respectively for the 5, 10 and 25 µg/g doses (n=2). The plot of (D) (Y-axis) Vs. (D)/(T) (X-axis) where, D=dose of haditoxin and T=survival time, was plotted (**Fig 3.4**). The LD_{50} value of haditoxin was calculated by the point of intersection of the regression line on the Y-axis. The LD_{50} of haditoxin was determined to be 4.4 µg/g in male Swiss albino mice.

3.3.4 Effect of haditoxin on the cholinergic transmission mediated by nicotinic receptors

The observed peripheral neurotoxic symptoms produced by haditoxin *in vivo*, warranted detailed pharmacological characterization of this protein on neuromuscular transmission mediated by nicotinic receptors. Accordingly, different isolated muscle preparations such as- CBCM and RHD are used for the study.

3.3.5 Effect of haditoxin on neuromuscular transmission in CBCM

Haditoxin produced a time-dependent blockade of the nerve evoked twitch responses of CBCM (**Fig. 3.5**). The contractile response to exogenous agonists (ACh and CCh) was completely inhibited by haditoxin whereas, response to exogenous KCl and twitches evoked by direct muscle stimulation were not inhibited. No contracture or increase in muscle tone was observed with any of the doses of haditoxin tested for up to 180 min following the addition of the toxin. This indicates a post-synaptic neuromuscular blockade and an absence of direct

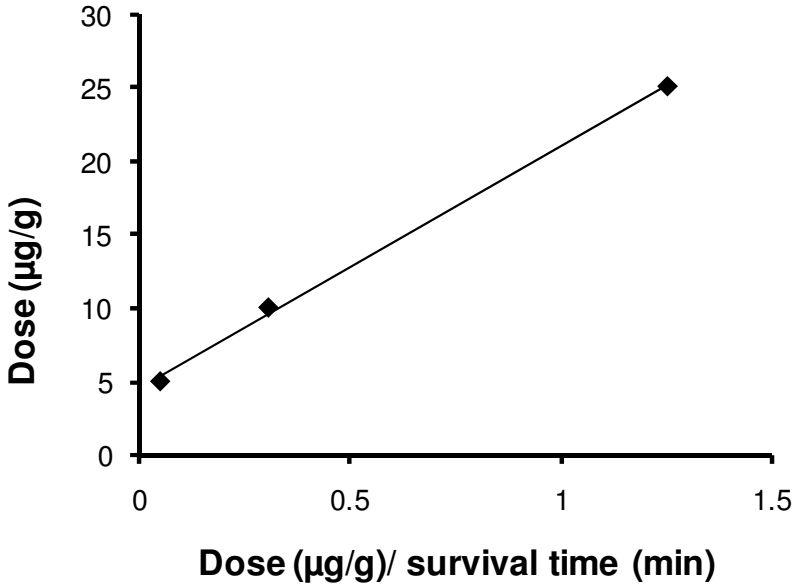

Figure 3.4: Determination of LD_{50} of haditoxin.

The method described by Meier and Theakston (1986) was followed to determine the LD_{50} of haditoxin. Haditoxin was injected intraperitoneally with doses of 5, 10 and 25 µg/g into male Swiss albino mice, using two animals for each dose. The time between injection and death (survival time) was recorded for each animal and the average for each group was calculated. A plot of dose vs. dose/survival time was constructed. The LD_{50} (the smallest dose of the toxin that kills 50% of the experimental animals in an unlimited time) is represented by the point where the extrapolated regression line intersected the ordinate. The LD_{50} of haditoxin was thus determined to be 4.4 µg/g.

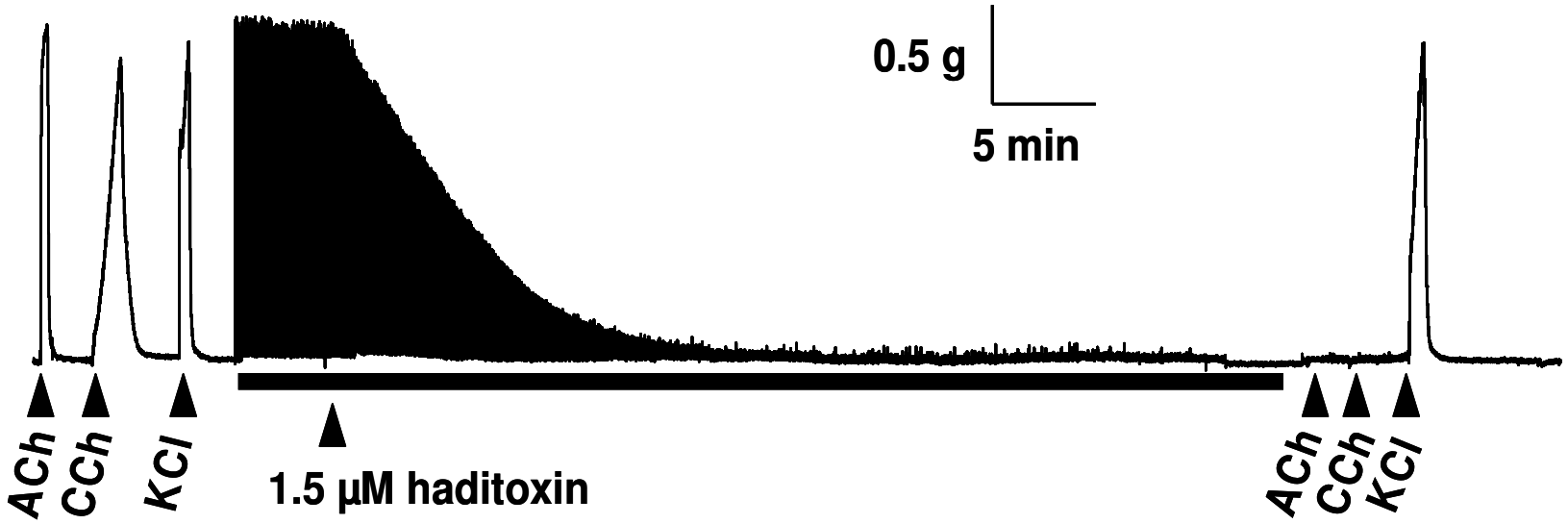

Figure 3.5: Effect of haditoxin on the twitch response of CBCM elicited by nerve stimulation and exogenously applied acetylcholine, carbachol and potassium chloride.

A segment of tracing showing the effect of haditoxin (1.5 µM) on chick biventer cervicis muscle preparations (CBCM) (n=3). Twitch response of the muscle was elicited by electrical field stimulation (EFS, indicated by the black bar) and by applying exogenous agonists, acetylcholine (ACh; 300 µM), carbachol (CCh; 10 µM) and potassium chloride (KCl; 30 mM). The vertical bar represents the magnitude of twitch response in gram tension and the horizontal bar depicts the time in minute.

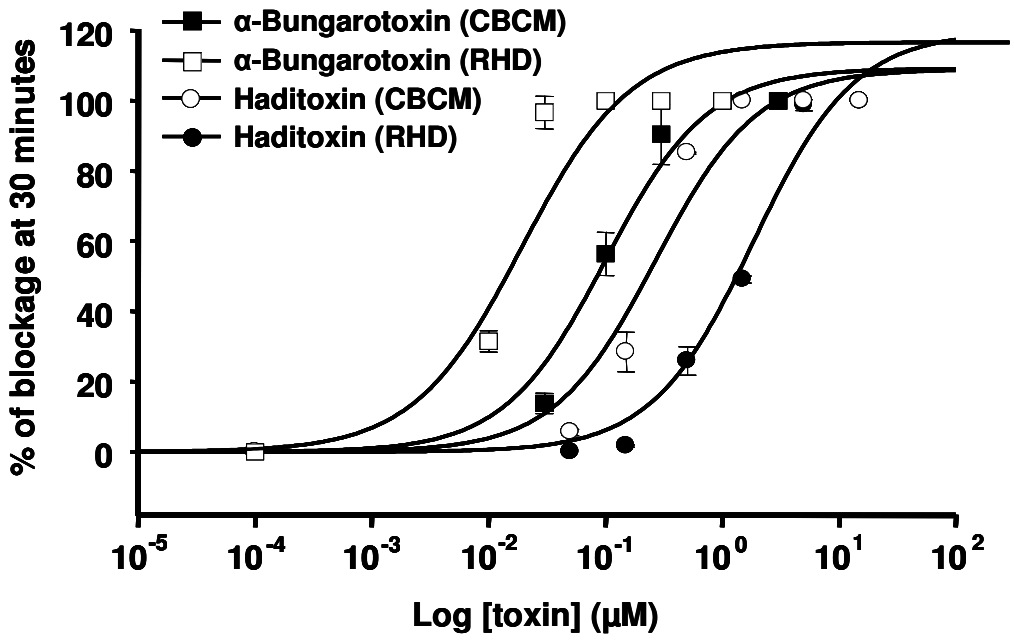

Figure 3.6: Dose-response curve of haditoxin and α-bungarotoxin on CBCM and RHD.

The concentration-response curves for the blockade of nerve-evoked twitch responses in the chick and rat muscle by of haditoxin and α-bungarotoxin. The block is calculated as a percentage of the control twitch responses of the muscle to supramaximal nerve stimulation in the absence of toxins. Each data point is the mean ± S.E. of at least three experiments.

myotoxicity. The effect of different dose of haditoxin was examined on CBCM. It was observed that haditoxin produces a dose-dependent effect. A dose-response curve was constructed and the IC_{50} of haditoxin on CBCM 0.27 ± 0.07 μM (**Fig. 3.6**) (considering the fact that the protein exists as dimer in solution; see in chapter 4).

Addition of α-bungarotoxin also completely inhibited the nerve evoked twitch responses of CBCM in a time-dependent fashion, without affecting the twitch response elicited by direct muscle stimulation or the response to exogenously applied KCl. A dose-response curve was constructed for α-bungarotoxin on CBCM and the IC_{50} of α-bungarotoxin was determined to be 12.1 ± 5.4 nM (**Fig 3.6**). Hence, when compared to the α-bungarotoxin, haditoxin was found to be ~20 times less potent on avian (CBCM) neuromuscular junctions.

3.3.6 Effect of haditoxin on neuromuscular transmission in RHD

The neuromuscular blockade properties of haditoxin were also evaluated on mammalian system. Haditoxin produced a complete time-dependent blockade of the nerve-evoked twitch responses in RHD (**Fig. 3.7**). Like CBCM, the twitch response due to direct muscle stimulation was not affected by the protein as well as the muscle tone was maintained at baseline for the entire duration of the experiment. When tested with was α-bungarotoxin a similar response was observed. The dose-dependent relationship for both haditoxin and α-bungarotoxin was evaluated for RHD and subsequently, a dose-response curve was constructed. The half inhibition (IC_{50}) for haditoxin and α-bungarotoxin was calculated to be 1.85 ± 0.39 μM and 100.5 ± 22.5 nM) (**Fig. 3.6**) respectively. A comparison of

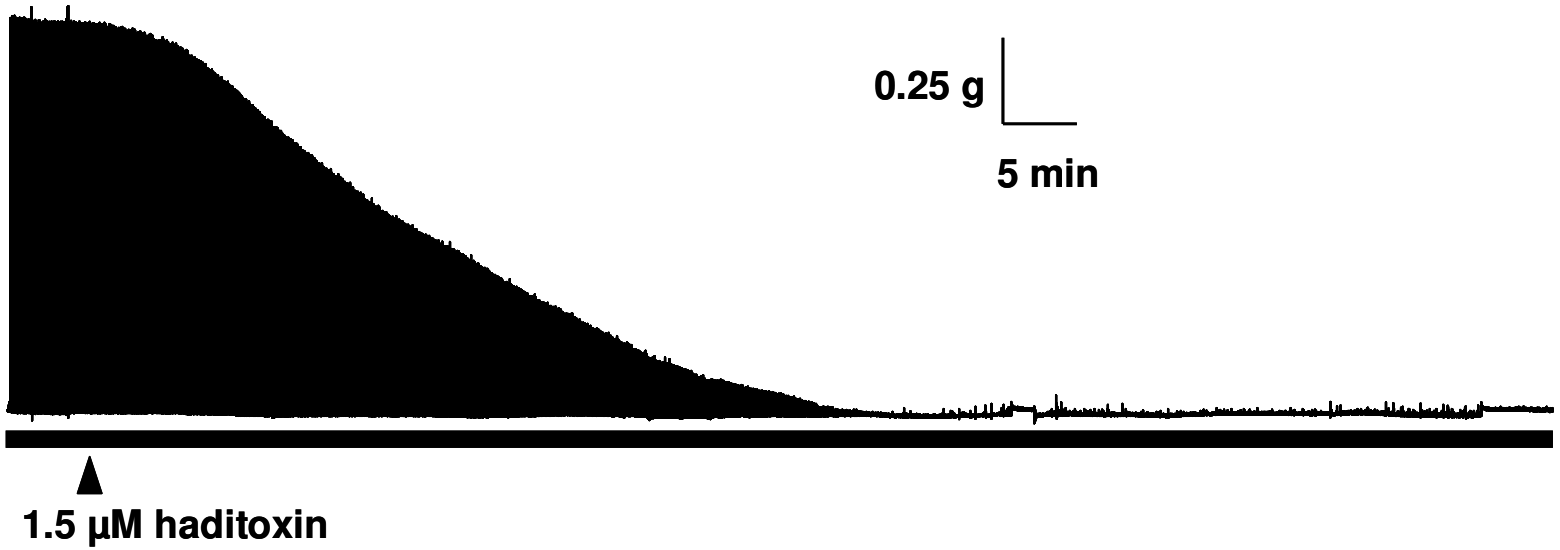

Figure 3.7: Effect of haditoxin on the twitch response of RHD elicited by nerve stimulation.

A segment of tracing showing the effect of haditoxin (1.5 µM) on rat anococcygeus muscle preparations (CBCM) (n=3). Twitch response of the muscle was elicited by electrical field stimulation (EFS), which is indicated by the black bar. The vertical bar represents the magnitude of twitch response in gram tension and the horizontal bar depicts the time in minute.

both the IC_{50} revealed that haditoxin was about ~18 times less potent on mammalian (RHD) neuromuscular junction.

3.3.7 Reversal of neuromuscular blockade produced by haditoxin

Reversibility of the neuromuscular blockade produced by haditoxin was tested for both the preparations (CBCM and RHD) with intermittent washing (indicated by black arrows in **Fig 3.8** and **3.9**). Partial recovery of the nerve evoked twitch response (~60% recovery in 120 min) was observed in the CBCM (**Fig. 3.8**) but not in the RHD (**Fig. 3.9**). In contrast, the neuromuscular blockade produced by α-bungarotoxin was practically irreversible even after prolonged washing. The reversibility was also assessed by the addition of anticholinesterase neostigmine which transiently reverses the neuromuscular blockade produced by haditoxin for CBCM (**Fig 3.10**) but failed to produce a long-lasting effect. These results indicate that, unlike typical α-neurotoxins like α-bungarotoxin, haditoxin exhibits partial reversibility in action, at least in the CBCM. The reversibility of haditoxin on CBCM was compared to that of a practically irreversible neurotoxin (α-bungarotoxin) and a readily reversible neurotoxin (candoxin) (Nirthanan *et al*, 2002) (**Fig. 3.11**).

3.3.8 Effect of haditoxin on human nAChRs

Since haditoxin blocked the muscle activity of the CBCM and RHD, we examined its activity on the human αβδε-nAChRs. Xenopus oocytes expressing human receptors were challenged with different concentrations of haditoxin. Haditoxin at a concentration of 10 μM completely inhibited the ACh-induced currents

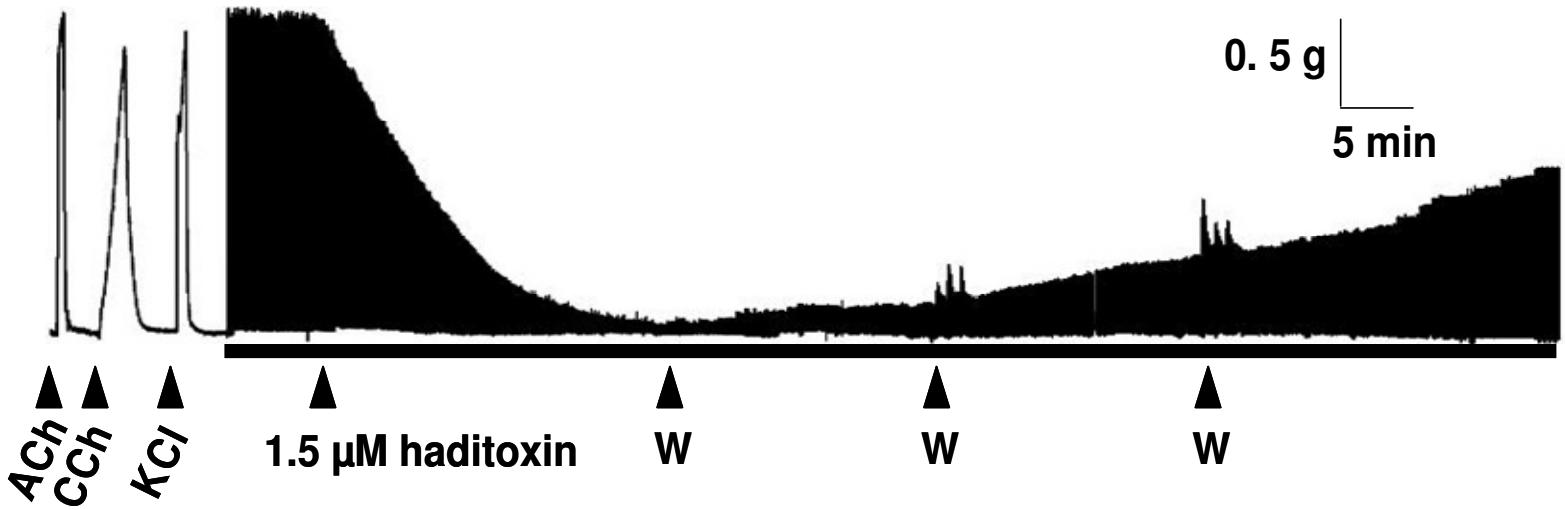

Figure 3.8: Reversibility of the nerve evoked twitch response blockade produced by haditoxin in CBCM.

Segment of tracing showing the complete blockade of nerve evoked twitch response in chick biventor cervicis muscle produced by haditoxin (1.5 µM). After the complete blockade was achieved, haditoxin was removed from the bath chamber by extensive washing (3 cycles of 30 sec on 30 sec off pulse with a flow rate of 20 ml/min) with fresh Krebs solution and it was continued at 30 min intervals over a period of 120 minutes (indicated as 'W' in the tracing). The vertical bar represents the magnitude of twitch response in gram tension and the horizontal bar depicts the time in minute.

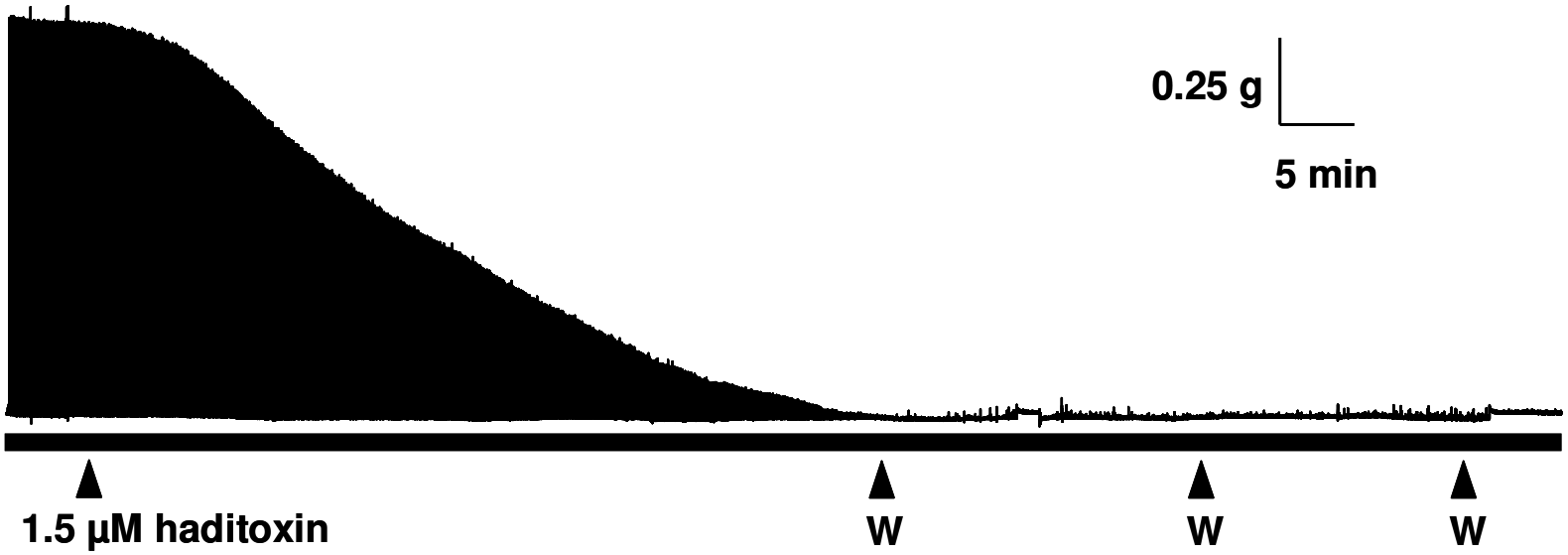

Figure 3.9: Reversibility of the nerve evoked twitch response blockade produced by haditoxin in RHD.

Segment of tracing showing the complete blockade of nerve evoked twitch response in rat hemidiaphragm muscle produced by haditoxin (1.5 µM). After the complete blockade was achieved, haditoxin was removed from the bath chamber by extensive washing (3 cycles of 30 sec on 30 sec off pulse with a flow rate of 20 ml/min) with fresh Krebs solution and it was continued at 30 min intervals over a period of 120 minutes (indicated as 'W' in the tracing). The vertical bar represents the magnitude of twitch response in gram tension and the horizontal bar depicts the time in minute.

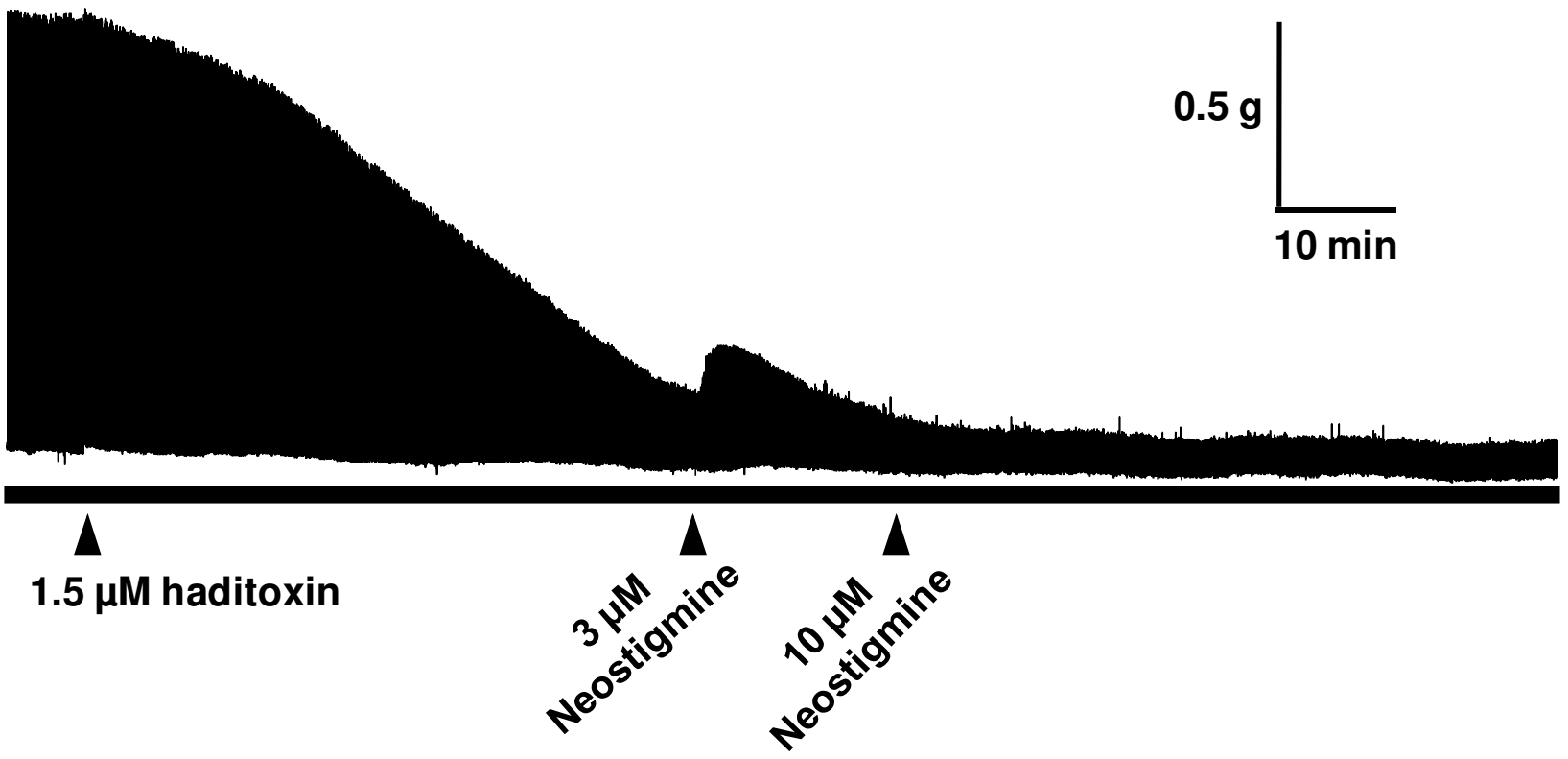

Figure 3.10: Reversibility of the nerve evoked twitch response blockade produced by haditoxin in CBCM by neostigmine.

Segment of tracing showing the blockade of nerve evoked twitch response in chick biventor cervicis muscle produced by haditoxin (1.5 µM). After the 80% blockade was achieved, neostigmine (anticholinesterase) was added to the bath chamber cumulatively up to 10 µM at the points indicated. The vertical bar represents the magnitude of twitch response in gram tension and the horizontal bar depicts the time in minute.

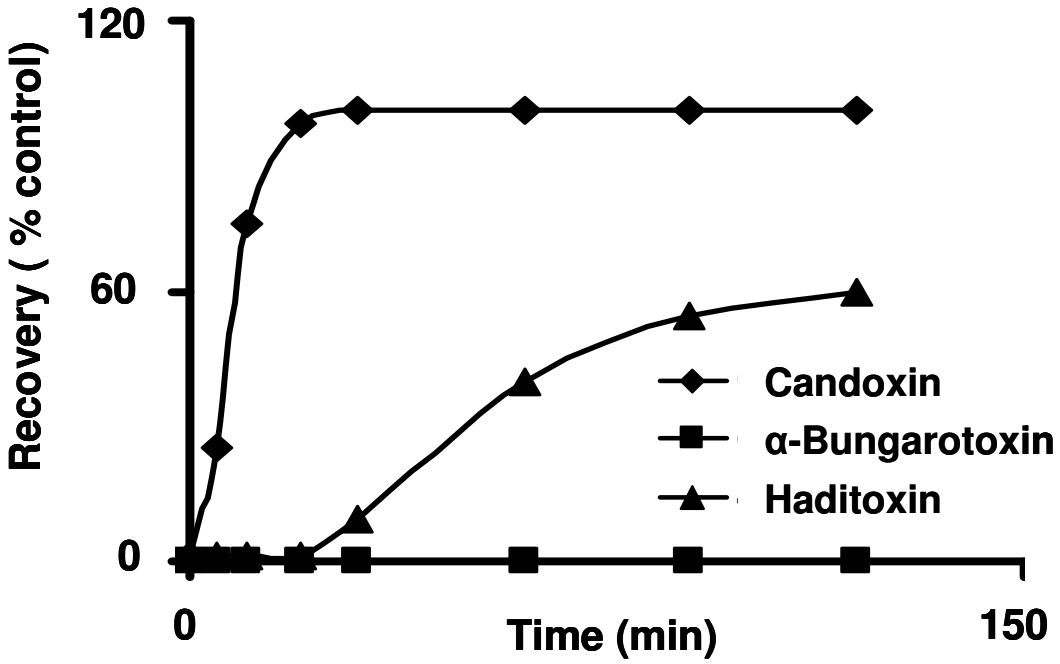

Figure 3.11: Comparative reversibility profile of haditoxin, α-bungarotoxin and candoxin on CBCM.

The reversibility of haditoxin was compared with α-bungarotoxin, a practically irreversible neurotoxin and candoxin, a readily reversible neurotoxin on chick biventer cervicis muscle.

produced by human αβδε-receptors (**Fig. 3.12 A**), whereas when applied alone no detectable current was produced. The inhibition of the ACh-induced currents by haditoxin was practically irreversible within 8 min washout. A dose-response curve was constructed and the IC_{50} value was found to be 550 nM (n=13) (**Fig. 3.12 B**). The inhibition curve was adequately described by a single Hill equation with a Hill coefficient (nH) of 0.7. This result is in good agreement with the findings on e*x vivo* studies with RHD as discussed earlier.

Further to determine the subtype specificity, we tested the activity of haditoxin on neuronal nACRs (α_7-, $\alpha_3\beta_2$- and $\alpha_4\beta_2$-nAChRs). Application of haditoxin alone to the oocytes expressing α_7-nAChRs produced no effect. However, 10 μM of haditoxin completely blocked the ACh-induced current produced by the α_7-receptors (**Fig 3.13 A**). Similar to the αβδε-receptors the blockade of the ACh-induced current observed by haditoxin on α_7-nAChRs was irreversible (**Fig 3.13 A**). An IC_{50} value of 180 nM (n=4) from the inhibition curve **(Fig 3.13 B)** with a Hill coefficient of 0.8. As shown in figure 3.14 A, haditoxin (10 μM) fully blocked the ACh-induced current produced by the $\alpha_3\beta_2$-nAChRs but notably, this blockade was fully reversible compared to the long lasting blockade observed at α_7-nAChRs (**Fig. 3.13 A**). The construction of the inhibition curve revealed an IC_{50} value of 500 nM (n=4) for $\alpha_3\beta_2$-nAChRs with a nH value of 1.1 (**Fig 3.14 B**). Finally, we tested the effect of haditoxin on $\alpha_4\beta_2$-nAChRs. Application of 10 μM haditoxin blocked only 70% of the ACh-induced current with partial reversibility (**Fig. 3.15 A**). The IC_{50} value of the blockade is in the micromolar range (IC_{50} = 2.6 μM, n=3) (**Fig. 3.15 B**). These results exhibited that haditoxin had a higher potency for α_7-nAChRs than for the other nAChRs. IC_{50} values for αβδε- and

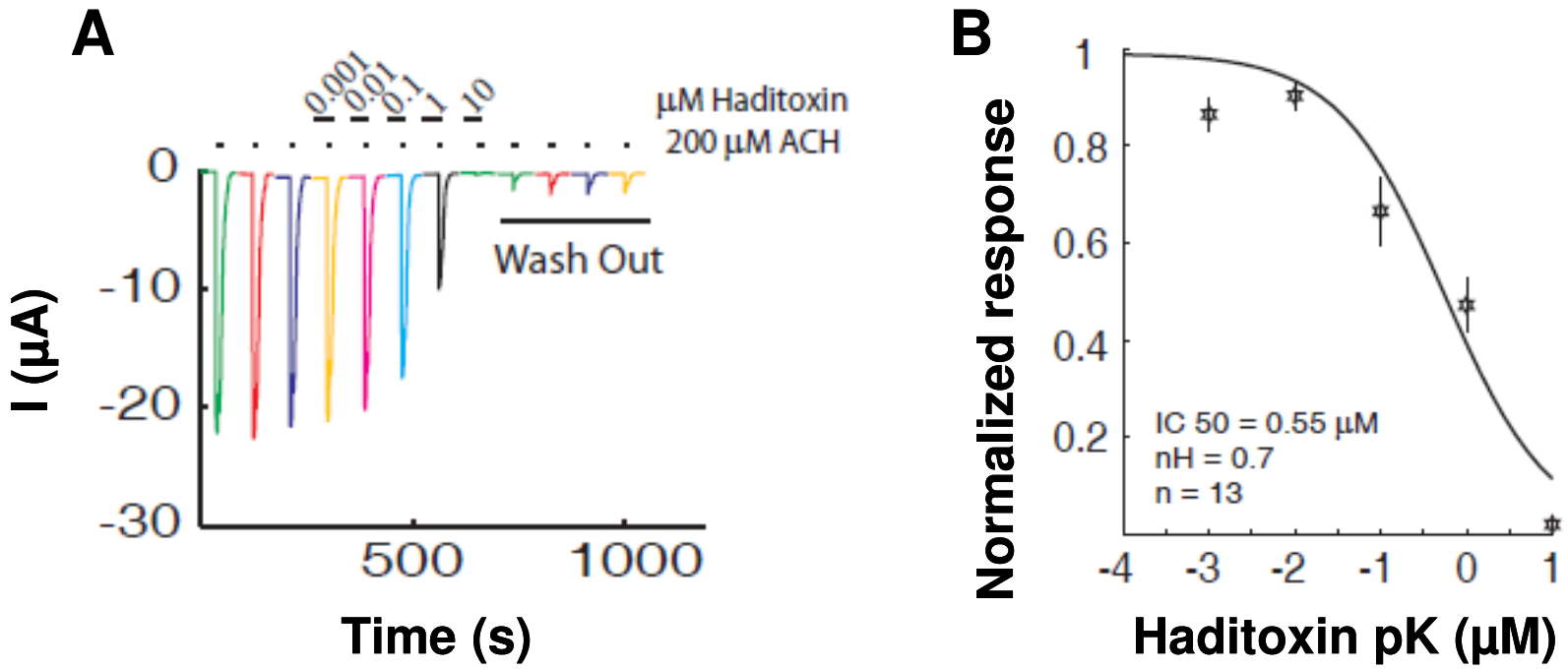

Figure 3.12: Effect of haditoxin on human αβδε-nAChRs expressed in *Xenopus* oocytes.

(A) Inhibition of ACh-induced currents in αβδε-nAChRs (neuromuscular junction). 200 µM was used to activate αβδε-nAChRs. First three traces are controls, followed by 2 minutes exposure to several haditoxin concentrations ranging from 10 nM to 10 µM. (B) Inhibition curves of the fitted data, IC_{50} and Hill coefficient (nH) for αβδε-nAChRs were 0.55 µM and 0.7.

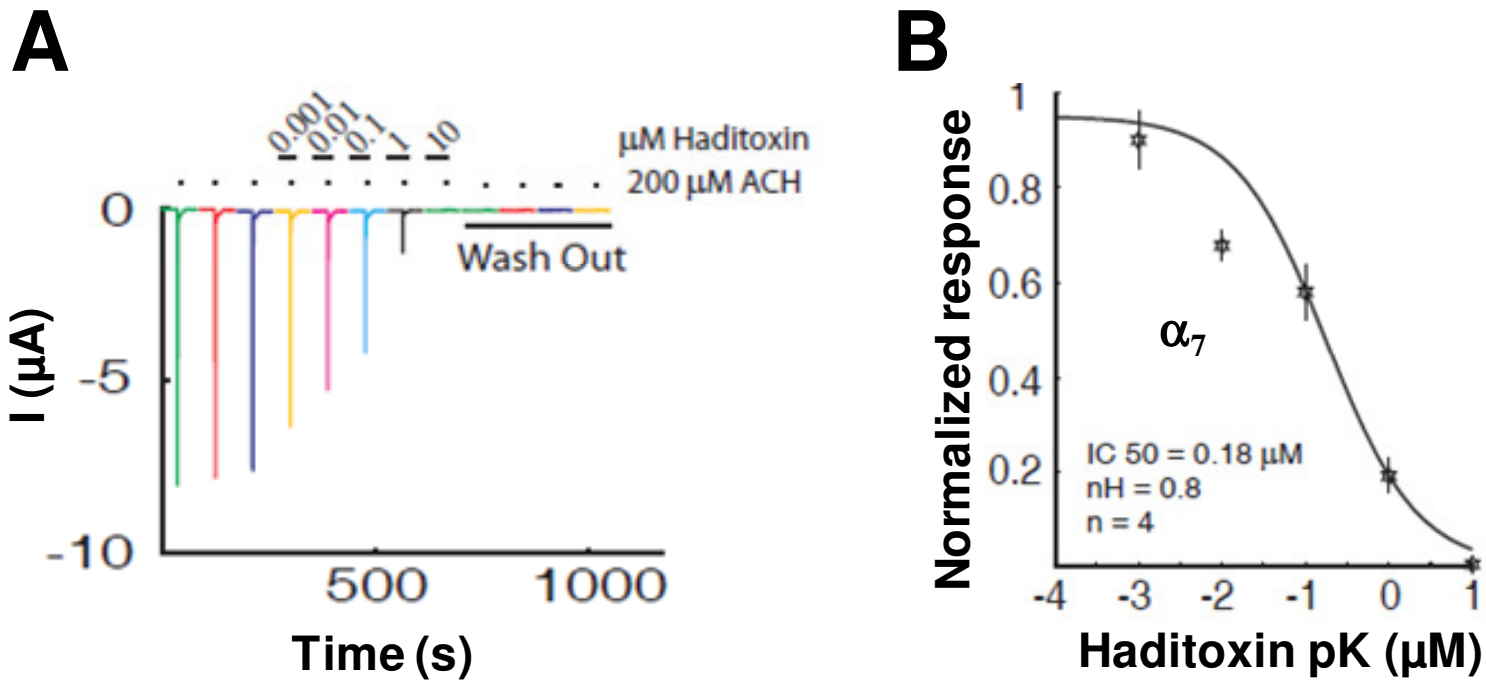

Figure 3.13: Effect of haditoxin on human α_7-nAChRs expressed in *Xenopus* oocytes.

(A) Inhibition of ACh-induced currents in α_7-nAChRs. 200 µM was used to activate α_7-nAChRs. First three traces are controls, followed by 2 minutes exposure to several haditoxin concentrations ranging from 10 nM to 10 µM. (B) Inhibition curves of the fitted data, IC_{50} and Hill coefficient (nH) for α_7-nAChRs were 0.18 µM and 0.8.

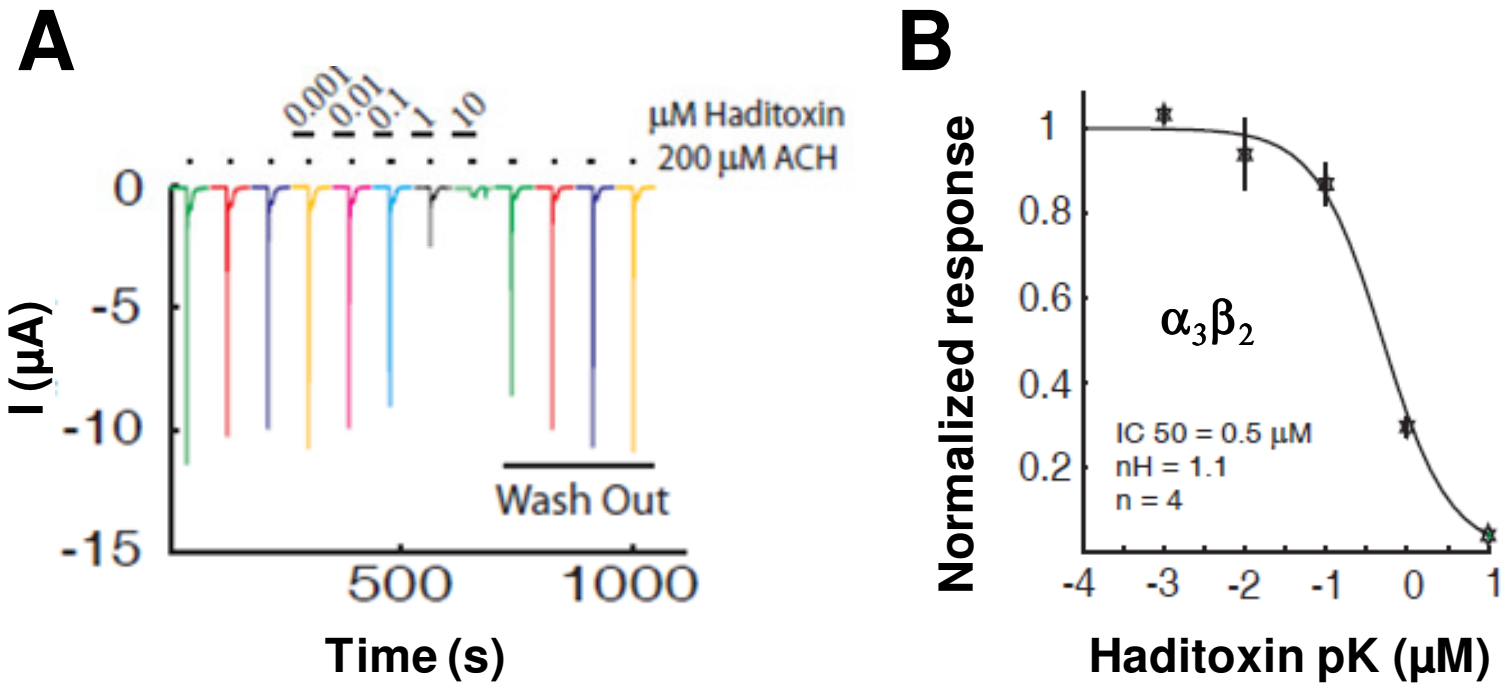

Figure 3.14: Effect of haditoxin on human $\alpha_3\beta_2$-nAChRs expressed in *Xenopus* oocytes.

(A) Inhibition of ACh-induced currents in $\alpha_3\beta_2$-nAChRs. 200 µM was used to activate $\alpha_3\beta_2$-nAChRs. First three traces are controls, followed by 2 minutes exposure to several haditoxin concentrations ranging from 10 nM to 10 µM. (B) Inhibition curves of the fitted data, IC_{50} and Hill coefficient (nH) for $\alpha_3\beta_2$-nAChRs were 0.5 µM and 1.1.

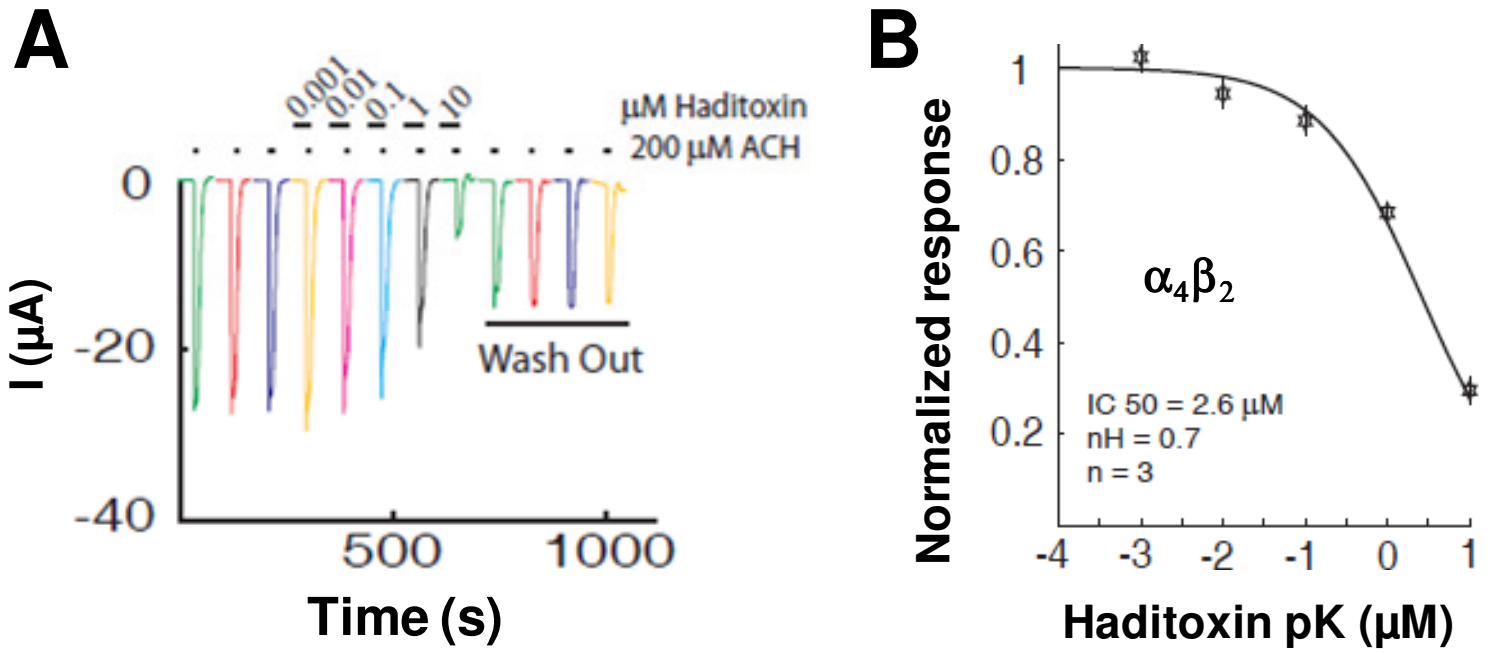

Figure 3.15: Effect of haditoxin on human $\alpha_4\beta_2$-nAChRs expressed in *Xenopus* oocytes.

(A) Inhibition of ACh-induced currents in $\alpha_4\beta_2$-nAChRs. 200 µM was used to activate $\alpha_4\beta_2$-nAChRs. First three traces are controls, followed by 2 minutes exposure to several haditoxin concentrations ranging from 10 nM to 10 µM. (B) Inhibition curves of the fitted data, IC_{50} and Hill coefficient (nH) for $\alpha_4\beta_2$-nAChRs were 2.6 µM and 0.7.

$\alpha_3\beta_2$-nAChRs were in the same nanomolar range, whereas for $\alpha_4\beta_2$-nAChRs was in the micromolar range (**Table 3.2**). However, further experiments will be necessary to discriminate between the different mechanisms of blockade and recovery.

Table 3.2: Effect of haditoxin on human nicotinic receptors expressed in *Xenopus* oocytes

Nicotinic receptor subtype	IC_{50} (μM)	Hill coefficient (nH)	Number of experiments (n)
αβδε-nAChRs (muscle)	0.55	0.7	13
α_7-nAChRs (neuronal)	0.18	0.8	4
$\alpha_3\beta_2$-nAChRs (neuronal)	0.5	1.1	4
$\alpha_4\beta_2$-nAChRs (neuronal)	2.6	0.7	3

3.4 DISCUSSION

Nonenzymatic neurotoxins from snake venom belonging to the 3FTx family consist of closely related polypeptides with a MW range of 6500 to 8000 Daltons. Functionally, most interfere with cholinergic neurotransmission with high affinity and are highly specific for different subtypes of muscarinic or nicotinic cholinergic receptors (for details see, chapter 1). This underscores their immense potential as lead molecules in drug discovery and as research tools in the detailed characterization of different cholinergic receptor subtypes.

In this chapter, we have described the pharmacological characterization of a novel neurotoxin, haditoxin isolated from the venom of *O. hannah*. Haditoxin belongs to the nonenzymatic three-finger toxin family of snake venom proteins. Based on the observed sequence homology with muscarinic toxins and their homologs when haditoxin was examined for muscarinic activity, the protein failed to show any effect on muscarinic receptors present in the smooth muscle of rat ileum and anococcygeus muscle. Under physiological conditions the contractile response elicited by cholinergic agonist in rat ileum is mediated by M3-subtype of muscarinic receptors. Activation of these receptors by ACh activates the G-protein which in turn through a series of secondary messenger molecules leads to an increase of intracellular calcium levels resulting in contraction of the smooth muscle (Eglen *et al*, 1994). Under exceptional circumstances M2 receptors in the ileum may produce an indirect contractile response by opposing the relaxing effect of cGMP (Ehlert and Thomas, 1995). The anococcygeus muscle preparation consists of cholinergic (muscarinic receptor), adrenergic and nitrergic innervation. The cholinergic innervations in this muscle consist of a single type of muscarinic

receptors (M3-subtype) (Weiser *et al*, 1997). It is obvious from the experimental results that haditoxin did not interact with the M_3-subtype of muscarinic receptors present in the both the smooth muscle preparations. Therefore, it is likely that the observed sequence similarity of haditoxin with muscarinic toxin homologs is probably coincidental due to either phylogeny or structure, including the presence of the core disulfide bridges, and not the function. This demands further investigation, including electrophysiological studies and/or binding assays on other subtypes of mAChRs.

Typical symptoms of peripheral neurotoxicity (Warrell *et al*, 1983; Laothong and Sitprija, 2001), which are very similar to the observations following the experimental envenomation by curare-mimetic neurotoxins (Chang *et al*, 1979), were observed in live mice with the administration of haditoxin. There was complete absence of any hemorrhage in the internal organs, indicating the fact that haditoxin might not have any cytolytic activity unlike few neurotoxins isolated from *D. r. russelli* and *O. hannah* venom (Shelke *et al*, 2002; Jing *et al*, 2006). This suggests, there is a possibility that haditoxin might exert its biological function by affecting the neurotransmission like the curare-mimetic neurotoxins. They are referred to as "curare-mimetic toxins" because of their similarity in mode of action to that of the arrow poison ‘curare’ (Endo and Tamiya, 1991). They interact with the postsynaptic acetylcholine receptors in the neuromuscular junction and block the interaction of the receptors with the endogenous ligand such as- ACh. This interaction subsequently prevents the opening of the ion channel associated with the acetylcholine receptor and results in neuromuscular blockade (Changeux *et al*, 1970 and Paterson & Nordberg, 2000) producing

paralysis. The snake venom curare-mimetic neurotoxins (also known as α-neurotoxins) are divided into two major groups: the short-chain α-neurotoxins, (60 to 65 amino acids long), which are arranged in a single polypeptide chain and cross-linked by four disulphide bridges and the long-chain α-neurotoxins, (66 to 87 amino acids long), which are also arranged in a single polypeptide chain but are cross-linked by five disulphide bridges (Dufton and Harvey, 1989 and Endo and Tamiya, 1991). Both the short and the long α-neurotoxins act as antagonists to acetylcholine receptors, preventing the interaction between ACh and postsynaptic receptors, resulting neuromuscular blockade.

A sequence comparison of haditoxin (65 amino acids and four disulfide bridges) with the α-neurotoxins showed a similarity of 54-60% with the short-chain neurotoxins (**Fig. 2.12** in chapter 2) and 52-57% with the long-chain neurotoxins (**Fig. 2.13** in chapter 2). The identity of haditoxin was about 10% higher for short-chain neurotoxin when compared to long-chain neurotoxins. This could be because of the resemblance of the primary structural characteristics of haditoxin (65 amino acid residues with 4 conserved disulfide bridges) with short-chain neurotoxins which are known to be composed of 60-65 amino acid residues with four intramolecular disulfide bridges. Additionally, it was observed that some of critical residues involved in the recognition of nAChRs by the α-neurotoxins (Endo and Tamiya, 1991; Pillet *et al*, 1993; Tremeau *et al*, 1995; Antil *et al*, 1999; Teixeira-Clerc *et al*, 2002; Fruchart-Gaillard *et al*, 2002; Bourne *et al*, 2005; Dellisanti *et al*, 2007) were conserved in haditoxin (Trp29, Asp31 and Arg33). This led us to investigate of neuromuscular blockade properties of haditoxin. It produced a potent postsynaptic neuromuscular blockade of the avian (IC_{50} = 0.27

± 0.07 μM) and mammalian (IC_{50} = 1.85 ± 0.39 μM) muscle (αβγδ) nAChRs (**Fig. 3.8 and 3.9**). This proved the fact that haditoxin has exerted its biological function by blocking the neuromuscular junction, similar to that of α-neurotoxins, in the mice which is followed by paralysis and subsequent death of the animal.

Interestingly, the reversibility of this neuromuscular blockade produced by haditoxin in the isolated tissues was taxa-specific; it was partially reversible by washing on the avian (chick) neuromuscular junction, whereas it was almost irreversible on the mammalian (rat) neuromuscular junction. Earlier, we reported taxa-specific neurotoxicity of denmotoxin from *Boiga dendrophila* (Pawlak *et al*, 2006) and irditoxin from *Boiga irregularis* (Pawlak *et al*, 2009). Taxa-specificity manifests the natural targeting of the venom toxins towards their prey *(*Pawlak *et al*, 2009; Barlow *et al*, 2009; Daltry *et al*, 1996; Pahari *et al*, 2007a). Venom composition of snake species is closely associated with its diet. Snakes from the *Boiga* sp. mainly feeds on the non-mammalian prey like birds (Prado-Franceschi *et al*, 1996; Mackessy *et al*, 2006; Pawlak *et al*, 2006; Pawlak *et al*, 2009), whereas elapids including the king cobra, mainly prey on snakes and rodents, and only occasionally and opportunistically on birds (Mehrtens, 1987; Coborn, 1991). Venom compositions of snakes are known to be dependent on prey specificity, in order to ensure efficiency in their capture and killing (Daltry *et al*, 1996). Therefore, the taxa-specific reversibility of the neuromuscular blockade produced by haditoxin is likely due to the natural species-specificity of the king cobra venom and not because of low toxicity.

In electrophysiological studies, it was an antagonist of muscle (αβδε) (IC_{50} = 0.55 μM), as well as neuronal α_7- (IC_{50} = 0.18 μM), $\alpha_3\beta_2$- (IC_{50} = 0.50 μM) and $\alpha_4\beta_2$-

(IC_{50} = 2.60 μM) nAChRs (**Fig 3.12 to 3.15**). Interestingly, haditoxin exhibited a novel pharmacology with combined blocking activity on muscle (αβδε) as well as neuronal (α_7, $\alpha_3\beta_2$ and $\alpha_4\beta_2$) nAChRs but with the highest potency on α_7-nAChRs. Although the primary structural features of haditoxin was similar to that of the short chain α-neurotoxins, which recognize only the muscle subtype of nAChRs, but haditoxin targets both muscle and neuronal nAChRs. Hitherto, the neuronal nAChRs are known to be recognized by either long-chain α-neurotoxins targeting the α_7-nAChRs (Servent *et al*, 1997; Servent *et al*., 2000) or κ-neurotoxins targeting the $\alpha_3\beta_2$- and $\alpha_4\beta_2$-nAChRs (Grant and Chiappinelli, 1985; Wolf *et al*, 1988). Both long-chain α-neurotoxins and κ-neurotoxins possess an additional fifth disulfide bridge at the tip of loop II which is reported to be critical to interact with neuronal nAChRs (Servent *et al*, 1997). Haditoxin is the first one to retain the functional properties of both long-chain α-neurotoxins and κ-neurotoxins although it lacks the fifth disulfide bridge as well as the long C-terminal tail of long-chain α-neurotoxins.

The blockade produced by haditoxin on $\alpha_3\beta_2$-nAChRs was fully reversible (**Fig 3.14 A**) whereas the blockade observed at α_7-nAChRs (**Fig. 3.13 A**) was long lasting and practically irreversible. This suggests that the dissociation of haditoxin from the $\alpha_3\beta_2$-nAChRs is faster when compared to the α_7-nAChRs. Hence, the dissociation constant (K_{Off}) value of haditoxin for the α_7 receptor is much smaller than at $\alpha_3\beta_2$-nAChRs. Although these two receptors (α_7 and $\alpha_3\beta_2$) display about equivalent IC_{50}'s their respective association constant (K_{On}) values towards haditoxin can be significantly different. However, the experimental protocol used herein prevents the detailed analysis of the K_{On} and K_{Off} values and further

binding experiments are needed to elucidate these values. An additional difference between these two receptors resides in their structural composition. As the α_7-nAChRs are composed of five α-subunits (this subunit contains the ligand binding site) thus it is thought that they display five identical ligand binding sites (Rang *et al*, 2003), while only two binding sites are proposed for the $\alpha_3\beta_2$-nAChRs (because these receptors are composed of two α_3-subunits and three β_2-subunits) (Colquhoun and Patrick, 1997; Itier and Bertrand, 2001). The difference in number of binding sites and effects on competitive blockade was previously discussed for α_7- and $\alpha_4\beta_2$-nAChRs showing significant functional outcomes (Palma *et al*, 1996). Interestingly, the electrophysiological results showed that haditoxin was almost 3-fold more potent to block ACh-induced responses mediated by α_7- (IC_{50} = 180 nM) compared with αβδε-. and $\alpha_3\beta_2$-nAChRs and only 70% blockade of ACh-induce current was observed with $\alpha_4\beta_2$-nAChRs. The reversibility profile was also different for the various subtypes which explain that the molecular mechanism of interaction for haditoxin with these receptors is entirely different. However, further experiments will be necessary to discriminate between the different mechanisms of blockade and recovery.

3.5 CONCLUSIONS

In summary, we have described the mechanism of action of haditoxin in this chapter in detail. Its unique functional features reside in its novel pharmacological profiles for the two subtypes of nicotinic receptors. Till date, only long-chain α-neurotoxins (α-bungarotoxin, α-cobratoxin) and κ-neurotoxins (κ-bungarotoxin) have been reported to bind with neuronal nAChRs with high affinity. The additional disulfide bridge present in these toxins play a vital role for the interaction. Haditoxin is distinctly an exception since it lacks the additional disulfide bond at the tip of middle loop but, nonetheless, blocks the neuronal receptors (α_7- and $\alpha_3\beta_2$-nAChRs) with nanomolar affinity. Moreover, primary structure-wise haditoxin is similar to short-chain α-neurotoxin whereas, unlike the conventional short-chain α-neurotoxin it interacts with the neuronal receptors with nanomolar affinity. Thus, this is the first report of a short-chain interacting with neuronal nAChRs. Finally, haditoxin is the first elapid neurotoxin to produce a taxa-specific blockade. These novel and interesting findings further led us to elucidate the structure as well as structure-function relationship of haditoxin (discussed in chapter 4 and 5).

Chapter Four

Biophysical and structural characterization of haditoxin

CHAPTER FOUR

Biophysical and structural characterization of haditoxin

4.1 INTRODUCTION

As discussed in the earlier chapters, with the unique functional properties, haditoxin is a novel member of the 3FTX family. Additionally, it was observed that during protein purification from crude venom, haditoxin eluted earlier compared to the other 3FTX members (discussed in chapter 1), which raises the possibility for this toxin to exist in an oligomeric state. Thus, there was a need to elucidate the structure of haditoxin, to clearly understand the biological function of this protein. Hitherto, the only available structural data for haditoxin was the information on its secondary structure as revealed by CD spectroscopy (discussed in chapter 2). Similar to all other 3FTXs haditoxin was also composed of predominantly β-sheet secondary structure. But this data was not enough to vividly understand the structure-function relationship of haditoxin. Hence, we proceed to determine the oligomeric nature of this protein using different biophysical techniques as well as the three-dimensional structure of this novel protein.

Several methods are employed to study the three-dimensional structures of proteins. The two techniques that have been widely used in structural biology to elucidate protein structure are: single-crystal X-ray diffraction and nuclear magnetic resonance (NMR) spectroscopy. X-ray crystallography is a long-standing and commonly used technique to determine three-dimensional structures of macromolecules. The technique is based on the scattering of X-rays by the

electrons in the atoms forming the crystal, which generates particular diffraction pattern. From this diffraction pattern scientists can reconstruct the position of each atom in the crystal and thereby, a three-dimensional map of the molecule can be made. To solve the three-dimensional structure of a protein using X-ray crystallography it is mandatory to obtain a good quality crystal but, not all proteins can be crystallized. An alternative technique to analyze the structure of proteins in solution is nuclear magnetic resonance (NMR) spectroscopy. It is based on the principle that the nuclei of some elements' atoms (such as hydrogen) resonate when they are placed in a powerful magnetic field. Thus, when a molecule containing such atoms, like- protein, peptides, organic polymers etc, are placed in a powerful magnetic field nuclear magnetic resonance occurs. The NMR signal is measured as chemical shifts of the atoms' nuclei in the molecule. The chemical shift of a nucleus depends on the chemical environment of that specific atom to which the nucleus belongs. The chemical environment in turn is defined by the nearby atoms and on their distances from each other. The signals that NMR produces are converted to a set of distances between specific pairs of atoms and this data is further used to generate models of possible structures. Thus, NMR generates a number of possible conformations of protein and the three-dimensional structure of a protein is the average of all these conformations rather than a single structure.

In this chapter, first we describe the biophysical techniques used to determine the oligomeric state of the protein followed by the crystallization, X-ray diffraction and data collection of haditoxin. With the purified protein gel filtration chromatography was performed to gain an idea about the relative molecular

weight (Mr) of haditoxin and thereby the oligomeric state of the protein. Further, we also tried to run a SDS-PAGE using a cross-linker to trap any possible oligomers. To elucidate the three-dimensional structure of this protein we set up crystal drops using different crystallization screens. The crystals were optimized further and diffracted using X-ray. Thus, we obtained the three-dimensional structure of haditoxin which was further analyzed for the presence of novel structural elements.

4.2 MATERIALS AND METHODS

4.2.1 Proteins and reagents

Haditoxin was purified from the venom of *O. hannah* as described in chapter 2. All the crystallization screens (Hampton and Index screens), crystallization trays, coverslips and grease were purchased from Hampton Research (Aliso Viejo, CA). The PACT Suite for crystallization was purchased from QIAgen (Hilden, Germany). The superdex 75 column (1 cm x 30 cm) was purchased from GE Healthcare Life Sciences (Piscataway, NJ, USA). The protein markers used for gel filtration studies were purchased from Sigma-Aldrich (St. Louis, MO, USA) and the SDS-PAGE markers were bought from Bio-Rad Laboratories (Hercules, CA, USA). The cross-linker Bis(sulfosuccinimidyl) suberate were purchased from Pierce (Rockford, IL, USA). All other chemicals and reagents used were of analytical grade.

4.2.2 Gel filtration chromatography

The oligomeric states of the protein were examined by gel filtration chromatography on a Superdex 75 column (1 cm x 30 cm) equilibrated with 50 mM Tris-HCl buffer (pH 7.4) using an ÄKTA purifier system at a flow rate of 0.6 ml/min. Calibration was done using bovine serum albumin (66 kDa), carbonic anhydrase (29 kDa), cytochrome C (12.4 kDa), aprotinin (6.5 kDa) and blue dextran (200 kDa) as molecular weight markers. Native protein (0.25-10 µM) as well as samples (0.25-10 µM) treated 0.6% sodium dodecyl sulfate (SDS) (2 h of incubation at room temperature) (Chiappinelli and Lee, 1985) were loaded separately onto the column and respective elution profiles were recorded. For the

SDS treated samples the column was equilibrated with the same buffer as mentioned above containing 0.1% SDS.

4.2.3 CD spectroscopy

Far-UV CD spectra (260-190 nm) for the protein samples with/without SDS were recorded using a Jasco J-810 spectropolarimeter (Jasco Corporation, Tokyo, Japan). All measurements were carried out at room temperature using a 0.1 cm path length capped cuvette. The instrument optics and cuvette chamber were continuously flushed with 10 L of nitrogen/min before and during the recording of the spectra to provide an oxygen-free environment. The spectra were recorded using a scanning speed of 50 nm/min, a resolution of 0.1 nm and a bandwidth of 1 nm. A total of three scans were recorded and averaged for each spectrum, and the baseline was subtracted with the blank. All samples were dissolved 50 mM Tris-HCl buffer (pH 7.4) with (0.6%) or without SDS.

4.2.4 Electrophoresis

Tris-Tricine SDS-PAGE (Schagger and von Jagow, 1987; Schagger, 2006) of the protein of interest in the presence or absence of cross-linker Bis(sulfosuccinimidyl) suberate (BS3) (Jennings and Nicknish, 1985; Staros, 1982; Staros and Anjaneyulu, 1989) was performed on a 12% gel (composition described in Appendix figure A.3), under reducing conditions, using Bio-Rad Mini-Protean II electrophoresis system. The concentration of BS3 used was 5 mM. The protein bands were visualized by Coomassie Blue staining (Merril, 1990).

4.2.5 Crystallization of haditoxin

Crystallization conditions for the protein were screened with Hampton Research screens, index screen and Pact suite screen using hanging-drop vapor-diffusion method. Lyophilized protein was dissolved in 10 mM Tris-HCl buffer pH 7.4 with 100 mM NaCl. The protein concentration was kept at 10 mg/ml and the drops were prepared by mixing equal volumes (1 µl) of protein solution (dissolved in 25 mM Tris buffer pH 7.4) and crystallization solutions. 500 µl reservoir solution was placed in each well. Crystallization experiments were performed at room temperature 297 K (24 °C). Small rod-shaped crystals were formed within 2-3 days. Further, optimization was done for few weeks to produce diffraction quality crystals. They were briefly soaked in the reservoir solution supplemented with 10% glycerol as cryo-protectant, prior to the X-ray diffraction data collection. Then these crystals were flash-frozen in a nitrogen cold stream at 100 K (-173 °C).

4.2.6 X-ray diffraction and data collection

The crystals were picked up with a nylon cryo-loop and frozen at 100 K in a nitrogen-gas cold stream. Diffraction up to 1.55 Å was obtained using a CCD detector mounted on a Bruker V8 rotating anode generator (Bruker AXS, Madison, WI, USA). A complete data set was collected, processed and scaled using the program HKL2000 (Otwinowski and Minor, 1997).

4.3 RESULTS

4.3.1 Haditoxin is a dimer

During the gel filtration of the crude venom we observed that haditoxin eluted earlier compared to other 3FTXs (**Fig. 2.2**, most of the 3FTXs elutes in peak 3 whereas haditoxin elutes in peak 2). This led us to investigate the oligomeric states of this protein. So, we carried out analytical gel filtration experiments using a Superdex G-75 column. Protein at concentrations (0.25 to 10 μM) covering the IC_{50} in CBCM (0.27 ± 0.07μM) and RHD (1.85 ± 0.39 μM) preparations, was loaded onto the column. At all of these concentrations, the presence of a single peak corresponding to a relative molecular weight (Mr) of 16.25 kDa was observed **(Fig. 4.1)**, supporting the existence of a dimeric species (the monomeric mass is ~7535 Da as observed in ESI-MS, discussed in chapter 2).

To find out the nature of interaction between the monomers, we observe the effect of SDS on dimerization, we treated the protein (0.25 to 10 μM) with SDS (0.6% w/v) and eluted using the same gel filtration column. SDS is a well known anionic surfactant which is commonly used as detergent. In biochemistry, it is used to disrupt any non-covalent interaction in the proteins, denaturing them, and causing the molecules to lose their native shape (conformation) (Shapiro *et al*, 1967). In presence of SDS, haditoxin eluted out as a single peak with a Mr of 8.16 kDa **(Fig. 4.1)** similar to the monomeric species, which indicates the involvement of non-covalent interactions in the dimerization process.

To elucidate the consequence of dimerization on the secondary structure of protein we performed CD spectroscopy of the SDS-treated and non-treated protein samples. As observed in Fig. 4.2 the non-treated protein retains its original β-sheet

structure which confers that the dimerization has no effect on the secondary structure of the protein. Whereas, in presence of SDS the protein had lost its original conformation and acquired a random-coil structure as revealed by the intense minima around 203 nm in the CD spectrum (**Fig. 4.2**). This indicates that the overall conformation of the protein may play crucial role for dimerization.

The dimerization was further confirmed by Tris-Tricine SDS-PAGE analysis in the presence and absence of a cross-linker, BS3 **(Fig. 4.3)**. BS3 is a chemical cross-linker which is homobifunctional, water-soluble, non-cleavable and membrane impermeable. It forms an amine to amine covalent bond with the protein complexes and thus, the conjugate is available for further analysis (Knoller *et al*, 1991; Dihazi and Sinz, 2003). In the presence of BS3, both the dimeric and monomeric species were visualized **(Fig. 4.3, lane 1)** whereas only the monomeric species were observed in its absence **(Fig. 4.3, lane 2)**. Altogether, these results indicate the existence of haditoxin as a homodimer in solution at pharmacologically relevant concentrations and the dimerization occurs through non-covalent interactions. Further, as observed from the CD studies, the overall conformation of haditoxin has a high impact on the dimerization as the dimeric species did not appear with the loss of the native conformation upon addition of SDS.

4.3.2 X-ray crystal structure of haditoxin

In order to determine the three-dimensional structure of haditoxin we used X-ray crystallographic method. Diffraction quality crystals of haditoxin were obtained with 0.1 M Tris, pH 8.5, 20% v/v ethanol (Hampton Research crystal screen 2,

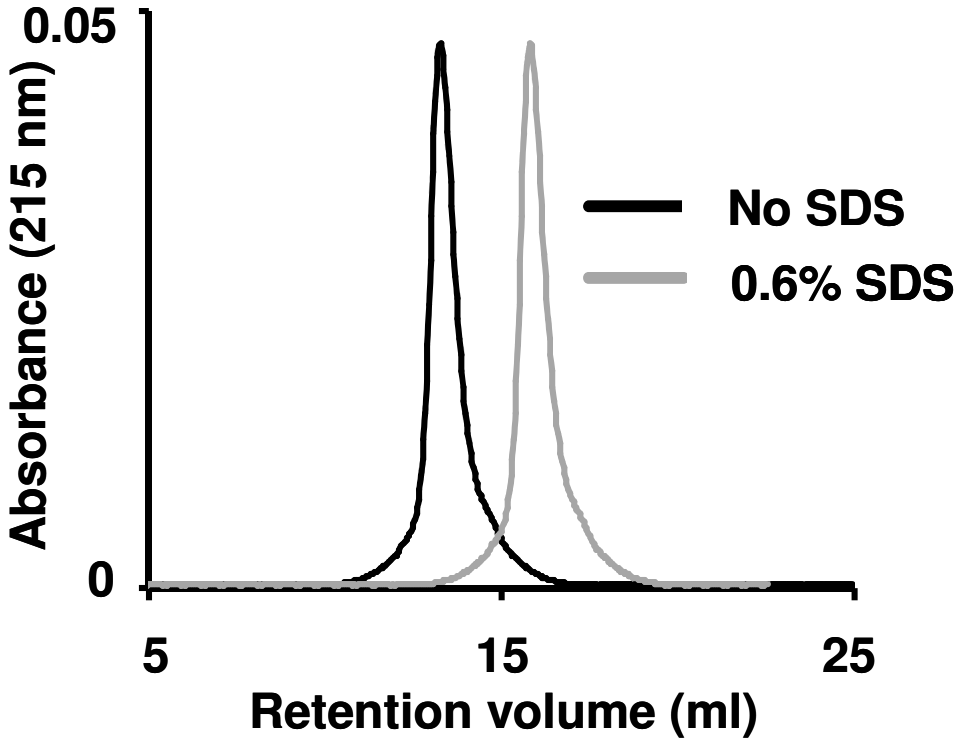

Figure 4.1: Dimerization of haditoxin observed in gel filtration studies.

Gel filtration profile of haditoxin with (gray) and without (black) SDS. 1 μM of haditoxin was loaded onto a Superdex 75 column (1 cm x 30 cm) equilibrated with 50 mM Tris-HCl buffer (pH 7.4). The protein was eluted out with the 50 mM Tris-HCl buffer (pH 7.4) or 50 mM Tris-HCl buffer (pH 7.4) containing 0.6% SDS at flow rate of 0.6 ml/min.

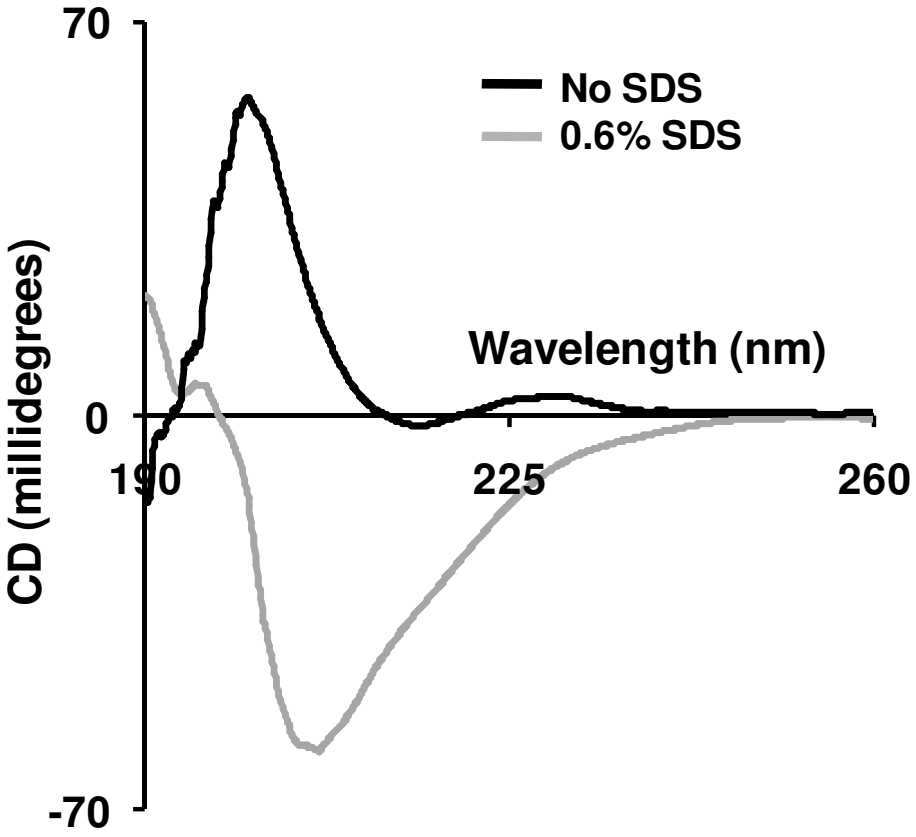

Figure 4.2: Effect of dimerization on secondary structure of haditoxin.

Far-UV CD spectrum of haditoxin (gray) and without (black) SDS. The protein (1 μM) was dissolved in 50 mM Tris-HCl buffer (pH 7.4) or 50 mM Tris-HCl buffer (pH 7.4) containing 0.6% SDS, and their CD spectra were recorded using a 0.1 cm path-length cuvette.

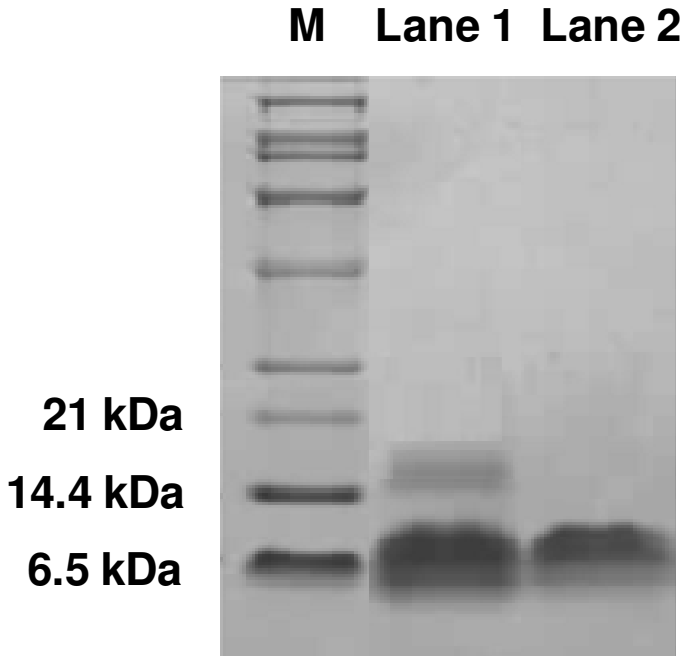

Figure 4.3: Tris-tricine SDS-PAGE analysis of haditoxin for dimerization.

Tris-tricine SDS-PAGE (12%) analysis of haditoxin with (lane 1) and without (lane 2) cross linker, bis(sulfosuccinimidyl)suberate (BS3). M is the marker lane. Concentration of BS3 used was 5 mM. Bands for monomer and dimer was observed in lane 1 with BS3 whether in lane 2 in the absence of BS3 band for monomer was only observed.

Table 4.1: X-ray data collection and refinement statistics

Data collection	
Cell parameters (Å)	a=37.27,b=41.29,c=40.98, β=106.4°
Space group	$P2_1$
Molecules /AU	2
Resolution range (Å)	50-1.55
Wavelength (Å)	1.5418
Observed reflections	82388
Unique reflections	17366
Completeness (%)	99.1(92.9)
Rsym (%)[a]	0.093
$I/\sigma(I)$	40.2(6.0)
Refinement and quality	
Resolution range (Å)	20-1.55
R_{work} (%) [b]	19.4
R_{free} (%)[c]	22.5
rmsd bond lengths (Å)	0.009
rmsd bond angles(deg)	1.274
Average B-factors ($Å^2$)	15.1
Number of protein atoms	130
Number of waters	117
Ramachandran plot (%)	
Most favored regions	88.9
Additional allowed regions	9.3
Generously allowed regions	1.9
Disallowed regions	0

[a] $R_{sym}=\sum|I_i-\langle I\rangle|/\sum|I|$, where I_i is the intensity of the *i*th measurement, and $\langle I\rangle$ is the mean intensity for that reflection.

[b] $R_{work}=\sum|F_{obs}-F_{calc}|/\sum|F_{obs}|$, where F_{calc} and F_{obs} are the calculated and observed structure factor amplitudes, respectively.

[c] R_{free}=as for R_{work}, but for 10 % of the total reflections chosen at random and omitted from refinement.

condition no. 44). Diffraction up to 1.55 Å was observed and the crystals belonged to the space group $P2_1$ **(Table 4.1)**.

4.3.3 Structure determination and refinement

The structure of haditoxin was solved by molecular replacement method (Molrep) (Vagin and Teplyakov, 1997). Initially, toxin-α, isolated from *Naja nigricollis* venom (Gilquin *et al*, 2003) was used as a search model (pdb code 1IQ9; sequence identity ~48%). The rotation and translation resulted in a correlation factor of 0.07 and R_{cryst} of 0.57. Further minimization in Refmac (Vagin *et al*, 2004) reduced the R factor to 0.42. An excellent quality electron density map was calculated at this stage which allowed to auto-build 90% of the haditoxin model with ARP/wARP (Perrakis *et al*, 1999). Resulting model with the electron density map was examined to manually build the rest of the model using Coot program (Emsley and Cowtan, 2004). After a few cycles of map fitting and refinement, we obtained an R factor of 0.194 (R_{free}=0.225) for reflections $I>\sigma I$ within 20-1.55 Å resolution. Throughout the refinement **(Table 4.1)** no NCS restraint was employed. All the 65 residues (considering one subunit) are well defined in the electron density map **(Fig. 4.4)** and statistics for the Ramachandran plot using PROCHECK (Laskowski *et al*, 1993) showed the presence of 88.9% of non-glycine residues in the most favored region. The asymmetric unit consisted of two monomers forming a tight dimer having an approximate dimension of 25 X 13 X 4 Å **(Fig. 4.5)**. This crystallographic dimer was consistent with the gel filtration and SDS-PAGE observations **(Fig. 4.1 ad 4.2)**.

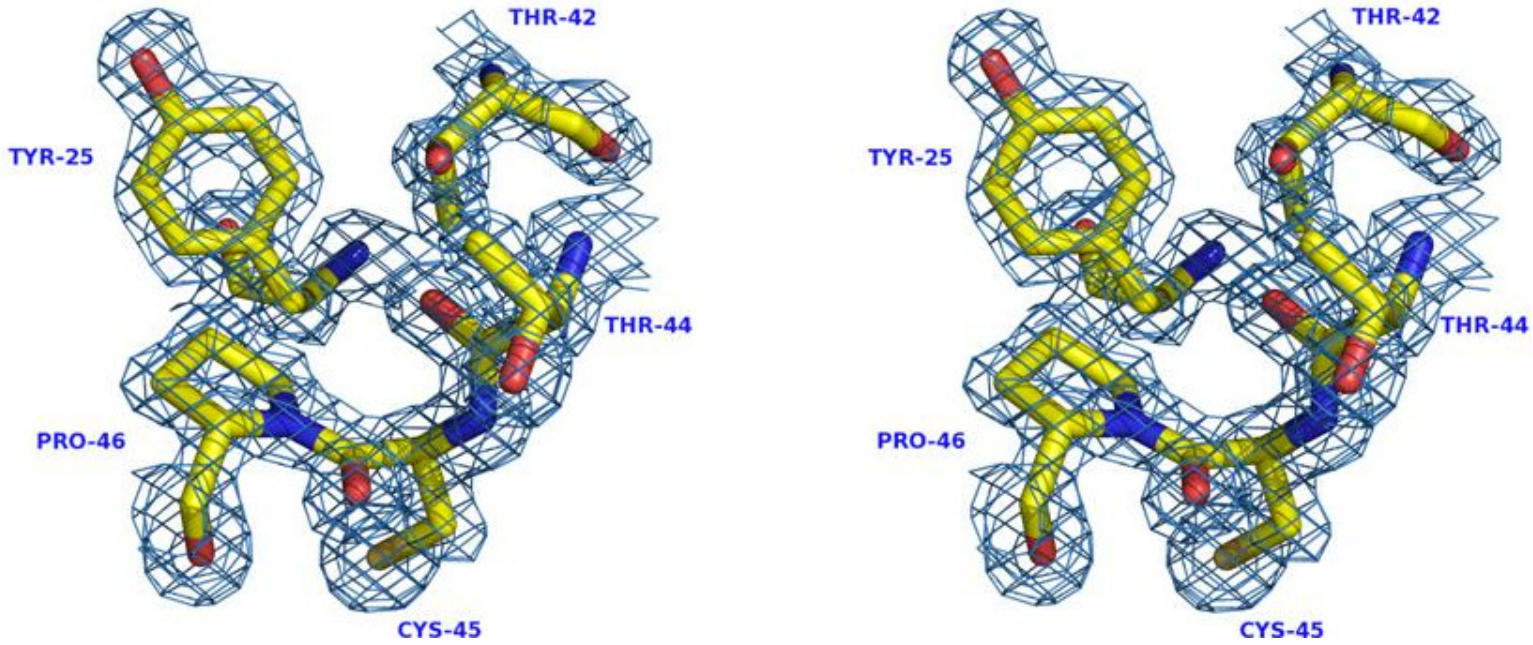

Figure 4.4: 2Fo-Fc map of haditoxin. The map was contoured at a level of 2.0.

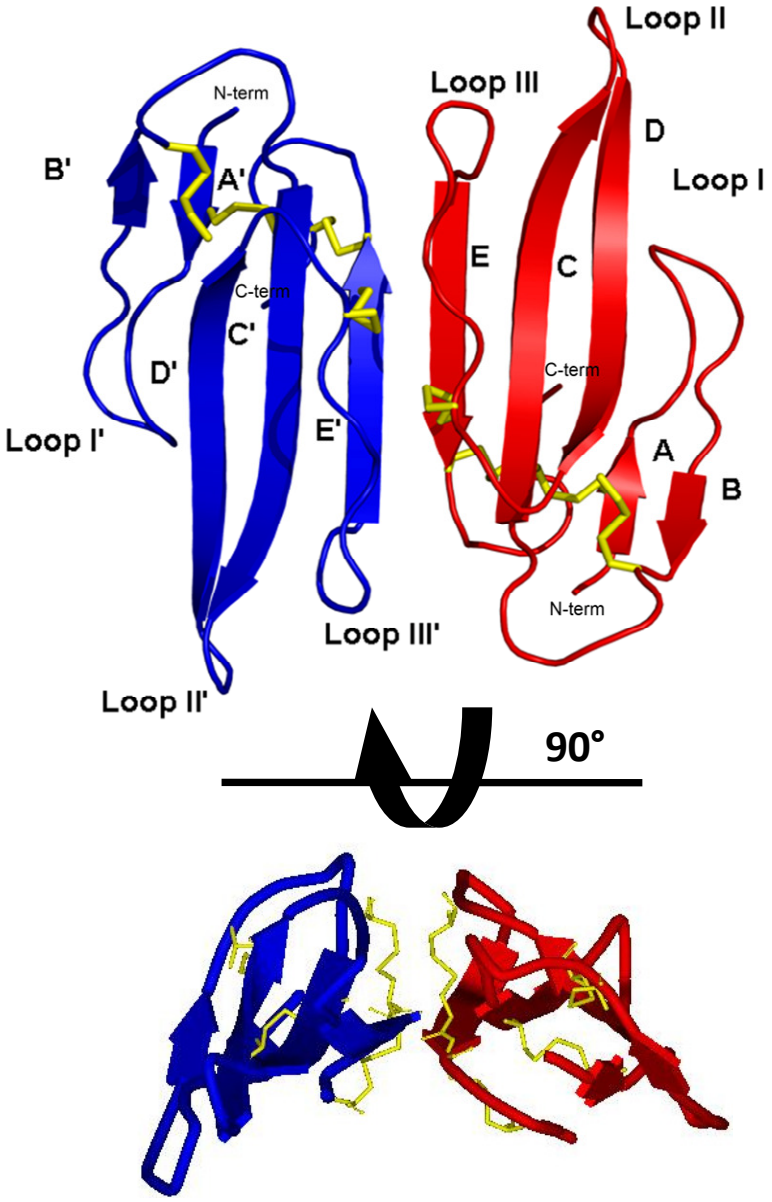

Figure 4.5: Overall crystal structure of haditoxin.

Monomer A is shown in red, monomer B is shown in yellow. β-strands and loops I-III are labeled. Disulphide bridges are shown in blue.

Each monomer adopted the common "three-finger" fold (Kini, 2002 and Kini and Doley, 2010) consisting of three β-sheeted loops protruding from a central core, tightened by four highly conserved disulfide bridges (Cys3–Cys24, Cys17–Cys41, Cys45–Cys57 and Cys58–Cys63) **(Fig. 4.5 and 4.6)**. Both the monomers were related by a 2-fold symmetry and their superposition yielded an rmsd of 0.2 Å for 65 Cα atoms **(Fig. 4.7)**. They were structurally similar to short-chain α-neurotoxins like toxin-α and erabutoxins **(Fig. 4.8)**. Loop I formed a two-stranded β-sheet (Lys2–Tyr4 and Thr14–Ile16), whereas loops II and III formed a three-stranded β-sheet (Glu34–Thr42, Phe23–Asp31 and Lys53–Cys58). The anti-parallel β-strands of the β-sheet were stabilized by mainchain–mainchain hydrogen bonding.

4.3.4 Dimeric interface

The dimeric interface was analysed using the PISA server (Krissinel and Henrick, 2007). It is mainly formed by loop III of each subunit. Strands D, C, E, E', C' and D' form a six β-pleated sheet with an overall right-handed twist **(Fig. 4.5)** in the dimer. Approximately 565 $Å^2$ (or 12 % of the total) surface areas and 17 residues of each monomer contributed to the dimerization. The close contacts between the monomers were maintained by 14 hydrogen bonds (<3.2 Å) and extensive hydrophobic interactions **(Table 4.2)**. Six mainchain–mainchain hydrogen bonding contacts existed across the interface involving strand E of monomer A and strand E' of monomer B **(Table 4.2, Fig. 4.9)**. Four of the hydrogen bonds were observed between the mainchain amide hydrogen and carbonyl oxygen of Val55 and Cys57 from monomer A and Val55' and Cys57' from monomer B; and

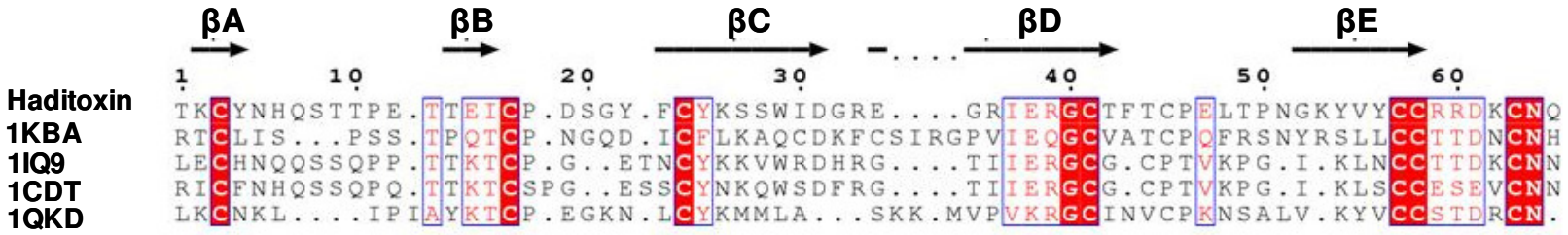

Figure 4.6: Structure based alignment of haditoxin with other three finger toxins.

Color coding of conserved residues are denoted by boxed red text and invariant residues by red highlight. Accession numbers are shown on the left. Secondary structure elements of haditoxin are shown on the top. Numbering is shown for the haditoxin sequence only. Sequence alignment was done by program Strap and displayed with ESPript.

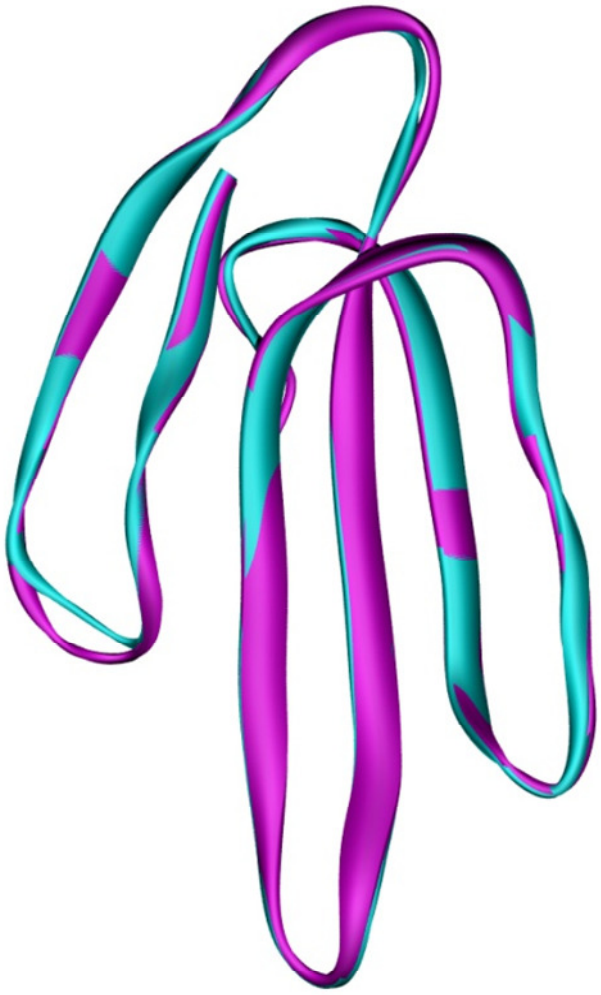

Figure 4.7: Superimposition of both the subunits of haditoxin.

Subunit A and B is shown in cyan and magenta respectively. Both the monomers are related by a 2-fold symmetry and their superposition yielded an rmsd of 0.2 Å for 65 α-carbon atoms.

Figure 4.8: Superimposition subunit A of haditoxin with short-chain α-neurotoxins.

Subunit A is shown in cyan, erabutoxin-a in magenta, erabutoxin-b in yellow and toxin-α in red

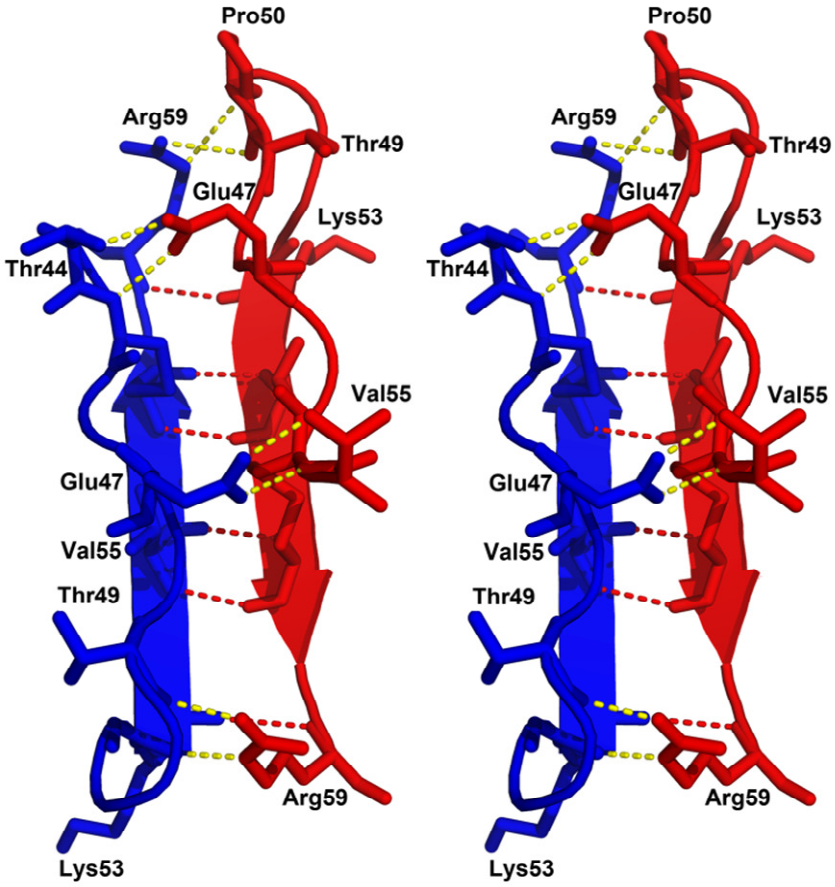

Figure 4.9: Stereo diagram of the dimeric interface of haditoxin.

The residues to form the hydrogen bonds are labeled. The mainchain-mainchain hydrogen bonds are shown in red. The other hydrogen bonds are shown in yellow. For details refer to table 4.2.

Table 4.2: Hydrogen bonds in the dimeric interface of haditoxin

Monomer A	Monomer B	Distance (Å)
Main chain		
Cys-57 (O)	Val-55 (N)	2.93
Val-55 (O)	Cys-57 (N)	2.85
Cys-57 (N)	Val-55 (O)	2.86
Val-55 (N]	Cys-57 (O)	2.90
Lys-53 (O)	Arg-59 (N)	3.10
Arg-59 (N)	Lys-53 (O)	3.40
Side chain		
Glu-47 (OE1)	Thr-44 (OG1)	2.63
Glu-47 (OE2)	Cys-45 (N)	2.76
Pro-50 (O)	Arg-59 (NE)	3.39
Thr-49 (O)	Arg-59 (NH_2)	3.37
Thr-44 (OG1)	Glu-47 (OE1)	2.68
Cys-45 (N)	Glu-47 (OE2)	2.81
Arg-59 (NH_2)	Thr-49 (O)	2.66
Arg-59 (NE)	Gly-52 (O)	2.76

the remaining two existed between the carbonyl oxygen of Lys53 (and Lys53') and the amide hydrogen of Arg59 (and Arg59') **(Table 4.2, Fig. 4.9)**.

In addition, there were another eight hydrogen bonding contacts mediated through the side chains of Thr44, Cys45, Glu47, Pro50 and Arg59 **(Table 4.2, Fig. 4.9)**. Two hydrophobic clusters further stabilized the dimeric structure. The side chains of Phe23 and Leu48 from both monomers formed one cluster, whereas the disulphide bridge between Cys45-Cys57 and Val55 of both monomers formed the other. These observations strongly suggest the existence of haditoxin as non-covalent homodimeric species.

4.4 DISCUSSION

Three-finger toxins from snake venom consist of a multitude of pharmacologically active peptides. All members of this family share a similar scaffold, which consists of three finger-like loops made of β-sheet structure, emerging from a globular core and stabilized by four conserved intramolecular disulfide linkages giving rise to the compact "β-cross" motif (Endo and Tamiya, 1987; Harrison and Sternberg, 1996; Kini 2002; Nirthanan *et al*, 2003; Kini and Doley, 2010). Although the members of this family of proteins share similar structural scaffold, it has been shown that the subtle differences in their structure contribute to the differences in affinity and specificity towards the diverse physiological targets of these peptides (Rees *et al*, 1987; Bilwes *et al*, 1994; Tsetlin, 1999). Thus, the three-dimentional structure of haditoxin essentially helped us to understand the novel structural elements present in this protein as well as its structure-function relationship.

This study provides, till date, the first report of a dimeric short-chain α-neurotoxin, which showed clear differences in structure and function hitherto attributed to this class of toxins. Haditoxin was a non-covalent homodimer where the monomers were oriented in an opposite direction. Structurally, the dimeric quaternary structure of haditoxin was similar to κ-neurotoxins, whereas individual monomers were similar to short-chain α-neurotoxins. Functionally, this homodimer antagonized muscle (αβγδ) and neuronal (α_7, $\alpha_3\beta_2$ and $\alpha_4\beta_2$) nAChRs, with highest affinity towards α_7-nAChRs. Thus, haditoxin was the first dimeric neurotoxin to interact with muscle nAChRs as well as the first short-chain α-neurotoxin to interact with neuronal α_7-nAChRs. On analyzing the primary and tertiary structures of haditoxin, it was observed that several structurally invariant residues, essential to maintain the three-finger fold, together with few functionally important residues reported to be critical for

binding of short-chain α-neurotoxins to muscle (αβγδ) and long-chain α/κ-neurotoxins to both muscle (αβγδ) and neuronal α7 receptors, were conserved in haditoxin.

Structurally invariant residues for haditoxin

Haditoxin contained all eight conserved cysteine residues that are essential for the three-finger folding (Menez *et al*, 1980; Endo and Tamiya, 1991). They formed four disulfide bridges located in the core region of the molecule. It was reported that the chemical reduction of these four disulfide bridges disrupt the native conformation of neurotoxins, resulting a total loss of neurotoxicity (Menez *et al*, 1980).

In addition, haditoxin possessed several other structurally invariant residues, responsible for the stability of the three-finger fold. For example, Tyr25 (numbering of the residues are according to erabutoxin-a, unless stated otherwise), the crucial residue stabilizing the antiparallel β-sheet structure (Torres *et al*, 2001), was conserved in a similar three-dimensional orientation in haditoxin. Similarly, the structurally invariant Gly40, involved in the tight packing of the three-dimensional fold by accommodating the bulky side chain of the Tyr25 (Menez *et al*, 1984; Endo and Tamiya, 1991) was also conserved. The two proline residues Pro44 and Pro48, potentially associated with the formation of the β-turn (Endo and Tamiya, 1991) were conserved in haditoxin as Pro46 and Pro50. Interestingly, some charged amino acid residues forming salt bridges had also been conserved in three-finger toxins for structural stability. The salt bridge between the N-terminal amino group and the carboxyl group of Glu58 in erabutoxin-a maintains the native conformation (Endo and Tamiya, 1991) of the toxin. A similar role had been found for the salt bridge between the N-terminal amino group and the carboxyl group of Asp58 in haditoxin. The electrostatic interaction between the C-terminal carboxyl group and the guanidinium group of Arg39 in erabutoxin-a (Endo and

Tamiya, 1991) was conserved as well in haditoxin by the bond between the C-terminal carboxyl group and the guanidinium group of the Arg39. Thus, presence of these structurally invariant residues contributed to the stable three-finger fold of haditoxin.

Functionally invariant residues for haditoxin

The subtle structural variations that exist between different classes of three-finger toxins may often reflect some functional significance (Menez, 1998). For instance, the high affinity binding of long-chain α-neurotoxins, but not short-chain α-neurotoxins, to neuronal α_7 receptors has been clearly attributed to structural variations in loop II of long-chain α-neurotoxins (Servent *et al*, 1997; Fruchart-Gaillard *et al*, 2002) compared to the short-chain ones. The crystal structure of haditoxin revealed the characteristic three-finger scaffold with the core containing four conserved disulfide bridges. The superimposition of the α-carbon backbone structure of haditoxin with that of a short-chain α-neurotoxin (erabutoxins, toxin-α) (**Fig. 4.8**) and a long-chain α-neurotoxin (α-cobratoxin) (**Fig. 4.10**) showed a better overall fit between haditoxin and short-chain α-neurotoxin, especially with respect to loop sizes and the short C-terminal tail. However, haditoxin differed markedly from the long-chain α-neurotoxins such as- α-cobratoxin in the region of the middle loop because of the fifth disulfide bridge present at the tip of this loop as well as the size and disposition of the first (N-terminus) loop and the C-terminus tail. The possible functional implications of these differences are discussed below in details.

Extensive structure-function relationship studies on the short-chain α-neurotoxin, erabutoxin-a (Teixeira-Clerc *et al*, 2002; Pillet *et al*, 1993; Tremeau *et al*, 1995; Endo and Tamiya, 1991), and long-chain α-neurotoxins, α-cobratoxin (Bourne *et al*, 2005; Antil *et al*, 1999) and α-bungarotoxin (Fruchart-Gaillard *et al*, 2002; Dellisanti *et al*, 2007), revealed the critical

Figure 4.10: Superimposition subunit A of haditoxin with α-cobratoxin.

Subunit A is shown in red, α-cobratoxin (long-chain α-neurotoxin) in blue. The conserved disulfide bridges are shown in yellow sticks.

residues involved in the recognition of nAChRs by snake neurotoxins. The crucial residues for α-neurotoxins to bind to muscle (αβγδ) nAChRs are Lys27, Trp29, Asp31, Phe32, Arg33, and Lys47. Haditoxin possessed three of them (Trp29, Asp31 and Arg33) in homologous positions. Additionally, each type of toxin possesses specific residues that recognized muscle or neuronal nAChRs. For muscle (αβγδ) nAChRs, these are His6, Gln7, Ser8, Ser9, and Gln10 in loop I and Tyr25, Gly34, Ile36, and Glu38 in loop II of short-chain α-neurotoxins such as-erabutoxin-a (Teixeira-Clerc *et al*, 2002) and Arg36 in loop II and Phe65 in the C-terminus tail of long-chain α-neurotoxins such as - α-cobratoxin (Bourne *et al*, 2005). His6, Gln7 and Ser8 in the loop I and Tyr25, Gly34, Ile37 and Glu38 in the loop II were conserved in haditoxin as the muscle-subtype specific determinants of short-chain α-neurotoxins. Moreover, Arg36, muscle-subtype specific determinant of long-chain α-neurotoxins was also conserved in haditoxin. The presence of these multiple functional determinants might explain the potent neurotoxicity exhibited by haditoxin on mammalian and avian muscle (αβγδ) nAChR.

On the contrary, the specific determinants (Ala28 and Lys35; α-cobratoxin numbering) of long-chain α-neurotoxins towards the neuronal (α_7) nAChRs (Antil-Delbeke *et al*, 2000) were not conserved in haditoxin. Significantly, haditoxin also lacked the 5^{th} disulfide bridge responsible for the cyclization of loop II which is considered to be a hallmark determinant for the ability of neurotoxins such as α-bungarotoxin and κ-bungarotoxins to interact with their specific neuronal nAChR targets (Antil-Delbeke *et al*, 2000; Osipov *et al*, 2008; Grant *et al*, 1998; Servent *et al*, 1997; Servent *et al*, 1998; Bourne *et al*, 2005). This is somewhat surprising given the high affinity of haditoxin for the neuronal α_7- (IC_{50} = 0.18 μM), $\alpha_3\beta_2$- (IC_{50} = 0.5 μM) and $\alpha_4\beta_2$- (IC_{50} = 2.6 μM) nAChRs.

The crystal structure of cobratoxin in complex with AChBP revealed the critical residues of cobratoxin incolved in the interaction with the binding protein, AChBP (a homolog for the

homopentamaric neuronal nicotinic receptors). This structure provides a lead template resembling a curaremimetic α-neurotoxin bound to homopentamaric neuronal nicotinic receptors. The residues of cobratoxin involved in the interaction are Thr6, Pro7, Ile9 in loop I; **Trp25**, **Cys26-Cys30**, **Asp27**, **Ala28**, **Phe 29**, Ser31, Ile32, Arg33, Gly34, **Lys35**, **Arg36**, Val37 in loop II and **Phe65**, Arg68 in the C-terminal tail (**Fig. 4.11 A**). This correlates well with the previous mutagenesis studies as the replacement of residues indicated in bold results in more than 5-7 folds decrease in the affinity towards the target receptor (Fruchart-Gaillard *et al*, 2002). Based on these residues we have aligned the sequence of α-cobratoxin with haditoxin (**Fig, 4.11** top). The putative residues of haditoxin which might be critical to interact with α_7-nAChRs are highlighted, the red and green residues are identical whereas the magenta ones are similar (**Fig. 4.11 B**).

Previously, candoxin, a non-conventional 3FTX (Nirthanan *et al*, 2002) was found to be an exception of a 3FTX that did not have the 5th disulfide bridge in loop II (candoxin has a 5th disulfide bridge in loop I), but still retained the ability to interact with neuronal (α_7) nAChRs (Nirthanan *et al*, 2003a). A superimposition of haditoxin and candoxin is represented in figure 4.12. It was suggested thus that candoxin may likely interact with neuronal α_7-nAChRs using alternate, novel points of contact. Likewise, it is plausible that haditoxin possesses unique combinations of determinants which enabled its interaction with α_7-, as well as $\alpha_3\beta_2$- and $\alpha_4\beta_2$-nAChRs. A detailed structure-function analysis to decipher these novel determinants is beyond the scope of this report.

Until now, the only dimeric neurotoxins known to interact with neuronal nAChRs are the κ-neurotoxins. In the case of κ-neurotoxins which interact with neuronal $\alpha_3\beta_2$- and $\alpha_4\beta_2$-nAChRs with high affinity (Grant and Chiappinelli, 1985; Wolf *et al*, 1988), the critical functional residue was identified as Arg34 (Fiordalisi *et al*, 1994). Haditoxin had Arg33 in a homologous

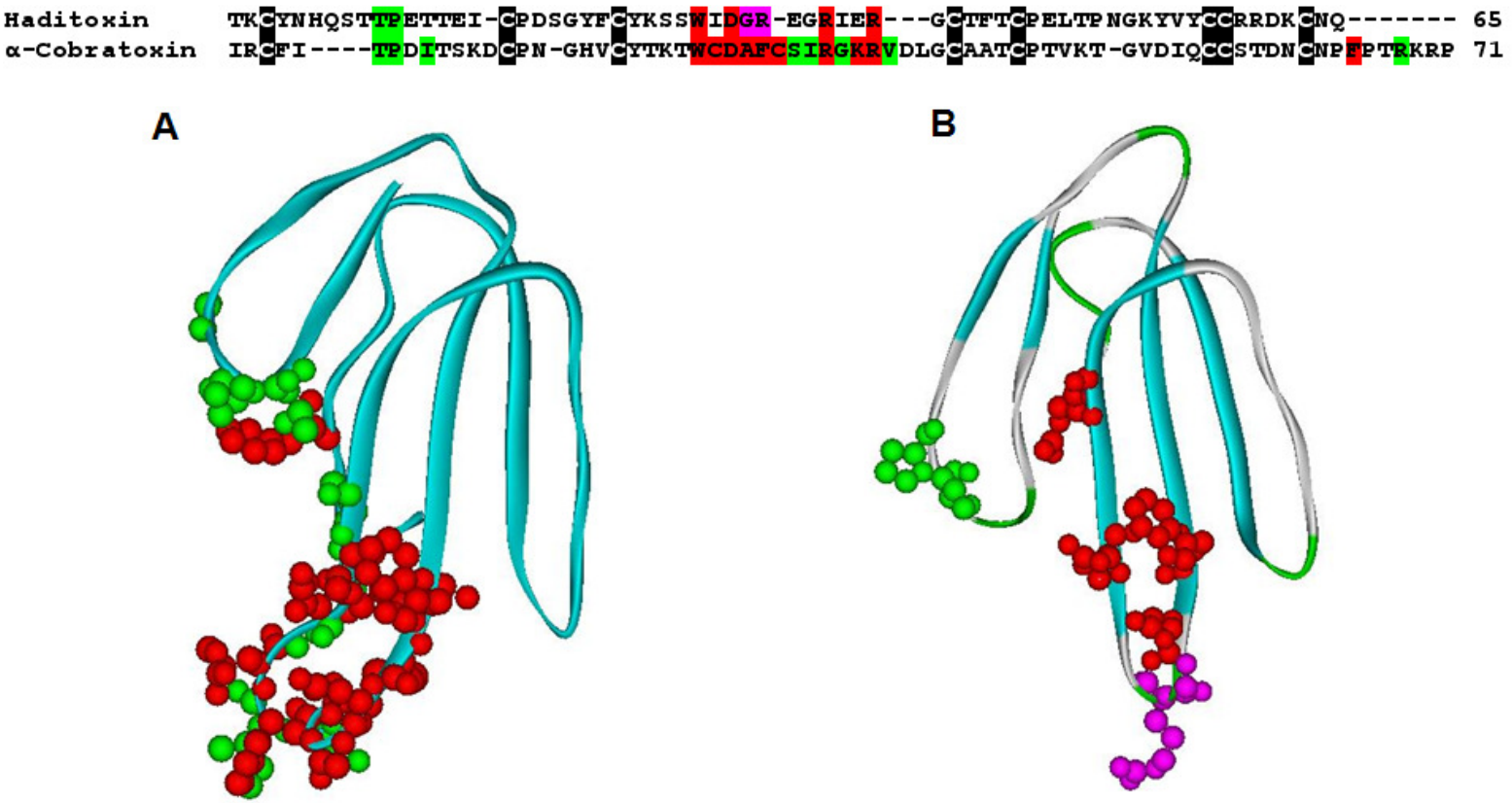

Figure 4.11: Critical residues for α-cobratoxin and haditoxin to interact with α7-nAChRs.

(A) The critical residues of α-cobratoxin to interact with AChBP, as identified in Bourne *et al*, (2005), are highlighted in CPK representation. The red coloured residues are those whose mutations cause an affinity decrease of more than 5-7 folds as proved by mutagenesis studies, green indicates the rest. On top, alignment of α-cobratoxin and haditoxin, the red highlighted residues are identical whereas the magenta ones are similar. (B) Putative functional residues of haditoxin for interaction with α7 receptors (colour coding is same as the top alignment figure).

Figure 4.12: Superimposition subunit A of haditoxin with candoxin.

Subunit A of haditoxin is shown in red, candoxin (a non-conventional neurotoxin) in green. The conserved disulfide bridges are shown in yellow sticks.

position, which may contribute in part to high affinity interaction with $\alpha_3\beta_2$- (IC_{50} = 0.5 μM) and $\alpha_4\beta_2$- (IC_{50} = 2.6 μM) nAChRs. Mutagenesis studies on κ-bungarotoxin revealed that the replacement of Pro36 to an amino acid residue bearing a bulky charged sidechain, like the Lys found in α-bungarotoxin, causes a 16 fold decrease in the efficacy of the toxin to block neurotransmission in the chick ciliary ganglion assay (Fiordalisi *et al*, 1994). Haditoxin bore an equivalent glycine residue, lacking bulky charged sidechain, which could explain the high affinity of this toxin towards the neuronal ($\alpha_3\beta_2$ and $\alpha_4\beta_2$) nAChRs.

Comparison of haditoxin with snake venom derived dimeric 3FTXs

Few known examples of dimeric three-finger neurotoxins derived from snake venoms exist (Chiappinelli and Lee, 1985; Osipov *et al*, 2008; Pawlak *et al*, 2009). Amongst them, the most well studied and characterized are the κ-neurotoxins, known to be composed of two identical monomers held together by non-covalent interactions (Dewan *et al*, 1994; Oswald *et al*, 1991). The observed dimeric form of haditoxin, with the characteristic six β-pleated sheets, was similar to that formed by κ-bungarotoxin (Dewan *et al*, 1994). Superposition of both molecules yielded an rmsd of 1.95 Å for 104 Cα atoms **(Fig. 4.13)**. The major deviations were located in the loops between the antiparallel β-strands.

Each monomer in κ-bungarotoxin was structurally homologous to long-chain α-neurotoxins, with the additional fifth disulfide bridge in the middle loop unlike haditoxin, which resembled short-chain α-neurotoxins **(Fig. 4.9)** with only four disulfide bridge. The dimeric interface for both haditoxin and κ-bungarotoxin was maintained by six mainchain-mainchain hydrogen bonds (Dewan *et al*, 1994). In addition, haditoxin had eight sidechain hydrogen bonding contacts between the monomers, whereas only three similar contacts were observed in κ-bungarotoxin **(Fig. 4.14)** (Dewan *et al*, 1994), suggesting that haditoxin formed tighter dimers

Figure 4.13: Haditoxin vs κ-bungarotoxin.

Superimposition of the Cα atoms of haditoxin with κ-bungarotoxin. Haditoxin and κ-bungarotoxin is shown in red and yellow respectively.

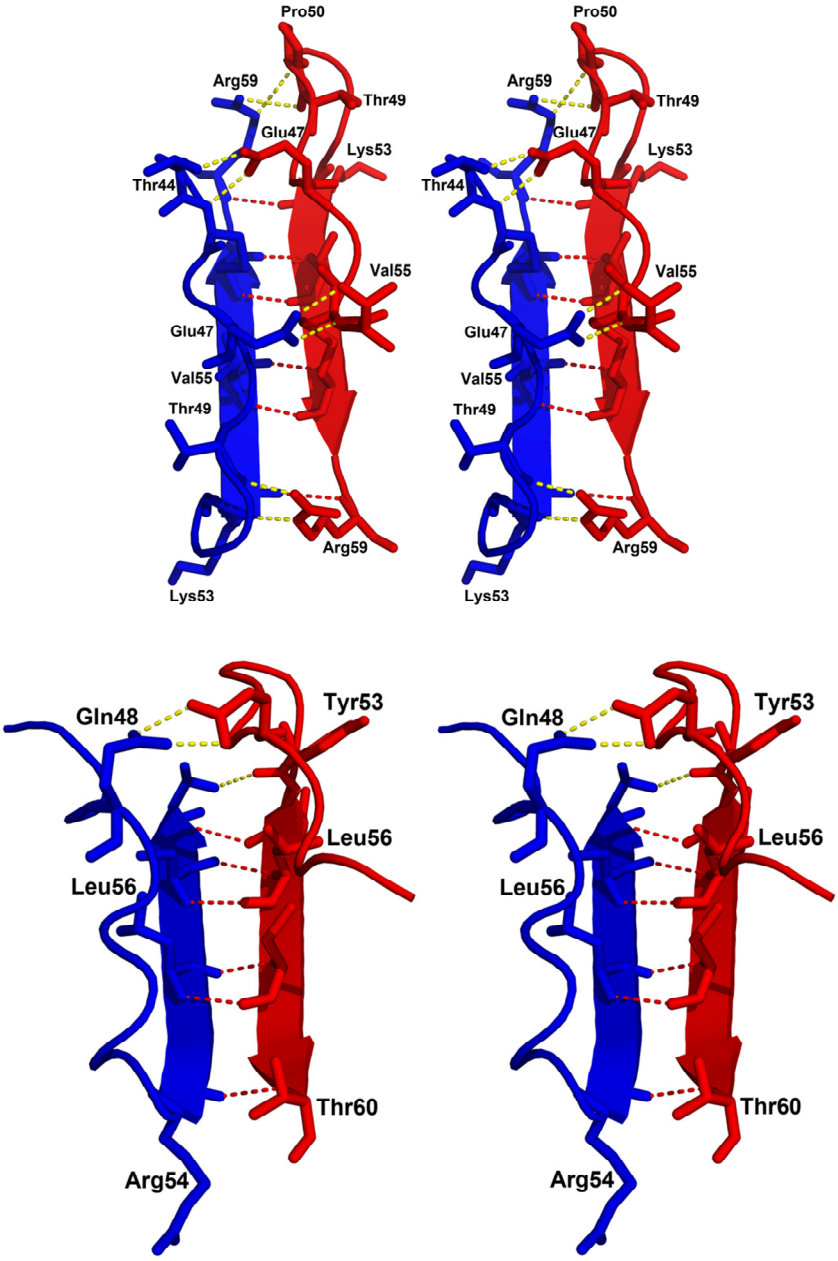

Figure 4.14: Stereo diagram of comparison of dimer interface of haditoxin (top) and κ-bungarotoxin (bottom).

The residues to form the hydrogen bonds are labeled. The mainchain-mainchain hydrogen bonds are shown in red. The other hydrogen bonds are shown in yellow.

than κ-bungarotoxin. The side chain interactions in κ-bungarotoxin are maintained by Phe49, Leu57, and Ile20, which are strictly conserved in all κ-neurotoxins (Dewan *et al*, 1994; Grant *et al*, 1997). Mutagenesis studies have proven that replacing Phe49 or Ile20 with alanines renders a toxin with an apparent lack of ability to fold into the native structure, even as a monomer (Grant *et al*, 1997). The same result has been observed with deletion studies (deletion of Arg54) with an aim to generate a 65 residue long protein, as found in the α-neurotoxins, from the 66 residue long κ-bungarotoxin (Grant *et al*, 1997). Whereas haditoxin being a 65 residue long protein lacked both Phe49 and Ile20 but still retained the intact dimeric structure. The electrostatic surface potential for both the molecules were apparently similar except for the tip of loop II which revealed a strong positive patch for haditoxin compared to κ-bungarotoxin **(Fig. 4.15)** (Dewan *et al*, 1994).

Functionally κ-neurotoxins interact with the neuronal ($\alpha_3\beta_2$ and $\alpha_4\beta_2$) nAChRs with high affinity (Grant and Chiappinelli, 1985; Wolf *et al*, 1988), whereas haditoxin interacted with both muscle ($\alpha\beta\gamma\delta$) and a variety of neuronal (α_7, $\alpha_3\beta_2$ and $\alpha_4\beta_2$) nAChRs. The crystal structure of the κ-bungarotoxin dimer showed that the guanidinium groups of the essential arginine residues, situated at the tip of the loop II, maintains nearly identical distance (44 Å) (Dewan *et al*, 1994) as like the acetylcholine binding sites in the pentameric receptor (30-50 Å) (Herz *et al*, 1989; Unwin, 1993). The κ-bungarotoxin dimer may interact with both the acetylcholine binding sites on a single neuronal receptor and physically block ion flow by spanning the channel (Dewan *et al*, 1994; Grant *et al*, 1997). But this mode of interaction did not explain the inability of the κ-neurotoxins to block the muscle nAChRs. Haditoxin maintained a distance of ~52 Å between the guanidinium groups of the critical arginine residues present in the turn region of the second loop which is almost similar to the acetylcholine binding sites in the pentameric receptor mentioned above. But unlike the κ-

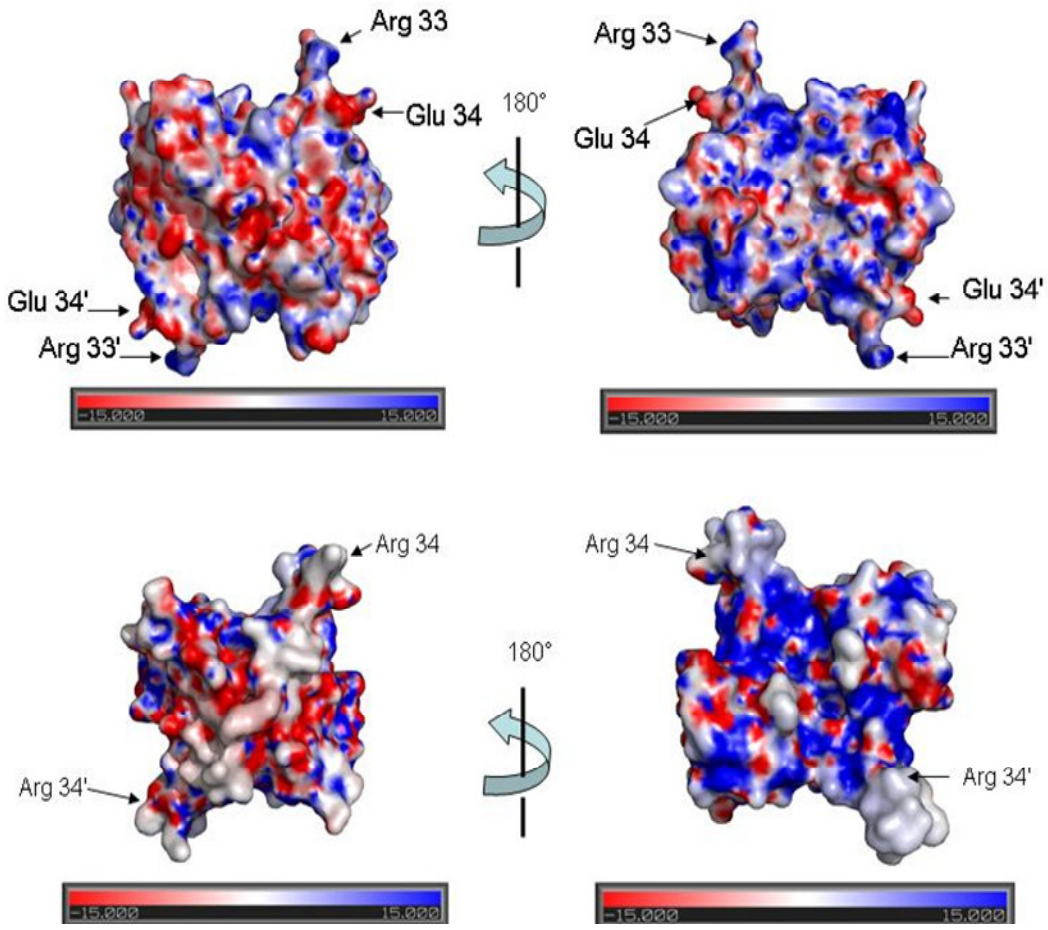

Figure 4.15: Comparison of the electrostatic surface of haditoxin and κ-bungarotoxin.

Electrostatic surface of haditoxin (top) and κ-bungarotoxin (bottom). The irientation are the same as the Figure 2 (top) before rotation. The location of Arg33 and Glu34 of haditoxin and Arg34 of k-bungarotoxin are indicated.

neurotoxins, haditoxin interacted with both muscle and neuronal nAChRs. This supports the fact that the dimeric toxins may have a unique mode of interaction with the nAChRs which demands further investigation.

More recently, other heterodimeric 3FTXs from elapid venoms have been reported, including covalently (disulfide) linked homodimers of a long-chain α-neurotoxin (α-cobratoxin) and heterodimers of α-cobratoxin in combination with a variety of three-finger cytotoxins (Osipov *et al*, 2008). Unlike haditoxin, all of these dimers were formed by covalent bonding (disulfide linkage) of the monomeric units. Functionally, the α-cobratoxin-cytotoxin heterodimers were able to block neuronal (α_7) nAChRs whereas the α-cobratoxin homodimer exhibited blockade of both neuronal α_7 and $\alpha_3\beta_2$ nAChRs, unlike monomeric α-cobratoxin which interacts with muscle ($\alpha\beta\gamma\delta$) and neuronal (α_7) nAChRs (Osipov *et al*, 2008).

Our laboratory has also reported on a colubrid venom derived covalently linked heterodimeric 3FTX, irditoxin (Pawlak *et al*, 2009), which was found to target muscle ($\alpha\beta\gamma\delta$) nAChRs, in sharp contrast to the reported function of elapid dimeric toxins (Osipov *et al*, 2008). Another distinguishing feature was that the subunits of irditoxin structurally resemble nonconventional three-finger neurotoxins (Pawlak *et al*, 2009). A comparison of the three-dimensional structures for haditoxin and irditoxin is presented in figure 4.16. Haditoxin, was both structurally and functionally distinct from the α-cobratoxin hetero/homodimers as well as irditoxin. Structurally, haditoxin was a non-covalently-linked homodimer of the short-chain α-neurotoxin type and functionally, it has a broad pharmacological profile with high affinity and selectivity for muscle ($\alpha\beta\gamma\delta$) and neuronal (α_7, $\alpha_4\beta_2$ and $\alpha_3\beta_2$) nAChRs.

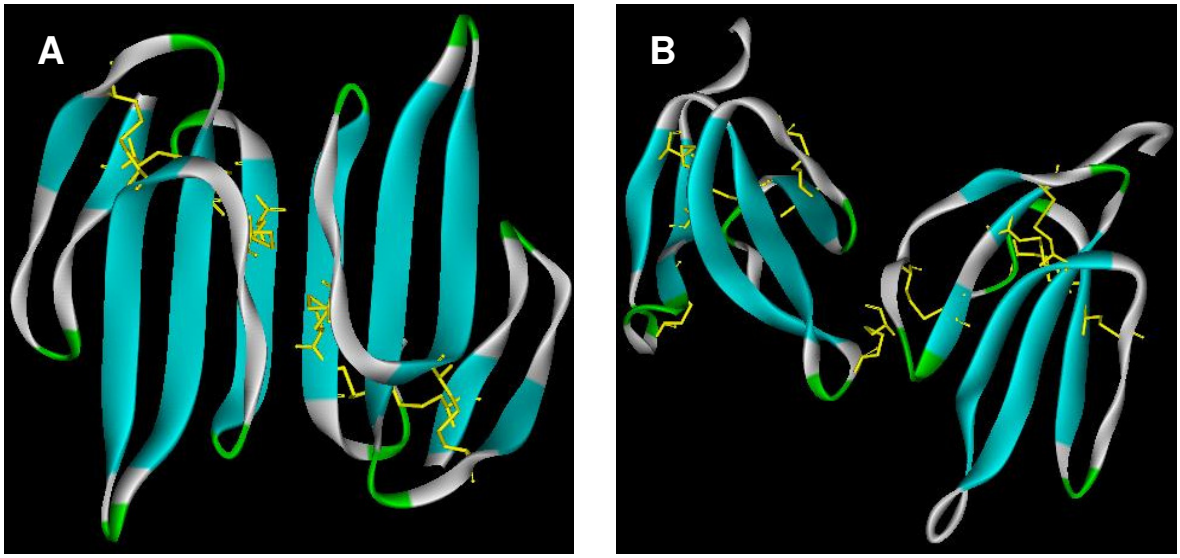

Figure 4.16: Structural comparison of haditoxin and irditoxin.

(A) Homodimeric structure of haditoxin. The dimer is composed of two non-covalently attached subunits, each of which is similar to short-chain neurotoxins with four disulfide bridges (shown in yellow sticks), (B) Heterodimeric structure of irditoxin. This dimer consists of two different monomers attached together with a disulfide bridge (shown in yellow stick) each subunit of irditoxin adopts a structure similar to the non-conventional neurotoxins with additional disulfide bridge in loop I (all disulfide bridges are shown in yellow).

4.5 CONCLUSIONS

To conclude, we have characterized a novel neurotoxin, haditoxin, with unique structural and functional profile. The three-dimentional crystal structure of the protein revealed that it exists as a homodimeric species in solution at pharmacologically relevant concentrations. Each monomer is similar to short-chain α-neurotoxins with respect to the number of amino acid residues and the four conserved disulfide bridges. Functionally, haditoxin interacts with the muscle and a variety of neuronal nAChRs, with the highest affinity for α_7-nAChRs. Thus, haditoxin is the first reported dimeric three-finger toxin recognizing the muscle ($\alpha\beta\gamma\delta$) nAChRs as well as the first short-chain α-neurotoxin to target the neuronal α_7-nAChR with nanomolar affinity.

Chapter Five

Structure-function relationships of haditoxin

CHAPTER FIVE

Structure-function relationship of haditoxin

5.1 INTRODUCTION

There is an intimate correlation between protein structure and function. The interaction of the proteins, via the molecular recognition site, with their target molecules results the specific biological function. Despite the complexity in size, structure and conformation of the proteins, the molecular recognition or interaction sites are compact and well defined. These protein-protein interaction sites may be continuous or discontinuous. Continuous interaction sites are formed by a stretch of amino acid residues linked directly to each other such as- the snake venom disintegrins, the potent inhibitors of the platelet aggregation, interact with the fibrinogen receptor, integrin $\alpha_{IIb}\beta_3$ (Huang *et al*, 1987), using a conserved tripeptide motif consisting of arginine-glycine-aspartic acid (RGD) residues (for review see, Calvete, 2005; Calvete *et al*, 2005). On the contrary, the discontinuous protein-protein interaction sites can be brought together through a specific three-dimensional fold of the protein. For example, the long-chain and short-chain α-neurotoxins from snake venom recognize the muscle nicotinic acetylcholine receptor though specific determinants which are common for both the subclass (Servent *et al*, 2000; Servent and Menez, 2001). These specific determinants consist of amino acid residues which are brought together to form the interaction site by the unique three dimensional fold of these neurotoxins.

Certainly, the task of delineating the molecular recognition site of a protein is a formidable challenge. This may involve the identification of structural epitopes from the three-

dimensional structure of the protein, preferably by co-crystallizing the ligand-receptor complex (Cunningham and Wells, 1993). An example will be the co-crystallization of a long-chain α-neurotoxin, α-cobratoxin with acetylcholine binding protein (AChBP), a homolog of the ligand-binding (amino-terminal) domain of nicotinic receptors, isolated from marine and fresh water snails (Smit *et al*, 2001; Brejc *et al*, 2001; Brejc *et al*, 2002; Hansen *et al*, 2004 and Bourne *et al*, 2005). This was a major breakthrough in understanding the mechanism of interaction between a snake venom α-neurotoxin and the nicotinic receptor.

On the other hand, the functional determinants of a protein can also be analyzed using site-directed mutagenesis, chemical modification and design of synthetic peptides derived from potential interaction sites as well as molecular modeling based on known structural templates (Menez, 1998; Servent and Menez, 2001). These methods, combined with available literature on the tertiary structure of neurotoxins, have now permitted the accurate delineation of the interaction sites by which different classes of neurotoxins recognize various subsets of nicotinic acetylcholine receptors (Pillet *et al*, 1993; Trémeau *et al*, 1995; Servent *et al*, 1997; Grant *et al*, 1998; Antil *et al*, 1999; Antil-Delbeke *et al*, 2000; Boulain and Menez, 1993; Zeng *et al*, 2001; Moise *et al*, 2002; Bourne *et al*, 2005 ; Dellisanti *et al*, 2007).

As discussed earlier, we have purified and characterized haditoxin, a novel member of the three-finger neurotoxin family, with unique structural and functional profile. It is the first reported dimeric three-finger toxin recognizing the muscle (αβγδ) nAChR as well as the first short-chain α-neurotoxin to target the neuronal α_7-nAChR with nanomolar affinity. In chapter four, the three-dimensional structure of haditoxin was analyzed in details with

respect to its function (specifically its inhibition of muscle ($\alpha\beta\gamma\delta$) and neuronal (α_7, $\alpha_4\beta_2$ and $\alpha_3\beta_2$) nicotinic acetylcholine receptors) as well as structure (especially the quaternary structure similar to snake venom dimeric neurotoxins) based on current knowledge of the structure-function relationships between snake venom neurotoxins and nicotinic acetylcholine receptors.

In this chapter, we describe the preliminary results of the structure-function relationship studies of haditoxin. Initially, we observed the interaction of haditoxin with acetylcholine binding protein using radioligand binding assays with an ultimate aim of co-crystallization. Using Ca^{2+} dependent fluorescence assay (Ca^{2+}/Fluo4) we also observed the interaction of haditoxin with other ion-channel receptors, such as- 5-hydroxytriptamine type 3 (5-HT_3) receptors, to find out the cross-reactivity, if any. Finally, we expressed haditoxin using a heterologous expression system and characterized the recombinant haditoxin functionally using tissue organ bath system.

5.2 MATERIALS AND METHODS

5.2.1 Reagents and kits

The details of reagents and kits used for this part of the study are as follows: Agarose, LB Broth, LB agar, oligonucletides (1st Base Pte. Ltd., Singapore), long PCR enzyme mix and restriction endonucleases (Fermentas International Inc., Burlinton, Ontario, Canada), DNA ladders, X-gal, IPTG (Promega Corporation, Madison, WI, USA), gel red stain and SeeBlue® Plus2 prestained protein ladder (Invitrogen by Life Technologies, Carlsbad, CA, USA), Gel extraction kit and PCR purification kit, (Qiagen, Hilden, Germany), Gene All Exprep Plasmid Quick kit (Gene All, Seoul, Korea), Cleanseq sequencing cleanup magnetic beads (Agencourt Bioscience, Beverly, MA) and ABI PRISM BigDye Terminator v3.1 cycle sequencing kit (PE Applied Biosystems, Foster City, CA). All the kits employed in this study were used according to the manufacturer's instructions. Haditoxin was purified from the venom of *O. hannah* as described in chapter 2 and the lyophilized powder was used for the radioligand and Ca^{2+}/Fluo4 assay. For recombinant expression the gene was obtained from the cDNA clone. The Ni-NTA (Nickle-Nitrolotriacetic acid) agarose resin was purchased from Qiagen (Hilden, Germany). Empty columns for gravity flow were obtained from Biorad (Hercules, CA, USA). All the reverse phase (RP) columns, Semiprep (5 µ, 300 Å, 10 mm x 250 mm) and analytical (5 µ, 300 Å, 4.6 mm x 250 mm), for High Performance Liquid Chromatography (HPLC) were purchased from Phenomenex (Torrance, CA, USA). Most of the standard drugs and chemicals used for the organ bath assay are the same as mentioned in chapter 3. Deionized water was purified with a MilliQ system (Millipore, Billerica, MA, USA). All other

chemicals were purchased from Sigma Aldrich, Milwaukee, WI, USA and 1st Base (Singapore).

5.2.2 Radioligand binding assay with acetylcholine binding protein

The interaction studies of haditoxin with acetylcholine binding protein (AChBP), described below were carried out in the collaborating laboratory of Professor Palmer Taylor, Skaggs School of Pharmacy and Pharmaceutical Sciences, University of California, San Diego, 9500 Gilman Drive, La Jolla, California 92093, United States of America.

An antimouse scintillation proximity assay (SPA, Amersham Biosciences, Piscataway, NJ, USA) was adapted for use in a soluble radioligand binding assay as described previously (Hibbs *et al*, 2004 and Utsintong *et al*, 2009). A total of five soluble acetylcholine-binding proteins (AChBP) were used for the study, AChBP from the freshwater snail *Lymnaea stagnalis* (Ls), from the marine species *Aplysia californica* (Ac) together with three mutants of Ac binding protein. All the binding proteins are recombinantly expressed and purified in Professor Taylor's lab. AChBP (final concentration ~500 pM binding sites for *Lymnaea stagnalis*, Ls; ~1 nM binding sites for *Aplysia californica*, Ac and its mutants), polyvinyltoluene anti-mouse SPA scintillation beads (0.1 mg/ml), monoclonal anti-FLAG M2 antibody from mouse, and [^{3}H] epibatidine (5 nM final concentration for Ls, 20 nM for Ac and mutants) were combined in a phosphate buffer (0.1 M, pH 7.0) with fixed concentrations of the haditoxin at 10 μM in a final volume of 100 μL. Nicotine at a concentration of 10 μM was used as positive control. The resulting mixtures were allowed to equilibrate at room temperature for a minimum of 2 h and measured on a Beckman LS

6500 liquid scintillation counter. The result was calculated by the fraction of [^{3}H]epibatidine.

5.2.3 Ca^{2+}/Fluo-4 assay on 5-HT_3 receptors

The interaction studies of haditoxin on human (h) 5-HT_3 receptors, described below were carried out in the collaborating laboratory of Assoc. Professor Anders Asbjørn Jensen, Faculty of Pharmaceutical sciences, University of Copenhagen, Universitetsparken 2, 2100 Copenhagen, Denmark.

The functional characterization of haditoxin at h5-HT_{3A} and h5-HT_{3AB} cell lines was performed using the Ca^{2+}/Fluo-4 assay as previously described (Jenson *et al*, 2010 and Jørgensen *et al*, 2011). Cell lines containing 5-HT_3 receptor subtypes were split into poly-d-lysine-coated black 96- well plates with clear bottom. Following 16–24 h incubation with the 5-HT_3 receptor cell lines, the culture medium was aspirated and the cells were incubated in assay buffer (50 µL) (Hank's Buffered Saline Solution containing 20 mm HEPES, 10 mm $CaCl_2$, 1 mm $MgCl_2$ and 2.5 mm probenecid, pH 7.4) supplemented with 6 mm Fluo-4/AM at 37 °C for 1 h. Then the buffer was aspirated, the cells were washed once with assay buffer (100 µL), and finally 100 µL of assay buffer was added to the cells. The 96-well plate was assayed in a NOVOstarTM microplate reader measuring emission (in fluorescence units, FU) at 520 nm caused by excitation at 485 nm before and up to 60 sec after addition of agonist/antagonist solution (33 µL) in assay buffer. Serotonin was used as agonist for both h5-HT_{3A} and h5-HT_{3AB} receptors. The experiments were performed in duplicate at least three times for each compound tested. For the testing of the compounds as potentiators, they were co-applied to the cells with EC_{10}-EC_{20}

concentrations of the agonist for the respective receptors. For the testing of the compounds as antagonists, an EC_{70}-EC_{95} concentration of the agonist was used.

5.2.4 Bacterial strains and plasmids

E. coli bacterial strains (DH5α and BL21(DE3)) were obtained from Novagen (EMD chemicals Inc., Darmstadt, Germany) and the expression vector (pLICC) was a kind gift from Professor Glenn King (Institute for Molecular Bioscience, University of Queensland, Australia). The schematic representation of the vector is shown in figure 5.1. In the pLICC vector, the gene of interest is encoded as a MalE-His6-MBP-fusion protein, with a tobacco etch virus (TEV) protease site engineered between the MBP and toxin coding regions. At the beginning of the construct the MalE signal sequence is used to ensure the export of the protein of interest into the redox environment of the periplasm (the signal sequence is cleaved off during this process). The hexahistidine tag enables purification of the MBP-fusion protein using nickel affinity chromatography. The maltose binding protein (MBP) is used to facilitate the folding and solubility of the protein of interest. The TEV cleavage site enables the pure recombinant toxin to be realised from the MBP tag. The pLICC vector contains an ampicillin resistance gene (AmpR) for selection, and T7 promoter to induce the expression of the target gene via IPTG.

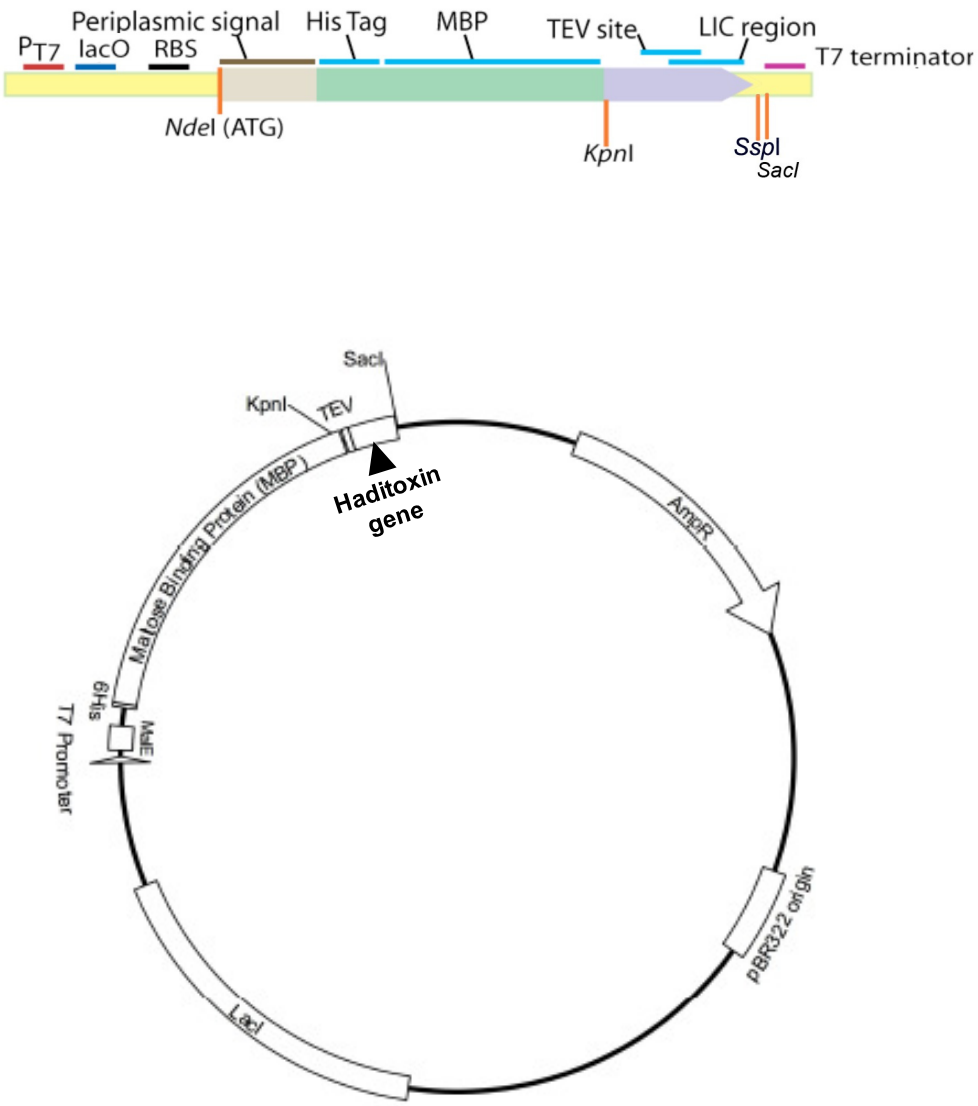

Figure 5.1: Schematic representation of the (A) plasmid pLICC and (B) pLICC:Haditoxin.

The regions encoding the restriction sites (KpnI and Sac I), His6 tag, MBP, MalE (periplasmic signal peptide), TEV cleavage site, and Haditoxin are indicated, as are the T7 promoter and ampicillin resistance gene. The plasmid used to produce a MalE-His6-MBP-Sf1a fusion protein via bacterial expression.

5.2.5 Cloning of haditoxin gene into pLICC plasmid

Haditoxin gene was cloned into pLICC vector flanking restriction enzyme sites KpnI and SacI at 5' and 3' end, respectively. As a result of using KpnI restriction site in the 5' end, the TEV cleavage site present in the vector was removed. Hence, we incorporated the new TEV cleavage site in the forward primer to generate the tag free protein. An additional glycine (Gly) residue was incorporated in the forward primer at the beginning of the haditoxin sequence for TEV protease recognition. The primers used for amplification were forward primer- (Fwd:ATAGGTACCGAAAACCTGTACTTCCAAGGCACCAAATGC) and reverse primer- (Rev: AGCGCGAGCTCCTGGTTGCATTTATCGCGGCG). The amplified product was double digested and ligated into pLICC plasmid followed by transformation (using heat shock) into DH5α competent cells. The sequence of the gene of interest was confirmed by DNA sequencing. Upon confirmation the plasmid containing the gene of interest was isolated from DH5α cells and transformed (using heat shock) into BL21(DE3) cells for test expression.

5.2.6 Sequence Analysis

The nucleotide sequences were read using Chromas Lite and Gene Runner. Sequence analysis was carried out using the BLAST program at the NCBI Database (www.ncbi.nlm.nih.gov) and ExPASy proteomics tools (www.expasy.org). Sequence alignments were carried out using the ClustalW program (www.ebi.ac.uk).

5.2.7 Recombinant protein expression

For 50 ml expression, a single colony harboring recombinant vector was used for inoculation of 2 ml of LB medium containing appropriate antibiotic (as mentioned above) and incubated at 37 °C with overnight shaking. The overnight grown culture was inoculated into 50 ml of fresh LB ampicillin medium. The flask with the bacterial culture was incubated at 37 °C with shaking until the optical density (OD) of the culture reached in between 0.8-1.3. At this stage, 1 ml of culture is taken out as 'uninduced sample' and incubated for 4 hours at 37 °C without being induced by IPTG. This is used as negative control. The rest of the culture is induced with 1 mM IPTG and incubated for further 4 hours 37 °C. After each hour 1 ml of culture was taken out for a time course evaluation of expression. After incubation the cells were harvested by centrifugation at 8,000 rpm for 10 mins at room temperature and the cell pellets were stored at -80 °C until mini-purification. Later, for large scale production of protein BL21(DE3) cells harboring pLICC with the gene of interest were induced with 1 mM IPTG and incubated at 37 °C for about 4 h. Before incubation, 1 ml aliquot was kept aside as unduced control. After the induction time is over, the cells were harvested by centrifuging the cultures at 8,000 rpm for 30 min. The cell pellets were stored at -80 °C until further purification. The expression of recombinant protein in E. coli was analyzed by Tris-tricine SDS-PAGE as described in chapter 4 (section 4.2.4).

5.2.8 Extraction of the recombinant protein

The cells expressing the protein were thawed on ice to prevent cell lysis. The pellets from the induced and uninduced samples were resuspended in 30 mM Tris, 40% sucrose, 2 mM

EDTA buffer (TSE buffer) pH 8.0, using magnetic stirrer until a uniform suspension was obtained. The volume of TSE buffer added was 100 µL for 1 ml culture, 5 ml for 50 ml of culture and 60 ml for 1 L culture. A 30 µL aliquot of each suspension (hereafter referred to as "whole cell extract" (WE)) was removed and set aside for SDS-PAGE analysis. The remainder was centrifuged at 12,000 rpm for 10 min and the supernatant was discarded. The pellets were resuspended in ice-chilled water to induce hypotonic shock and break the outer membrane. The volume of water used depends on the culture volume- 100 µL for 1 ml, 5 ml for 50 ml and 60 ml for 1 L of culture. 9. Light stirring on the magnetic stirrer was done to resuspend the pellets and to ensure that all the cells receive the osmotic shock induced by water uniformly. 30 µL aliquot of each suspension (hereafter referred to as "Whole cell Suspension in water" (WW)) was removed and set aside for SDS-PAGE analysis. After this the mixture was again centrifuged at 12,000 rpm for a further 10 min and similarly, 30 µL sample of the supernatant was collected (hereafter referred to as "periplasmic cell extract" (PE)). Then a small scraping of the pellets were taken out and resuspended in 100 µL SDS-PAGE running buffer, and a 30 µL aliquot was retained (henceforth referred to as "cytoplasmic cell extract" (CE)). For the uninduced sample (1 ml) the pellet is boiled with 1% SDS for 10 min and 30 µL was taken for SDS-PAGE analysis. All the samples (Uninduced, WE, WW, PE and CE) was analyzed by 12% tris-tricine SDS-PAGE.

5.2.9 Affinity purification

The Ni-NTA resin stored in 20% ethanol was poured into gravity flow column and washed extensively with MilliQ water. The beads were equilibrated with TNG buffer (20

mM Tris, 200 mM NaCl, 10% glycerol, pH 8.0). The periplasmic extract (PE) was collected in a beaker on ice and 2.6 mL 0.5 M Tris pH 8.0, 2.6 mL 5 M NaCl and 6.5 mL 100% glycerol was added to get final concentration of ~20 mM Tris, ~200 mM NaCl and ~10% glycerol (i.e. TNG buffer). The addition of the components was split into three steps. The 6mL of pre-equilibrated Ni-NTA resin slurry was then added to the buffered PE. The mixture was stirred for 1 h to allow binding to resin. This was then poured into an empty gravity flow column. The flow through was collected and the column was washed extensively (5-6 times, each with 50 ml for pellet from 1 L culture) with wash buffer (TNG buffer with 15 mM imidazole). The protein bound to the beads was eluted out using TNG buffer with 250 mM imidazole (20 ml). The imidazole was removed from the eluate with an Amicon Ultra 3 kDa centrifugal filter (Millipore, Billerica, MA, USA) using TNG buffer. The final solution was made up to 10 mL by the addition of redox buffer (final concentration of GSSH:GSG = 1:10). TEV protease (expressed and purified) was added to the solution, before incubation for 12–13 h with shaking, in order to release the recombinant haditoxin from the MBP fusion protein. TEV enzyme was used in a w/w ratio of 1:20 with that of the fusion protein. Finally, the solution was passed over the Ni-NTA Superflow matrix in order to capture the His6-MBP and His6-TEV. The flow through containing recombinant peptide toxin was collected in TNG buffer.

5.2.10 Purification of the cleaved protein using RP-HPLC

The recombinant tag free haditoxin was further purified using RP-HPLC. The cleaved protein was filtered before injecting into a Jupiter C18 analytical column preequilibrated with buffer A (0.1% (v/v) Trifluoroacetic acid; TFA in water). The untagged protein (after

TEV protease cleavage) was eluted with a linear gradient of 25%-45% of buffer B (80% acetonitrile (v/v) in 0.1% (v/v) TFA) at a flow rate of 1 ml/min. The fractions were collected and further they were subjected to ESI-MS for mass determination.

5.2.11 Mass determination

Fractions obtained from the RP-HPLC were directly injected into an API-300 LC/MS/MS system (PerkinElmer Life Sciences, Wellesley, MA, USA) to determine the mass of the proteins present. Electrospray ionization mass spectrum (ESI-MS) was acquired in a same method as described in chapter 2 (section 2.2.4). Analyte software (PerkinElmer Life Sciences, Wellesley, MA, USA) was used to analyze and deconvolute the raw mass data. Fractions showing the expected MW were pooled and lyophilized.

5.2.12 *Ex vivo* organ bath studies with recombinant haditoxin

Isolated tissue experiments with chick biventor cervicis muscle (CBCM) using organ bath were performed following the same procedure as described in chapter 3 (section 3.2.6 and 3.2.11). The effects of various concentrations of haditoxin (0.03 to 10 μM; n=3) on the response of exogenous ACh, CCh or KCl on CBCM were investigated. Blockade of the responses to ACh, CCh and KCl by haditoxin are expressed as a percentage of the respective control response prior to the addition of the toxin.

5.2.13 Statistical analysis

The data were expressed as mean ± standard error of mean (SEM) of at least 3 experiments. The experiments with higher dose of haditoxin (like- 5 and 15 μM) were

done with n=3. The data was analyzed using Origin software version 5.0 (OriginLab, Northampton, MA, USA).

5.3 RESULTS

5.3.1 Interaction of haditoxin with AChBP

The soluble acetylcholine-binding protein (AChBP) is a structural homologue of the extracellular ligand binding domain of muscle-type and neuronal nAChRs (Smit *et al*, 2001; Brejc *et al*, 2001; Hansen *et al*, 2004). 10 μM of haditoxin was screened for its ability to compete or interfere with the binding of [^{3}H]epibatidine to the 5 AChBPs (Ls, Ac and the three Ac mutants, AcY55W, Ac5', Ac2'3''6), as measured by a scintillation proximity assay (**Fig. 5.2**). As shown in the figure haditoxin failed to show significant interference for the binding of [^{3}H]epibatidine to the binding proteins. These results suggested that either haditoxin did not interact with the binding protein or it did not competed with [^{3}H]epibatidine for the same binding site. As expected, significant interference for the binding of [^{3}H]epibatidine to the binding proteins was observed with nicotine except for the mutant Ac2'3''6.

5.3.2 Interaction of haditoxin with 5-HT$_3$ receptors

We have characterized haditoxin for its interaction with 5-HT$_3$ receptors using Ca2+/Fluo4 asaay. This experiment was done to find out the specificity of the toxin towards nicotinic receptors, since ligands targeting nicotinic receptors (especially α_7-nAChR) often hit other cys-loop receptors belonging to the super family ligand-gated ion channel receptors (for review see, Connolly and Wafford 2004; Ortells and Lunt, 1995). The cross reactivity was mostly observed with the 5-HT$_3$ receptors because of the high (30%) sequence homology observed between these two class of receptors (Maricq *et al*, 1991; Werner *et al*, 1994). We have checked the cross

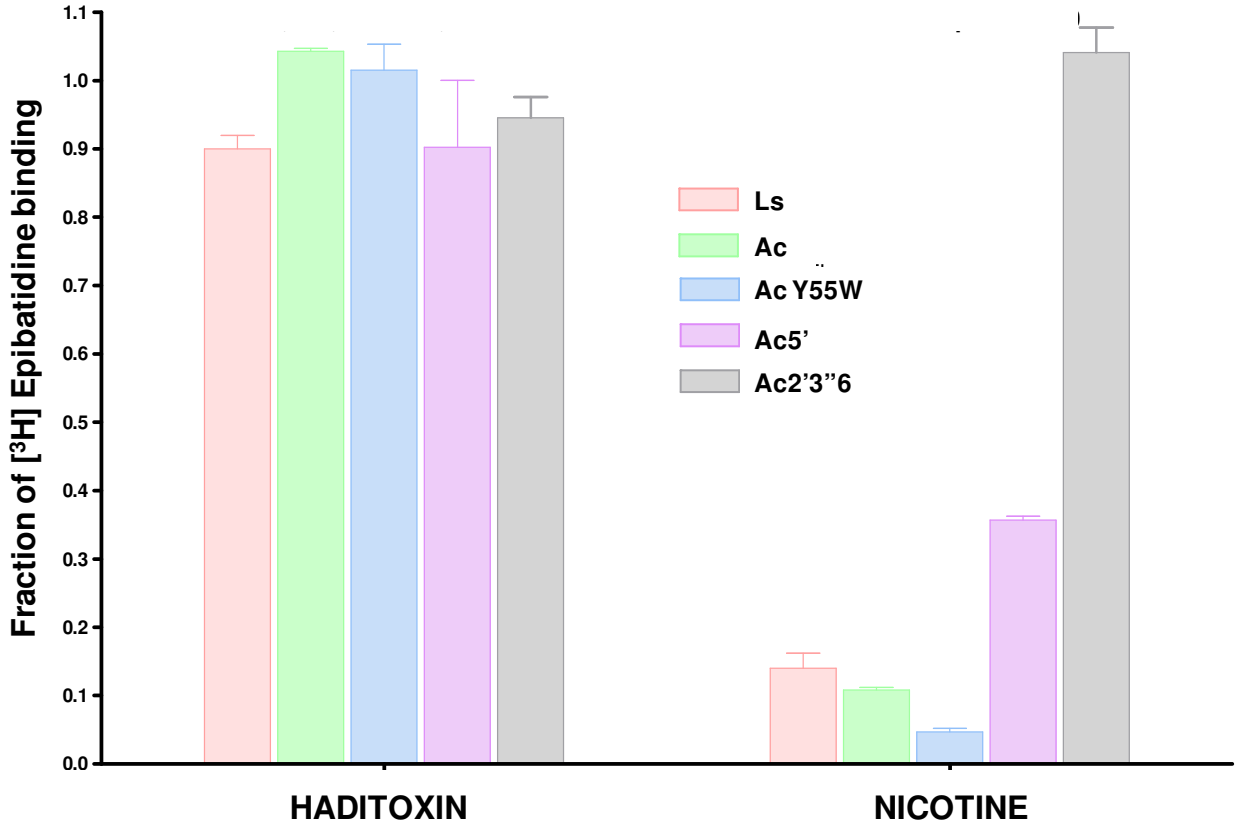

Figure 5.2: Interaction of haditoxin with acetylcholine binding protein and mutants.

Compititive radioligand binding assay of haditoxin vs. Acetylcholine binding proteins (Ls: *Lymnaea stagnalis*; Ac: *Aplysia californica* and Ac y55W, Ac5' & Ac2'3"6: *Aplysia californica* mutants). The concentration of haditoxin used was 10 µM. Nicotine (10 µM) was used as positive control. The radioligand used was [^{3}H] Epibatidine. Results were expressed as fraction of epibatidine binding.

reactivity of haditoxin towards 5-HT_{3A} and 5-HT_{3AB} receptors using $Ca^{2+/}$Fluo4 assay. As observed in table 5.1 and figure 5.3 haditoxin did not exhibited any kind of activity (neither as antagonists or potentiators) at these receptors up to a concentration of 30 µM. As expected, 5-hydroxytryptamine or serotonin exhibited a potent agonistic effect and ondansetron, 5-HT_3 receptor blocker (Zoldan *et al*, 1996), exhibited a potent antagonistic effect. Hence, it can be concluded that haditoxin did not interact with 5-HT_3 receptors and it is a selective blocker for the nicotinic receptors, unlike the small molecular nicotinic ligands including acetylcholine (Gurley and Lanthorn, 1998; Steward *et al*, 2000; Machu *et al*, 2001; Broad *et al*, 2002; Drisdel *et al*, 2008).

5.3.3 Recombinant expression and purification of haditoxin

Recombinant haditoxin was successfully produced using the *E. coli* periplasmic expression system. The denaturing gel (SDS-PAGE) showing over-expression and initial purification of the toxins can be seen in figure 5.4. Comparison of the whole-cell extracts for the negative control (lane 1, labeled "Un") and the periplamic extract after IPTG induction (lane 5, labeled "PE") reveals that an intense band at ~49 kDa, consistent with the expected size of the His6-MBP-haditoxin fusion protein, is only present after IPTG induction. Moreover, as expected, this protein was found predominantly in the periplasmic fraction (labeled "PE"), with only minimal amounts, if any, present in the cytoplasmic extract (lane 6, labeled "CE"). Hence, it was concluded that the MBP-haditoxin fusion proteins have been highly over-expressed in *E. coli* and are found almost exclusively in the periplasmic extract.

Table 5.1: Interaction of the Haditoxin with human 5-HT_3A and 5-HT_3AB receptors.

	5-HT_3A	5-HT_3AB
Agonist		
Serotonin	0.32 [6.49 ± 0.02]	0.65 [6.18 ± 0.05]
Compounds		
Haditoxin	> 30 [< 4.5]	> 30 [< 4.5]

The IC_{50} values were obtained using the Ca2+/Fluo-4 assay at 5-HT_3A- and 5-HT_3AB-HEK293 cell lines. An assay concentration of 1 µM serotonin was used as agonist in the antagonist experiments. The EC_{50} values for serotonin and the IC_{50} values for the antagonists are given in µM with pEC_{50} ± S.E.M. and pIC_{50} ± S.E.M. values in brackets, respectively, and represent the means of 3-4 experiments performed in duplicate.

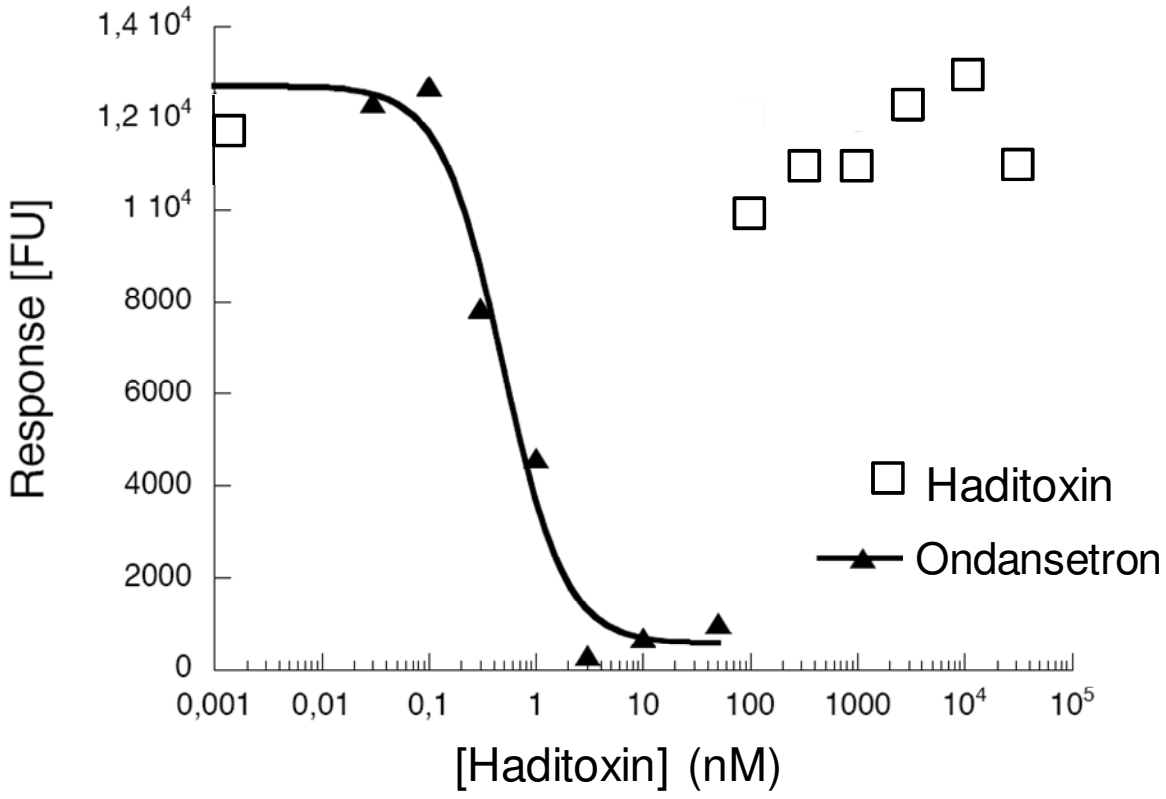

Figure 5.3: Dose-dependent inhibition curve of haditoxin on 5-HT_3A receptors.

The data points were obtained from the Fluo4-Ca2+ assay using 5-HT_3A/ HEK293 cell lines. Ondansetron, a standard antagonist was used as a positive control. Antagonism was observed at a concentration of 1 μM 5-HT.

Lane 7, 8, 9 and 10 in figure 5.4 shows the result of the affinity chromatography using Ni-NTA beads. The flow through (lane 7, labeled as "Flt") and washes (lane 8 and 9, labeled as "W1" and "W2" respectively) showed that the MBP-haditoxin fusion protein was bound to the Ni-NTA beads and the intense band in lane 10 (labeled as "Elu") indicates that the protein was eluted out from the column along with the elution buffer. Following nickel affinity chromatography, TEV cleavage of the fusion protein was performed. The intense bands in lane 2, 3, 4 and 5 in figure 5.5 indicates the successful cleavage of the fusion protein and release of both the fusion partners (one band at ~ 7 kDa, which is probably of the toxin and the other band at ~45 kDa, which is probably the His6-MBP. The untagged recombinant toxin was eluted out from the Ni-NTA column whereas the His6-MBP remained in the column and was further eluted out using elution buffer containing imidazole as shown in lane 7 and 8 of figure 5.5. Post cleavage the toxin was further purified using RPHPLC. The resulting HPLC chromatogram is shown in figure 5.6. The peak indicated by the black arrow is the fraction containing recombinant haditoxin. All the peaks obtained from the RP-HPLC was subjected to ESI-MS for mass confirmation and hence identity. The molecular weight of the peak indicate by the black arrow in figure 5.6 showed three peaks with mass/charge ratios ranging from +5 to +7 charges (**Fig. 5.7 A**), and the final reconstructed spectrum showed a molecular weight of 7592.01 ± 0.66 Da (**Fig. 5.7 B**) similar to the calculated mass of the recombinant haditoxin with all the cysteines oxidized.

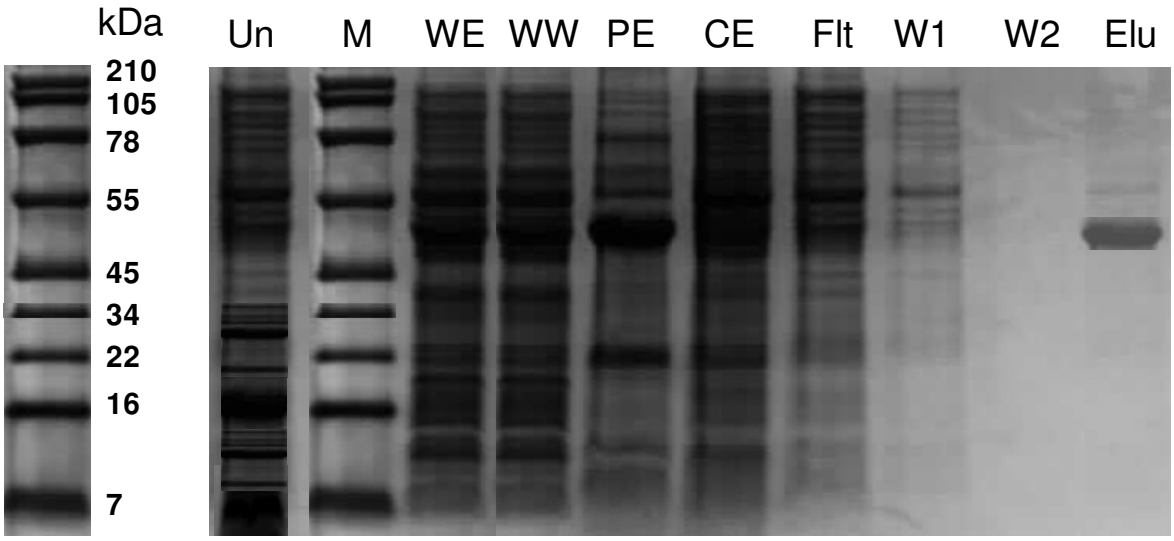

Figure 5.4: SDS-PAGE picture showing over-expression and affinity purification of recombinant haditoxin.

Lane markings on the top indicate- Un: uninduced whole cell extract, M: Marker for protein molecular-weight standards, WE: induced whole cell extract, WW: whole cell extracts of cells suspended in water, PE: periplasmic extract, CE: cytoplasmic extract, Flt: flowthrough, W1: wash first time, W2: wash second time and Elu: Elution of recombinant haditoxin. The masses for each of the standard are shown on the left of the gel. The thick band in between 55 and 45 Da as seen in lane 5, in the periplasmic extract is presumed to be the MBP-toxin fusion proteins (calculated molecular weight ~ 50 kDa).

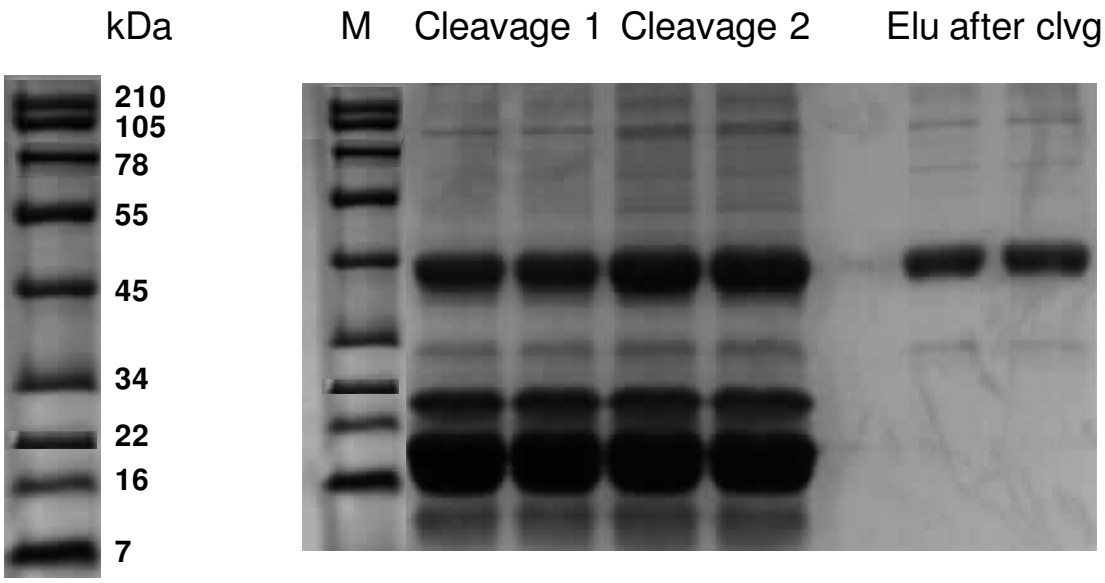

Figure 5.5: SDS-PAGE picture showing TEV cleavage of recombinant haditoxin.

Lane markings on the top indicate- M: Marker for protein molecular-weight standards, Cleavage 1: Cleavage reaction was set up with lower concentration of fusion protein, Cleavage 2: Cleavage reaction was set up with higher concentration of fusion protein and Elu aftr clvg: Elution of MBP after separating the tag free recombinant haditoxin. The masses for each of the standard are shown on the left of the gel. The thick bands near 7 kDa as seen in lane 1, 2, 3 and 4 are presumed to be the tag free haditoxin (calculated molecular weight ~ 7592 Da) and the bands near 43 kDa as seen in lane 1, 2, 3, 4, 6 and 7 are presumed to be the MBP tag (calculated molecular weight ~ 43 kDa).

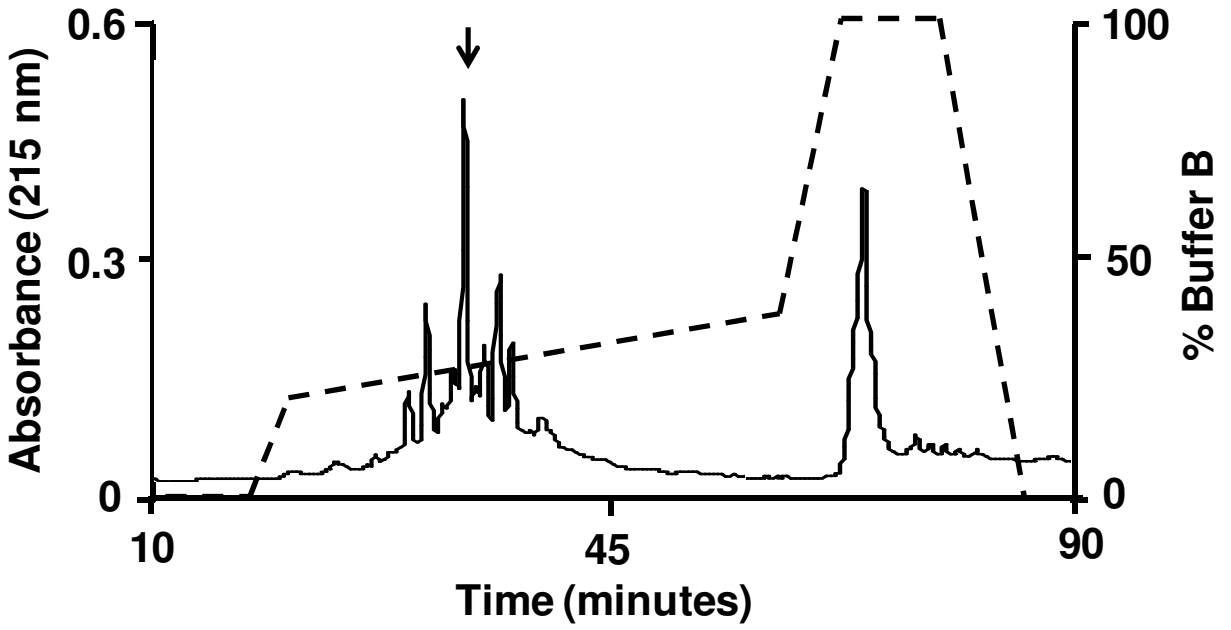

Figure 5.6: RP-HPLC profile of recombinant haditoxin.

After TEV cleavage recombinant haditoxin was subjected to RP-HPLC using a Jupiter C18 (5 µ, 300 Å, 4.5 x 250 mm) analytical column was equilibrated with aqueous 0.1% (v/v) TFA (buffer A). The protein was eluted from the column with a flow rate of 1 ml/min with a gradient of 23-49% (over a time period of about 90 minutes) buffer B (80% acetonitrile in 0.1% TFA). The dotted line (- - -) indicates the gradient of the buffer B. The black downward arrow indicates the peak containing recombinant haditoxin. Elution of protein was monitored at 215 nm.

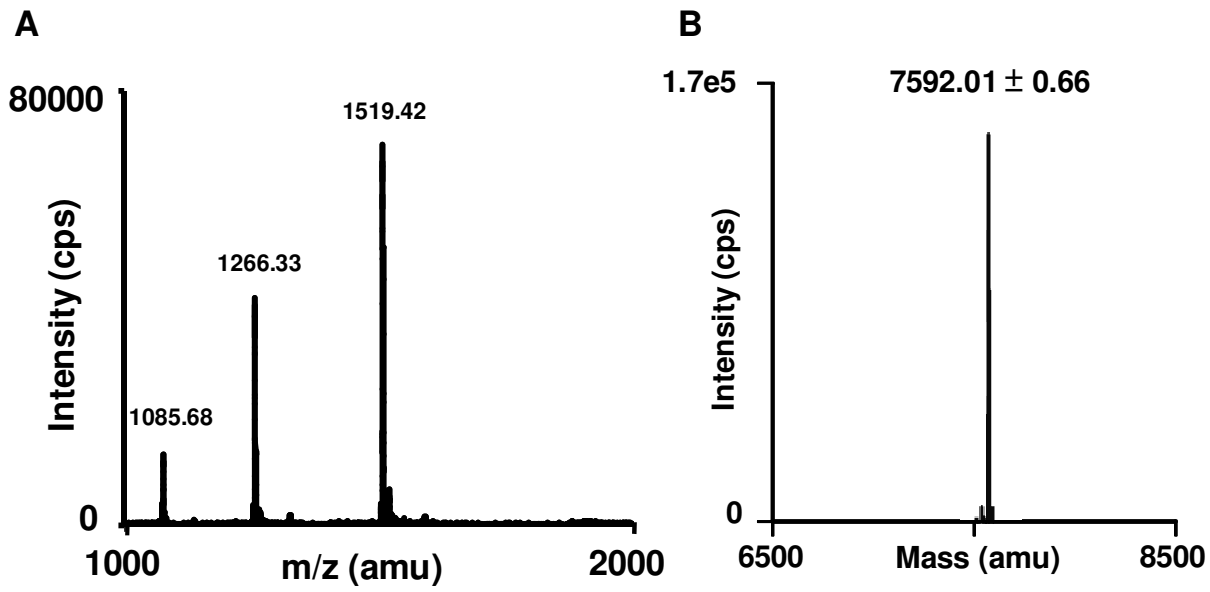

Figure 5.7: ESI-MS spectrum of the recombinant haditoxin.

RP-HPLC fraction containing recombinant haditoxin was subjected to ESI-MS using an API-300 liquid chromatography/tandem mass spectrometry system. The spectrum shows a series of multiply charged ions ranging from +5 to +7 charges (A), corresponding to a single, homogenous peptide with a molecular weight of 7592.01 ± 0.66 Da (B).

5.3.4 Functional characterization of recombinant haditoxin using CBCM

Recombinant haditoxin produced a time-dependent blockade of the nerve evoked twitch responses of CBCM **(Fig. 5.8)**. The contractile response to exogenous agonists (ACh and CCh) was completely inhibited by haditoxin whereas, response to exogenous KCl and twitches evoked by direct muscle stimulation were not inhibited. No contracture or increase in muscle tone was observed with any of the doses of haditoxin tested for up to 180 minutes following the addition of the toxin. This indicates a post-synaptic neuromuscular blockade and an absence of direct myotoxicity. The dose-dependent effect of recombinant haditoxin was examined on CBCM. A dose-response curve was constructed and the IC_{50} of recombinant haditoxin on CBCM was calculated to be 0.25 ± 0.10 μM **(Fig. 5.9)** (considering the monomeric mass of the protein).

Addition of native haditoxin, purified from the venom (as described in chapter 2) also completely inhibited the nerve evoked twitch responses of CBCM in a time-dependent fashion, without affecting the twitch response elicited by direct muscle stimulation or the response to exogenously applied KCl (already discussed in chapter 3). A dose-response curve was constructed for native haditoxin on CBCM and the IC_{50} was determined to be 0.27 ± 0.07 μM (**Fig 3.6**, chapter 3). Hence, compared to the native haditoxin the recombinant one was found to be equipotent on avian (CBCM) neuromuscular junctions.

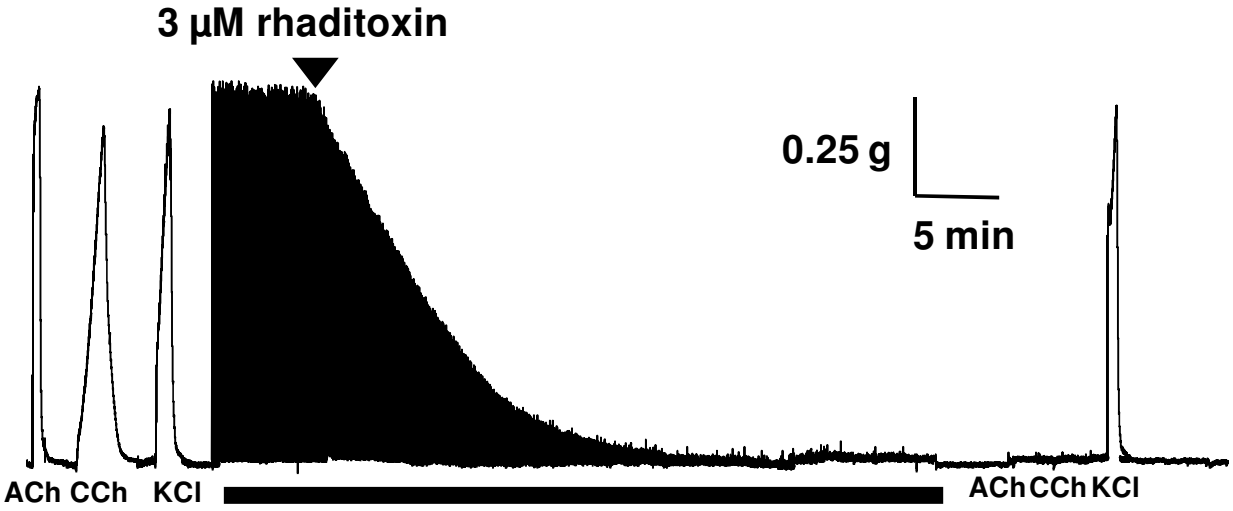

Figure 5.8: Effect of recombinant (r) haditoxin on the twitch response of CBCM elicited by nerve stimulation and exogenously applied acetylcholine, carbachol and potassium chloride.

A segment of tracing showing the effect of haditoxin (3 µM) on chick biventer cervicis muscle preparations (CBCM) (n=3). Twitch response of the muscle was elicited by electrical field stimulation (EFS, indicated by the black bar) and by applying exogenous agonists, acetylcholine (ACh; 300 µM), carbachol (CCh; 10 µM) and potassium chloride (KCl; 30 mM). The vertical bar represents the magnitude of twitch response in gram tension and the horizontal bar depicts the time in minute.

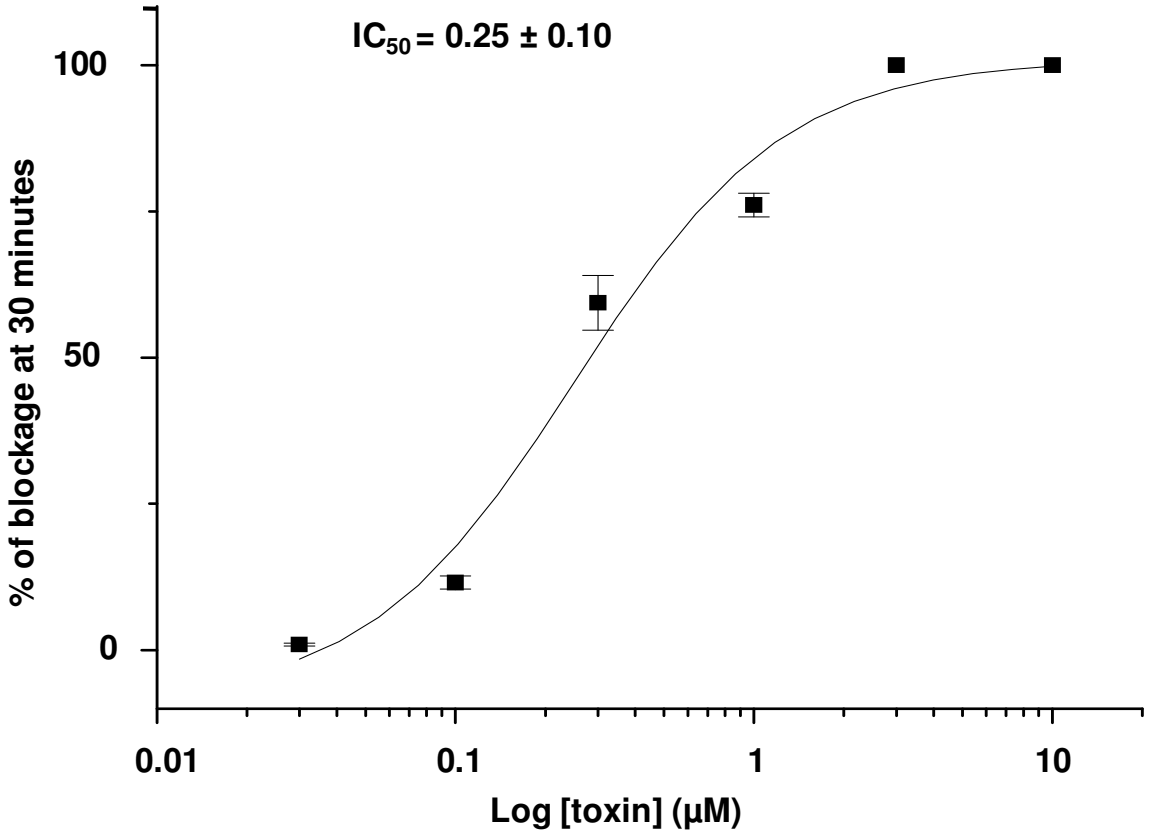

Figure 5.9: Dose-response curve of recombinant haditoxin on CBCM.

The concentration-response curve for the blockade of nerve-evoked twitch responses in the chick muscle by of recombinant haditoxin. The block is calculated as a percentage of the control twitch responses of the muscle to supramaximal nerve stimulation in the absence of toxins. Each data point is the mean ± S.E. of at least three experiments.

5.4 DISCUSSION

Mother Nature has always reengineered proteins for new functions through evolutionary processes. Understanding how protein architectures evolve to accommodate a variety of functions remains a primary focus in protein chemistry. Knowledge about the relationships between protein structure and function has the potential to reveal fundamental characteristics of protein structures as well as the explicit manner in which they deliver their associated functions. To vivdly understand the structure-function paradigm, particularly useful structural information is extracted from the primary amino acid sequences and the associated tertiary/quaternary structures. The task becomes more difficult when the group of proteins being investigated belongs to a structurally similar family but functionally diverse. A classical example of such a family is the snake venom three-finger toxins. All the proteins in this family share a similar pattern of protein folding: three β-stranded loops extending from a central core, which is stabilized by the four conserved disulfide bonds. Because of their appearance, this family of proteins is called the three-finger toxin family. However, they exhibit distinct pharmacological properties including neurotoxic, cardiotoxic, anticoagulant and antiplatelet effects. It has been observed that slight alterations in the primary structure (the amino acid residues) of these proteins may result a completely different physiological function, while retaining the same three-finger fold. Therefore, their structure-function relationships are subtle and complicated.

We have characterized a novel three-finger neurotoxin, haditoxin from the venom of king cobra. Haditoxin In this chapter, we have described few experiments which have been performed to understand the very basics of the structure-function relationship of this

protein. Haditoxin is the first dimeric α-neurotoxin to interact with the muscle type nicotinic receptors as well as the first short-chain α-neurotoxin to interact with the neuronal α_7 nicotinic receptors although it lacks the extra disulfide bridge at the tip of the loop 2, known to be essential to interact with neuronal receptors. Therefore, to find out the novel structural elements through which haditoxin interacts with the nicotinic receptors we tried to observe the interaction of haditoxin with acetylcholine binding protein (AChBP). AChBP is a novel glial-derived soluble protein, which is an analogue of the ligand-binding domains of the nicotinic acetylcholine receptor (nAChRs) (Brejc *et al*, 2001; Smith *et al*, 2001; Brejc *et al*, 2001). Like the nAChRs, it assembles into a homopentamer with ligand-binding characteristics that are typical for a nicotinic receptor. Until now, several nicotinic small molecular ligands and α-conotoxins have been co-crystallized with AChBP (Hansen, *et al*, 2004; Celie *et al*, 2004; Ulen *et al*, 2006). Structures of such complexes have provided insights into the ligand binding site present at the cleft formed by subunit-subunit interface of nAChR. Till date, the first and only snake venom neurotoxin co-crystallized with AChBP was the long-chain α-neurotoxin, α-cobratoxin, isolated from the venom of *Naja kauothia* (Bourne *et al*, 2005). This revealed the toxin/receptor interaction site present at subunit-subunit interface. The interaction sites deduced from the structure of AChBP-toxin complex contribute greatly to the understanding of nAChR-snake neurotoxin interactions. However, there are not much structural details available on how a dimeric neurotoxin interacts with the nicotinic receptor.

Therefore, with an ultimate aim to co-crystallize haditoxin with AChBP we observed the interaction between haditoxin and AChBP using competitive radioligand binding assay.

As shown by the results haditoxin did not show any competition with epibatidine to interact with the AChBP or its mutants. This could be because of the specificity of haditoxin towards vertebrate nicotinic acetylcholine receptors and not to the invertebrate analog. There is also another possibility that haditoxin may bind to a different site compared to epibatidine, which made it non-competitive, but this can only be confirmed with further experiments.

Nicotinic receptors are pentamaric ligand-gated ion channel receptors (for review see, Karlin, 2002). The ligand binding site of this receptor is characterized by a cysteine loop between Cys^{119} and Cys^{132} (Torpedo α-subunit numbering). This is common with other members of the ligand gated ion channels including gamma amino butyric acid ($GABA_{A,C}$), glycine, and 5-hydroxytryptamine (5-HT_3) receptors. Hence, together, these receptors belong to the "Cys-loop" superfamily of ligand-gated ion channels (Ortells and Lunt, 1995; Le Novère and Changeux, 1999; Corringer *et al*, 2000). Among all these receptors 5-HT_3 receptor shares about 30% sequence homology with the nicotinic receptors (Maricq *et al*, 1991; Werner *et al*, 1994). As a result of this, the ligands which binds to nicotinic receptors (including acetylcholine) also interacts with 5-HT_3 receptors and vice-versa. Because of this cross interaction there are several disadvantages when using either nicotinic ligands or 5-HT_3 receptor ligands in clinical practice. Hence, we wanted to check the interaction of haditoxin, which is a nicotinic ligand, towards 5-HT_3 receptors using Ca^{2+}/Fluo4 assay. Haditoxin did not exhibit any kind of interaction with 5-HT_3 receptors. Therefore, it can be concluded that haditoxin is specific towards nicotinic receptors only, without any cross reactivity with 5-HT_3 receptors. Thus, haditoxin can be further analyzed to find out the novel structural elements which are specific towards the

nicotinic receptors and these elements can be used as a model to design drugs specific towards nicotinic receptors.

Haditoxin is the first dimeric α-neurotoxin interacting with the muscle nicotinic receptors. Therefore, we wanted to know what will happen if the protein become monomeric. To answer this question we decided to perform mutagenesis studies of the interface residues, but this demands the recombinant expression of haditoxin. Hence, we proceeded for the recombinant expression of wild-type haditoxin in bacterial system. Haditoxin was expressed successfully in bacteria using a periplasmic expression vector. The expressed toxin was purified and the tag was cleaved off. The untagged protein was further purified using RP-HPLC and the identity was confirmed by mass spectrometry. Next, it was necessary to assess the functional properties of recombinant haditoxin thus, we performed *ex vivo* organ bath studies using chick biventer cervicis muscle. It was observed that the recombinant haditoxin acts similar to the native one producing a potent post-synaptic neuromuscular blockade. The IC_{50} of the recombinant toxin (0.25 ± 0.10 μM in Fig. 5.9), as determined from the dose-response curve, was comparable to that of the native one (0.27 ± 0.07 μM in Fig 3.6, chapter 3). Currently, we are designing the mutants to alter the dimeric interface of wild-type haditoxin which will allow us to express the monomeric toxin. This will be followed by the tissue organ bath assay and/or electrophysiological assay to evaluate the functional properties of the monomeric haditoxin. It will reveal the role of the dimeric three-dimensional structure of haditoxin towards its neuromuscular blockade function.

5.5 CONCLUSIONS

In summary, haditoxin does not compete with the radioligand to interact with the invertebrate nicotinic receptor homolog, AChBP, possibly because of its specificity towards vertebrate nicotinic receptors or the binding site for the radioligand and haditoxin is different in the AChBP. Haditoxin did not show any cross reactivity toward other cys-loop ion channel receptors such as- 5-HT_3 receptors and it was found to be a specific antagonist for nicotinic receptors. We have successfully expressed recombinant haditoxin and it was found to be equipotent on CBCM compared to the native one. Further site-directed mutagenesis studies are in progress.

Chapter Six

Conclusions and future perspective

CHAPTER SIX

Conclusions and future prospective

6.1 CONCLUSIONS

This thesis reports the isolation and characterization of a novel three-finger toxin, haditoxin. It was first identified in the cDNA library of the venom gland tissue of *O. hannah*. According to the cDNA sequence, haditoxin consists of a single polypeptide chain of 66 amino acid residues with a calculated molecular mass of 7534.42 Da. The primary structure of haditoxin revealed that the cysteine bonding pattern is conserved with the members of the three-finger family of snake venom proteins, which shows that the protein is a members of this family. Based on the primary structure, haditoxin exhibited about 37-57% of homology with other 3FTXs including, muscarinic toxins, short-chain α-neurotoxins, long-chain α-neurotoxins, κ-neurotoxins and non-conventional neurotoxins. Interestingly, it was found that haditoxin shared the highest sequence homology (~ 80%) with the muscarinic toxins homologs, MTLP-3 (the name 'MTLP' was given based on the observed sequence identity with muscarinic toxins), with unknown molecular targets.

For detailed structural and functional analysis haditoxin was purified to homogeneity from the crude venom of *O. hannah*, by successive gel filtration chromatography and reverse-phase HPLC. The identity of the purified protein was confirmed by N-terminal sequencing. Purified haditoxin was found to be homogeneous by mass spectrometry and capillary electrophoresis. The secondary

structure was found to be predominantly β-sheet similar to other three-finger toxins. Surprisingly, when we tested haditoxin for muscarinic activity (based on the observed sequence homology), it failed to show any activity. Further *in vivo* assay in mice with haditoxin showed symptoms of peripheral neurotoxicity similar to α-neurotoxins. Hence, we observed the effect of haditoxin on the neuromuscular junction. The toxin produced a potent neuromuscular blockade in isolated nerve-muscle preparation. The reversibility of this blockade was species specific, probably because of the dietary nature of the snake. Based on the primary sequence (65 amino acids with four disulfide bridges) and the neuromuscular blocking property haditoxin was more likely similar to a short-chain α-neurotoxin. The neuromuscular blockade effect was further confirmed by electrophysiology studies on expressed muscle (αβγδ) type nAChRs.

Surprisingly, in the electrophysiology experiments haditoxin showed nanomolar affinity towards α_7-nAChRs. This was a very interesting finding because, till date none of the other short-chain α-neurotoxins are known to interact with neuronal nAChRs. This is the first report of a short-chain α-neurtoxins targeting the neuronal α_7-nAChRs. Haditoxin also produced a potent blockade on $\alpha_3\beta_2$-nAChRs, but the blockade for $\alpha_4\beta_2$-nAChRs is in micromolar range. Moreover, in these experiments it was also observed that haditoxin produced a readily reversible blockade for the $\alpha_3\beta_2$-nAChRs whereas the blockade for the α_7-receptors was long lasting. These data strongly suggest that the nature of binding for haditoxin toward these receptors is very different.

Another interesting finding of this study was the high probability for the oligomeric nature of haditoxin. In the initial gel filtration studies during protein purification it was observed that this protein elutes earlier compared to other three-finger toxins. This could be as a consequence of oligomerization. To investigate the issue we performed gel filtration chromatography with purified haditoxin. It eluted with a relative molecular weight of 8.16 kDa, which is approximately double the molecular weight of haditoxin as observed in ESI-MS (~ 7.535 Da). The dimerization was further confirmed by SDS-PAGE in presence of a cross-linker. Thus, it is clear that haditoxin existed as a homodimer in solution.

The high resolution crystal structure of haditoxin supported the dimeric nature of the protein. The molecule was composed of two identical monomers held together by non-covalent interactions, similar to the κ-neurotoxins. Each of the monomer adapted a structure similar to the short-chain α-neurotoxins with four intramolecular disulfide bridges. Thus, haditoxin is the first dimeric short-chain α-neurotoxins.

The three dimensional structure of haditoxin revealed the presence of some functionally invariant residues in α-neurotoxins and κ-neurotoxins that are important for binding to muscle ($\alpha\beta\gamma\delta$) and neuronal ($\alpha_3\beta_2$ and $\alpha_4\beta_2$) nAChRs. These putative functionally important residues were found to be located in homologous positions and in similar spatial disposition in the tertiary structure of haditoxin which can explain the potent neuromuscular blockade as well as the ACh-induced current blockade in $\alpha_3\beta_2$- and $\alpha_4\beta_2$-nAChRs produced by haditoxin.

Interestingly however, haditoxin lacked the fifth disulfide bridge at the tip of loop II in long-chain α-neurotoxins, hitherto considered to be crucial for neurotoxins to bind to α_7-nicotinic receptors with high affinity. Moreover, haditoxin also lacks the specific determinants of long-chain α-neurotoxins known to be critical for the interaction with α_7-nicotinic receptors. Thus, haditoxin is the first known toxin documented that lacks this important structural configuration, and yet still capable of mediating a functional block of α_7 nicotinic receptors at nanomolar concentrations. Clearly therefore, haditoxin utilizes other, yet undetermined, functional determinants in its interaction with the neuronal α_7-nAChRs.

To investigate these novel structural elements we have initiated the structure-function relationship studies of haditoxin. In order to co-crystallize the protein with the acetylcholine binding protein (AChBP), the homolog for the ligand binding domain of nicotinic receptors, we studied the interaction of haditoxin with AChBP using competitive radioligand binding experiments. Haditoxin did not compete with the radioligand to interact with AChBP. We have also examined the interaction of haditoxin towards other ligand-gated ion channel receptors, but unlike the small molecular ligands, haditoxin did not show any interaction with them. Finally, we expressed recombinant haditoxin in bacterial expression system for further site-directed mutagenesis studies. The recombinant protein was functionally equipotent as the native protein as observed on the chick neuromuscular junction.

6.2 FUTURE PERSPECTIVE

The work described in this thesis has addressed some fundamental issues related to the structure and function of haditoxin, a novel three-finger neurotoxin from king cobra venom. We have also initiated preliminary structure-function relationship studies to understand novel elements responsible for the unique pharmacological properties of the toxin. However, there are some pertinent questions, answers for which will open up new and exciting avenues of investigation in the future. Some of them are discussed in the following sections.

6.2.1 Role of the dimeric structure of haditoxin towards neuromuscular blockade

Haditoxin is the first dimeric neurotoxin to interact with muscle type nicotinic receptors. It will be interesting to examine the function of haditoxin in a monomeric form. This can be achieved by mutating the amino acid residues which present at the dimeric interface and important to maintain the non-covalent interaction. This can be followed by expression and functional characterization of the mutant protein(s).

6.2.2 Novel structural elements of haditoxin to interact with α_7-nAChR

Haditoxin lacks the extra disulfide bridge compared to all the snake venom neurotoxins that interact with the α_7-nAChRs. It also lacks the specific

determinants of long-chain α-neurotoxins (Ala28 and Lys35; α-cobratoxin numbering) towards the neuronal (α_7) nAChRs. Thus, it is of great interest to find out the structural elements responsible for the nanomolar affinity of haditoxin towards α_7-nAChRs, possibly by site-directed mutagenesis studies followed by the functional characterization of the mutants on the same receptor.

6.2.3 Binding mode of haditoxin to α_7-nAChR

The mode of binding of haditoxin towards the α_7-nAChR is also crucial to understand. One of our collaborators has constructed a series of receptor mutants with mutations in the orthosteric binding site of α_7-nAChR. Binding mode of haditoxin can be investigated, by characterizing the impact of different mutations on the antagonism produced on α_7-nAChR.

6.2.4 Structural determinants of haditoxin conferring reversibility

It has already been suggested that the reversibility of neuromuscular blockade produced by some neurotoxins may be associated with a specific area of interaction on the toxin molecule, distinct from the receptor recognition site (Harvey and Rodger, 1978). Site directed mutagenesis of individual residues in haditoxin may be able to identify specific residue(s), if any, that may be involved in conferring the reversibility to the nicotinic receptor blockade produced by

haditoxin. Understandably, this will be a formidable challenge because of the lack of information to postulate the possible residues that could be involved.

6.2.5 Kinetics of interaction between haditoxin and neuronal receptors

In the electrophysiology experiments there was a 3-fold difference in the EC_{50} of haditoxin towards α_7- and $\alpha_3\beta_2$-nAChRs but the blockade on $\alpha_3\beta_2$-nAChRs was readily reversible, whereas the blockade for the α_7-nAChRs was practically irreversible. This reveals that the association and dissociation of haditoxin for these two receptors are very different. Radioligand binding experiments can be performed to analyze in details the kinetics of binding for haditoxin towards these receptors in order to elucidate this mechanism involved.

Bibliography

BIBLIOGRAPHY

Adem A, Asblom A, Johansson G, Mbugua PM, Karlsson E. (1988) Toxins from the venom of the green mamba Dendroaspis angusticeps that inhibit the binding of quinuclidinyl benzilate to muscarinic acetylcholine receptors. *Biochim Biophys Acta* 968(3), 340–345.

Adem A, Karlsson E. (1997) Muscarinic receptor subtype selective toxins. *Life Sci.* 60(13-14), 1069-1076.

Aird SD, Kaiser II. (1985) Toxicity Assays. *Toxicon.* 23(1), 11-13.

Aird SD, Womble GC, Yates JR 3rd, Griffin PR. (1999) Primary structure of gamma-bungarotoxin, a new postsynaptic neurotoxin from venom of *Bungarus multicinctus*. *Toxicon*. 37(4), 609-625.

Albrand JP, Blackledge MJ, Pascaud F, Hollecker M, Marion D. (1995) NMR and restrained molecular dynamics study of the three-dimensional solution structure of toxin FS2, a specific blocker of the L-type calcium channel, isolated from black mamba venom. *Biochemistry.* 34(17), 5923-5937.

Antil S, Gaillard C, Tamiya T, Corringer PJ, Changeux JP, Servent D, Menez A. (2000) Molecular determinants by which a long chain toxin from snake venom interacts with the neuronal alpha 7-nicotinic acetylcholine receptor. *J Biol Chem.* 275(38), 29594-29601.

Antil S, Servent D, Ménez A. (1999) Variability among the sites by which curaremimetic toxins bind to torpedo acetylcholine receptor, as revealed by identification of the functional residues of alpha-cobratoxin. *J Biol Chem.* 274(49), 34851-34858.

Arredondo J, Chernyavsky AI, Jolkovsky DL, Webber RJ, Grando SA. (2006) SLURP-2: A novel cholinergic signaling peptide in human mucocutaneous epithelium. *J Cell Physiol.* 208(1), 238-245.

Arias HR. (2000) Localization of agonist and competitive antagonist binding sites on nicotinic acetylcholine receptors. *Neurochem Int.* 36, 595-645.

Ashcroft FM (2000) *Ion channels and disease: channelopathies.* Academic Press: California.

Bailey GS. (1998) Enzymes from snake venom. Alaken Inc., Fort Collins, Colarado.

Barchan D, Kachalsky S, Neumann D, Vogel Z, Ovadia M, Kochva E, Fuchs S. (1992) How the mongoose can fight the snake: the binding site of the mongoose acetylcholine receptor. *Proc Natl Acad Sci*. 89(16), 7717-21.

Baraka A. (1974) Nerve and muscle stimulation of the rat isolated phrenic nervedaiphragm preparation. *Anesth Analg.* 53(4), 594-596.

Bargmann C. (2005) Neuroscience: Genomics reaches the synapse. *Nature* 436, 473-474.

Barlow A, Pook CE, Harrison RA, Wüster W. (2009) Coevolution of diet and prey-specific venom activity supports the role of selection in snake venom evolution. *Proc Biol Sci.* 276(1666), 2443-2449.

Bertrand D, Cooper E, Valera S, Rungger D, Ballivet M. (1991) Electrophysiology of neuronal nicotinic acetylcholine receptors expressed in *Xenopus* oocytes following nuclear injection of genes or cDNAs. In: Conn M, Editor, *Methods in Neuroscience,* Vol. 4. Academic Press, San Diego, pp. 174-193.

Bilwes A, Rees B, Moras D, Menez R, Menez A. (1994) X-ray structure at 1.55 A of toxin gamma, a cardiotoxin from Naja nigricollis venom. Crystal packing reveals a model for insertion into membranes. *J Mol Biol.* 239(1), 122-136.

Birrell GW, Earl ST, Wallis TP, Masci PP, de Jersey J, Gorman JJ, Lavin MF. (2007) The diversity of bioactive proteins in Australian snake venoms. *Mol Cell Proteomics.* 6(6), 973-986.

Bogin O. (2005) Venom peptides and their mimetics as potential drugs. *Modulator.* 19, 14–20. **(www.almone.com)**

Bourne Y, Talley TT, Hansen SB, Taylor P, Marchot P. (2005) Crystal structure of a Cbtx-AChBP complex reveals essential interactions between snake alpha-neurotoxins and nicotinic receptors. *EMBO J.* 24(8), 1512-1522.

Bourne Y, Taylor P, Marchot P. (1995) Acetylcholinesterase inhibition by fasciculin: crystal structure of the complex. *Cell.* 83(3), 503-512.

Bradley KN. (2000) Muscarinic toxins from the green mamba. *Pharmacol Ther.* 85(2), 87–109.

Brejc K, van Dijk WJ, Klaassen RV, Schuurmans M, van Der Oost J, Smith AB, Sixma TK. (2001) Crystal structure of an Ach-binding protein reveals the ligand binding domain of nicotinic receptors. *Nature.* 411(6835), 269-276.

Brejc K, van Dijk WJ, Smit AB, Sixma TK. (2002) The 2.7 A structure of AChBP, homologue of the ligand-binding domain of the nicotinic acetylcholine receptor. *Novartis Found Symp.* 245, 22-29.

Broad LM, Felthouse C, Zwart R, McPhie GI, Pearson KH, Craig PJ, Wallace L, Broadmore RJ, Boot JR, Keenan M, Baker SR, Sher E. (2002) PSAB-OFP, a selective alpha 7 nicotinic receptor agonist, is also a potent agonist of the 5-HT_3 receptor. *Eur J Pharmacol.* 452(2), 137-144.

Buckley NJ, Caulfield MP. (1992) Transmission: acetylcholine. In: Burnstock G. and Hoyle CHV. (Ed.), Autonomic Neuroeffector Mechanisms. Harwood Academic Publishers, USA. pp. 265–322.

Bulbring E. (1946) Observations on the isolated phrenic nerve diaphragm preparations of the rat. *Br J Pharmacol.* 1, 38 - 61.

Calvete JJ. (2005) Structure-function correlations of snake venom disintegrins. *Curr Pharm Des.* 11(7), 829-835.

Calvete JJ, Marcinkiewicz C, Monleón D, Esteve V, Celda B, Juárez P, Sanz L. (2005) Snake venom disintegrins: evolution of structure and function. *Toxicon.* 45(8), 1063-1074.

Calvete JJ, Sanz L, Angulo Y, Lomonte B, Gutiérrez JM. (2009) Venoms, venomics, antivenomics. *FEBS Lett.* 583(11), 1736-1743.

Caulfield MP, Birdsall NJ. (1998) International Union of Pharmacology. XVII. Classification of muscarinic acetylcholine receptors. *Pharmacol Rev.* 50(2), 279–290.

Celie PH, van Rossum-Fikkert SE, van Dijk WJ, Brejc K, Smit AB, Sixma TK. (2004) Nicotine and carbamylcholine binding to nicotinic acetylcholine receptors as studied in AChBP crystal structures. *Neuron.* 41(6), 907-914.

Cervenansky C, Dajas F, Harvey AL, Karlsson E. (1991) Fasciculins, anticholinesterase toxins from mamba venoms: biochemistry and pharmacology. In: Harvey AL. (Ed.), Snake Toxins. Pergamon Press, New York. pp. 303-321.

Chang CC. (1979) The action of snake venoms on nerve and muscle. In: Lee CY. (Ed.) Snake Venoms, Handbook of Experimental Pharmacology, Vol. 52, Springer-Verlag, Berlin, pp. 309-376.

Chang CC, Lee CY. (1963) Isolation of neurotoxins from the venom of Bungarus multicinctus and their modes of neuromuscular blocking action. *Arch Int Pharmacodyn Ther.* 144, 241-257.

Changeux JP. (1990) The TiPS lecture. The nicotinic acetylcholine receptor: an allosteric protein prototype of ligand-gated ion channels. *Trends Pharmacol Sci.* 11(12), 485-492.

Changeux J, Edelstein SJ. (2001) Allosteric mechanisms in normal and pathological nicotinic acetylcholine receptors. *Curr Opin Neurobiol*. 11(3), 369-77.

Changeux JP, Edelstein S J. (1998) Allosteric receptors after 30 years. *Neuron.* 21, 959-980.

Changeux JP, Kasai M, Lee CY. (1970) Use of a snake venom toxin to characterize the cholinergic receptor protein. *Proc Natl Acad Sci USA*. 67(3), 1241-1247.

Chatrath ST, Chapeaurouge A, Lin Q, Lim TK, Dunstan N, Mirtschin P, Kumar PP, Kini RM. (2011) Identification of novel proteins from the venom of a cryptic snake Drysdalia coronoides by a combined transcriptomics and proteomics approach. *J Proteome Res.* 10(2), 739-750.

Chen D, Patrick JW. (1997) The α-bungarotoxin-binding nicotinic acetylcholine receptor from rat brain contains only the α7 subunit. *J Biol Chem.* 272, 24024-24029.

Chiappinelli VA, Lee JC. (1985) kappa-Bungarotoxin. Self-association of a neuronal nicotinic receptor probe. *J Biol Chem.* 260(10), 6182-6186.

Chiappinelli,V.A. and Wolf,K.M. (1989). Kappa-neurotoxins: heterodimer formation between different neuronal nicotinic receptor antagonists. *Biochemistry*. 28, 8543-8547.

Chicheportiche R, Vincent JP, Kopeyan C, Schweitz H, Lazdunski M. (1975) Structure-function relationship in the binding of snake neurotoxins to the torpedo membrane receptor. *Biochemistry*. 14(10):2081-91.

Chimienti F, Hogg RC, Plantard L, Lehmann C, Brakch N, Fischer J, Huber M, Bertrand D, Hohl D. (2003) Identification of SLURP-1 as an epidermal neuromodulator explains the clinical phenotype of Mal de Meleda. *Hum Mol Genet.* 12(22), 3017-3024.

Coborn J. (1991) The Atlas of Snakes of the World, TFH Publications, New Jersey, USA.

Cogger HG. (2000) Reptiles & Amphibians of Australia. Reed New Holland: Sydney, Australia.

Colquhoun LM, Patrick JW. (1997) Alpha3, beta2, and beta4 form heterotrimeric neuronal nicotinic acetylcholine receptors in Xenopus oocytes. *J Neurochem*. 69(6), 2355-2362.

Colubridae species list at the TIGR Reptile Database. Accessed 4 December 2008.
Conant R, Collins JT. (1991) A Field Guide to Reptiles and Amphibians: Eastern and Central North America. Houghton Mifflin, Boston. pp. 450, 48 plates.

Connolly CN, Wafford KA. (2004) The Cys-loop superfamily of ligand-gated ion channels: the impact of receptor structure on function. *Biochem Soc Trans.* 32(Pt3), 529-534.

Corringer PJ, Le Novère N, Changeux JP. (2000) Nicotinic receptors at the amino-acid level. *Annu Rev Pharmacol Toxicol.* 40, 431-458.

Crachi MT, Hammer LW, Hodgson WC. (1999) A pharmacological examination of venom from the Papuan taipan (*Oxyuranus scutellatus canni*). *Toxicon*. 37(12), 1721-1734.

Cunningham BC, Wells JA. (1993) Comparison of a structural and a functional epitope. *J Mol Biol.* 234(3), 554 –563.

Daltry JC, Wüster W, Thorpe RS. (1996) Diet and snake venom evolution. *Nature.* 379(6565), 537-540.

de Weille JR, Schweitz H, Maes P, Tartar A, Lazdunski M. (1991) Calciseptine, a peptide isolated from black mamba venom, is a specific blocker of the L-type calcium channel. *Proc Natl Acad Sci U S A.* 88(6), 2437-2440.

Deacock ARD, Davies TDW. (1958) The influence of certain ganglionic blocking agents on neuromuscular transmission. *Brit J Anaesth.* 30(5), 217-225.

Dellisanti CD, Yao Y, Stroud JC, Wang ZZ, Chen L. (2007) Crystal structure of the extracellular domain of nAChR alpha1 bound to alpha-bungarotoxin at 1.94 A resolution. *Nat Neurosci.* 10(8), 953-962.

Dewan JC, Grant GA, Sacchettini JC. (1994) Crystal structure of kappa-bungarotoxin at 2.3-A resolution. *Biochemistry.* 33(44), 13147-13154.

Dihazi GH, Sinz A. (2003) Mapping low-resolution three-dimensional protein structures using chemical cross-linking and Fourier transform ion-cyclotron resonance mass spectrometry. *Rapid Commun Mass Spectrom.* 17(17), 2005-2014.

Doley R, Mackessy SP, Kini RM. (2009) Role of accelerated segment switch in exons to alter targeting (ASSET) in the molecular evolution of snake venom proteins. *BMC Evol Biol.* 9, 146.

Drenth J, Low BW, Richardson JS, Wright CS. (1980) The toxinagglutinin fold. A new group of small protein structures organized around a four-disulfide core. *J Biol Chem.* 255(7), 2652-2655.

Drisdel RC, Sharp D, Henderson T, Hales TG, Green WN. (2008) High affinity binding of epibatidine to serotonin type 3 receptors. *J Biol Chem.* 283(15), 9659-9665.

Dufton MJ. (1993) Kill and cure: the promising future for venom research. *Endeavour.* 17(3), 138-140.

Dufton MJ, Harvey AL. (1989) The long and the short of snake toxins. *Trends Pharmacol Sci.* 10(7), 258-259.

Dufton MJ, Hider RC. (1988) Structure and pharmacology of elapid cytotoxins. *Pharmacol Ther.* 36(1), 1-40.

Durand JF. (2004) "The origin of snakes." Geoscience Africa 2004. Abstract Volume, University of the Witwatersrand, Johannesburg, South Africa. pp. 187.

Durant NN. (1984) The physiology of neuromuscular transmission. In: Katz R (Ed.) *Muscle Relaxants.* Grune and Stratton Inc., Orlando, Florida, pp. 19-52.

Eglen RM, Hegde RS, Watson N. (1996) Muscarinic receptor subtypes and smooth muscle function. *Pharmacol Rev.* 48, 531–565.

Eglen RM, Reddy H, Watson N, Challis RAJ. (1994) Muscarinic receptor subtypes in smooth muscle. *Trends Pharmacol Sci.* 15(4), 114–117.

Ehlert FJ, Thomas EA. (1995) Functional role of M2 muscarinic receptors in the guinea pig ileum. *Life Sci.* 56(11-12), 965-971.

Emsley P, Cowtan K. (2004) Coot: model-building tools for molecular graphics. *Acta Crystallogr D Biol Crystallogr.* 60(P 12 Pt 1), 2126-2132.

Endo T, Tamiya N. (1987) Current view on the structure-function relationship of postsynaptic neurotoxins from snake venoms. *Pharmacol Ther.* 34(3), 403-451.

Endo T, Tamiya N. (1991) Structure-function relationships of postsynaptic neurotoxins from snake venoms. In: Harvey AL. (Ed.), Snake Toxins. Pergamon Press, New York. pp. 165-222.

Fairley NH. (1929a) The dentition and biting mechanism of Australian snakes. *Med J Aust.* 1, 313-317.

Fairley NH. (1929b) The present position of snake bite and the snake bitten in Australia. *Med J Aust.* 1, 296-312.

Feldman, S. (1996) *Neuromuscular block*. Butterworth – Heinemann, Oxford.

Fernandez JH, Neshich G, Camargo ACM. (2004) Using bradykininpotentiating peptide structures to develop new antihypertensive drugs. *Genet Mol Res.* 3(4), 554–563.

Fiordalisi JJ, al Rabiee R, Chiappinelli VA, Grant GA. (1994) Site-directed mutagenesis of kappa-bungarotoxin: implications for neuronal receptor specificity. *Biochemistry.* 33(13), 3872-3877.

Fleming TJ, O'hUigin C, Malek TR. (1993) Characterization of two novel Ly-6 genes. Protein sequence and potential structural similarity to α-bungarotoxin and other neurotoxins. *J Immunol.* 150(12), 5379–5390.

Fletcher CM, Harrison RA, Lachmann PJ, Neuhaus D. (1994) Structure of a soluble, glycosylated form of the human complement regulatory protein CD59. *Structure,* 2(3), 185-199.

Freitas MA, Geno PW, Sumner LW, Cooke ME, Hudiburg SA, Ownby CL, Kaiser II, Odell GV. (1992) Citrate is a major component of snake venoms. *Toxicon*. 30(4), 461-464.

Friedrich C, Tu AT. (1971) Role of metals in snake venoms for hemorrhagic, esterase and proteolytic activities. *Biochem Pharmacol.* 20(7), 1549-1556.

Fruchart-Gaillard C, Gilquin B, Antil-Delbeke S, Le Novère N, Tamiya T, Corringer P-J, Changeux J-P, Ménez A, Servent D. (2002) Experimentally based

model of a complex between a snake toxin and the alpha7 nicotinic receptor. *Proc Natl Acad Sci USA.* 99(5), 3216-3221.

Fry BG. (2005) From genome to "venome": molecular origin and evolution of the snake venom proteome inferred from phylogenetic analysis of toxin sequences and related body proteins. *Genome Res.* 15(3), 403-420.

Fry BG, Scheib H, van der Weerd L, Young B, McNaughtan J, Ramjan SF, Vidal N, Poelmann RE, Norman JA. (2008) Evolution of an arsenal: structural and functional diversification of the venom system in the advanced snakes (Caenophidia). *Mol Cell Proteomics* 7(2), 215–246.

Fry BG, Vidal N, Norman JA, Vonk FJ, Scheib H, Ramjan SF, Kuruppu S, Fung K, Hedges SB, Richardson MK, Hodgson WC, Ignjatovic V, Summerhayes E, Kochva E. (2006) Early evolution of the venom system in lizards and snakes. *Nature*. 439(7076), 584–588.

Fry BG, Vidal N, van der Weerd L, Kochva E, Renjifo C. (2009) Evolution and diversification of the Toxicofera reptile venom system. *J Proteomics.* 72(2), 127–136.

Fry BG, Wuster W, Kini RM, Brusic V, Khan A, Venkataraman D, Rooney AP. (2003) Molecular evolution and phylogeny of elapid snake venom three-finger toxins. *J Mol Evol.* 57(1), 110–129.

Fujimi TJ, Nakajyo T, Nishimura E, Ogura E, Tsuchiya T, Tamiya T. (2003) Molecular evolution and diversification of snake toxin genes, revealed by analysis of intron sequences. *Gene.* 313, 111-118.

Furchgott RF. (1972) The classification of adrenoceptors (adrenergic receptors): An evaluation from the standpoint of receptor theory. In: Blaschko H. and Muscholl E. (Ed.), Handbook of Experimental Pharmacology, Catecholamines. Springer-Verlag, New York and Heidelberg. Vol. 33, pp. 283-335.

Galzi JL, Revah F, Black D, Goeldner M, Hirth C, Changeux JP. (1990) Identification of a novel amino acid α- tyrosine 93 within the cholinergic ligand-binding sites of the acetylcholine receptor by photolabeling. Additional evidence for a three-loop model of the cholinergic ligand-binding site. *J Biol Chem* 265, 10430–10437.

Gay EA, Bienstock RJ, Lamb PW & Yakel JL (2007). Structural determinates for apolipoprotein E-derived peptide interaction with the *α*7 nicotinic acetylcholine receptor. *Mol Pharmacol* 72, 838–849.

Geh SL, Rowan EG, Harvey AL. (1992) Neuromuscular effects of three phospholipases A2 from the venom of *Pseudechis australis,* the Australian king brown snake. *Toxicon.* 30(9), 1051 – 1057.

Geh SL, Vincent A, Rang S, Abrahams T, Jacobson L, Lang B, Warrell DA. (1997) Identification of phospholipase A2 and neurotoxic activities in the venom of the New Guinean small-eyed snake (*Micropechis ikaheka*). *Toxicon.* 35(1), 101 - 109.
Gibson A, McFadzean I. (2001) Biology of the anococcygeus muscle. *Int Rev Cyt.* 205, 1-35.

Gidrol X, Chrestin H, Tan HL, Kush A. (1994) Hevein, a lectin-like protein from Hevea brasiliensis (rubber tree) is involved in the coagulation of latex. *J Biol Chem*. 269(12), 9278-9283.

Gillespie JS. (1972) The rat anococcygeus muscle and its response to nerve stimulation and to some drugs. *Br J Pharmacol*. 45(3), 404 - 416.

Gilquin B, Bourgoin M, Menez R, le Du MH, Servent D, Zinn-Justin S, Menez A. (2003) Motions and structural variability within toxins: implication for their use as scaffolds for protein engineering. *Protein Sci.* 12(2), 266-277.

Ginsborg BL, Warriner JN. (1960) The isolated chick biventer cervicis nervemuscle preparation *Br J Pharmacol.* 15, 410 - 411.

Gold BS, Dart RC, Barish RA. (2002) Bites of venomous snakes. *N Engl J Med.* 347(5), 347-356.

Gopalakrishnakone P, Chou LM (1990) Snake of medical importance. Singapore: Venom and toxins research group.

Gottschall J. (1981) The diaphragm of the rat and its innervation. Muscle fiber composition; perikarya and axons of efferent and afferent neurons. *Anat Embryol (Berl).* 161(4), 405–417.

Grant GA, al Rabiee R, Xu XL, Zhang Y. (1997) Critical interactions at the dimer interface of kappa-bungarotoxin, a neuronal nicotinic acetylcholine receptor antagonist. *Biochemistry.* 36(11), 3353-3358.

Grant GA, Chiappinelli VA. (1985) kappa-Bungarotoxin: complete amino acid sequence of a neuronal nicotinic receptor probe. *Biochemistry*. 24(6), 1532-1537.

Grant GA, Luetje CW, Summers R, Xu XL. (1998) Differential roles for disulfide bonds in the structural integrity and biological activity of kappa-Bungarotoxin, a neuronal nicotinic acetylcholine receptor antagonist. *Biochemistry.* 37(35), 12166-12171.

Greenwald J, Fischer WH, Vale WW, Choe S. (1999) Three-finger toxin fold for the extracellular ligand-binding domain of the type II activin receptor serine kinase. *Nat Struct Biol.* 6(1) 18-22.

Grutter T, Changeux JP. (2001) Nicotinic receptors in wonderland. *Trends Biochem Sci.* 26, 459-463.

Gumley TP, McKenzie IFC, Sandrin MS. (1995) Tissue expression, structure and function of the murine Ly-6 family of molecules. *Immunol Cell Biol.* 73(4), 277–296.

Gurley DA, Lanthorn TH. (1998) Nicotinic agonists competitively antagonize serotonin at mouse 5-HT_3 receptors expressed in Xenopus oocytes. *Neurosci Lett.* 247(2-3), 107–110.

Hansen SB, Talley TT, Radic Z, Taylor P. (2004) Structural and ligand recognition characteristics of an acetylcholine-binding protein from Aplysia californica. *J Biol Chem.* 279(23), 24197-24202.

Harris JB. (1991) Phospholipases in snake venoms and their effects on nerve and muscle. In: Harvey AL. (Ed.), Snake Toxins. Pergamon Press, New York. pp. 91–129.

Harrison PM, Sternberg MJ. (1996) The disulphide beta-cross: from cystine geometry and clustering to classification of small disulphide-rich protein folds. *J Mol Biol.* 264(3), 603-623.

Harvey AL. (1991) Snake Toxins. Pergamon Press, New York, USA.

Harvey AL. (2002) Toxins 'R' Us: more pharmacological tools from nature's superstore. *Trends Pharmacol Sci.* 23(5), 201-203.

Harvey AL, Barfaraz A, Thomson E, Faiz A, Preston S, Harris JB. (1994) Screening of snake venoms for neurotoxic and myotoxic effects using simple in vitro preparations from rodents and chicks. *Toxicon.* 32(3), 257-265.

Harvey AL, Bradley KN, Cochran SA, Rowan EG, Pratt JA, Quillfeldt JA, Jerusalinsky DA. (1998) What can toxins tell us for drug discovery? *Toxicon* 36(11), 1635–1640.

Harvey AL, Rodger IW. (1978) Reversibility of neuromuscular blockade produced by toxins isolated from the venom of the sea snake *Laticauda semifasciata. Toxicon* 16, 219-255.

Herz JM, Johnson DA, Taylor P. (1989) Distance between the agonist and noncompetitive inhibitor sites on the nicotinic acetylcholine receptor. *J Biol Chem.* 264(21), 12439-12448.

Hibbs RE, Talley TT, Taylor P. (2004) Acrylodan-conjugated cysteine side chains reveal conformational state and ligand site locations of the acetylcholine-binding protein. *J Biol Chem*. 279(27), 28483-28491. (SPA Assay)

Hider RC, Karlsson E, Namiranian S. (1991) Separation and purification of toxins from snake venoms. In: Harvey AL. (Ed.), Snake Toxins. Pergamon Press, New York. pp. 1-34.

Hogg RC, Bandelier F, Benoit A, Dosch R, Bertrand D. (2008) An automated system for intracellular and intranuclear injection. *J Neurosci Methods.* 169(1), 65-75.

Huang TF, Holt JC, Lukasiewicz H, Niewiarowski S. (1987) Trigramin. A low molecular weight peptide inhibiting fibrinogen interaction with platelet receptors expressed on glycoprotein IIb-IIIa complex. *J Biol Chem.* 262(33), 16157-16163.

Ibanez-Tallon I, Miwa JM, Wang HL, Adams NC, Crabtree GW, Sine SM, Heintz N. (2002) Novel modulation of neuronal nicotinic acetylcholine receptors by association with the endogenous prototoxin lynx1. *Neuron*. 33(6), 893-903.

Itier V, Bertrand D. (2001) Neuronal nicotinic receptors: from protein structure to function. *FEBS letters*. 504(3), 118–125.

Iwanaga S, Suzuki T. (1979) Enzymes in snake venom. In: Lee CY. (Ed.) Snake Venoms, Handbook of Experimental Pharmacology, Vol. 52. Springer-Verlag, Berlin, pp. 61-158.

Jennings ML, Nicknish JS. (1985) Localization of a site of intermolecular cross-linking in human red blood cell band 3 protein. *J Biol Chem.* 260(9), 5472-5479.

Jensen AA, Bergmann ML, Sander T, Balle T. (2010) Ginkgolide X is a potent antagonist of anionic Cys-loop receptors with a unique selectivity profile at glycine receptors. *J Biol Chem.* 285(13), 10141-10153. (Fluo4 assay)

Jerusalinsky D, Harvey AL. (1994) Toxins from mamba venoms: small proteins with selectivities for different subtypes of muscarinic acetylcholine receptors. *Trends Pharmacol Sci.* 15(11), 424-430.

Jerusalinsky D, Kornisiuk E, Alfaro P, Quillfeldt J, Ferreira A, Rial VE, Durán R, Cerveñansky C. (2000) Muscarinic toxins: novel pharmacological tools for the muscarinic cholinergic system. *Toxicon*. 38(6), 747-761.

Jiang M, Haggblad J, Heilbronn E. (1987) Isolation and pharmacological characterization of a new alpha-neurotoxin (alpha-AgTx) from venom of the viper Agkistrodon halys (Pallas). *Toxicon.* 25(9), 1019-1022.

Jørgensen CG, Frølund B, Kehler J, Jensen AA. (2011) Discovery of benzamide analogues as a novel class of 5-HT_3 receptor agonists. *ChemMedChem.* 6(4), 725-736. (Fluo4 assay)

Junqueira-de-Azevedo IL, Ching AT, Carvalho E, Faria F, Nishiyama MY Jr, Ho PL, Diniz MR. (2006) Lachesis muta (Viperidae) cDNAs reveal diverging pit viper molecules and scaffolds typical of cobra (Elapidae) venoms: implications for snake toxin repertoire evolution. *Genetics*. 173(2), 877-889.

Kao PN, Dwork AJ, Kaldany RR, Silver ML, Wideman J, Stein S, Karlin A. (1984) Identification of the α subunit half-cystine specifically labeled by an affinity reagent for the acetylcholine receptor binding site. *J Biol Chem* 259, 11662–11665.

Karlin A. (2002) Emerging structure of the nicotinic acetylcholine receptors. *Nature Rev. Neurosci.* 3(2), 102-114.

Karlsson E. (1979) Chemistry of protein toxins in snake venoms. In: Lee CY. (Ed.) Snake venoms, Handbook of Experimental Pharmacology, Vol. 52. Springer-Verlag, Berlin, pp. 159 – 212.

Karlsson E, Eaker DL, Porath J. (1966) Purification of a neurotoxin from the venom of *Naja nigricollis. Biochim Biophys Acta.* 127(2), 505-520.

Karlsson E, Jolkonen M, Mulugeta E, Onali P, Adem A. (2000) Snake toxins with high selectivity for subtypes of muscarinic acetylcholine receptors. *Biochimie*. 82(9-10), 793–806.

Karlsson E, Mbugua PM, Rodriguez-Ithurralde D. (1984) Fasciculins, anticholinesterase toxins from the venom of the green mamba *Dendroaspis angusticeps*. *J Physiol (Paris).* 79(4), 232-240.

Kasheverov IE, Zhmak MN, Fish A, Rucktooa P, Khruschov AY, Osipov AV, Ziganshin RH, D'hoedt D, Bertrand D, Sixma TK, Smit AB, Tsetlin VI. (2009) Interaction of alpha-conotoxin ImII and its analogs with nicotinic receptors and acetylcholine-binding proteins: additional binding sites on Torpedo receptor. *J Neurochem.* 111(4), 934-944.

Kasturiratne A, Wickremasinghe AR, de Silva N, Gunawardena NK, Pathmeswaran A, Premaratna R, Savioli L, Lalloo DG, de Silva HJ. (2008) Estimation of the global burden of snakebite. *PloS Med.* 5(11), e218.

Katz B, Thesleff S. (1957) A study of the desensitization produced by acetylcholine at the motor end-plate. *J Physiol*. 138(1), 63-80.

Kenakin TP. (2006) A Pharmacology Primer: Theory, Application and Methods, 2nd ed. Academic Press/Elsevier, Amsterdam.

Kieffer B, Driscoll PC, Campbell ID, Willis AC, van der Merwe A, Davis SJ. (1994) Three-dimensional solution structure of the extracellular region of the complement regulator protein CD59, a new cell-surface protein domain related to snake venom neurotoxins. *Biochemistry.* 33(15), 4471-4482.

Kini RM. (2002) Molecular moulds with multiple missions: functional sites in three-finger toxins. *Clin Exp Pharmacol Physiol.* 29(9), 815–822.

Kini RM. (2010) A protein biochemist's sandbox Toxin treasure in. Features, Poisons and antidotes. *The Biochemical Society.*

Kini RM, Chan YM. (1999) Accelerated evolution and molecular surface of venom phospholipase A2 enzymes. *J Mol Evol*. 48(2) 125-132.

Kini RM, Doley R. (2010) Structure, function and evolution of three-finger toxins: mini proteins with multiple targets. *Toxicon.* 56(6), 855-67.

Kirsch T, Sebald W, Dreyer MK. (2000) Crystal structure of the BMP-2- BRIA ectodomain complex. *Nat Struct Biol.* 7(6), 492-496.

Knoller S, Shpungin S, Pick E. (1991) The membrane-associated component of the amphiphile-activated, cytosol-dependent superoxide-forming NADPH oxidase of macrophages is identical to cytochrome b559. *J Biol Chem.* 266(5), 2795-2804.

Koh DCI, Armugam A, Jeyaseelan K. (2006) Snake venom components and their applications in biomedicine. *Cell Mol Life Sci*. 63(24), 3030–3041.

Kolbe HVJ, Huber A, Cordier P, Rasmussen UB, Bouchon B, Jaquinod M, Vlasak R, Delot EC, Kreil G. (1993) Xenoxins, a family of peptides from dorsal gland secretion of *Xenopus laevis* related to snake venom cytotoxins and neurotoxins. *J Biol Chem.* 268(22), 16458-16464.

Kordis D, Gubensek F. (2000) Adaptive evolution of animal toxin multigene families. *Gene.* 261(1), 43-52.

Krebs HA. (1950) Body size and tissue respiration. *Biochim Biophys Acta.* 4(1-3), 249-269.

Krebs HA, Henseleit K. (1932) Untersuchungenuber die Harnstoffbildung im Tierkorper. *Z Physiol Chem.* 210, 33-66.

Kreienkamp HJ, Sine SM, Maeda RK, Taylor P. (1994) Glycosylation sites selectively interfere with α-toxin binding to the nicotinic acetylcholine receptor. *J Biol Chem.* 269, 8108-8114.

Krissinel E, Henrick K. (2007) Inference of macromolecular assemblies from crystalline state. *J Mol Biol.* 372(3), 774-797.

Kukhtina VV, Weise C, Muranova TA, Starkov VG, Franke P, Hucho F, Wnendt S, Gillen C, Tsetlin VI, Utkin YN. (2000) Muscarinic toxin-like proteins from cobra venom. *Eur J Biochem.* 267(23), 6784-6789.

Kumar TK, Jayaraman G, Lee CS, Arunkumar AI, Sivaraman T, Samuel D, Yu C. (1997) Snake venom cardiotoxins-structure, dynamics, function and folding. *J Biomol Struct Dyn.* 15(3), 431-463.

Kuruppu S, Reeve S, Smith AI, Hodgson WC. (2005) Isolation and pharmacological characterisation of papuantoxin-1, a postsynaptic neurotoxin from the venom of the Papuan black snake (Pseudechis papuanus). *Biochem Pharmacol.* 70(5), 794-800.

Langley JN. (1907) On the contraction of muscle, chiefly in relation to the presence of "receptive" substances: Part I. *J Physiol*. 36(4-5), 347-384.

Langmead CJ, Watson J, Reavill C. (2008) Muscarinic acetylcholine receptors as CNS drug targets. *Pharmacol Ther.* 117(2), 232–243.

Laothong C, Sitprija V. (2001) Decreased parasympathetic activities in Malayan krait (*Bungarus candidus*) envenoming. *Toxicon.* 39(9), 1353-1357.

Laskowski RA, MacArthur MW, Moss DS, Thornton JM. (1993) Procheck: a program to check the stereochemical quality of protein structures. *J Appl Crystallogr.* 26, 283-291.

Lawson R, Slowinski JB, Crother BI, Burbrink FT. (2005) Phylogeny of the Colubroidea (Serpentes): new evidence from mitochondrial and nuclear genes. *Mol Phylogenet Evol.* 37(2), 581–601.

le Du MH, Housset D, Marchot P, Bougis PE, Navaza J, Fontecilla-Camps JC. (1996) Structure of fasciculin 2 from green mamba snake venom: evidence for unusual loop flexibility. *Acta Crystallogr D Biol Crystallogr.* 52(Pt 1), 87-92.

Le Novère N, Changeux JP. (1999) The ligand gated ion channel database. *Nucleic Acids Res.* 27(1), 340-342.

Lee AM, Jacoby DB, Fryer AD. (2001) Selective muscarinic receptor antagonists for airway diseases. *Curr Opin Pharmacol.* 1(3), 223–229.

Lee CY. (1972) Chemistry and pharmacology of polypeptide toxins in snake venoms. *Annu Rev Pharmacol.* 12, 265-286.

Léna C, Changeux JP. (1997) Pathological mutations of nicotinic receptors and nicotine-based therapies for brain disorders. *Curr Opin Neurobiol.* 7, 674-682.

Lewis RJ, Garcia ML. (2003) Therapeutic potential of venom peptides. *Nat Rev Drug Discov.* 2(10), 790-802.

Li J, Zhang H, Liu J, Xu K. (2006) Novel genes encoding six kinds of three-finger toxins in *Ophiophagus hannah* (king cobra) and function characterization of two recombinant long-chain neurotoxins. *Biochem J.* 398(2), 233–242.

Lindstrom J. (1997) Nicotinic acetylcholine receptors in health and disease. *Mol Neurobiol.* 15, 193-222.

Llinas P, Le Du MH, Gardsvoll H, Dano K, Ploug M, Gilquin B, Stura EA, Menez A. (2005) Crystal structure of the human urokinase plasminogen activator receptor bound to an antagonist peptide. *EMBO J.* 24(9), 1655-1663.

Louw AI, Visser L. (1978) The synergism of cardiotoxin and phospholipase A2 in hemolysis. *Biochim Biophys Acta* 512(1), 163-171.

Lumsden NG, Fry BG, Ventura S, Kini RM, Hodgson WC. (2005) Pharmacological characterisation of a neurotoxin from the venom of Boiga dendrophila (mangrove catsnake). *Toxicon*. 45(3), 329-334.

Machu TK, Hamilton ME, Frye TF, Shanklin CL, Harris MC, Sun H, Tenner Jr, TE, Soti FS, Kem WR. (2001) Benzylidene analogs of anabaseine display partial agonist and antagonist properties at the mouse 5-hydroxytryptamine(3A) receptor. *J Pharmacol Exp Ther.* 299(3), 1112 – 1119.

Mackessy SP, Sixberry NM, Heyborne WH, Fritts T. (2006) Venom of the Brown Treesnake, Boiga irregularis: ontogenetic shifts and taxa-specific toxicity. *Toxicon.* 47(5), 537-548.

Marchot P, Bourne Y, Prowse CN, Bougis PE, Taylor P. (1998) Inhibition of mouse acetylcholinesterase by fasciculin: crystal structure of the complex and mutagenesis of fasciculin. *Toxicon.* 36(11), 1613-1622.

Maricq AV, Peterson AS, Brake AJ, Myers RM, Julius D. (1991) Primary structure and functional expression of the $5HT_3$ receptor, a serotonin-gated ion channel. *Science.* 254(5030), 432-437.

Mark O'Shea. (2005) Venomous Snakes of the World. New Holland Publishers: London, UK. pp. 14.

Mc Dowell, Samuel B. (1972) The evolution of the tongue of snakes and its bearing on snake origins. *Evolutionary Biology* .6, 191–273.

McDowell RS, Dennis MS, Louie A, Shuster M, Mulkerrin MG, Lazarus RA. (1992) Mambin, a potent glycoprotein IIb-IIIa antagonist and platelet aggregation inhibitor structurally related to the short neurotoxins. *Biochemistry.* 31(20), 4766-4772.

McGehee DS, Role LW (1995) Physiological diversity of nicotinic acetylcholine receptors expressed by vertebrate neurons. *Annu Rev Physiol.* 57, 521–546.

Mehrtens J. (1987) Living Snakes of the World, Sterling, New York, USA.

Meier J, Theakston RDG. (1986) Approximate LD50 determinations of snake venoms using eight to ten experimental animals. *Toxicon.* 24(4), 395 – 410.

Menez A. (1998) Functional architectures of animal toxins: a clue to drug design? *Toxicon.* 36(11), 1557-1572.

Ménez A. (2002) Perspectives in Molecular Toxinology. John Wiley & Sons Ltd., Chichester, UK.

Menez A, Bouet F, Guschlbauer W, Fromageot P. (1980) Refolding of reduced short neurotoxins: circular dichroism analysis. *Biochemistry.* 19(18), 4166-4172.

Menez A, Boulain JC, Bouet F, Couderc J, Faure G, Rousselet A, Tremeau O, Gatineau E, Fromageot P. (1984) On the molecular mechanisms of neutralization of a cobra neurotoxin by specific antibodies. *J Physiol (Paris).* 79(4), 196-206.

Ménez A, Stöcklin R, Mebs D. (2006) ‘‘Venomics” or: the venomous systems genome project. *Toxicon* 47(3), 255–259.

Merril CR. (1990) Gel-staining techniques. *Methods Enzymol.* 182, 477-488.

Meyer MD, Decker MW, Rueter LE, Anderson DJ, Dart MJ, Kim KH, Sullivan JP Williams M (2000) The identification of novel structural compound classes exhibiting high affinity for neuronal nicotinic acetylcholine receptors and analgesic efficacy in preclinical models of pain. *Eur J Pharmacol.* 393, 171-177.

Miwa JM, Ibanez-Tallon I, Crabtree GW, Sanchez R, Sali A, Role LW, Heintz N. (1999) Lynx1, an endogenous toxin-like modulator of nicotinic acetylcholine receptors in the mammalian CNS. *Neuron.* 23(1), 105 – 114.

Middleton RE, Cohen JB. (1991) Mapping of the acetylcholine binding site of the nicotinic acetylcholine receptor: [3H]nicotine as an agonist photoaffinity label. *Biochemistry*. 30, 6987–6997.

Mishina M, Takai T, Imoto K, Noda M, Takahashi T, Numa S, Methfessel C, Sakmann B. (1986) Molecular distinction between fetal and adult forms of muscle acetylcholine receptor. *Nature*. 321(6068):406-11.

Miyazawa A, Fujiyoshi Y, Stowell M & Unwin N. (1999) Nicotinic acetylcholine receptor at 4.6 Å resolution: transverse tunnels in the channel wall. *J Mol Biol*. 288, 765–786.

Moise L, Piserchio A, Basus VJ, Hawrot E. (2002) NMR structural analysis of α-bungarotoxin and its complex with the principal α-neurotoxin-binding sequence on the α7 subunit of a neuronal nicotinic acetylcholine receptor. *J. Biol. Chem.* 277(14), 12406-12417.

Nakashima K, Nobuhisa I, Deshimaru M, Nakai M, Ogawa T, Shimohigashi Y, Fukumaki Y, Hattori M, Sakaki Y, Hattori S. (1995) Accelerated evolution in the protein-coding regions is universal in crotalinae snake venom gland phospholipase A2 isozyme genes. *Proc Natl Acad Sci U S A*. 92(12), 5605-5609.

Nakashima K, Ogawa T, Oda N, Hattori M, Sakaki Y, Kihara H, Ohno M. (1993) Accelerated evolution of Trimeresurus flavoviridis venom gland phospholipase A2 isozymes. *Proc Natl Acad Sci U S A*. 90(13), 5964-5968.

Nau F, Guérin-Dubiard C, Désert C, Gautron J, Bouton S, Gribonval J, Lagarrigue S. (2003) Cloning and characterization of HEP21, a new member of the uPAR/Ly6 protein superfamily predominantly expressed in hen egg white. *Poult Sci.* 82(2), 242-250.

Neubig RR, Cohen JB. (1979) Equilibrium binding of [^{3}H] tubocurarine and [^{3}H] acetylcholine by *Torpedo* postsynaptic membranes: stoichiometry and ligand interactions. *Biochemistry* 18, 5464-5475.

Nirthanan S, Charpantier E, Gopalakrishnakone P, Gwee MC, Khoo HE, Cheah LS, Bertrand D, Kini RM. (2002) Candoxin, a novel toxin from Bungarus candidus, is a reversible antagonist of muscle (alphabetagammadelta) but a poorly reversible antagonist of neuronal alpha 7 nicotinic acetylcholine receptors. *J Biol Chem.* 277(20), 17811-17820.

Nirthanan S, Charpantier E, Gopalakrishnakone P, Gwee MC, Khoo HE, Cheah LS, Kini RM, Bertrand D. (2003a) Neuromuscular effects of candoxin, a novel toxin from the venom of the Malayan krait (*Bungarus candidus*). *Br J Pharmacol.* 139(4), 832-844.

Nirthanan S, Gopalakrishnakone P, Gwee MC, Khoo HE, Kini RM. (2003) Non-conventional toxins from Elapid venoms. *Toxicon.* 41(4), 397-407.

Nirthanan S, Gwee MC. (2004) Three-finger alpha-neurotoxins and the nicotinic acetylcholine receptor, forty years on. *J Pharmacol Sci.* 94(1), 1-17.

Nobuhisa I, Nakashima K, Deshimaru M, Ogawa T, Shimohigashi Y, Fukumaki Y, Sakaki Y, Hattori S, Kihara H, Ohno M. (1996) Accelerated evolution of Trimeresurus okinavensis venom gland phospholipase A2 isozyme-encoding genes. *Gene*. 172(2), 267-272.

Odell GV, Fenton AW, Ownby CL, Doss MP, Schmidt JO. (1999) The role of venom citrate. *Toxicon.* 37(3), 407-409.

Ohno M, Menez R, Ogawa T, Danse JM, Shimohigashi Y, Fromen C, Ducancel F, Zinn-Justin S, le Du MH, Boulain JC, Tamiya T, Menez A. (1998) Molecular evolution of snake toxins: is the functional diversity of snake toxins associated with

a mechanism of accelerated evolution? *Prog Nucleic Acid Res Mol Biol.* 59, 307-364.

Olianas MC, Ingianni A, Maullu C, Adem A, Karlsson E, Onali P. (1999) Selectivity profile of muscarinic toxin 3 in functional assays of cloned and native receptors. *J Pharmacol Exp Ther.* 288(1), 164-170.

OmPraba G, Chapeaurouge A, Doley R, Devi KR, Padmanaban P, Venkatraman C, Velmurugan D, Lin Q, Kini RM. (2010) Identification of a novel family of snake venom proteins Veficolins from Cerberus rynchops using a venom gland transcriptomics and proteomics approach. *J Proteome Res.* 9(4), 1882-1893.

Ortells MO, Lunt GG. (1995) Evolutionary history of the ligand-gated ion-channel superfamily of receptors. *Trends Neurosci.* 18(3), 121-127.

Osipov AV, Kasheverov IE, Makarova YV, Starkov VG, Vorontsova OV, Ziganshin RK, Andreeva TV, Serebryakova MV, Benoit A, Hogg RC, Bertrand D, Tsetlin VI, Utkin YN. (2008) Naturally occurring disulfide-bound dimers of three-fingered toxins: a paradigm for biological activity diversification. *J Biol Chem.* 283(21), 14571-14580.

Oswald RE, Sutcliffe MJ, Bamberger M, Loring RH, Braswell E, Dobson CM. (1991) Solution structure of neuronal bungarotoxin determined by two-dimensional NMR spectroscopy: sequence-specific assignments, secondary structure, and dimer formation. *Biochemistry*. 30(20), 4901-4909.

Otwinowski Z, Minor W. (1997) Processing of X-ray Diffraction Data Collected in Oscillation Mode. In Carter CW and Sweet JRM editors. *Methods Enzymol*. Academic Press, New York.

Pahari S, Bickford D, Fry BG, Kini RM. (2007a) Expression pattern of three-finger toxin and phospholipase A2 genes in the venom glands of two sea snakes, Lapemis curtus and Acalyptophis peronii: comparison of evolution of these toxins in land snakes, sea kraits and sea snakes. *BMC Evol Biol.* 7, 175.

Pahari S, Mackessy SP, Kini RM. (2007) The venom gland transcriptome of the Desert Massasauga rattlesnake (Sistrurus catenatus edwardsii): towards an understanding of venom composition among advanced snakes (Superfamily Colubroidea). *BMC Mol Biol.* 8, 115.

Pal SK, Gomes A, Dasgupta SC, Gomes A. (2002) Snake venom as therapeutic agents: from toxin to drug development. *Indian J Exp Biol.* 40(12), 1353-1358.

Pan HL, Chen SR, Eisenach JC (1999) Intrathecal clonidine alleviates allodynia in neuropathic rats: Interaction with spinal muscarinic and nicotinic receptors. *Anesthesiology* 90, 509-514.

Palma E, Bertrand S, Binzoni T, Bertrand D. (1996) Neuronal nicotinic α7 receptor expressed in *Xenopus oocytes* presents five putative binding sites for methyllycaconitine. *J Physiol.* 491, 151-161.

Palmer CA, Hollis DM, Watts RA, Houck LD, McCall MA, Gregg RG, Feldhoff PW, Feldhoff RC, Arnold SJ. (2007) Plethodontid modulating factor, a hypervariable salamander courtship pheromone in the three-finger protein superfamily. *FEBS J*. 274(9), 2300-2310.

Parascandola J. (1986) The development of receptor theory. In: Parnham MJ. and Bruinvels J. (Ed.), Pharmacological Methods, Receptors and Chemotherapy. Elsevier/North-Holland, Amsterdam. Vol. 3, pp. 129-158.

Paterson D, Nordberg A. (2000) Neuronal nicotinic receptors in the human brain. *Prog Neurobiol*. 61(1), 75-111.

Pawlak J, Mackessy SP, Fry BG, Bhatia M, Mourier G, Fruchart-Gaillard C, Servent D, Menez R, Stura E, Menez A, Kini RM. (2006) Denmotoxin, a three-finger toxin from the colubrid snake Boiga dendrophila (Mangrove Catsnake) with bird-specific activity. *J Biol Chem.* 281(39), 29030-29041.

Pawlak J, Mackessy SP, Sixberry NM, Stura EA, le Du MH, Menez R, Foo CS, Menez A, Nirthanan S, Kini RM. (2009) Irditoxin, a novel covalently linked heterodimeric three-finger toxin with high taxon-specific neurotoxicity. *FASEB J.* 23(2), 534-545.

Perrakis A, Morris R, Lamzin VS. (1999) Automated protein model building combined with iterative structure refinement. *Nat Struct Biol.* 6(5), 458-463.

Phelps T. (1981) In: Poisonous Snakes. Blandford Press: Dorset.

Picciotto MR, Zoli M, Lena C, Bessis A, Lallemand Y, LeNovere N, Vincent P, Pich EM, Brulet P, Changeux JP. (1995) Abnormal avoidance learning in mice lacking functional high-affinity nicotine receptor in the brain. *Nature* 374, 65-67.

Pillet L, Tremeau O, Ducancel F, Drevet P, Zinn-Justin S, Pinkasfeld S, Boulain JC, Menez A. (1993) Genetic engineering of snake toxins. Role of invariant residues in the structural and functional properties of a curaremimetic toxin, as probed by site-directed mutagenesis. *J Biol Chem.* 268(2), 909-916.

Ploug M, Ellis V. (1994) Structure-function relationships in the receptor forurokinase-type plasminogen activator. Comparison to other members of the Ly-6 family and snake venom α-neurotoxins. *FEBS Lett.* 349(2), 163-168.

Pollard BJ. (1994) Components of the neuromuscular junction. In: Pollard, B.J. (Ed.) *Applied Neuromuscular Pharmacology.* Oxford University Press, New York, pp.17-43.

Prado-Franceschi J, Hyslop S, Cogo JC, Andrade AL, Assakura M, Cruz-Höfling MA, Rodrigues-Simioni L. (1996) The effects of Duvernoy's gland secretion from the xenodontine colubrid Philodryas olfersii on striated muscle and the neuromuscular junction: partial characterization of a neuromuscular fraction. *Toxicon.* 34(4), 459-466.

Pung YF, Wong PT, Kumar PP, Hodgson WC, Kini RM. (2005) Ohanin, a novel protein from king cobra venom, induces hypolocomotion and hyperalgesia in mice. *J Biol Chem.* 280(13), 13137-13147.

Pyron RA, Burbrink FT, Colli GR, de Oca AN, Vitt LJ, Kuczynski CA, Wiens JJ. (2011) The phylogeny of advanced snakes (Colubroidea), with discovery of a new subfamily and comparison of support methods for likelihood trees. *Mol Phylogenet Evol.* 58(2), 329-342.

Rajagopalan N, Pung YF, Zhu YZ, Wong PT, Kumar PP, Kini RM. (2007) Beta-cardiotoxin: a new three-finger toxin from Ophiophagus hannah (king cobra) venom with beta-blocker activity. *FASEB J.* 21(13), 3685-3695.

Ramanathan VK, Hall ZW. (1999) Altered glycosylation sites of the delta subunit of the acetylcholine receptor (AChR) reduce alpha delta association and receptor assembly. *J Biol Chem.* 274(29), 20513-20.

Rang HP, Dale MM, Ritter JM Moore PK. (2003) Pharmacology, 5th ed. Churchill Livingstone: Philadelphia, US. pp. 138.

Rees B, Samama JP, Thierry JC, Gilibert M, Fischer J, Schweitz H, Lazdunski M, Moras D. (1987) Crystal structure of a snake venom cardiotoxin. *Proc Natl Acad Sci U S A.* 84(10), 3132-3136.

Reiter MJ, Cowburn DA, Prives JM, Karlin A. (1972) Affinity labeling of the acetylcholine receptor in the electroplax: electrophoretic separation in sodium dodecyl sulfate. *Proc Natl Acad Sci*. 69, 1168–1172.

Ricciardi A, le Du MH, Khayati M, Dajas F, Boulain JC, Menez A, Ducancel F. (2000) Do structural deviations between toxins adopting the same fold reflect functional differences? *J Biol Chem.* 275(24), 18302-18310.

Rocha e Silva M, Beraldo WT, Rosenfeld G. (1949) Bradykinin, a hypotensive and a smooth muscle stimulating factor released from plasma globulin by snake venom and by trypsin. *Am J Physiol.* 156(2), 261–273.

Rowan EG, Harvey AL, Takasaki C, Tamiya N. (1989) Neuromuscular effects of three phospholipase A2 from the venom of the Australian king brown snake *Pseudechis australis. Toxicon.* 27(5), 551-560.

Savitzky AH. (1980) The role of venom delivery strategies in snake evolution. *Evolution.* 34(6), 1194-1204.

Scanziani M, Häusser M. (2009) Electrophysiology in the age of light. *Nature.* 461(7266), 930-939.

Scarr E, Dean B. (2008) Muscarinic receptors: do they have a role in the pathology and treatment of schizophrenia? *J Neurochem.* 107(5), 1188–1195.

Schägger H. (2006) Tricine-SDS-PAGE. *Nat Protoc.* 1(1), 16-22.

Schägger H, von Jagow G. (1987) Tricine-sodium dodecyl sulfate-polyacrylamide gel electrophoresis for the separation of proteins in the range from 1 to 100 kDa. *Anal Biochem.* 166(2), 368-379.

Segalas I, Roumestand C, Zinn-Justin S, Gilquin B, Menez R, Menez A, Toma F. (1995) Solution structure of a green mamba toxin that activates muscarinic acetylcholine receptors, as studied by nuclear magnetic resonance and molecular modelling. *Biochemistry.* 34(4), 1248-60.

Seguela P, Wadiche J, Dineley-Miller K, Dani JA, Patrick JW. (1993) Molecular cloning, functional properties, and distribution of rat brain α7: a nicotinic cation channel highly permeable to calcium. *J Neurosci.* 13, 596-604.

"Serpentes". Integrated Taxonomic Information System. Retrieved 3 December 2008.

Servent D, Antil S, Gaillard C, Corringer PJ, Changeux JP, Menez A. (2000) Molecular characterization of the specificity of interactions of various neurotoxins on two distinct nicotinic acetylcholine receptors. *Eur J Pharmacol.* 393(1-3), 197-204.

Servent D, Fruchart-Gaillard C. (2009) Muscarinic toxins: tools for the study of the pharmacological and functional properties of muscarinic receptors. *J. Neurochem.* 109(5), 1193-1202.

Servent D, Menez A. (2001) Snake neurotoxins that interact with nicotinic acetylcholine receptors. In: Massaro, EJ. (Ed.), Handbook of Neurotoxicology. Humana, Totowa, New Jersey. Vol. 1, pp 385-425.

Servent D, Mourier G, Antil S, Menez A. (1998) How do snake curaremimetic toxins discriminate between nicotinic acetylcholine receptor subtypes. *Toxicol Lett.* 102-103, 199-203.

Servent D, Winckler-Dietrich V, Hu HY, Kessler P, Drevet P, Bertrand D, Menez A. (1997) Only snake curaremimetic toxins with a fifth disulfide bond have high affinity for the neuronal alpha7 nicotinic receptor. *J Biol Chem.* 272,(39) 24279-24286.

Shapiro AL, Viñuela E, Maizel JV Jr. (1967) Molecular weight estimation of polypeptide chains by electrophoresis in SDS-polyacrylamide gels. *Biochem Biophys Res Commun.* 28(5), 815-820.

Shelke RRJ, Sathish S, Gowda TV. (2002) Isolation and characterization of a novel postsynaptic/cytotoxic neurotoxin from *Daboia russelli russelli* venom. *J Peptide Res*. 59(6), 257–263.

Shine R. (1998) Australian Snakes: A natural history. Sydney: Reed New Holland.

Smit AB, Syed NI, Schaap D, van Minnen J, Klumperman J, Kits KS, Lodder H, van der Schors RC, van Elk R, Sorgedrager B, Brejc K, Sixma TK, Geraerts WP. (2001) A glia-derived acetylcholine-binding protein that modulates synaptic transmission. *Nature.* 411(6835), 261-268.

Starkov VG, Poliak I, Vul'fius EA, Kriukova EV, Tsetlin VI, Utkin I. (2009) New weak toxins from the cobra venom. *Bioorg Khim.* 35(1), 15-24.

Staros JV. (1982) N-hydroxysulfosuccinimide active esters: bis(N-hydroxysulfosuccinimide) esters of two dicarboxylic acids are hydrophilic, membrane-impermeant, protein cross-linkers. *Biochemistry.* 21(17), 3950-3955.

Staros JV, Anjaneyulu PS. (1989) Membrane-impermeant cross-linking reagents. *Methods Enzymol.* 172, 609-628.

Steward LJ, Boess FG, Steele JA, Liu D, Wong N, Martin IL. (2000) Importance of phenylalanine 107 in agonist recognition by the 5-hydroxytryptamine(3A) receptor. *Mol. Pharmacol.* 57(6), 1249– 1255.

Tan LC, Kuruppu S, Smith AI, Reeve S, Hodgson WC. (2006) Isolation and pharmacological characterisation of hostoxin-1, a postsynaptic neurotoxin from the venom of the Stephen's banded snake (Hoplocephalus stephensi). *Neuropharmacology*. 51(4), 782-788.

Tassonyi E, Charpantier E, Muller D, Dumont L, Bertrand D. (2002) Role of nicotinic acetylcholine receptors in the mechanisms of anesthesia. *Brain Res Bull.* 57, 133-150.

Teixeira-Clerc F, Menez A, Kessler P. (2002) How do short neurotoxins bind to a muscular-type nicotinic acetylcholine receptor? *J Biol Chem.* 277(28), 25741-25747.

Torres AM, Kini RM, Selvanayagam N, Kuchel PW. (2001) NMR structure of bucandin, a neurotoxin from the venom of the Malayan krait (*Bungarus candidus*). *Biochem J.* 360(Pt 3), 539-548.

Torres AM, Wong HY, Desai M, Moochhala S, Kuchel P W, Kini RM. (2003) Identification of a novel family of proteins in snake venoms. *J Biol Chem.* 278(41), 40097-40104.

Trémeau O, Lemaire C, Drevet P, Pinkasfeld S, Ducancel F, Boulain JC, Menez A. (1995) Genetic engineering of snake toxins. The functional site of erabutoxin a, as delineated by site-directed mutagenesis, includes variant residues. *J Biol Chem.* 270(16), 9362-9369.

Tsetlin V. (1999) Snake venom alpha-neurotoxins and other 'three-finger' proteins. *Eur J Biochem.* 264(2), 281-286.

Tsuneki H, Kimura I, Dezaki K, Kimura M, Sala C, Fumagalli G. (1995) Immunohistochemical localization of neuronal nicotinic receptor subtypes at the preand postjunctional sites in mouse diaphragm muscle. *Neurosci Lett.* 196, 13–16.

Tyrode MV. (1910) Mode of action of some purgative salts. *Arch Int Pharmacodyn Ther*. 20, 205-210.

Ulens C, Hogg RC, Celie PH, Bertrand D, Tsetlin V, Smit AB, Sixma TK. (2006) Structural determinants of selective alpha-conotoxin binding to a nicotinic acetylcholine receptor homolog AChBP. *Proc Natl Acad Sci U S A*. 103(10), 3615-3620.

Unwin N. (1993) Nicotinic acetylcholine receptor at 9 A resolution. *J Mol Biol.* 229(4), 1101-1124.

Unwin N. (2005) Refined structure of the nicotinic acetylcholine receptor at 4A resolution. *J Mol Biol.* 346(4):967-89.

Utkin YN, Kukhtina V V, Kryukova EV,Chiodini F, Bertrand D, Methfessel C, Tsetlin VI. (2001) "Weak toxin" from Naja kaouthia is a nontoxic antagonist of alpha 7 and muscle-type nicotinic acetylcholine receptors. *J Biol Chem.* 276:15810-15815.

Utsintong M, Talley TT, Taylor PW, Olson AJ, Vajragupta O. (2009) Virtual screening against alpha-cobratoxin. *J Biomol Screen.* 14(9), 1109-1118. (SPA assay)

Vagin A, Steiner RA, Lebedev AA, Potterton L, McNicholas S, Long F, Murshudov GN. (2004) REFMAC5 dictionary: organization of prior chemical knowledge and guidelines for its use. *Acta Crystallogr D Biol Crystallogr.* 60(Pt 12 Pt 1), 2184-2195.

Vagin A, Teplyakov A. (1997) MOLREP: an Automated Program for Molecular Replacement. *J Appl Crystallogr*. 30, 1022-1025.

Vidal N, Delmas AS, David P, Cruaud C, Couloux A, Hedges SB. (2007) The phylogeny and classification of caenophidian snakes inferred from seven nuclear protein-coding genes. *C R Biol*. 330(2), 182–187.

Viljoen CC, Botes DP. (1973) Snake venom toxins. The purification and amino acid sequence of toxin F VII from *Dendroaspis angusticeps* venom. *J Biol Chem.* 248(14), 4915-4919.

Voitenko SV, Bobryshev AY, Skok VI. (2000) Intracellular regulation of neuronal nicotinic cholinoreceptors. *Neurosci Behav Physiol.* 30, 19–25.

Wang D, Chiara DC, Xie Y, Cohen JB. (2000) Probing the structure of the nicotinic acetylcholine receptor with 4-benzoylbenzoylcholine, a novel photoaffinity competitive antagonist. *J Biol Chem* 275, 28666–28674.

Wang ZZ, Hardy SF, Hall ZW. (1996) Assembly of the nicotinic acetylcholine receptor. The first transmembrane domains of truncated alpha and delta subunits are required for heterodimer formation in vivo. *J Biol Chem.* 271(44):27575-84.

Warrell DA, Looareesuwan S, White NJ, Theakston RDG, Warrell MJ, Kosakarn W, Reid HA. (1983) Severe neurotoxic envenoming by Malayan krait *Bungarus candidus* (Linnaeus): response to antivenom and anticholinesterase. *Br Med J.* 286(6366), 678-682.

Weiser M, Mutschler E, Lambrecht G. (1997) Characterization of postjunctional muscarinic receptors mediating contraction in rat anococcygeus muscle. *Naunyn Schmiedebergs Arch Pharmacol.* 356(5), 671 - 677.

Welsh JH. (1967) Acetylcholine in snake venoms. In: Russell EE. and Sanders PR. (Ed.), Animal Toxins. Pergamon Press, New York. pp. 363 – 368.

Werner P, Kawashima E, Reid J, Hussy N, Lundström K, Buell G, Humbert Y, Jones KA. (1994) Organization of the mouse 5-HT_3 receptor gene and functional expression of two splice variants. *Brain Res Mol Brain Res.* 26(1-2), 233-241.

White J. (1998) Venomous Snakes. In: Geordie T. (Ed.), Australia's Most Dangerous Spiders, Snakes and Marine Creatures: Australian geographic field guide. Sydney: Australian Geographic Pty. Ltd. pp. 11-54.

Wolf KM, Ciarleglio A, Chiappinelli VA. (1988) kappa-Bungarotoxin: binding of a neuronal nicotinic receptor antagonist to chick optic lobe and skeletal muscle. *Brain Res.* 439(1-2), 249-258.

Wonnacott S. (1997) Presynaptic nicotinic acetylcholine receptors. *Trends Neurosci.* 20, 92-98.

Xu W, Gelber S, Orr-Urtreger A, Armstrong D, Lewis RA, Ou CN, Patrick JW, Role L, De Biasi M, Beaudet AL. (1999a) Megacystis, mydriasis, and ion channel defect in mice lacking the α3 neuronal nicotinic acetylcholine receptor. *Proc Natl Acad Sci.* 96, 5746-5751.

Xu W, Orr-Urtreger A, Nigro F, Gelber S, Sutcliffe SB, Armstrong D, Patrick JW, Role L, Beaudet AL, M De Biasi. (1999b) Multiorgan autonomic dysfunction in mice lacking the β2 and the β4 subunits of neuronal nicotinic acetylcholine receptors. *J Neurosci.* 19, 9298-9305.

Yakel JL. (2010) Gating of nicotinic ACh receptors: latest insights into ligand binding and function. *J Physiol*. 588(4), 597-602.

Zaher H, Grazziotin FG, Cadle JE, Murphy RW, Moura-Leite JC, Bonatto SL. (2009) Molecular phylogeny of advanced snakes (Serpentes, Caenophidia) with an emphasis on South America xenodontines: a revised classification and descriptions of new taxa. *Pap Av Zool.* 49, 115–153.

Zeng H, Moise L, Grant M A, Hawrot E. (2001) The solution structure of a complex formed between α-bungarotoxin and an 18-mer cognate peptide derived from the α1 subunit of the nicotinic acetylcholine receptor from *Torpedo californica. J Biol Chem.* 276(25), 22930-22940.

Zoldan J, Friedberg G, Livneh M, Melamed E. (1995) Psychosis in advanced Parkinson's disease: treatment with ondansetron, a 5-HT_3 receptor antagonist. *Neurology.* 45(7), 1305-1308.

Appendix

APPENDIX

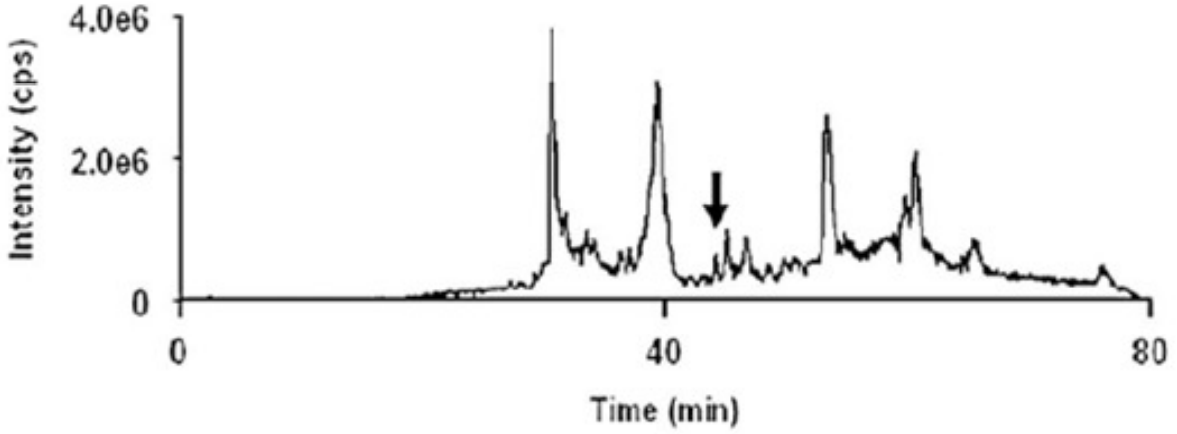

Masses of peptides and proteins detected by LC/MS from king cobra venom

25-30 min	30-35 min	35-40 min	40-45 min	45-50 min
3,571.02 ± 1.42[a]	7,020.03 ± 0.01	6,324.49 ± 0.72	7,013.80 ± 1.27	7,100.02 ± 0.01
3,936.03 ± 0.04[a]	7,535.67 ± 0.60	6,339.99 ± 0.01	7,294.35 ± 2.07	10,164.54 ± 0.75[a]
4,123.04 ± 1.44[a]	7,942.00 ± 2.86	7,013.80 ± 1.27	7,570.00 ± 1.98	24,989.51 ± 2.42
7,451.34 ± 1.17	7,944.50 ± 0.67	7,055.52 ± 0.70	11,951.35 ± 3.92[a]	
7,941.35 ± 2.32	7,975.02 ± 1.01	7,294.35 ± 2.07	13,667.48 ± 4.91	
		7,306.52 ± 2.13	13,682.62 ± 3.47	
		7,395.51 ± 0.73	13,838.42 ± 2.01	
		7,524.34 ± 0.56		
		7,557.00 ± 2.67		
		7,975.02 ± 1.01		

[a] Peptides and proteins that may belong to new families of venom proteins

Figure A.1: LC/MS profile of *O. hannah* crude venom.

The masses of 4 novel proteins identified from the cDNA library are highlighted with green boxes. The proteins and peptide eluted during 30-35 min showed the presence of a protein with molecular weight of 7,535.67 ± 0.60 Da, similar to the mass of haditoxin. Reproduced with permission from Prof. R Manjunatha Kini, Department of Biological Sciences, National University of Singapore (Pung *et al*., 2005).

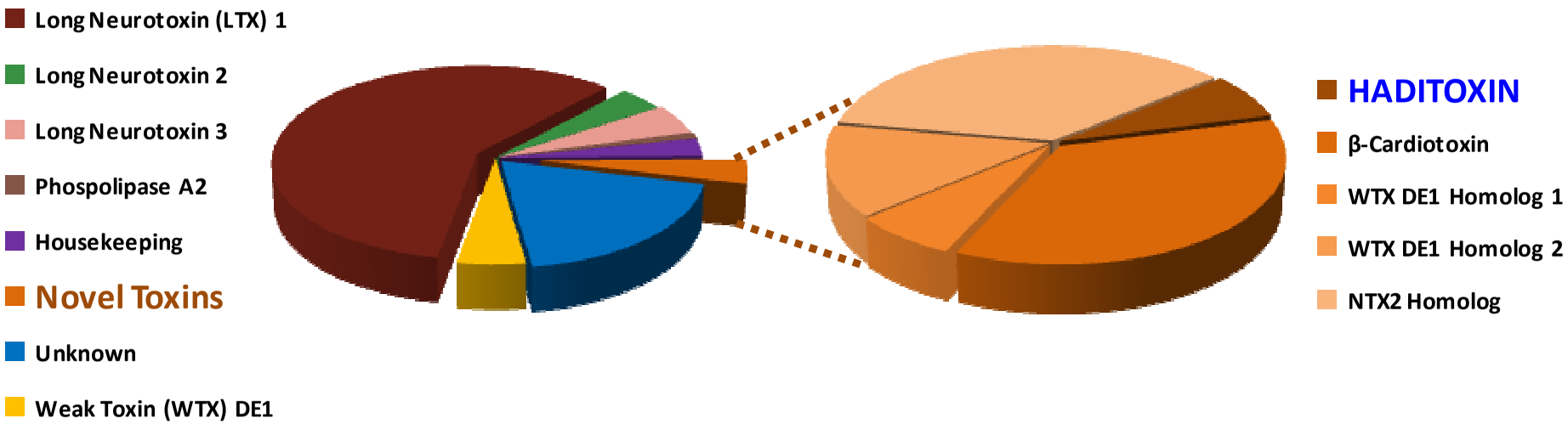

Figure A.2: Abundance of various genes in the venom gland cDNA library *O. hannah*.

Pie diagram shows the major groups of genes found in the library and their abundance. Inset, abundance of various novel toxin genes found in the library. Reproduced with permission from Prof. R Manjunatha Kini, Department of Biological Sciences, National University of Singapore (Rajagopalan *et al*, 2007).

the journal of biological chemistry

jbc

MARCH 12, 2010
VOLUME 285
NUMBER 11

ASBMB AMERICAN SOCIETY FOR BIOCHEMISTRY AND MOLECULAR BIOLOGY

THE JOURNAL OF BIOLOGICAL CHEMISTRY VOL. 285, NO. 11, pp. 8302–8315, March 12, 2010

Structural and Functional Characterization of a Novel Homodimeric Three-finger Neurotoxin from the Venom of *Ophiophagus hannah* (King Cobra)*[S]◆

Received for publication, October 13, 2009, and in revised form, December 23, 2009 Published, JBC Papers in Press, January 13, 2010, DOI 10.1074/jbc.M109.074161

Amrita Roy[‡], Xingding Zhou[‡], Ming Zhi Chong[‡], Dieter D'hoedt[§], Chun Shin Foo[‡], Nandhakishore Rajagopalan[‡1], Selvanayagam Nirthanan[¶‖], Daniel Bertrand[§], J. Sivaraman[‡], and R. Manjunatha Kini[‡2]**

*From the [‡]Department of Biological Sciences, National University of Singapore, Singapore 117543, the [§]Department of Neuroscience, Medical Faculty, University of Geneva, 1211 Geneva 4, Switzerland, the [¶]School of Medical Science, Griffith University Gold Coast Campus, Queensland 4222, Australia, the [‖]Department of Pharmacology, School of Medicine, National University of Singapore, Singapore 117597, and the **Department of Biochemistry and Molecular Biophysics, Medical College of Virginia, Virginia Commonwealth University, Richmond, Virginia 23298*

Snake venoms are a mixture of pharmacologically active proteins and polypeptides that have led to the development of molecular probes and therapeutic agents. Here, we describe the structural and functional characterization of a novel neurotoxin, haditoxin, from the venom of *Ophiophagus hannah* (King cobra). Haditoxin exhibited novel pharmacology with antagonism toward muscle ($\alpha\beta\gamma\delta$) and neuronal (α_7, $\alpha_3\beta_2$, and $\alpha_4\beta_2$) nicotinic acetylcholine receptors (nAChRs) with highest affinity for α_7-nAChRs. The high resolution (1.5 Å) crystal structure revealed haditoxin to be a homodimer, like κ-neurotoxins, which target neuronal $\alpha_3\beta_2$- and $\alpha_4\beta_2$-nAChRs. Interestingly however, the monomeric subunits of haditoxin were composed of a three-finger protein fold typical of curaremimetic short-chain α-neurotoxins. Biochemical studies confirmed that it existed as a non-covalent dimer species in solution. Its structural similarity to short-chain α-neurotoxins and κ-neurotoxins notwithstanding, haditoxin exhibited unique blockade of α_7-nAChRs (IC_{50} 180 nM), which is recognized by neither short-chain α-neurotoxins nor κ-neurotoxins. This is the first report of a dimeric short-chain α-neurotoxin interacting with neuronal α_7-nAChRs as well as the first homodimeric three-finger toxin to interact with muscle nAChRs.

Snake venoms are a rich source of pharmacologically active proteins and polypeptides targeting a variety of receptors with high affinity and specificity (1). Because of their high specificity, some of these molecules have contributed significantly (*a*) to the isolation and characterization of different receptors and their subtypes in the field of molecular pharmacology and (*b*) as lead compounds in the development of therapeutic agents (2, 3). For example, the discovery of α-bungarotoxin, a postsynaptic neurotoxin from the venom of *Bungarus multicinctus*, led to the identification of the nicotinic acetylcholine receptor (nAChR),[3] the first isolated receptor protein (4) as well as the first one to be characterized electrophysiologically (5) and biochemically (6, 7). Subsequently, it was also used to characterize several other nAChRs (8–10).

Snake venom proteins can be broadly classified as enzymatic and non-enzymatic proteins. Three-finger toxins (3FTxs) are the largest group of non-enzymatic snake venom proteins (1, 11). They are most commonly found in the venoms of elapid and hydrophiid snakes. Recently, our laboratory has also demonstrated the presence of 3FTxs from colubrid venoms (12, 13), and 3FTx transcripts have been found in the venom gland transcriptome of viperid snakes (14, 15). The proteins in this family of toxins share a common structural scaffold of three β-sheeted loops emerging from a central core (11, 16). Despite the overall similarity in structure, these proteins have diverse functional properties. Members of this family include neurotoxins targeting the cholinergic system (7, 11, 16), cytotoxins/cardiotoxins interacting with the cell membranes (17), calciseptine and related toxins that block the L-type Ca^{2+} channels (18), dendroaspins, which are antagonists of various cell adhesion processes (19), and β-cardiotoxin antagonizing the β-adrenoceptors (20). The subtle variations in their structures, such as the presence of extra disulfide bonds, differences in size and overall conformation (twists and turns) of the loops, and longer C-terminal and/or N-terminal extensions (21), may contribute to the observed functional diversity as well as specificity of these toxins (22).

* This work was supported by research grant from the Biomedical Research Council (BMRC), Agency for Science and Technology, Singapore (BMRC Grant R154-000-172-316) (to R. M. K.) and by Academic Research Fund funding support (Grant R154000438112) from National University of Singapore, Singapore (to J. S.).

◆ This article was selected as a Paper of the Week.

The atomic coordinates and structure factors (code 3HH7) have been deposited in the Protein Data Bank, Research Collaboratory for Structural Bioinformatics, Rutgers University, New Brunswick, NJ (http://www.rcsb.org/).

[S] The on-line version of this article (available at http://www.jbc.org) contains supplemental Fig. 1.

[1] Present address: ZMBH, University of Heidelberg, 69120 Heidelberg, Germeny.

[2] To whom correspondence should be addressed: Protein Science Laboratory, Dept. of Biological Sciences, Faculty of Science, National University of Singapore, Singapore 117543. Tel.: 65-6516-5235; Fax: 65-6779-2486; E-mail: dbskinim@nus.edu.sg.

[3] The abbreviations used are: nAChR, nicotinic acetylcholine receptor; mAChR, muscarinic acetylcholine receptors; 3FTx, three-finger toxin; MT, muscarinic toxin; BS^3, bis(sulfosuccinimidyl) suberate; CBCM, chick biventer cervicis muscle; RHD, rat hemidiaphragm muscle; r.m.s.d., root mean square deviation; RP-HPLC, reverse phase-high performance liquid chromatography; MS, mass spectrometry; ESI-MS, electrospray mass ionization-MS; Tricine, *N*-[2-hydroxy-1,1-bis(hydroxymethyl)ethyl]glycine; MTLP, muscarinic toxin-like protein.

This family contains several types of neurotoxins that interact with different subtypes of nicotinic and muscarinic receptors involved in central and peripheral cholinergic transmission. Depending on the target receptors, these neurotoxins can be broadly divided into various groups. Curaremimetic or α-neurotoxins that target muscle ($\alpha\beta\gamma\delta$ or α_1 subtype) nAChRs (7, 16, 23) belong to short-chain and long-chain neurotoxins (classified based on size and number of disulfide bridges (24)). Long-chain neurotoxins, but not short-chain neurotoxins, also target neuronal α_7-nAChRs associated with neurotransmission in the brain (25). κ-Neurotoxins, such as κ-bungarotoxin (*B. multicinctus*), show specificity for other neuronal subtypes, $\alpha_3\beta_2$- and $\alpha_4\beta_2$-nAChRs (26, 27). Muscarinic 3FTxs, unlike many small molecule ligands, can distinguish between different types of muscarinic acetylcholine receptors (mAChRs) (for review, see Ref. 28) and hence are useful in the characterization of these receptor subtypes. Muscarinic toxin 1, isolated from the venom of *Dendroaspis angusticeps*, interacts with mAChR subtype 1 (M1) (29), whereas muscarinic toxin 3 (MT3), isolated from the same snake, interacts with M4 mAChRs (30). In recent years, new 3FTxs with distinct and novel receptor specificities have been characterized and added to this growing library (12, 13, 31–36), justifying their usefulness as pharmacological tools to dissect the cholinergic circuitry to understand the role of individual receptor subtypes or offer clues to the rational design of specific therapeutics.

All neurotoxins characterized to date exist as monomers with the exception of κ-neurotoxins from *Bungarus* sp. (37, 38), which is a non-covalently linked homodimer that binds neuronal ($\alpha_3\beta_2$ and $\alpha_4\beta_2$) but not muscle ($\alpha\beta\gamma\delta$) nAChRs. More recently, we published the first report of a covalent heterodimeric neurotoxin, irditoxin from the venom of *Boiga* sp., which was a uniquely irreversible inhibitor of muscle ($\alpha\beta\gamma\delta$) nAChRs (13). Here, we report the purification, pharmacological characterization, and a high resolution crystal structure of a novel non-covalent homodimeric neurotoxin from the venom of *Ophiophagus hannah* (King cobra). Although its quaternary structure is similar to κ-neurotoxins, it exhibited novel pharmacology with potent blocking activity on muscle ($\alpha\beta\gamma\delta$) as well as neuronal (α_7, $\alpha_3\beta_2$, and $\alpha_4\beta_2$) nAChRs. Based on the high resolution crystal structure (1.55 Å) we have explored its structural similarities with other neurotoxins. This new toxin was named haditoxin (*O. hannah* dimeric neurotoxin) and is the first homodimeric three-finger neurotoxin interacting with α_1-nAChRs.

EXPERIMENTAL PROCEDURES

Materials—Lyophilized *O. hannah* venom was obtained from PT Venom Indo Persada (Jakarta, Indonesia) and Kentucky Reptile Zoo (Slade, KY). Reagents for N-terminal sequencing by Edman degradation are from Applied Biosystems (Foster City, CA). KCl, acetonitrile, and trifluoroacetic acid were from Merck KGaA, Darmstadt, Germany. Precision Plus protein standards, dual color (marker for SDS-PAGE), and bis(sulfosuccinimidyl) suberate (BS^3) were purchased from Bio-Rad Laboratories and Pierce, respectively. Superdex 30 HiLoad (16/60) column and Jupiter C18 (5 μ, 300 Å, 4.6 × 150 mm) were purchased from GE Healthcare and Phenomenex (Torrance, CA), respectively. Crystal screening solution and accessories were obtained from Hampton Research (Aliso Viejo, CA). All other chemicals including α-bungarotoxin from *B. multicinctus* were purchased from Sigma-Aldrich. All the reagents were of the highest purity grade. Water was purified using a MilliQ system (Millipore, Billerica, MA).

Animals—Animals (Swiss albino mice and Sprague-Dawley rats) were acquired from the National University of Singapore Laboratory Animal Center and acclimatized to the Department Animal Holding Unit for at least 3 days before the experiments. They were housed, four per cage, with food and water available *ad libitum* in a light controlled room (12-h light/dark cycle, light on at 7:00 a.m.) at 23 °C and 60% relative humidity. Domestic chicks (*Gallus gallus domesticus*) were purchased from Chew's Agricultural Farm, Singapore, and delivered on the day of experimentation. Animals were sacrificed by exposure to 100% carbon dioxide. All experiments were conducted according to the Protocol (021/07a) approved by the Institutional Animal Care and Use Committee of the National University of Singapore.

Purification of the Protein—*O. hannah* crude venom (100 mg dissolved in 1 ml of MilliQ water and filtered) was loaded onto a Superdex 30 gel filtration column, equilibrated with 50 mM Tris-HCl buffer; pH 7.4, and eluted with the same buffer using an ÄKTA purifier system (GE Healthcare). Fractions containing the toxin of interest were further subfractionated by reverse phase-high performance liquid chromatography (RP-HPLC) using a Jupiter C18 column, equilibrated with 0.1% (v/v) trifluoroacetic acid, and eluted with a linear gradient of 80% (v/v) acetonitrile in 0.1% (v/v) trifluoroacetic acid. Elution was monitored at 280 and 215 nm. Fractions were directly injected into an API-300 liquid chromatography-tandem MS system (PerkinElmer Life Sciences) to determine the mass and homogeneity of the protein as described previously (20). Analyte software (PerkinElmer Life Sciences) was used to analyze and deconvolute the raw mass data. Fractions showing the expected molecular mass were pooled and lyophilized.

Capillary Electrophoresis—Capillary electrophoresis was performed on a BioFocus3000 system (Bio-Rad) to determine the homogeneity of the protein after RP-HPLC. The native protein (1 μg/μl) was injected to a 25 μm × 17 cm coated capillary using a pressure mode (5 p.s.i./s) and run in 0.1 M phosphate buffer (pH 2.5) under 18 kV at 20 °C for 7 min. The migration was monitored at 200 nm.

N-terminal Sequencing—N-terminal sequencing of the native protein was performed by automated Edman degradation using a Procise 494 pulsed liquid-phase protein sequencer (Applied Biosystems) with an on-line 785A phenylthiohydantoin derivative analyzer. The phenylthiohydantoin amino acids were sequentially identified by mapping the respective separation profiles with the standard chromatogram.

CD Spectroscopy—Far-UV CD spectra (260–190 nm) were recorded using a Jasco J-810 spectropolarimeter (Jasco Corp., Tokyo, Japan) as described previously (20). The protein samples (concentration range 0.25–1 mg/ml) were dissolved in MilliQ water.

In Vivo Toxicity Study—Native protein (200 μl dissolved in 0.89% NaCl) was injected intraperitoneally using a 27-gauge 0.5-inch needle (BD Biosciences) into male Swiss albino mice (15 ± 2 g) at doses of 5, 10, and 25 mg/kg ($n = 2$). The symptoms of envenomation were observed, and in the event of death, the time of death was noted. The control group was injected with 200 μl of 0.89% NaCl. Postmortem examinations were conducted on all animals.

Ex Vivo Organ Bath Studies—Isolated tissue experiments were performed as described previously (13, 31) using a conventional organ bath (6 ml) containing Krebs solution of the following composition (in mM): 118 NaCl, 4.8 KCl, 1.2 KH_2PO_4, 2.5 $CaCl_2$, 25 $NaHCO_3$, 2.4 $MgSO_4$, and 11 D-(+)glucose); pH 7.4, at 37 °C. This is continuously aerated with carbogen (5% carbon dioxide in oxygen). The resting tension of the tissues was maintained at 1–2 g, and the preparations were allowed to equilibrate for 30–45 min. Electrical field stimulation was carried out through platinum ring electrodes using a Grass stimulator S88 (Grass Instruments, West Warwick, RI). The magnitude of the contractile response was measured in gram tension. Data were continuously recorded on PowerLab/Chart 5 data acquisition system via a force displacement transducer (Model MLT0201) (AD Instruments, Bella Vista NSW, Australia). Neuromuscular blockade produced by a toxin is expressed as a percentage of the original twitch height in the absence of exposure to toxin. Dose-response curves representing the percent blockade after 30 min of exposure to the respective toxins were plotted.

Chick Biventer Cervicis Muscle (CBCM) Preparations—The CBCM nerve-skeletal muscle preparation (39) was isolated from chicks (6 days old) and mounted in the organ bath chamber under similar experimental conditions as described previously (12, 31). The effect of haditoxin (0.05–5 μM; $n = 3$) or α-bungarotoxin (0.01–1.0 μM; $n = 3$) on nerve-evoked twitch responses of the CBCM were studied. In separate experiments, the recovery from complete neuromuscular blockade was assessed by washing out the toxin with Krebs solution at 30-min intervals (three cycles of 30-s on pulse, 30-s off pulse) over a 120-min period.

Rat Hemidiaphragm Muscle (RHD) Preparations—The RHD muscle associated with the phrenic nerve (40) was isolated and mounted in a 5-ml organ bath chamber under similar conditions as stated for CBCM, as described previously (13). The effects of haditoxin (0.15–15 μM; $n = 3$) or α-bungarotoxin (0.01–1.0 μM; $n = 3$) on nerve-evoked twitch responses of the RHD were investigated. Recovery of neuromuscular blockade was assessed similarly as described above for CBCM.

Electrophysiology—Two-electrode voltage clamp experiments were done using *Xenopus* oocytes. The oocytes were prepared and injected as described by Hogg *et al.* (41). Briefly, 2 ng of cDNA encoding for human $\alpha_4\beta_2$-, $\alpha\beta\delta\epsilon$-, α_7-, and $\alpha_3\beta_2$-nAChRs were injected into the oocytes. Two-electrode voltage clamp measurements were done 2–3 days after injection. During recordings, the oocytes were perfused with OR2 (oocyte ringer) containing (in mM): 82.5 NaCl, 2.5 KCl, 1 $MgCl_2$, 2.5 Ca_2Cl, 5 HEPES, and 20 μg/ml bovine serum albumin; pH 7.4. Atropine (0.5 μM) was added to all solutions to block activity of endogenous muscarinic receptors. Just before use, acetylcholine (ACh) and haditoxin were dissolved the OR2 solution. All recordings were performed with an automated two-electrode voltage clamp robot. Oocytes were clamped at −100 mV, and data were digitized and analyzed off-line using MATLAB (Mathworks, Natick, MA).

Gel Filtration Chromatography—The oligomeric states of the protein were examined by gel filtration chromatography on a Superdex 75 column (1 × 30 cm) equilibrated with 50 mM Tris-HCl buffer (pH 7.4) using an ÄKTA purifier system at a flow rate of 0.6 ml/min. Calibration was done using bovine serum albumin (66 kDa), carbonic anhydrase (29 kDa), cytochrome *c* (12.4 kDa), aprotinin (6.5 kDa), and blue dextran (200 kDa) as molecular mass markers. Native protein (0.25–10 μM) as well as samples (0.25–10 μM) treated with 0.6% SDS (2 h of incubation at room temperature) (37) were loaded separately onto the column, and respective elution profiles were recorded. For the SDS-treated samples, the column was equilibrated with the same buffer containing 0.1% SDS.

Electrophoresis—Tris-Tricine SDS-PAGE of the protein of interest in the presence or absence of cross-linker BS^3 (42) was performed on a 12% gel, under reducing conditions, using the Bio-Rad Mini-Protean II electrophoresis system. The concentration of BS^3 used was 5 mM. The protein bands were visualized by Coomassie Blue staining.

Crystallization and Data Collection—Crystallization conditions for the protein were screened with Hampton Research screens using the hanging-drop vapor diffusion method. Lyophilized protein was dissolved in 10 mM Tris-HCl buffer, pH 7.4, with 100 mM NaCl. Crystallization experiments were performed at room temperature 297 K (24 °C) with drops containing equal volumes (1 μl) of reservoir and protein solution. Small rod-shaped crystals were formed within 2–3 days and grew to diffraction quality after 3 weeks. They were briefly soaked in the reservoir solution supplemented with 10% glycerol as cryo-protectant prior to the x-ray diffraction data collection. Then these were flash-frozen in a nitrogen cold stream at 100 K (−173 °C). Diffraction up to 1.55 Å was obtained using a CCD detector (Platinum135) mounted on a Bruker Microstar Ultra rotating anode generator (Bruker AXS, Madison, WI). A complete data set was collected, processed, and scaled using the program HKL2000 (43).

RESULTS

Five novel 3FTxs were identified from the cDNA library of the venom gland tissue of *O. hannah*, and one of them, named β-cardiotoxin, has been characterized previously (20). Here, we describe the characterization of the second novel toxin, identified previously as an MTLP-3 homolog based on sequence homology (20) (Fig. 1). The liquid chromatography/MS profile of *O. hannah* venom (44) showed the presence of a 7,535.67 ± 0.60 Da protein, similar to the expected molecular mass of the protein being characterized. This protein was purified from the crude venom using a two-step chromatographic approach. Firstly, the venom components were separated based on their sizes into five peaks using gel filtration chromatography (Fig. 2*A*). Subsequently, each peak was fractionated by RP-HPLC, and the fractions were analyzed by ESI-MS to identify the presence of the protein of interest (Fig. 2*A*, *black bar*). Further, these

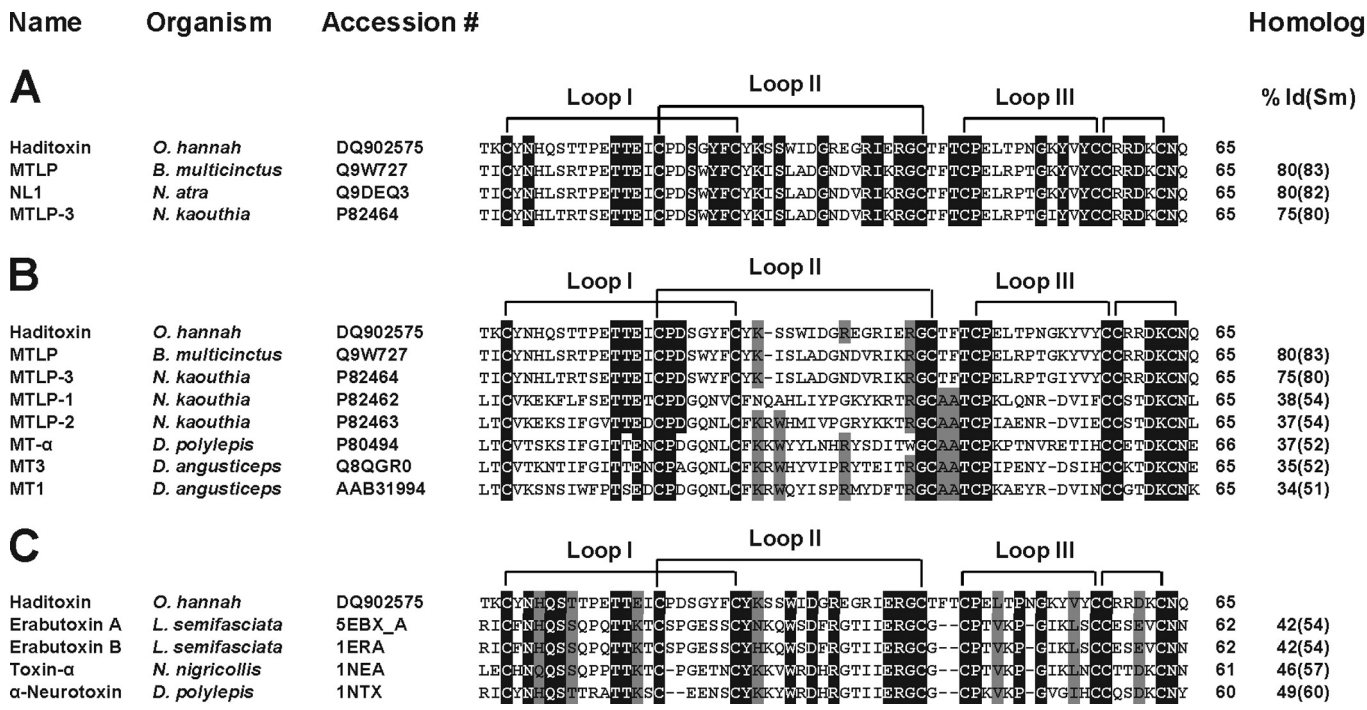

FIGURE 1. **Multiple sequence alignment of novel proteins.** *A–C*, sequence alignment of haditoxin with the most homologous sequences (*A*), muscarinic toxin homologs (*B*), and short-chain α-neurotoxins (*C*). Toxin names, species, and accession numbers are shown. Conserved residues in all sequences are highlighted in *black*. Disulfide bridges and loop regions are also shown. At the end of each sequence, the numbers of amino acids are stated. The homology (sequence identity and similarity (*% Id(Sm)*)) of each protein is compared with haditoxin and shown at the end of each sequence. *N. atra*, *Naja atra*; *N. kaouthia*, *Naja kaouthia*; *D. polylepis*, *Dendroaspis polylepis*; and *L. semifasciata*, *Laticauda semifasciata*.

fractions were pooled and separated by RP-HPLC (Fig. 2*B*). The ESI-MS of fraction 2a (Fig. 2*C*, *black arrow*) showed three peaks with mass/charge (*m*/*z*) ratios ranging from +4 to +6 charges (Fig. 2*C*), and the final reconstructed mass spectrum showed a molecular mass of 7,535.67 ± 1.25 Da, which matched the calculated mass of 7,534.42 Da (Fig. 2*C*, *inset*). The secondary structural elements of haditoxin were analyzed using far-UV CD spectroscopy. The spectrum shows maxima at 230 and 198–200 nm and a minimum at 215 nm (Fig. 2*D*). Thus, haditoxin was found to be composed of β-sheeted structure similar to all other 3FTxs (11, 16). The presence of a single protein peak in the electropherogram (Fig. 2*E*) indicates the homogeneity of the protein, ensuring the absence of contaminants, especially other α-neurotoxin(s) and cytotoxins present in the venom. Identification was further confirmed by N-terminal sequencing of the first 36 residues, which matched the cDNA sequence of the MTLP-3 homolog (20). This protein was found to be a homodimer (see below) and hence was renamed as haditoxin (*O. hannah* dimeric neurotoxin) following the nomenclature of dimeric 3FTxs (12, 13).

Investigation of Haditoxin for Muscarinic Effects—As detailed in Fig. 1, *A* and *B*, haditoxin showed high similarity (80–83%) with muscarinic toxin homologs (MTLP and MTLP-3) as well as similarity with muscarinic toxins (MT-α, MT7, and MT3) (51–52%). As such, we examined the effects of haditoxin on *in vitro* smooth muscle preparations, the rat ileum and rat anococcygeus muscle, pharmacologically characterized to represent M2 (45) and M3 mAChRs (46), respectively. In both preparations, the protein had no effect on the contractile response of the muscle to exogenously applied ACh or electrical field stimulation, suggesting that haditoxin does not interact with M2 and M3 mAChRs (supplemental Fig. 1). Therefore, it is likely that the observed sequence similarity with muscarinic toxin homologs is probably coincidental due to either phylogeny or structure, including the presence of the core disulfide bridges, and not the function. This merits further investigation, including electrophysiological studies and/or binding assays on other subtypes of mAChRs.

In Vivo Toxicity of Haditoxin—In preliminary experiments to observe the biological effects of haditoxin, all mice injected with the toxin (5, 10, and 25 mg/kg) showed typical symptoms of peripheral neurotoxicity, such as paralysis of hind limbs and labored breathing, and finally died, presumably due to respiratory paralysis (47, 48). The time of death was recorded for each animal, with the average calculated to be 94, 32.5, and 20 min, respectively, for the 5, 10, and 25 mg/kg doses. On postmortem, no gross changes in the internal organs, notably hemorrhage, were observed.

Ex Vivo Neurotoxic Effects of Haditoxin—The observed peripheral neurotoxic symptoms produced by haditoxin *in vivo* warranted detailed pharmacological characterization on neuromuscular transmission using CBCM and RHD preparations. Haditoxin (1.5 μM) produced a reproducible time- and dose-dependent neuromuscular blockade in both preparations (Fig. 3, *A* and *C*). In the CBCM, it completely inhibited the contractile response to exogenous agonists (ACh and carbachol (*CCh*)), whereas response to exogenous KCl and twitches evoked by direct muscle stimulation were not inhibited, indicating a postsynaptic neuromuscular blockade and an absence of direct myotoxicity.

The IC_{50} of haditoxin on CBCM and RHD was 0.27 ± 0.07 and 1.85 ± 0.39 μM, respectively (Fig. 3*E*) (considering the fact

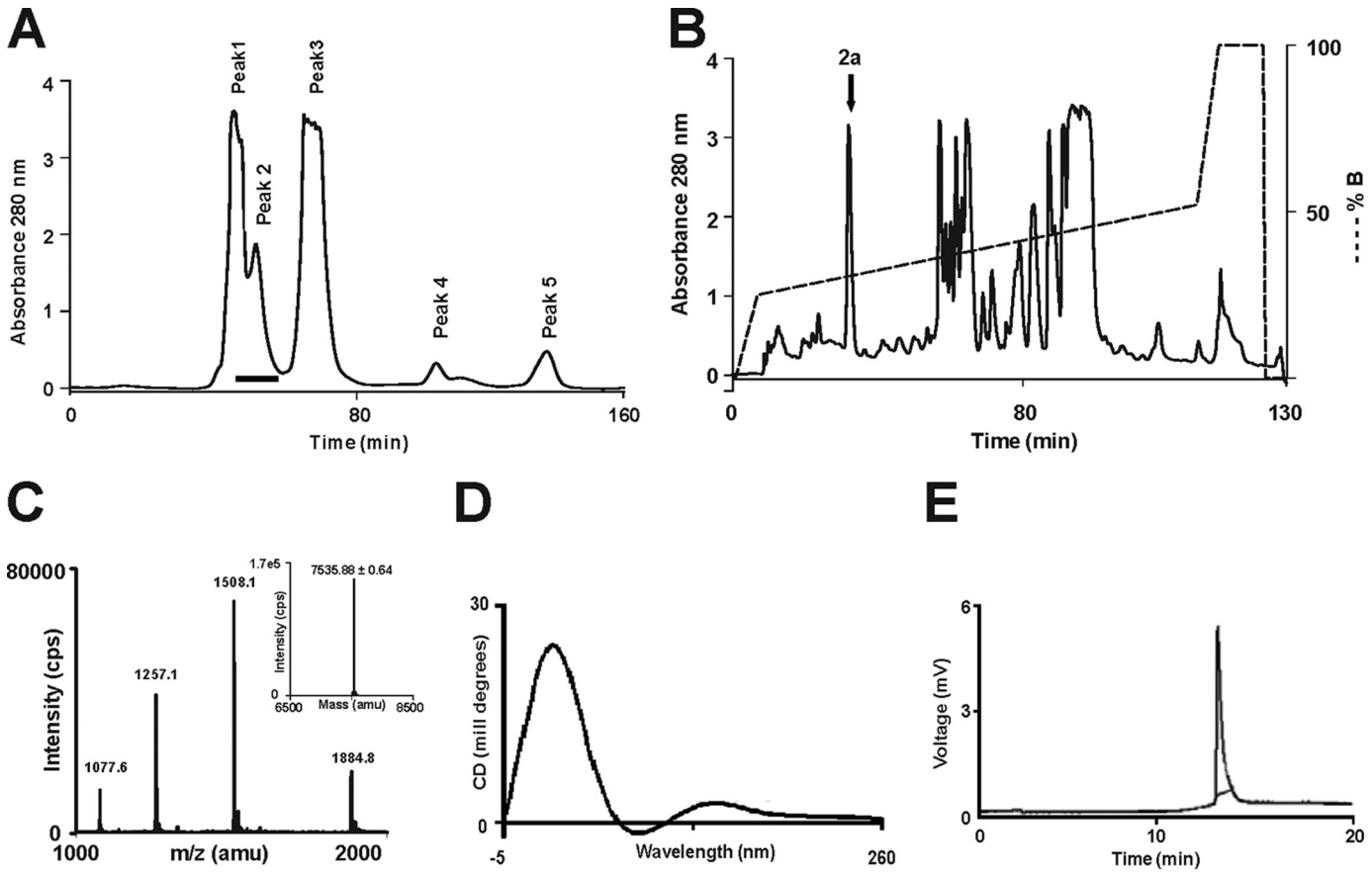

FIGURE 2. **Purification of haditoxin from the venom of *O. hannah*.** *A*, gel filtration chromatogram of crude venom. Crude venom (100 mg/ml) was fractionated using a Superdex 30 HiLoad (16/60) column. The column was pre-equilibrated with 50 mM Tris-HCl buffer (pH 7.4). Proteins were eluted at a flow rate of 1 ml/min using the same buffer. A *black bar* at *Peak 2* indicates the fractions containing haditoxin. *B*, RP-HPLC profile of the gel filtration fractions containing haditoxin. Jupiter C18 (5 μ, 300 Å, 4.5 × 250 mm) analytical column was equilibrated with 0.1% (v/v) trifluoroacetic acid. Protein of interest was eluted from the column with a flow rate of 1 ml/min with a gradient of 23–49% buffer B (80% acetonitrile in 0.1% trifluoroacetic acid). The *dotted line* indicates the gradient of the buffer B. The *downward arrow* at *Peak 2a* indicates fractions containing haditoxin. *C*, ESI-MS profile of the RP-HPLC fraction containing haditoxin. The spectrum shows a series of multiply charged ions, corresponding to a single, homogenous peptide with a molecular mass of 7,535.88 Da. *Inset*, reconstructed mass spectrum of haditoxin; *CPS* = counts/s; *amu* = atomic mass units. *D*, far-UV CD spectrum of haditoxin. The protein was dissolved in MilliQ water (0.5 mg/ml), and the CD spectra were recorded using a 0.1-cm path length cuvette. *E*, electropherogram of haditoxin. The sample was injected using pressure mode 5 p.s.i./s, and electrophoresis runs were carried out using a coated capillary (17 cm × 25 μm) at 18 kV, with 0.1 M phosphate buffer (pH 2.5) at 20 °C for 7 min.

that the protein exists as dimer in solution; see below). When compared with α-bungarotoxin (IC_{50} on CBCM 12.1 ± 5.4 nM and RHD 100.5 ± 22.5 nM) (Fig. 3*E*), haditoxin was about 50 times less potent on both avian (CBCM) and mammalian (RHD) neuromuscular junctions.

Reversibility of the neuromuscular blockade was tested for both preparations with intermittent washing (Fig. 3, *D* and *F*, *black arrows*). Partial recovery of the contractile response (60% recovery in 2 h) was observed in the CBCM (Fig. 3*B*) but not in the RHD (Fig. 3*D*). These results indicate that unlike typical α-neurotoxins such as α-bungarotoxin, haditoxin exhibits partial reversibility in action, at least in the CBCM.

Effect of Haditoxin on Human nAChRs—Because haditoxin blocked the muscle activity of the CBCM and RHD, we examined its activity on human αβδε-nAChRs. Haditoxin completely inhibited the ACh-induced αβδε currents at a concentration of 10 μM (Fig. 4*A*) with an IC_{50} value of 550 nM ($n = 13$) (Fig. 4*B*). This inhibition was practically irreversible within 8 min of washout. This result is in good agreement with the findings on e*x vivo* studies with RHD as discussed earlier. Next, we tested the activity of haditoxin on α_7- and $\alpha_3\beta_2$-nAChRs. On α_7-nAChRs, an irreversible block was observed at 10 μM concentration of haditoxin (Fig. 4*C*) with an IC_{50} value was 180 nM ($n = 4$) (Fig. 4*D*). As shown in Fig. 4*E*, 10 μM haditoxin fully blocked the response of $\alpha_3\beta_2$-nAChRs, with an IC_{50} value of 500 nM ($n = 4$) (Fig. 4*F*). Notably, the blockade at $\alpha_3\beta_2$ was fully reversible, whereas long-lasting blockade was observed at α_7-nAChRs. This suggests that the K_{Off} value at the α_7 receptor is much smaller than at $\alpha_3\beta_2$-nAChRs. As these two receptors display about equivalent IC_{50} values, this indicates that their respective K_{On} values are probably significantly different. However, the experimental protocol used herein prevents the detailed analysis of the K_{On} and K_{Off} values. An additional difference between these two receptors resides in their structural composition. Although it is thought that α_7-nAChRs display five identical ligand binding sites, only two binding sites are proposed for the $\alpha_3\beta_2$-nAChRs. The difference in number of binding sites and effects on competitive blockade was previously discussed for α_7- and $\alpha_4\beta_2$-nAChRs, showing significant functional outcomes (49). Interestingly, haditoxin was almost 3-fold more potent to block ACh-induced responses mediated by α_7-nAChRs (IC_{50} = 180 nM, $n = 4$) when compared with

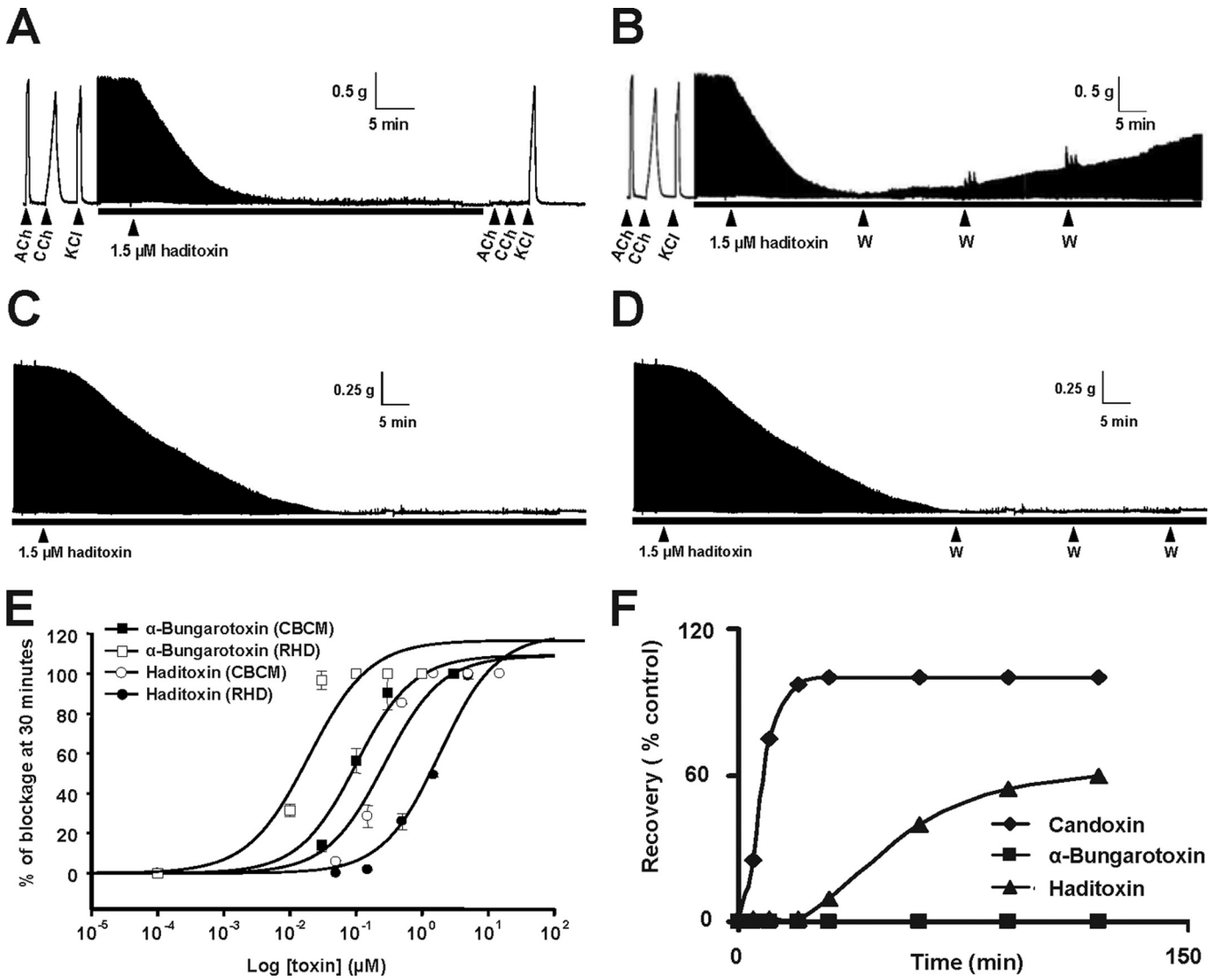

FIGURE 3. **Pharmacological profile of haditoxin.** *A–D*, a segment of tracing showing the effect of haditoxin (1.5 μM) on CBCM preparations (*A*), reversibility of CBCM preparation (*B*), RHD preparations (*C*), and reversibility of RHD preparation (*D*). Contractions were produced by exogenous ACh (300 μM), carbachol (*CCh*; 10 μM), and KCl (30 mM). The *black bar* indicates the electrical field stimulation. The point of washing out the toxin with Krebs solution in reversibility studies is indicated by the abbreviation *W*. *E*, dose-response curve of haditoxin and α-bungarotoxin on CBCM and RHD. The block is calculated as a percentage of the control twitch responses of the muscle to supramaximal nerve stimulation. Each data point is the mean ± S.E. of at least three experiments. *F*, comparative reversibility profile of α-bungarotoxin, haditoxin, and candoxin.

$\alpha\beta\delta\epsilon$- and $\alpha_3\beta_2$-nAChRs. There was no recovery after application of haditoxin. Finally, we tested the effect of haditoxin on $\alpha_4\beta_2$-nAChRs. Application of 10 μM haditoxin blocked only 70% of the current with partial reversibility (Fig. 4*G*). The IC_{50} value of the blockade is in the micromolar range (IC_{50} = 2.6 μM, n = 3) (Fig. 4*H*). However, further experiments will be necessary to discriminate between the different mechanisms of blockade and recovery. These results show that haditoxin had a higher potency for α_7-nAChRs than for the other nAChRs. IC_{50} values for $\alpha\beta\delta\epsilon$- and $\alpha_3\beta_2$-nAChRs were in the same nanomolar range, whereas for $\alpha_4\beta_2$-nAChRs, it was in the micromolar range.

Haditoxin Is a Dimer—During the gel filtration of the crude venom, we observed that haditoxin eluted earlier when compared with other 3FTxs (Fig. 2*A*, most of the 3FTxs elutes in *Peak 3*). This led us to investigate the oligomeric states of this protein. Thus, we carried out analytical gel filtration experiments using a Superdex G-75 column. Protein, at concentrations (0.25–10 μM) covering the IC_{50} in CBCM (0.27 ± 0.07 μM) and RHD (1.85 ± 0.39 μM) preparations, was loaded onto the column. At all of these concentrations, the presence of a single peak corresponding to a relative molecular mass of 16.25 kDa was observed (Fig. 5*A*), supporting the existence of a dimeric species. To observe the effect of SDS on dimerization, we treated the protein (0.25–10 μM) with SDS and eluted using the same column. It eluted as a single peak with a M_r of 8.16 kDa (Fig. 5*A*), similar to the monomeric species.

The dimerization was further confirmed by Tris-Tricine SDS-PAGE analysis in the presence and absence of a cross-linker, BS^3 (Fig. 5*B*). In the presence of BS^3, both the dimeric and the monomeric species were visualized (Fig. 5*B*, *lane 1*), whereas only the monomeric species were observed in its absence (Fig. 5*B*, *lane 2*). These results, together with MS data (showing monomeric mass, Fig. 2*C*), indicate the existence of

haditoxin as a homodimer in solution at pharmacologically relevant concentrations, and the dimerization occurs through non-covalent interactions. Further, as haditoxin loses its β-sheeted structure and becomes random coil in the presence of SDS (as indicated by CD studies; data not shown), its overall conformation may play a critical role in the dimerization.

Crystal Structure of Haditoxin—To determine the three-dimensional structure of haditoxin, we used the x-ray crystallographic method. Diffraction quality crystals of haditoxin were obtained with 0.1 M Tris, pH 8.5, 20% v/v ethanol (Hampton Research crystal screen 2, condition 44). Diffraction up to 1.55 Å was observed, and the crystals belonged to the space group $P2_1$ (Table 1).

Structure Determination and Refinement—The structure of haditoxin was solved by the molecular replacement method (Molrep) (50). Initially, toxin-α, isolated from *Naja nigricollis* venom, was used as a search model (Protein Data Bank (PDB) code 1IQ9; sequence identity ~48%). The rotation and translation resulted in a correlation factor of 0.07 and R_{cryst} of 0.57. Further minimization in Refmac (51) reduced the *R* factor to 0.42. An excellent quality electron density map was calculated at this stage, which allowed us to auto-build 90% of the haditoxin model with ARP/wARP (52). The resulting model with the electron density map was examined to manually build the rest of the model using the Coot program (53). After a few cycles of map fitting and refinement, we obtained an *R* factor of 0.194 (R_{free} = 0.225) for reflections $I > \sigma I$ within 20-1.55 Å resolution. Throughout the refinement (Table 1), no noncrystallographic symmetry restraint was employed. All 65 residues (considering one subunit) are well defined in the electron density map (Fig. 6*A*), and statistics for the Ramachandran plot using PROCHECK (54) showed the presence of 88.9% of non-glycine residues in the most favored region.

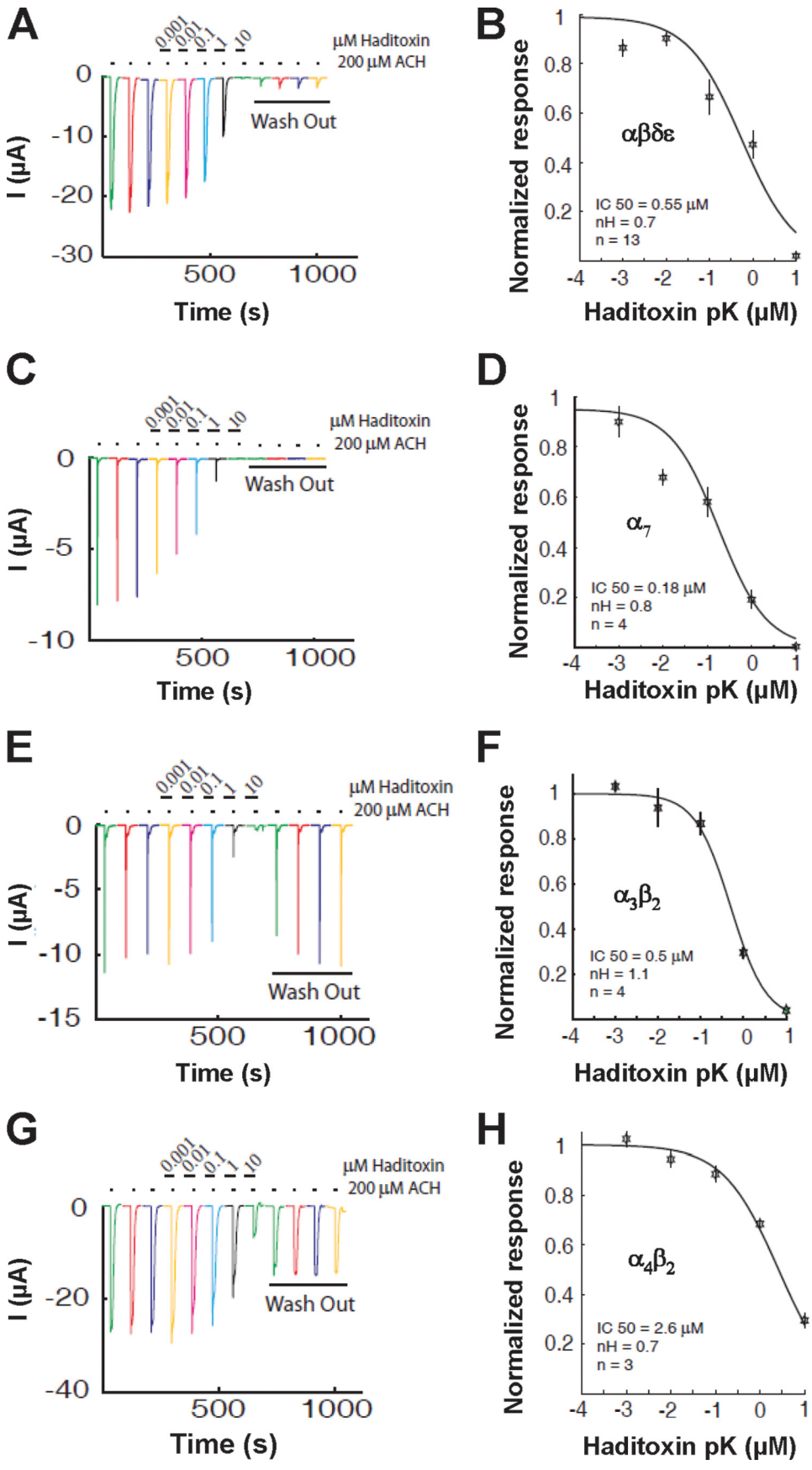

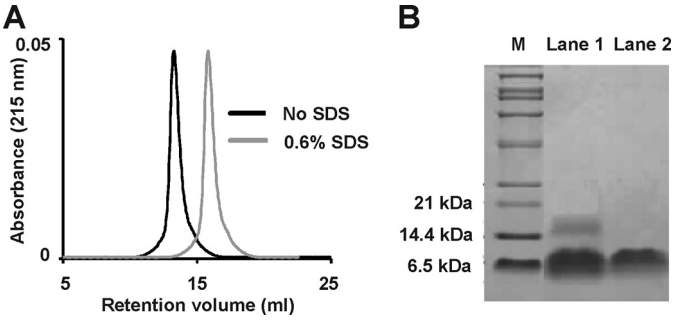

FIGURE 5. **Dimerization of haditoxin.** *A*, gel filtration profile of haditoxin with (*gray*) and without (*black*) SDS. 1 μM haditoxin was loaded onto a Superdex 75 column (1 × 30 cm) equilibrated with 50 mM Tris-HCl buffer (pH 7.4). The protein was eluted out with the 50 mM Tris-HCl buffer (pH 7.4) or 50 mM Tris-HCl buffer (pH 7.4) containing 0.6% SDS at flow rate of 0.6 ml/min. *B*, Tris-Tricine SDS-PAGE analysis of haditoxin with (*lane 1*) and without (*lane 2*) cross linker (BS^3). *M* is the marker lane. The concentration of BS^3 is 5 mM.

TABLE 1
X-ray data collection and refinement statistics

Data collection	
Cell parameters (Å)	$a = 37.27$, $b = 41.29$, $c = 40.98$, $\beta = 106.4°$
Space group	$P2_1$
Molecules/asymmetric unit	2
Resolution range (Å)	50–1.55
Wavelength (Å)	1.5418
Observed reflections	82,388
Unique reflections	17,366
Completeness (%)	99.1 (92.9)
R_{sym} (%)[a]	0.093
$I/\sigma(I)$	40.2 (6.0)
Refinement and quality	
Resolution range (Å)	20–1.55
R_{work} (%)[b]	19.4
R_{free} (%)[c]	22.5
r.m.s.d. bond lengths (Å)	0.009
r.m.s.d. bond angles (deg)	1.274
Average *B* factors (Å^2)	15.1
Number of protein atoms	1408
Number of waters	114
Ramachandran plot (%)	
Most favored regions	88.9
Additional allowed regions	9.3
Generously allowed regions	1.9
Disallowed regions	0

[a] $R_{sym} = \sum|I_i - \langle I\rangle|/\sum|I|$, where I_i is the intensity of the *i*th measurement, and $\langle I\rangle$ is the mean intensity for that reflection.
[b] $R_{work} = \sum||F_{obs}| - |F_{calc}||/\sum|F_{obs}|$, where F_{calc} and F_{obs} are the calculated and observed structure factor amplitudes, respectively.
[c] R_{free} = as for R_{work}, but for 10% of the total reflections chosen at random and omitted from refinement.

The coordinates and structure factors have been deposited with the Research Collaboratory for Structural Bioinformatics (RCSB) PDB (55) with the code 3HH7. The asymmetric unit consists of two monomers forming a tight dimer having an approximate dimension of 25 × 13 × 4 Å (Fig. 6*B*). This crystallographic dimer is consistent with the gel filtration and SDS-PAGE observations (Fig. 5). Both monomers are related by a two-fold symmetry, and their superposition yielded an r.m.s.d. of 0.2 Å for 65 Cα atoms (Fig. 7*A*). Each monomer adopts the common three-finger fold (11) consisting of three β-sheeted loops protruding from a central core, tightened by four highly conserved disulfide bridges (Cys-3–Cys-24, Cys-17–Cys-41, Cys-45–Cys-57, and Cys-58–Cys-63) (Fig. 6, *B* and *C*), and are structurally similar to short-chain α-neurotoxins such as toxin-α and erabutoxins (Fig. 7*B*). Loop I forms a two-stranded β-sheet (Lys-2–Tyr-4 and Thr-14–Ile-16), whereas loops II and III form a three-stranded β-sheet (Glu-34–Thr-42, Phe-23–Asp-31, and Lys-53–Cys-58). The antiparallel β-strands of the β-sheet are stabilized by main chain-main chain hydrogen bonding.

Dimeric Interface—The dimeric interface was analyzed using the Protein Interfaces, Surfaces and Assemblies (PISA) server (56). It is mainly formed by loop III of each subunit. Strands D, C, E, E′, C′, and D′ form a six β-pleated sheet with an overall right-handed twist (Fig. 6*B*) in the dimer. Approximately 565 Å^2 (or 12% of the total) surface areas and 17 residues of each monomer contribute to the dimerization. The close contacts between the monomers are maintained by 14 hydrogen bonds (<3.2 Å) and extensive hydrophobic interactions (Table 2). Six main chain-main chain hydrogen-bonding contacts exist across the interface involving strand E of monomer A and E′ of B (Table 2, Fig. 7*C*). Four are observed between the main chain amide hydrogen and carbonyl oxygen of Val-55 and Cys-57 from monomer A and Val-55′ and Cys-57′ from monomer B, and the remaining two exist between the carbonyl oxygen of Lys-53 (and Lys-53′) and the amide hydrogen of Arg-59 (and Arg-59′). In addition, there are another eight hydrogen-bonding contacts mediated through the side chains of Thr-44, Cys-45, Glu-47, Pro-50, and Arg-59 (Table 2, Fig. 7*C*). Two hydrophobic clusters further stabilize the dimeric structure. The side chains of Phe-23 and Leu-48 from both monomers form one cluster, whereas the disulfide bridge between Cys-45–Cys-57 and Val-55 of both monomers form the other. These observations strongly suggest the existence of haditoxin as non-covalent homodimeric species.

DISCUSSION

Nonenzymatic neurotoxins from snake venom belonging to the 3FTx family consist of closely related polypeptides with a molecular mass range of 6,500–8,000 Da. Functionally, most interfere with cholinergic neurotransmission and are highly specific for different subtypes of muscarinic or nicotinic cholinergic receptors (for details, see the Introduction). This underscores their immense potential as lead molecules in drug discovery and as research tools in the characterization of receptor subtypes.

Here, we have described the purification and characterization of a novel neurotoxin, haditoxin, from the venom of *O. hannah*. It is a non-covalent homodimer that produces potent postsynaptic neuromuscular blockade of the mammalian muscle (IC_{50} = 1.85 ± 0.39 μM) and avian muscle (IC_{50} = 0.27 ± 0.07 μM) (αβγδ)

FIGURE 4. **Effect of haditoxin on human nAChRs expressed in *Xenopus* oocytes.** *A*, *C*, *E*, and *G*, inhibition of ACh-induced currents in αβδε- (neuromuscular junction) (*A*), α_7- (*C*), $\alpha_4\beta_2$- (*E*), and $\alpha_3\beta_2$-nAChRs (*G*). Neuromuscular junction currents were activated by 10 μM ACh, whereas 200 μM was used to activate α_7-, $\alpha_4\beta_2$-, and $\alpha_3\beta_2$-nAChRs. The first three traces are controls, followed by a 2-min exposure to several haditoxin concentrations ranging from 10 nM to 10 μM. Each experiment was terminated by a 8-min wash out. Little or no recovery was observed for αβδε- and α_7-nAChRs, whereas partial to full recovery was observed for $\alpha_4\beta_2$- and $\alpha_3\beta_2$-nAChRs. Inhibition curves of the fitted data, IC_{50}, and Hill coefficient (*nH*) for αβδε-nAChRs (*B*) were 0.55 μM and 0.7; for α_7-nAChRs (*D*), they were 0.18 μM and 0.8; for $\alpha_3\beta_2$-nAChRs (*F*), they were 0.5 μM and 1.1; and for $\alpha_4\beta_2$-nAChRs (*H*), they were 2.6 μM and 0.7. *Error bars* indicate S.E.

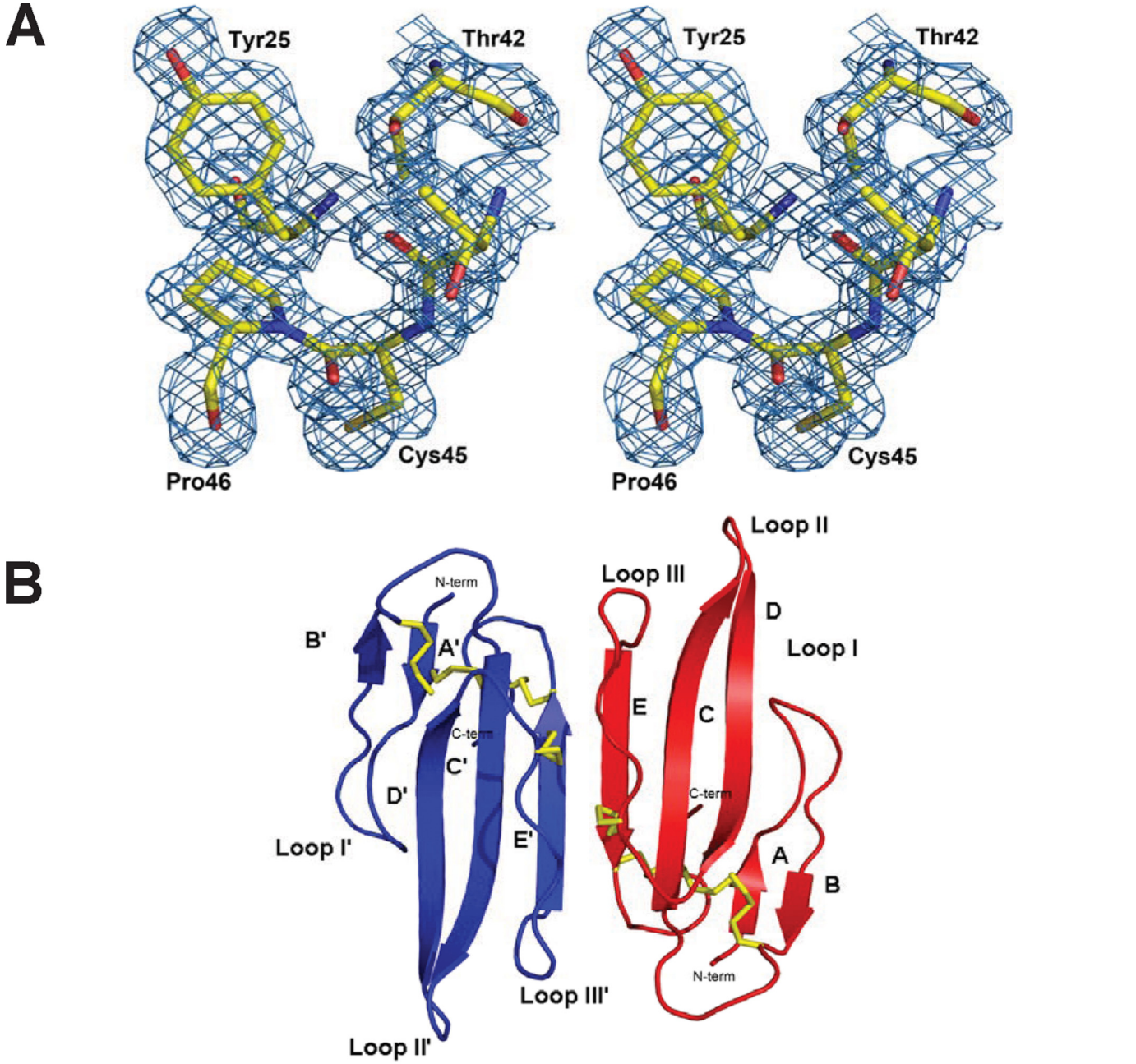

FIGURE 6. **Overall structure of haditoxin.** *A*, stereo view of a portion of the final $2F_o - F_c$ map of haditoxin. The map was contoured at a level of 1.0 σ. *B*, monomers A and B are shown in *blue* and *red*, respectively. Disulfide bonds are shown in *yellow*. N and C termini (*N-term* and *C-term*), β-strands, and loops I, II, and III are labeled. *C*, structure-based alignment of three-finger toxins. Color coding of conserved residues is provided by *boxed red text*, and color coding of invariant residues is provided by *red highlight*. Accession numbers are shown on the *left*, and secondary structural elements of haditoxin are shown on *top*. Numbering is shown for haditoxin only. Sequence alignment was done by Strap (82) and displayed with ESPript (83).

nAChRs (Fig. 3, *A* and *C*). In electrophysiological studies, it was an antagonist of muscle ($\alpha\beta\delta\epsilon$) ($IC_{50}$ = 0.55 μM) as well as neuronal α_7- (IC_{50} = 0.18 μM), $\alpha_3\beta_2$- (IC_{50} = 0.50 μM), and $\alpha_4\beta_2$- (IC_{50} = 2.60 μM) nAChRs (Fig. 4). Interestingly, haditoxin exhibited a novel pharmacology with combined blocking activity on muscle ($\alpha\beta\gamma\delta$) as well as neuronal (α_7, $\alpha_3\beta_2$, and $\alpha_4\beta_2$) nAChRs but with the highest potency on α_7-nAChRs, which is recognized by neither short-chain α-neurotoxins nor κ-neurotoxins.

The reversibility of this neuromuscular blockade was taxa-specific; it is partially reversible by washing in the chick neuromuscular junction, whereas it was almost irreversible in the rat neuromuscular junction. Earlier, we reported taxa-specific neurotoxicity of denmotoxin from *Boiga dendrophila* (12) and irditoxin from *Boiga irregularis* (13). Taxa specificity manifests the natural targeting of the venom toxins toward their prey (13, 57–59). Snakes from the *Boiga* sp. mainly feed on the non-mammalian prey such as birds (12, 13, 60), whereas elapids, including the king cobra, mainly prey on snakes and rodents and only occasionally and opportunistically on birds (61, 62). Venom compositions of snakes are known to be dependent on prey specificity to ensure efficiency in their capture and killing (58). Therefore, the taxa-specific reversibility of the neuromuscular blockade produced by haditoxin is likely due to the natural species specificity of the king cobra venom and not because of low toxicity.

Structurally Important Residues for Haditoxin—Haditoxin contains all 8 conserved cysteine residues that are essential for the three-finger folding (24, 63). They form four disulfide bridges located in the core region of the molecule. In addition, this molecule possesses several other structurally invariant residues, responsible for the stability of the three-finger fold. For example, Tyr-25 (numbering of the residues is according to erabutoxin-a, unless stated otherwise), the crucial residue stabilizing the antiparallel β-sheet structure (64), is conserved in a similar three-dimensional orientation. Similarly, the structurally invariant Gly-40, involved in the tight packing of the three-dimensional fold by accommodating the bulky side chain of the Tyr-25 (24), is also conserved. The 2 proline residues Pro-44 and Pro-48, potentially associated with the formation of the β-turn (24), are conserved in haditoxin as Pro-46 and Pro-50. The salt bridge between the

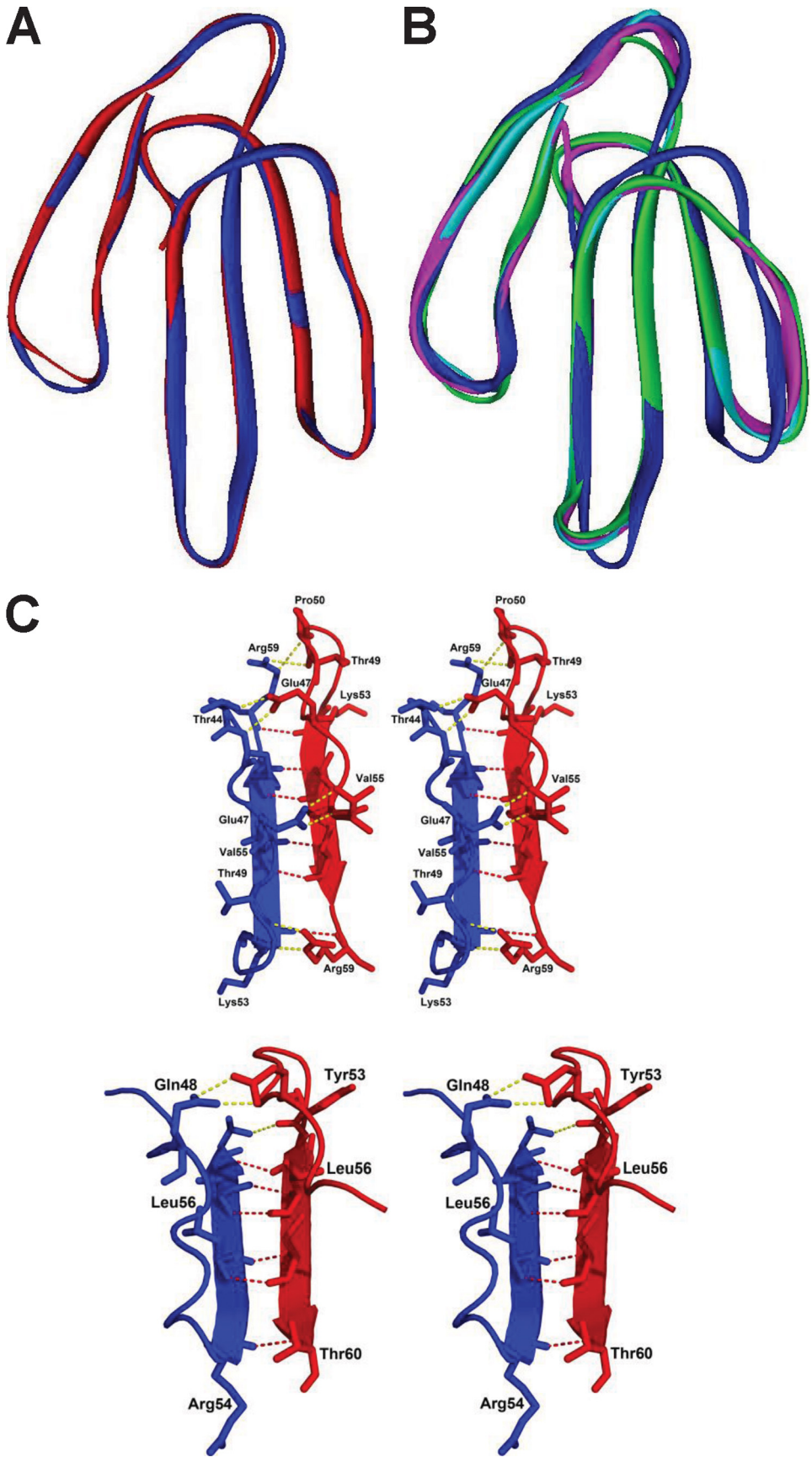

TABLE 2
Hydrogen bonds in the dimeric interface of the haditoxin

Hydrogen bonds	Monomer A	Monomer B	Distance
			Å
Main chain-main chain	Cys-57 (O)	Val-55 (N)	2.93
	Val-55 (O)	Cys-57 (N)	2.85
	Cys-57 (N)	Val-55 (O)	2.86
	Val-55 (N)	Cys-57 (O)	2.90
	Lys-53 (O)	Arg-59 (N)	3.10
	Arg-59 (N)	Lys-53 (O)	3.40
Side chain-side chain	Glu-47 (OE1)	Thr-44 (OG1)	2.63
	Glu-47 (OE2)	Cys-45 (N)	2.76
	Pro-50 (O)	Arg-59 (NE)	3.39
	Thr-49 (O)	Arg-59 (NH_2)	3.37
	Thr-44 (OG1)	Glu-47 (OE1)	2.68
	Cys-45 (N)	Glu-47 (OE2)	2.81
	Arg-59 (NH_2)	Thr-49 (O)	2.66
	Arg-59 (NE)	Gly-52 (O)	2.76

N-terminal amino group and the carboxyl group of Glu-58 as well as the C-terminal carboxyl group and the guanidinium group of Arg-39 in erabutoxin-a (24) is maintained by the N-terminal amino group and the carboxyl group of Asp-58 as well as the C-terminal carboxyl group and the guanidinium group of the Arg-39 in haditoxin. Thus, the presence of these structurally invariant residues contributes to the stable three-finger fold of haditoxin.

Functionally Important Residues for Haditoxin—Extensive structure-function relationship studies on the short-chain α-neurotoxin, erabutoxin-a (24, 65, 66), and the long-chain α-neurotoxins, α-cobratoxin (67, 68) and α-bungarotoxin (69, 70), revealed the critical residues involved in the recognition of nAChRs by snake neurotoxins. The crucial residues for α-neurotoxins to bind to muscle (αβγδ) nAChRs are Lys-27, Trp-29, Asp-31, Phe-32, Arg-33, and Lys-47. Haditoxin possesses three of them (Trp-29, Asp-31, and Arg-33) in homologous positions. Additionally, each type of toxin possesses specific residues that recognize muscle or neuronal nAChRs. For muscle (αβγδ) nAChRs, these are His-6, Gln-7, Ser-8, Ser-9, and Gln-10 in loop I and Tyr-25, Gly-34, Ile-36, and Glu-38 in loop II of short-chain α-neurotoxins (65) and Arg-36 in loop II and Phe-65 in the C terminus tail of long-chain α-neurotoxins (67). His-6, Gln-7, and Ser-8 in the loop I and Tyr-25, Gly-34, Ile-37, and Glu-38 in the loop II are conserved in haditoxin as the muscle subtype-specific determinants of short-chain α-neurotoxins. Moreover, Arg-36, muscle subtype-specific determinant of long-chain α-neurotoxins, is also conserved in haditoxin. The presence of these multiple functional determinants may explain the potent neurotoxicity exhibited by haditoxin on mammalian and avian muscle (αβγδ) nAChR.

On the contrary, the specific determinants (Ala-28 and Lys-35; α-cobratoxin numbering) of long-chain α-neurotoxins toward the neuronal (α_7) nAChRs (71) are not conserved in haditoxin. Significantly, haditoxin also lacks the fifth disulfide bridge responsible for the cyclization of loop II, which is considered to be a hallmark determinant for the ability of neurotoxins such as α-bungarotoxin and κ-bungarotoxins to interact with their specific neuronal nAChR targets (67, 71–74). This is somewhat surprising given the high affinity of haditoxin for α_7- (IC_{50} = 0.18 μM), $\alpha_3\beta_2$- (IC_{50} = 0.5 μM), and $\alpha_4\beta_2$- (IC_{50} = 2.6 μM) nAChRs. Previously, candoxin, a non-conventional 3FTx (31), was found to be an exception of a 3FTx that did not have the fifth disulfide bridge in loop II (candoxin has a fifth disulfide bridge in loop I) but still retained the ability to interact with neuronal (α_7) nAChRs (75). It was suggested thus that candoxin may likely interact with neuronal α_7-nAChRs using alternate, novel points of contact. Likewise, it is plausible that haditoxin possesses unique combinations of determinants that enable its interaction with α_7-, as well as $\alpha_3\beta_2$- and $\alpha_4\beta_2$-nAChRs. A detailed structure-function analysis to decipher these novel determinants is beyond the scope of this report.

In the case of κ-neurotoxins, which interact with neuronal $\alpha_3\beta_2$- and $\alpha_4\beta_2$-nAChRs with high affinity (26, 27), the critical functional residue was identified as Arg-34 (76). Haditoxin has Arg-33 in a homologous position, which may contribute in part to high affinity interaction with $\alpha_3\beta_2$- (IC_{50} = 0.5 μM) and $\alpha_4\beta_2$- (IC_{50} = 2.6 μM) nAChRs. Mutagenesis studies on κ-bungarotoxin revealed that the replacement of Pro-36 to an amino acid residue bearing a bulky, charged side chain, such as the Lys found in α-bungarotoxin, causes a 16-fold decrease in the efficacy of the toxin to block neurotransmission in the chick ciliary ganglion assay (76). Haditoxin bears an equivalent glycine residue, lacking a bulky, charged side chain, which can explain the high affinity of this toxin toward the neuronal ($\alpha_3\beta_2$ and $\alpha_4\beta_2$) nAChRs.

Comparison of Haditoxin with Other Dimeric 3FTxs—Few known examples of dimeric three-finger neurotoxins derived from snake venoms exist (13, 37, 72). Among them, the most well studied and characterized are the κ-neurotoxins, known to be composed of two identical monomers held together by non-covalent interactions (77, 78). The observed dimeric form of haditoxin, with the characteristic six β-pleated sheets, is similar to that formed by κ-bungarotoxin (77). Superposition of both molecules yielded an r.m.s.d. of 1.95 Å for 104 Cα atoms (Fig. 8*A*). The major deviations are located in the loops between the antiparallel β-strands. However, each monomer in κ-bungarotoxin is structurally homologous to long-chain α-neurotoxins unlike haditoxin, which resembles short-chain α-neurotoxins (Fig. 7*C*). The dimeric interface for both is maintained by six main chain-main chain hydrogen bonds (77). In addition, haditoxin has eight side chain hydrogen-bonding contacts between the monomers, whereas only three similar contacts were observed in κ-bungarotoxin (Fig. 7*A*) (77), suggesting that haditoxin forms tighter dimers than κ-bungarotoxin. The side chain interactions in κ-bungarotoxin are maintained by Phe-49, Leu-57, and Ile-20, which are strictly conserved in all κ-neurotoxins (77, 79). Mutagenesis studies have proven that replacing Phe-49 or Ile-20 with alanines renders a toxin with an apparent lack of ability to fold into the native structure, even as a monomer (79).

FIGURE 7. **Structural details of haditoxin.** *A*, superimposition of both subunits of haditoxin. Subunits A and B are shown in *blue* and *red*, respectively. *B*, superimposition subunit A of haditoxin with short-chain α-neurotoxins. Subunit A is shown in *blue*, erabutoxin-a is shown in *magenta*, erabutoxin-b is shown in *cyan*, and toxin-α is shown in *green*. *C*, stereo diagram of comparison of dimer interface of haditoxin (*top*) and κ-bungarotoxin (*bottom*). The residues to form the hydrogen bonds are labeled. The main chain-main chain hydrogen bonds are shown in *red*, and the other hydrogen bonds are shown in *yellow*.

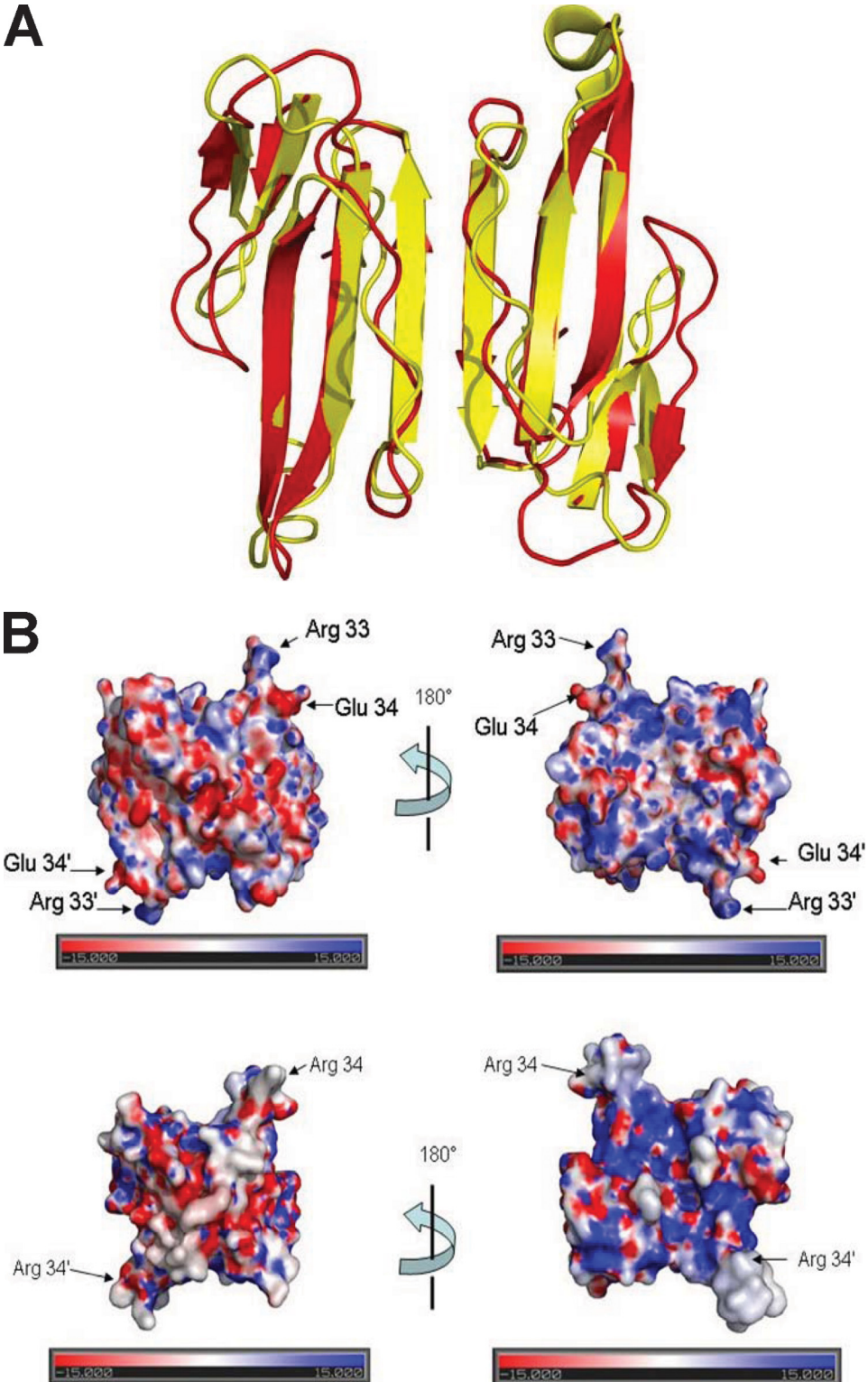

FIGURE 8. **Haditoxin *versus* κ-bungarotoxin.** *A*, superimposition of haditoxin with κ-bungarotoxin. Haditoxin and κ-bungarotoxin are shown in *red* and *yellow*, respectively. *B*, electrostatic surface of haditoxin (*top*) and κ-bungarotoxin (*bottom*). The orientation is the same as in Fig. 6*B*. The locations of Arg-33 and Glu-34 of haditoxin and Arg-34 of κ-bungarotoxin are indicated.

The same result has been observed with deletion studies (deletion of Arg-54) with an aim to generate a 65-residue-long protein, as found in the α-neurotoxins, from the 66-residue-long κ-bungarotoxin (79), whereas haditoxin being a 65-residue-long protein lacks both Phe-49 and Ile-20 but still retains the intact dimeric structure. The electrostatic surface potentials for both molecules were apparently similar (Fig. 8*B*) except for the tip of loop II, which revealed a strong positive patch for haditoxin when compared with κ-bungarotoxin (77).

Functionally, κ-neurotoxins interact with the neuronal ($\alpha_3\beta_2$ and $\alpha_4\beta_2$) nAChRs with high affinity (26, 27), whereas haditoxin interacts with both muscle ($\alpha\beta\gamma\delta$) and a variety of neuronal (α_7, $\alpha_3\beta_2$, and $\alpha_4\beta_2$) nAChRs. The crystal structure of the κ-bungarotoxin dimer showed that the guanidinium groups of the essential arginine residues, situated at the tip of the loop II, maintains nearly identical distance (44 Å) (77), like the acetylcholine binding sites in the pentameric receptor (30–50 Å) (80, 81). The κ-bungarotoxin dimer may both interact with the acetylcholine binding sites on a single neuronal receptor and physically block ion flow by spanning the channel (77, 79). However, this mode of interaction does not explain the inability of the κ-neurotoxins to block the muscle nAChRs. Haditoxin maintains a distance of ~52 Å between the guanidinium groups of the critical arginine residues present in the turn region of the second loop, which is almost similar to the acetylcholine binding sites in the pentameric receptor mentioned above. However, unlike the κ-neurotoxins, haditoxin interacts with both muscle and neuronal nAChRs. This supports the fact that the dimeric toxins may have a unique mode of interaction with the nAChRs, which demands further investigation.

More recently, other heterodimeric 3FTxs from elapid venoms have been reported, including covalently (disulfide) linked homodimers of a long-chain α-neurotoxin (α-cobratoxin) and heterodimers of α-cobratoxin in combination with a variety of three-finger cytotoxins (72). Unlike haditoxin, all of these dimers are formed by covalent bonding (disulfide linkage) of the monomeric units. Functionally, the α-cobratoxin-cytotoxin heterodimers were able to block neuronal (α_7) nAChRs, whereas the α-cobratoxin homodimer exhibited blockade of

both neuronal α_7- and $\alpha_3\beta_2$-nAChRs, unlike monomeric α-cobratoxin, which interacts with muscle ($\alpha\beta\gamma\delta$) and neuronal (α_7) nAChRs (72).

Our laboratory has also reported on a colubrid venom-derived covalently linked heterodimeric 3FTx, irditoxin (13), which was found to target muscle ($\alpha\beta\gamma\delta$) nAChRs, in sharp contrast to the reported function of elapid dimeric toxins (72). Another distinguishing feature was that the subunits of irditoxin structurally resemble non-conventional 3FTxs (13). Haditoxin is both structurally and functionally distinct from the α-cobratoxin hetero/homodimers as well as irditoxin. Structurally, haditoxin is a non-covalently linked homodimer of the short-chain α-neurotoxin type, and functionally, it has a broad pharmacological profile with high affinity and selectivity for muscle ($\alpha\beta\gamma\delta$) and neuronal (α_7, $\alpha_4\beta_2$, and $\alpha_3\beta_2$) nAChRs. Haditoxin exhibits a unique structural and functional profile and is the first reported dimeric 3FTx interacting with the muscle ($\alpha\beta\gamma\delta$) nAChR as well as the first short-chain type of α-neurotoxin to interact with neuronal α_7-nAChR with nanomolar affinity.

REFERENCES

1. Harvey, A. L. (1991) *Snake Toxins*, pp. 1–90, Pergamon Press, New York
2. Lewis, R. J., and Garcia, M. L. (2003) *Nat. Rev. Drug Discov.* **2,** 790–802
3. Harvey, A. L. (2002) *Trends Pharmacol. Sci.* **23,** 201–203
4. Langley, J. N. (1907) *J. Physiol.* **36,** 347–384
5. Katz, B., and Thesleff, S. (1957) *J. Physiol.* **138,** 63–80
6. Grutter, T., and Changeux, J. P. (2001) *Trends Biochem. Sci.* **26,** 459–463
7. Changeux, J. P. (1990) *Trends Pharmacol. Sci.* **11,** 485–492
8. Taylor, P., Molles, B., Malany, S., and Osaka, H. (2002) in *Perspectives in Molecular Toxinology* (Ménez, A., ed) pp. 271–280, John Wiley & Sons, Chichester, England
9. Changeux, J. P., Kasai, M., and Lee, C. Y. (1970) *Proc. Natl. Acad. Sci. U.S.A.* **67,** 1241–1247
10. Colquhoun, L. M., and Patrick, J. W. (1997) *Adv. Pharmacol.* **39,** 191–220
11. Kini, R. M. (2002) *Clin. Exp. Pharmacol. Physiol.* **29,** 815–822
12. Pawlak, J., Mackessy, S. P., Fry, B. G., Bhatia, M., Mourier, G., Fruchart-Gaillard, C., Servent, D., Ménez, R., Stura, E., Ménez, A., and Kini, R. M. (2006) *J. Biol. Chem.* **281,** 29030–29041
13. Pawlak, J., Mackessy, S. P., Sixberry, N. M., Stura, E. A., Le Du, M. H., Ménez, R., Foo, C. S., Ménez, A., Nirthanan, S., and Kini, R. M. (2009) *FASEB J.* **23,** 534–545
14. Pahari, S., Mackessy, S. P., and Kini, R. M. (2007) *BMC. Mol. Biol.* **8,** 115
15. Jiang, M., Häggblad, J., and Heilbronn, E. (1987) *Toxicon* **25,** 1019–1022
16. Tsetlin, V. (1999) *Eur. J. Biochem.* **264,** 281–286
17. Kumar, T. K., Jayaraman, G., Lee, C. S., Arunkumar, A. I., Sivaraman, T., Samuel, D., and Yu, C. (1997) *J. Biomol. Struct. Dyn.* **15,** 431–463
18. de Weille, J. R., Schweitz, H., Maes, P., Tartar, A., and Lazdunski, M. (1991) *Proc. Natl. Acad. Sci. U.S.A.* **88,** 2437–2440
19. McDowell, R. S., Dennis, M. S., Louie, A., Shuster, M., Mulkerrin, M. G., and Lazarus, R. A. (1992) *Biochemistry* **31,** 4766–4772
20. Rajagopalan, N., Pung, Y. F., Zhu, Y. Z., Wong, P. T., Kumar, P. P., and Kini, R. M. (2007) *FASEB J.* **21,** 3685–3695
21. Ricciardi, A., le Du, M. H., Khayati, M., Dajas, F., Boulain, J. C., Menez, A., and Ducancel, F. (2000) *J. Biol. Chem.* **275,** 18302–18310
22. Ohno, M., Ménez, R., Ogawa, T., Danse, J. M., Shimohigashi, Y., Fromen, C., Ducancel, F., Zinn-Justin, S., Le Du, M. H., Boulain, J. C., Tamiya, T., and Ménez, A. (1998) *Prog. Nucleic Acid Res. Mol. Biol.* **59,** 307–364
23. Nirthanan, S., and Gwee, M. C. (2004) *J. Pharmacol. Sci.* **94,** 1–17
24. Endo, T., and Tamiya, N. (1991) in *Snake Toxins* (Harvey, A. L., ed) pp. 165–222, Pergamon Press, New York
25. Servent, D., Antil-Delbeke, S., Gaillard, C., Corringer, P. J., Changeux, J. P., and Ménez, A. (2000) *Eur. J. Pharmacol.* **393,** 197–204
26. Grant, G. A., and Chiappinelli, V. A. (1985) *Biochemistry* **24,** 1532–1537
27. Wolf, K. M., Ciarleglio, A., and Chiappinelli, V. A. (1988) *Brain Res.* **439,** 249–258
28. Servent, D., and Fruchart-Gaillard, C. (2009) *J. Neurochem.* **109,** 1193–1202
29. Harvey, A. L., Kornisiuk, E., Bradley, K. N., Cerveñansky, C., Durán, R., Adrover, M., Sánchez, G., and Jerusalinsky, D. (2002) *Neurochem. Res.* **27,** 1543–1554
30. Olianas, M. C., Ingianni, A., Maullu, C., Adem, A., Karlsson, E., and Onali, P. (1999) *J. Pharmacol. Exp. Ther.* **288,** 164–170
31. Nirthanan, S., Charpantier, E., Gopalakrishnakone, P., Gwee, M. C., Khoo, H. E., Cheah, L. S., Bertrand, D., and Kini, R. M. (2002) *J. Biol. Chem.* **277,** 17811–17820
32. Lumsden, N. G., Fry, B. G., Ventura, S., Kini, R. M., and Hodgson, W. C. (2005) *Toxicon* **45,** 329–334
33. Starkov, V. G., Poliak, Iu. L., Vul'fius, E. A., Kriukova, E. V., Tsetlin, V. I., and Utkin, Iu. N. (2009) *Bioorg. Khim.* **35,** 15–24
34. Kuruppu, S., Reeve, S., Smith, A. I., and Hodgson, W. C. (2005) *Biochem. Pharmacol.* **70,** 794–800
35. Tan, L. C., Kuruppu, S., Smith, A. I., Reeve, S., and Hodgson, W. C. (2006) *Neuropharmacology* **51,** 782–788
36. Aird, S. D., Womble, G. C., Yates, J. R., 3rd, and Griffin, P. R. (1999) *Toxicon* **37,** 609–625
37. Chiappinelli, V. A., and Lee, J. C. (1985) *J. Biol. Chem.* **260,** 6182–6186
38. Chiappinelli, V. A., and Wolf, K. M. (1989) *Biochemistry* **28,** 8543–8547
39. Ginsborg, B. L., and Warriner, J. (1960) *Br. J. Pharmacol. Chemother.* **15,** 410–411
40. Bülbring, E. (1997) *Br. J. Pharmacol.* **120,** 3–26
41. Hogg, R. C., Bandelier, F., Benoit, A., Dosch, R., and Bertrand, D. (2008) *J. Neurosci. Methods* **169,** 65–75
42. Staros, J. V. (1982) *Biochemistry* **21,** 3950–3955
43. Otwinowski, Z., and Minor, W. (1997) *Methods Enzymol.* **276,** 307–326
44. Pung, Y. F., Wong, P. T., Kumar, P. P., Hodgson, W. C., and Kini, R. M. (2005) *J. Biol. Chem.* **280,** 13137–13147
45. Coulson, F. R., Jacoby, D. B., and Fryer, A. D. (2004) *J. Pharmacol. Exp. Ther.* **308,** 760–766
46. Weiser, M., Mutschler, E., and Lambrecht, G. (1997) *Naunyn Schmiedebergs Arch. Pharmacol.* **356,** 671–677
47. Warrell, D. A., Looareesuwan, S., White, N. J., Theakston, R. D., Warrell, M. J., Kosakarn, W., and Reid, H. A. (1983) *Br. Med. J.* (*Clin. Res. Ed.*) **286,** 678–680
48. Laothong, C., and Sitprija, V. (2001) *Toxicon* **39,** 1353–1357
49. Palma, E., Bertrand, S., Binzoni, T., and Bertrand, D. (1996) *J. Physiol.* **491,** 151–161
50. Vagin, A., and Teplyakov, A. (1997) *J. Appl. Crystallogr.* **30,** 1022–1025
51. Vagin, A. A., Steiner, R. A., Lebedev, A. A., Potterton, L., McNicholas, S., Long, F., and Murshudov, G. N. (2004) *Acta Crystallogr. D. Biol. Crystallogr.* **60,** 2184–2195
52. Perrakis, A., Morris, R., and Lamzin, V. S. (1999) *Nat. Struct. Biol.* **6,** 458–463
53. Emsley, P., and Cowtan, K. (2004) *Acta Crystallogr. D. Biol. Crystallogr.* **60,** 2126–2132
54. Laskowski, R. A., MacArthur, M. W., Moss, D. S., and Thornton, J. M. (1993) *J. Appl. Crystallogr.* **26,** 283–291
55. Berman, H. M., Westbrook, J., Feng, Z., Gilliland, G., Bhat, T. N., Weissig, H., Shindyalov, I. N., and Bourne, P. E. (2000) *Nucleic Acids Res.* **28,** 235–242
56. Krissinel, E., and Henrick, K. (2007) *J. Mol. Biol.* **372,** 774–797
57. Barlow, A., Pook, C. E., Harrison, R. A., and Wüster, W. (2009) *Proc. Biol. Sci.* **276,** 2443–2449
58. Daltry, J. C., Wüster, W., and Thorpe, R. S. (1996) *Nature* **379,** 537–540
59. Pahari, S., Bickford, D., Fry, B. G., and Kini, R. M. (2007) *BMC. Evol. Biol.* **7,** 175
60. Mackessy, S. P., Sixberry, N. M., Heyborne, W. H., and Fritts, T. (2006) *Toxicon* **47,** 537–548
61. Mehrtens, J. (1987) *Living Snakes of the World*, pp. 245–281, Sterling, New York
62. Coborn, J. (1991) *The Atlas of Snakes of the World*, pp. 452–453, TFH Publications, New Jersey

63. Ménez, A., Bouet, F., Guschlbauer, W., and Fromageot, P. (1980) *Biochemistry* **19,** 4166–4172
64. Torres, A. M., Kini, R. M., Selvanayagam, N., and Kuchel, P. W. (2001) *Biochem. J.* **360,** 539–548
65. Teixeira-Clerc, F., Ménez, A., and Kessler, P. (2002) *J. Biol. Chem.* **277,** 25741–25747
66. Trémeau, O., Lemaire, C., Drevet, P., Pinkasfeld, S., Ducancel, F., Boulain, J. C., and Ménez, A. (1995) *J. Biol. Chem.* **270,** 9362–9369
67. Bourne, Y., Talley, T. T., Hansen, S. B., Taylor, P., and Marchot, P. (2005) *EMBO J.* **24,** 1512–1522
68. Antil, S., Servent, D., and Ménez, A. (1999) *J. Biol. Chem.* **274,** 34851–34858
69. Fruchart-Gaillard, C., Gilquin, B., Antil-Delbeke, S., Le Novère, N., Tamiya, T., Corringer, P. J., Changeux, J. P., Ménez, A., and Servent, D. (2002) *Proc. Natl. Acad. Sci. U.S.A.* **99,** 3216–3221
70. Dellisanti, C. D., Yao, Y., Stroud, J. C., Wang, Z. Z., and Chen, L. (2007) *Nat. Neurosci.* **10,** 953–962
71. Antil-Delbeke, S., Gaillard, C., Tamiya, T., Corringer, P. J., Changeux, J. P., Servent, D., and Ménez, A. (2000) *J. Biol. Chem.* **275,** 29594–29601
72. Osipov, A. V., Kasheverov, I. E., Makarova, Y. V., Starkov, V. G., Vorontsova, O. V., Ziganshin, R. Kh., Andreeva, T. V., Serebryakova, M. V., Benoit, A., Hogg, R. C., Bertrand, D., Tsetlin, V. I., and Utkin, Y. N. (2008) *J. Biol. Chem.* **283,** 14571–14580
73. Grant, G. A., Luetje, C. W., Summers, R., and Xu, X. L. (1998) *Biochemistry* **37,** 12166–12171
74. Servent, D., Mourier, G., Antil, S., and Ménez, A. (1998) *Toxicol. Lett.* **102–103,** 199–203
75. Nirthanan, S., Charpantier, E., Gopalakrishnakone, P., Gwee, M. C., Khoo, H. E., Cheah, L. S., Kini, R. M., and Bertrand, D. (2003) *Br. J. Pharmacol.* **139,** 832–844
76. Fiordalisi, J. J., al-Rabiee, R., Chiappinelli, V. A., and Grant, G. A. (1994) *Biochemistry* **33,** 3872–3877
77. Dewan, J. C., Grant, G. A., and Sacchettini, J. C. (1994) *Biochemistry* **33,** 13147–13154
78. Oswald, R. E., Sutcliffe, M. J., Bamberger, M., Loring, R. H., Braswell, E., and Dobson, C. M. (1991) *Biochemistry* **30,** 4901–4909
79. Grant, G. A., Al-Rabiee, R., Xu, X. L., and Zhang, Y. (1997) *Biochemistry* **36,** 3353–3358
80. Herz, J. M., Johnson, D. A., and Taylor, P. (1989) *J. Biol. Chem.* **264,** 12439–12448
81. Unwin, N. (1993) *J. Mol. Biol.* **229,** 1101–1124
82. Gille, C., and Frömmel, C. (2001) *Bioinformatics* **17,** 377–378
83. Gouet, P., Courcelle, E., Stuart, D. I., and Métoz, F. (1999) *Bioinformatics* **15,** 305–308

doi: 10.1111/j.1472-8206.2008.00631.x

ORIGINAL ARTICLE

An insight on the neuropharmacological activity of *Telescopium telescopium* – a mollusc from the Sunderban mangrove

S.K. Samanta[a], K.T. Manisenthil Kumar[a], Amrita Roy[a], S. Karmakar[a], Shawon Lahiri[b], G. Palit[b], J.R. Vedasiromoni[c], T. Sen[a]*

[a]*Division of Pharmacology, Department of Pharmaceutical Technology, Jadavpur University, Kolkata 700032, India*
[b]*Central Drug Research Laboratory, Chatter Manzil, Lucknow 226001, India*
[c]*Drug Development Division, Indian Institute of Chemical Biology, 4, Raja S.C. Mullick Road, Kolkata 700032, India*

Keywords
catecholamines,
CNS depressant,
mollusc,
Telescopium telescopium

Received 14 September 2007;
revised 4 February 2008;
accepted 7 July 2008

*Correspondence and reprints:
tssen@hotmail.com
Dedication: This paper is dedicated to the loving memory of our mentor, Prof. A.K. Nag Chaudhuri.

ABSTRACT

The present study was carried out to evaluate the biological properties of the tissue extract of a marine snail *Telescopium telescopium*, collected from the coastal regions of West Bengal India. On extensive pharmacological screening, it was found that the biological extract of *T. telescopium* (TTE) produced significant central nervous system (CNS)-depressant activity as observed from the reduced spontaneous motility, potentiation of pentobarbitone induced sleeping time, hypothermia and respiratory depression with transient apnoea. The extract significantly decreased both residual curiosity and also muscle coordination. The fraction, obtained following saturation with 60–80% ammonium sulphate (80S), was also found to demonstrate predominant CNS-depressant activity. It was observed that both TTE and the 80S fraction significantly altered the brain noradrenaline and homovanillic acid levels without affecting the brain gamma amino butyric acid (GABA) concentration. Based on the present observations, it can be suggested that the CNS-depressant effects produced by TTE and 80S could be attributable to modified catecholamine metabolism in the brain.

INTRODUCTION

The coastline of peninsular India is bestowed with highly productive estuarine areas. The Sundarbans, a deltaic region of West Bengal, India, is the world's largest mangrove ecosystem, having a rich floral and faunal diversity. The mollusc, *Telescopium telescopium*, is one of the most dominant molluscan species found in the Sundarban mangrove and it is found to reside mainly in the estuarine environment. *Telescopium* has the ability to survive in the typical mangrove environment, thereby making them an attractive subject for scientific studies.

The molluscan species are known to produce potent bioactive molecules and according to available reports, some of these substances have been found to be useful in both defence and predation. The bioactive components identified so far in the molluscs indicate the presence of neurotoxin, haemolysin, cardiotoxin and different biogenic amines [1,2]. It has also been observed that the biological effects associated with molluscan tissue extracts are either dependent on any one of these active components or on the cumulative effect of these substances.

On survey of the literature, it was observed that the extracts from the spermathecal gland of *Telescopium telescopium* produced potent antimicrobial [3] and immunocontraceptive properties [4]. Moreover, two endo-(1 linked to 3)-beta-D-glucanases have also been isolated from this mollusc [5]. Moreover, a number of reports are available indicating the presence of various neuroactive components in different molluscan species [6]. However, on detailed survey of the literature, no

reports were available regarding its activity on the central nervous system (CNS). In this study, an attempt has been made to evaluate the neuropharmacological profile of *T. telescopium* tissue extract (TTE) and of its fraction(s).

MATERIALS AND METHODS

Collection and identification

Live molluscan species *T. telescopium* were collected from the creeks of the river Matla in Jharkhali, Sundarban, West Bengal, India. The molluscan specimens were identified by Zoological Survey of India, New Alipore, Kolkata, India.

Preparation of extract

On removal of the outer shell, the soft tissue portion was homogenized with three volumes of 20 mM phosphate buffer (pH 7.2) for 5 min, sonicated for 2 min and then centrifuged at 14 000 ***g*** (Biofuge Stratos, Hanau, Germany) at 4 °C. The pooled extract was subsequently defatted with dichloromethane (DCM) and concentrated under reduced pressure. The concentrated fraction was further subjected to successive precipitation with 30, 60 and 80% saturations of ammonium sulphate and then the salts were removed by dialysis. The DCM cut extract (TTE) and the precipitates thus obtained with 30 (30S), 60 (60S) and 80% (80S) were subsequently freeze dried and stored at −20 °C.

Protein estimation

Protein concentration was estimated following the method described by Bradford [7] using standard Bradford Kit (Genei, Bangalore, India) and all concentrations of extract (unless otherwise specified) were expressed in terms of protein equivalent.

Animals used

The pharmacological experiments were conducted using adult Swiss albino mice (18–22 gm) and rats of Charles Foster strain (120–180 gm). The animals were housed in standard plastic cages and maintained on 12 h dark–light cycle under regulated temperature (22 ± 2 °C). Animals were used after an acclimatization period of at least 10 days in the laboratory environment and were maintained on ad libitum food and water. Control vehicle or test materials were administered intraperitoneally unless otherwise specified. All experimental protocols were carried out according to the guidelines of the Institutional Ethical Committee (constituted under Committee for the Purpose of Control and Supervision of Experiments on Animals, India).

Acute toxicity study

Acute toxicity studies were carried out in male mice (n = 20). The extract (TTE) and 80S were administered (i.p.), in a dose range of 0.1–1.6 g/kg. The animals were observed for signs and symptoms of toxicity and number of mortality was recorded during a period of 24 h. The LD_{50} was determined according to the method of Litchfield and Wilcoxon [8]. The animals were also observed for any changes in the general behaviour pattern following the administration of TTE [9].

Spontaneous motility

Groups of mice (n = 10) were treated (i.p.) with either the test samples (TTE, 100 and 200 mg/kg; 80S, 50 mg/kg) or normal saline (0.1 mL/10 g). After 30 min of treatment, the activity was measured in a photoactometer (Techno, Lucknow, India) for 6 min and the procedure was repeated at 30-min intervals up to a period of 3 h [10].

Pentobarbitone-induced sleeping time

Groups (10 in each) of mice were treated with pentobarbitone sodium (Sigma, St Louis, MO, USA) (40 mg/kg, i.p.), 30 min after intraperitoneal administration of TTE (100 and 200 mg/kg), 30S (100 mg/kg), 60S (100 mg/kg), 80S (50 mg/kg), control vehicle (normal saline) or chlorpromazine (Sigma) (4 mg/kg, i.p.). The time interval between the loss and regaining of righting reflex was measured as sleeping time [11].

Anticonvulsant activity

Pentylenetetrazole (PTZ) (HiMedia, Mumbai, India) (80 mg/kg, i.p.) was injected into groups of mice (10 in each), 30 min after administration of TTE (100 and 200 mg/kg), 80S (50 mg/kg) or the control vehicle. The animals were then carefully observed for the signs and symptoms of convulsion [12]. Diazepam (East India Pharmaceutical Works Ltd, Kolkata, India) (10 mg/kg, i.p.) was used as the standard drug.

Body temperature

Rectal temperature was recorded at pre-determined time intervals (up to 5 h) in groups of male mice (n = 10), before and after the administration of TTE (100 and 200 mg/kg, i.p.), 80S (50 mg/kg, i.p.) or normal saline [13,14].

Rat respiration

The effect of TTE and 80S on abdominal respiration was evaluated in male anaesthetized rats. TTE (100 and 200 mg/kg) and 80S (50 mg/kg) were administered through the jugular vein [15]. Thereafter, one end of a thread was tied to the skin at the lower end of the sternum and the other end was carefully tied to a frontal writing lever. The abdominal respiration was then recorded.

Studies on exploratory behaviour

Head-dip test

Telescopium telescopium tissue extract (100 and 200 mg/kg), 80S (50 mg/kg), normal saline (0.1 mL/kg) or diazepam (10 mg/kg) were administered (i.p.) to groups (n = 10) of pre-screened mice. The animals were then placed singly on a wooden board (with 16 evenly spaced holes) and the number of times, the animals dipped their head inside the hole, during a period of 3 min was recorded [16].

Y-maze test

Previously screened rats were divided into groups (n = 10) and were treated with TTE (100 and 200 mg/kg), 80S (50 mg/kg) or the control vehicle. After 30 min, the rats were individually placed for 5 min in the centre of a symmetrical Y-shaped runway (13 × 38 × 33 cm) and the number of times, each rat (with all four feet) entered the arms of the Y-maze were recorded [17].

Evasion test

Groups of mice (n = 10) were kept in a rectangular box, having an inclined plane by which the mice could escape from the box. Those mice, which escaped within 5 min, were selected for further testing. Following administration of control vehicle or test materials (TTE, 100 and 200 mg/kg; 80S, 50 mg/kg), the animals were again placed in the box and thereafter, the numbers of mice remaining in the box, at the end of 5 min were recorded [18].

Studies on muscle relaxant activity

Rotarod test

The pre-screened mice (n = 10) were administered (i.p.) with normal saline (0.1 mL/10 g), test material (TTE, 100 and 200 mg/kg; 80S, 50 mg/kg) or diazepam (10 mg/kg). The animals were then placed (one at a time) on a horizontal rod (30 mm diameter, rotating at 5 rpm) and were observed for 3 min. The numbers of animals remaining on the rod were recorded and the procedure was repeated at intervals of 30 min up to a period of 2.5 h [19,20].

Chimney test

In a Pyrex glass tube (30 cm long and 2.8 cm diameter) marked at a point 20 cm from its base, a mouse was introduced at the end nearest to the mark. When the mouse reached the bottom, the tube was reoriented vertically, so that the mouse tried to climb backwards immediately. The animals, which reached the mark within 30 s, were selected for further testing. Thirty minutes after administration (i.p.) of either the test material (TTE, 100 and 200 mg/kg; 80S, 50 mg/kg), diazepam (10 mg/kg) or normal saline (0.1 mL/kg), the animals were placed individually in the glass tubes and were then observed for their ability to climb backwards during a time period of 30 s [21].

Traction test

Pre-screened albino mice (n = 10) were treated with the control vehicle, test material (TTE, 100 and 200 mg/kg; 80S, 50 mg/kg) or diazepam (10 mg/kg). Each animal was suspended through its forepaws on a metallic wire (0.2 cm diameter) stretched horizontally at a height of 25 cm. The number of animals that failed to grasp the wire (ataxia) with their hind paw within 10 s was recorded [22].

Estimation of GABA content of brain in mice

The effect of TTE (100 and 200 mg/kg, i.p.), 80S (50 mg/kg, i.p.) and the standard drug (diazepam, 10 mg/kg, i.p.) on the brain GABA (whole brain) content was evaluated following the method of Lowe et al. [23]. The brain tissue homogenate (1 mL) was treated with 0.14 M ninhydrin solutions (0.5 M carbonate–bicarbonate buffer, pH 9.95). The reaction mixture was then kept in a water bath (60 °C) for 30 min, cooled and treated with 5.0 mL of copper tartarate reagent. After 10 min, the fluorescence (377/451 nm) was measured in a spectrofluorimeter (Shimadzu Rf-5000; Shimadzu Corporation, Kyoto, Japan).

Effect on monoamine neurotransmitter

Biogenic amines in the different regions of the brain were estimated by high performance liquid chromatography-electrochemical detector (HPLC-EC) according to the modified method of Kim et al. [24]. The animals were pretreated with either TTE (100 mg/kg) or 80S (50 mg/kg). The animals were killed by decapitation and their brains were rapidly removed and placed on chilled containers. The striatum, hypothalamus, hippocampus and cerebellum were dissected out as described by Glowinski and Iversen [25]. The brain tissue samples

were then homogenized in 0.17 M perchloric acid (with dihydroxybenzylamine (DHBA) as internal standard in the range of 25 ng/mL) by Polytron homogenizer (Polytron, Littau-Lucerne, Switzerland). Homogenates were then centrifuged at 33 000 ***g*** (Biofuge Stratos, Hanau, Germany) at 4 °C. Thereafter, 20 μL of supernatant was injected via HPLC pump (Model 1525, Binary Gradient Pump; Waters, Milford, MA, USA) into a column (Spherisorb RP C18; Waters Corporation, Milford, MA, USA) (5 μm particle size, 4.6 mm i.d × 250 mm at 30 °C) connected to an Electrochemical detector (Model 2465; Waters) at a potential of +0.8 V with glassy carbon working electrode vs. Ag/AgCl reference electrode. Mobile phase consists of 32 mM citric acid, 12.5 mM disodium hydrogen orthophosphate, 1.4 mM sodium octyl sulphonate, 0.05 mM ethylenediamine tetra acetic acid (EDTA) and 16% (v/v) methanol (pH 4.2) at a flow rate of 1.2 mL/min. Amount of neurotransmitters were calculated from the standard curve prepared with DA-DHBA, 5HT-DHBA, DOPAC-DHBA, HVA-DHBA and 5HIAA-DHBA (Sigma).

Polyacrylamide gel electrophoresis (SDS–PAGE)

Sodium dodecyl sulphate–polyacrylamide gel electrophoresis (SDS–PAGE) was carried out according to the method of Lammeli [26]. TTE and the various ammonium sulphate precipitated fractions were loaded (15 μg of protein in each lane) in a 10% polyacrylamide gel (Sigma) containing 0.1% SDS and electrophoresis was performed in a Minigel electrophoresis system (Amersham Biosciences, Piscataway, NJ, USA). The broad range molecular weight standards (205–6.5 kDa; Genei) were run concurrently with the various samples.

Statistical analysis

Results were expressed as mean ± SE statistical analyses were performed with one way analysis of variance (ANOVA) followed by Student's *t*-test and $P < 0.05$ was considered to be statistically significant.

RESULTS

Acute toxicity

The LD_{50} of TTE (extract) and 80S (ammonium sulphate precipitated fraction) was found to be 800 and 1200 mg/kg (i.p. 24 h), respectively. It was also observed that administration of the test substances (TTE and 80S, i.p.) altered some behavioural responses in mice. The animals became quiet, aggregated at corner of the cages and also displayed reduced locomotor activity.

Spontaneous motility

In this experimental model, pretreatment with either TTE or 80S produced significant reduction of spontaneous motility. Moreover, the animals treated with the test samples showed such reduced motility during the entire duration (120 min) of the study (*Figure 1*).

Pentobarbitone-induced sleeping time

Prior administration of TTE (100 and 200 mg/kg, i.p.) significantly potentiated pentobarbitone-induced sleeping time in a dose-dependent manner. Among the ammonium sulphate precipitated fractions, the 80S fraction produced significant potentiation of pentobarbitone-induced sleeping time (*Figure 2*).

Anticonvulsant activity

Pretreatment with either TTE or 80S could not protect the experimental animals against PTZ-induced convulsion and mortality. However, both TTE and 80S significantly delayed the onset of tremor and convulsion. Diazepam pretreatment delayed the onset of tremor and convulsion; moreover, no mortality was recorded (*Table I*).

Body temperature

Administration of the TTE and 80S produced significant lowering of normal body temperature, in a dose-dependent manner. Maximum reduction in body temperature

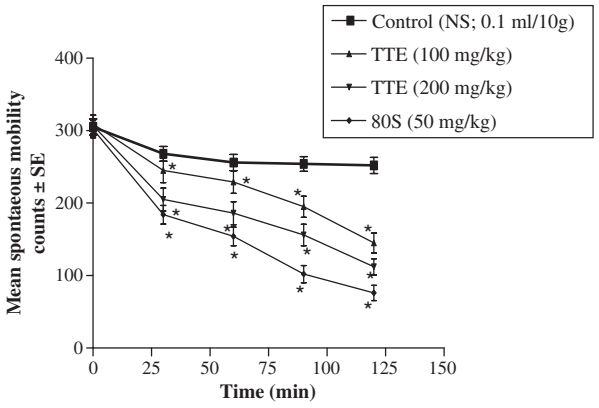

Figure 1 Effect of the *Telescopium telescopium* tissue extract (TTE) and 80% ammonium sulphate saturated precipitate (80S) on spontaneous motility in mice. TTE (100 and 200 mg/kg), 80S (50 mg/kg) or control vehicle (normal saline; 0.1 mL/10 g) were administered intraperitoneally. The spontaneous motility was measured after 30 min following the administration of the test substances. Values are expressed as mean ± SE ($n = 10$). *P* vs. control, by *t*-test, *<0.005.

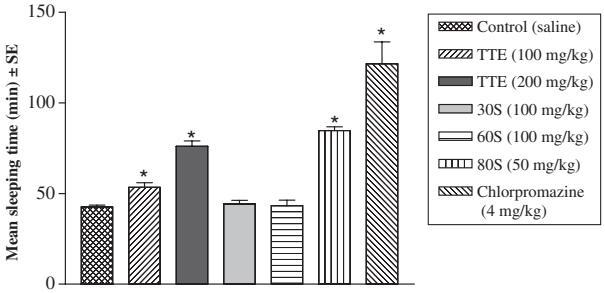

Figure 2 Effect of TTE (100 and 200 mg/kg) and the ammonium sulphate saturated precipitate (30S, 100 mg/kg; 60S, 100 mg/kg; 80S, 50 mg/kg), control vehicle (normal saline) and chlorpromazine (4 mg/kg) on Pentobarbitone sodium-induced sleeping time. The test substances were administered (i.p.), 30 min before the administration of pentobarbitone sodium. Values are expressed as mean ± SE (n = 10). P vs. control, by t-test, *<0.005.

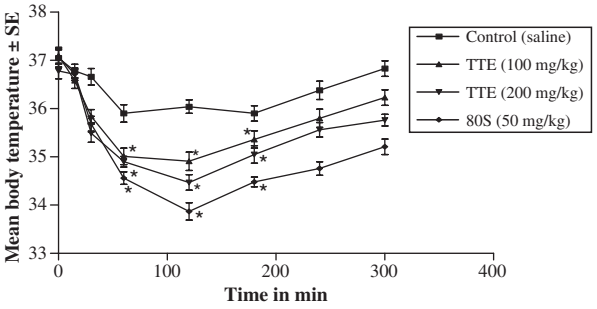

Figure 3 Effect of TTE and 80S on normal body temperature. After intraperitoneal administration of TTE (100 and 200 mg/kg), 80S (50 mg/kg) or of normal saline as control vehicle, body temperature was recorded at pre-determined intervals up to a period of 5 h. Values are expressed as mean ± SE (n = 10). P vs. control, by t-test, *<0.005.

was recorded after a period of 120 min and the normal body temperature was found to be restored after a period of about 4 h. (*Figure 3*).

Rat respiration

Intravenous administration of TTE (100 and 200 mg/kg) and 80S (50 mg/kg) produced respiratory depression in anaesthetized rats (*Figure 4*).

Exploratory behaviour patterns

Head-dip test

Pretreatment with different doses of TTE (100 mg/kg, 42%; 200 mg/kg, 65%), 80S (50 mg/kg, 78%) or diazepam (10 mg/kg, 80%) produced significant reduction in head-dip responses when compared with the control group of animals (*Figure 5*).

Y-maze test

Significant (dose-dependent) decrease in exploratory behaviour pattern was observed in the different groups of animals treated with TTE (100 mg/kg, 30%; 200 mg/kg, 39%), 80S (55%) or diazepam (10 mg/kg, 70%) used as the standard drug (*Figure 5*).

Evasion test

Telescopium telescopium tissue extract (100 mg/kg, 60%; 200 mg/kg, 70%), 80S (50 mg/kg, 90%) and diazepam (10 mg/kg, 100%) caused significant inhibition of residual curiosity in mice as observed in the evasion test (*Figure 5*).

Muscle relaxant activity

Results of rotarod, chimney test and traction test revealed significant loss in skeletal muscle co-ordination, following administration of TTE and 80S (*Figure 6*). The inhibitory activity of 80S fraction and diazepam (Diazepam; 10 mg/kg) were found to be considerably higher (compared with TTE) in the various experimental models studied.

Table I Effect of TTE, ammonium sulphate saturated precipitate (80S) and normal saline (control vehicle) on PTZ (80 mg/kg, i.p.) induced convulsion in mice.

Groups	Onset of tremor (min)	Onset of convulsion (min)	Average no. of seizure episodes	% Mortality
Control	4.2 ± 0.32	6.2 ± 0.46	5.3 ± 0.42	80
TTE (100 mg/kg)	5.4 ± 0.31*	8.0 ± 0.54*	4.4 ± 0.63	80
TTE (200 mg/kg)	8.1 ± 0.24*	10.4 ± 0.73*	4.0 ± 0.51	80
80S (50 mg/kg)	11.3 ± 0.34*	12.4 ± 0.85*	4.1 ± 0.67	70
Diazepam (10 mg/kg)	16.2 ± 0.34*	–	–	Nil

TTE, *Telescopium telescopium* tissue extract; PTZ, pentylenetetrazole.

Values are expressed as mean ± SE (n = 10). P vs. control, by t-test, *<0.05 (first appearance of pilo-erection was considered as the onset of tremor response).

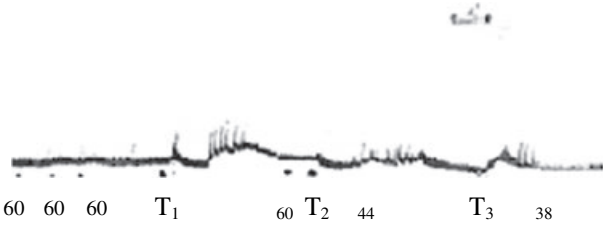

Figure 4 Effect of TTE and 80S on rat respiration. TTE (T_1, 100 mg/kg; T_2, 200 mg/kg) and 80S (T_3, 50 mg/kg) were administered to anaesthetized rats through the jugular vein, and the abdominal respiration was recorded.

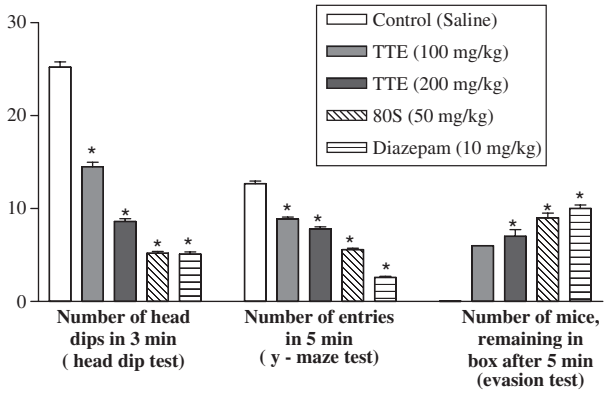

Figure 5 Effect of TTE and 80S on exploratory behaviour pattern using Head-dip, Y-maze and Evasion test models. TTE (100 and 200 mg/kg), 80S (50 mg/kg), control vehicle (normal saline) or Diazepam (10 mg/kg) were administered (i.p.), 30 min prior to the commencement of the experiments. Values are expressed as mean ± SE (n = 10). P vs. control, by t-test, *<0.005.

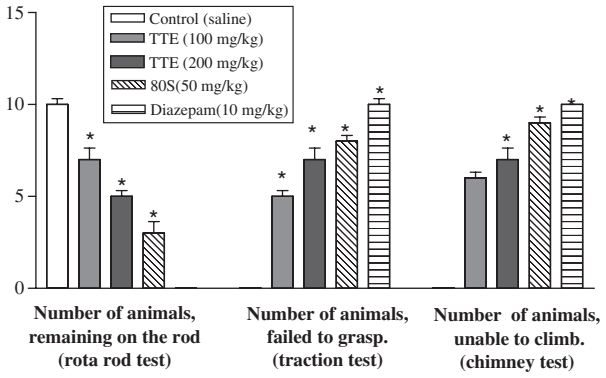

Figure 6 Effect of TTE, 80S and diazepam on motor coordination (using Rotarod, Traction and Chimney models). The test substances (TTE, 100 and 200 mg/kg; 80S, 50 mg/kg and Diazepam, 10 mg/kg) and the control vehicle were administered 30 min prior to the commencement of the experiments. Values are expressed as mean ± SE (n = 10). P vs. control, by t-test, *<0.005.

Table II Effect of TTE, ammonium sulphate saturated precipitate (80S) and normal saline (control vehicle) on brain catecholamines.

		Control	TTE (100 mg/kg)	TTE (200 mg/kg)	80S (50 mg/kg)
NA	CC	707 ± 44	529 ± 39*	476 ± 36*	354 ± 27*
	HPC	486 ± 38	379 ± 32	343 ± 34*	326 ± 33*
	HP	2098 ± 218	1894 ± 163	1695 ± 146*	1436 ± 125*
	ST	488 ± 61	362 ± 43	327 ± 41	285 ± 32
DOPAC	CC	226 ± 18	212 ± 24	202 ± 26	234 ± 24
	HPC	–	–	–	–
	HP	–	–	–	–
	ST	452 ± 54	475 ± 64	426 ± 58	448 ± 49
5HIAA	CC	867 ± 36	845 ± 41	823 ± 45	832 ± 42
	HPC	946 ± 112	895 ± 116	999 ± 119	954 ± 114
	HP	1326 ± 123	1233 ± 135	1239 ± 146	13351 ± 127
	ST	1368 ± 86	1246 ± 96	1286 ± 114	1314 ± 129
DA	CC	954 ± 76	965 ± 69	947 ± 82	1011 ± 114
	HPC	–	–	–	–
	HP	221 ± 11	257 ± 34	217 ± 28	247 ± 29
	ST	1949 ± 124	1882 ± 118	2066 ± 221	2132 ± 234
HVA	CC	31 ± 6	83 ± 13*	126 ± 23*	237 ± 19*
	HPC	–	–	–	–
	HP	–	–	–	–
	ST	172 ± 14	286 ± 19*	298 ± 21*	387 ± 23*
5HT	CC	495 ± 32	408 ± 26	386 ± 46	398 ± 33
	HPC	404 ± 29	383 ± 26	401 ± 34	384 ± 30
	HP	542 ± 36	567 ± 42	510 ± 39	533 ± 34
	ST	513 ± 62	506 ± 46	499 ± 39	536 ± 35

TTE, *Telescopium telescopium* tissue extract; NA, noradrenaline; DOPAC, 3,4-dihydroxyphenylacetic acid; HIAA, hydroxy indole acetic acid; DA, dopamine; HT, hydroxytryptamine; CC, cortex; HPC, hippocampus; HP, hypothalamus; ST, striatum.

P vs. control, by t-test, *<0.005.

Values are expressed as mean ± SE (n = 6) (concentrations of the biogenic amines are expressed as ng/gm of brain tissue).

Effect on GABA content

Telescopium telescopium tissue extract as well as the 80S fraction did not produce any significant change in the brain GABA content. However, the standard drug diazepam was found to increase the brain GABA content significantly when compared with the control group of animals.

Effect on brain biogenic amines

In this study, both TTE (100 and 200 mg/kg, i.p.) and 80S (50 mg/kg, i.p.) produced significant reduction of noradrenaline (NA) content in different regions (cortex, hippocampus and hypothalamus) of the brain, along with elevation of homovanillic acid (HVA) in the cortex and striatum. However, no significant changes in the levels of 5-hydroxytryptamine (HT), dihydroxyphenyl-

alaine (DOPA) and hydroxy indole acetic acid (HIIA) were observed following administration of TTE and 80S (*Table II*).

Polyacrylamide gel electrophoresis (SDS–PAGE)

The band pattern of SDS–PAGE indicated that ammonium sulphate precipitation produced distinct changes in the protein profile of the different fractions (*Figure 7*). The number of protein bands in the 80S fraction was considerably decreased and some prominent bands were observed at 104, 66 and 52 kD regions.

DISCUSSION

Our study was aimed towards the evaluation of neuropharmacological activity of *T. telescopium*. The initial findings with the *Telescopium* extract indicated definite alterations of general behaviour with reduced locomotor activity. As evident from the results, both TTE and the 80S fraction produced significant reduction of spontaneous motility, in a manner similar to that of the CNS-depressants (barbiturates and benzodiazepines), which are also known to produce identical effects in rodents [27]. Significant potentiation of pentobarbitone-induced sleeping time was also observed following pretreatment with either TTE or 80S.

It is well established that prolongation of barbital hypnosis is caused by sedative and/or hypnotic property [28], attributed to either inhibition of pentobarbitone metabolism [29] or to some central mechanisms involved in the regulation of sleep [30]. According to some reports, there may be some correlation between reduction in spontaneous motility and sedative activity [31], generally attributed to a reduced CNS excitability [32]. In this study, both TTE and the fraction 80S lowered spontaneous motility, increased (dose-dependently) pentobarbitone-induced sleeping time, reduced normal body temperature and also produced respiratory depression (with transient apnoea), similar to that of the benzodiazepines, which are also known to produce similar pharmacological effects [15,27,33]. Moreover, intraperitoneal administration of TTE and 80S significantly delayed the onset of tremor and convulsion induced by PTZ, even though no reduction in mortality could be observed with the test substances. These findings indicate the probable CNS depressant activity of the *Telescopium* products TTE and 80S.

Furthermore, pretreatment with both TTE and 80S, produced significant decrease in exploratory behaviour pattern (evident from head-dip and Y-maze test models). According to the published literature, such alteration of exploratory behaviour can be attributed to the sedative activity [34]. It was also observed that both TTE and the fraction (80S) produced significant inhibition of residual curiosity and these findings are in conformity with various other CNS-depressant drugs [16,35].

In another study, both the test substances (TTE and 80S) produced significant motor in coordination (in the rotarod, chimney and traction test models), and our

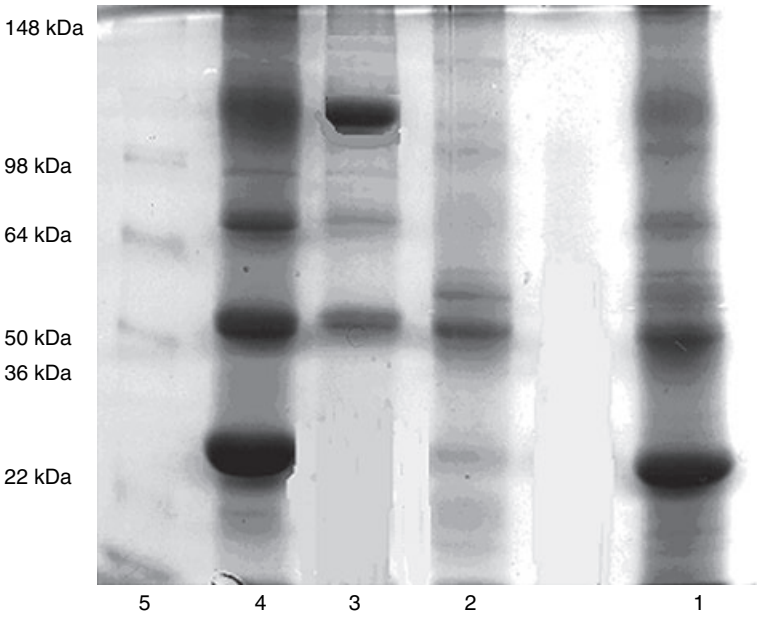

Figure 7 Polyacrylamide gel electrophoresis (with SDS; 0.1%) of TTE and different ammonium sulphate saturated precipitate fractions (30S, 60S and 80S). The separations were carried out with 10% polyacrylamide gel, and the bands were visualized after staining with Coomassie blue. Lanes: (1) TTE; (2) 60S; (3) 80S; (4) 30S; (5) standard molecular weight marker.

observations with the test samples were found to be similar to the standard drug diazepam [13,16], which is also known to produce generalized muscle relaxation [36].

The CNS-depressant effects of barbiturates and benzodiazepines have been reported to be mediated through $GABA_A$ receptors [37]. Moreover, many researchers have correlated CNS depressant activity with elevation of brain GABA levels [38]. However, in our studies neither TTE nor 80S produced any significant alteration of brain GABA levels.

In this context, it may be mentioned that besides GABA, catecholamines have also been found to promote wakefulness by inhibiting the sleep-active neurons [39]. According to the published reports, substances causing catecholamine deficiency are known to influence sleep. Amongst the different catecholamines, depletion of NA (reserpine, alpha methyl-P-tyrosine, 6-hydroxydopamine), often leads to depression [40,41] and has also been observed that mice with NA deficiency tend to fall asleep faster and are also difficult to awake, indicating the stimulating effect of NA on wakefulness [42]. NA is known to be a predominant target for different antidepressant drugs (with varying specificity towards the adrenergic system), which are known to influence the level of NA, thereby improving adrenergic signalling during depression [43]. Therefore, further studies were carried out to evaluate the role of TTE and 80S on catecholamine concentration in the different regions of the brain. From this study, it was evident that both TTE and 80S significantly diminished the concentration of NA in the cortex, hippocampus, hypothalamus and striatum, whereas the concentration of HVA was found to be increased in the cortex and striatum. However, the levels of dopamine and 5HT, in the different regions of the brain, remained unaltered. Hence, from the present findings, it is evident that intraperitoneal administration of the molluscan product(s), produced significant alteration of catecholamine metabolism, resembling certain CNS-depressant compounds [44,45] and centrally acting muscle relaxants.

From SDS–PAGE analysis of the test substances, it was observed that ammonium sulphate precipitation (80S fraction) caused a marked change in the protein band pattern as compared with the crude extract (TTE). Moreover, on the basis of the experimental findings, it may also be noted that the CNS-depressant activity of 80S fraction was found to be more pronounced in comparison with the crude sample (TTE). Thus, from the results of the current investigation, it was evident that both TTE and the fraction possess definite CNS-depressant activity. Further studies are presently being carried out to purify and characterize the bioactive peptide(s) present in the 80S fraction.

ACKNOWLEDGEMENT

This investigation was partly supported by a research grant from CSIR, New Delhi, India.

REFERENCES

1 Jha R.K., Zi-rong X. Biomedical compounds from marine organisms. Mar. Drugs (2004) **2** 123–146.
2 Ireland C., Copp B., Foster M., McDonald L., Radisky D., Swersey J. Marine Biology, Plenum Press, New York, USA, 1993.
3 Pakrashi A., Roy P., Datta U. Antimicrobial effect of protein(s) isolated from a marine mollusc *Telescopium telescopium*. Ind. J. Physiol. Pharmacol. (2000) **45** 249–252.
4 Pakrashi A., Datta U., Choudhury A. A search for immunocontraceptive agent from marine sources-role of antispermatheca globulin of *Telescopium telescopium* on fertility regulation in male rat. Ind. J. Exp. Biol. (1992) **30** 1066–1074.
5 Cutler R.L., Yellowlees D. Purification and characterisation of two endo-(1linked to 3)- beta-D-glucanases from *Telescopium telescopium*. Carbohydr. Res. (1979) **75** 221–229.
6 Myers P.A., Cruz L.Z., Rivier J.E., Olivera B.M. Conous peptides as chemical probes for receptors and ion channels. Chem. Rev. (1993) **93** 1923–1936.
7 Bradford M.M. A rapid and sensitive method for the quantitation of microgram quantities of protein utilizing the principle of protein dye- binding. Anal. Biochem. (1976) **72** 248–254.
8 Litchfield J.T., Wilcoxon F. A simplified method of evaluating dose effects experiments. J. Pharmacol. Expt. Ther. (1949) **96** 99–113.
9 Irwin S. Drug screening and evaluation procedure. Science (1962) **136** 123–132.
10 Irwin S. Comprehensive observational assessment: a systematic quantitative procedure for assessing the behavioural and physiologic state of the mouse. Psychopharmacolgia (1968) **13** 222–257.
11 Dandiya P.C., Collumbine H. Studies on Acorus calamus (III); some pharmacological action of the volatile oil. J. Pharmacol. Expt. Ther. (1959) **125** 353–359.
12 Soaje – Echague E., Lim R.K. Anticonvulsant activity of some carbonylureas. J. Pharmacol. Expt. Ther. (1962) **138** 224–228.
13 Pal S., Sen T., Nagchaudhuri A.K. Neuropsychopharmacological profile of methanolic fraction of *Bryophyllum pinnatum* leaf extract. J. Pharm. Pharmacol. (1999) **51** 313–318.
14 Bianchi C., Franceschini J. Experimental observation on Haffner's method for testing analgesic drugs. Br. J. Pharmacol. (1954) **9** 280–282.
15 Gaddum J.H. A method of recording the respiration. J. Physiol. (1941) **99** 257–264.

16 Dorr M., Steinberg H., Tomkiewics M., Joycee D., Persolt R.D., Summerfield A. Persistence of dose-related behaviour in mice. Nature (1971) **231** 121–123.
17 Rushton R., Steinberg H., Tinson C. Modification of the effect of an amphetamine barbiturate mixture by the past experience of rate (Y-shaped runway). Nature (1961) **192** 533–535.
18 Turner R.A. Screening methods in pharmacology, Academic Press, New York, USA & London, UK, 1965.
19 Dunham N.W., Miya T.S. A note on a simple apparatus for detecting neurological deficit in rats and mice. J. Am. Pharm. Assoc. Sci. (1957) **46** 208–209.
20 Vishwakarma S.L., Pal S.C., Kasture V.S. Anxiolytic and antiemetic activity of Zingiber officinale. Phytother. Res. (2002) **16** 621–626.
21 Boisser J.R., Dermont C., Robins R., Pagny J. Tentative de pharmacologie previsionelle dans de domain de neuroleptiquee: action sedative centralle et adrenolytique de la N (dimethoxy-3-4 phenethyl) N/ (chloro-2 phenyl) piperazine. J. Arch. Int. Pharmacodyn. (1961) **133** 29–32.
22 Rudzik A.D., Hester J.B., Tang A.H., Stray R.N., Friss W. The Benzodiazepines, Randall Raven Press, New York, USA, 1973.
23 Lowe I.P., Robins E., Eyerman G.S. The fluorometric measurement of glutamic decarboxylase and its distribution in brain. J. Neurochem. (1958) **3** 8–18.
24 Kim C., Speisky M.B., Kharoouba S.N. Rapid and sensitive method for measuring norepinephrine, dopamine, 5-Hydroxytryptamine and their major metabolites in rat brain by high performance liquid chromatography. J. Chromatogr. (1987) **69** 331–338.
25 Glowinski J., Iverson L.L. Regional studies of catecholamines in rat brain. I. The disposition of [3H] nor epinephrine, [3H] DA and [3H] dopa in various regions of brain. J. Neurochem. (1966) **13** 655–669.
26 Laemmli U.K. Cleavage of structural proteins during the assembly of the head of bacteriophage T4. Nature (1970) **227** 680–685.
27 Beninger R.J. The role of dopamine in locomotion activity and learning. Brain. Res. Rev. (1983) **287** 173–180.
28 Fujimori H., Cobb D.P. Central nervous system depressant activity of MA 1337: 3-(3,4,-m-chlorophenyl-l-piperazyl propyl)-2, 4, (1H, 3H) quinazolinedone hydrocholoride. J. Pharmacol. Exp. Ther. (1965) **148** 151–157.
29 Kaul P.N., Kulkarni S.K. New drug metabolism inhibitors of marine origin. J. Pharm. Sci. (1978) **67** 1293–1296.
30 N'Gouemo P., Nguemby-Bina C., Baldy-Moulinier M. Some neuropharmacological effects of an ethanol extract of Maprounea africina in rodents. J. Ethnopharmacol. (1994) **43** 161–166.
31 Ozturk Y., Aydini S., Beis R., Baser K.H.C., Berberoglu H. Effect of Hypericum perforatum L. and Hypericum calximu L. extract on central nervous system in mice. Phytomedicine (1996) **3** 139–146.
32 Masur J., Martz R.M., Carlini E.A. Effects of acute and chronic administration of Cannabis sativa and (-) 9-trans-tetra-hydrocannabinol on behaviour of rats in open field arena. Psychopharmacologia (1971) **19** 388–397.
33 Tang A.H., Code R.A., Himes C.S. Antagonism of hypothermia produced by benzodiazepine related compounds by U-78875 in mice. Eur. J. Pharmacol. (1993) **236** 1–5.
34 File S.E., Pello S. The effects of triazolobenzodiazepines in two animal tests of anxiety in the holeboard. Br. J. Pharmacol. (1985) **86** 729–735.
35 Dutta A.S., Nag Chaudhuri A.K. Neuropharmacological studies on the venom of Vipera russelli. Ind. J. Exp. Biol. (1991) **29** 937–942.
36 Range H.P., Dale M.M., Ritter J.M. A text book of pharmacology, Churchill Livingstone, Edinburgh, UK, 1996.
37 Whiting P.J. The $GABA_A$ receptor gene family: new opportunities for drug development. Curr. Opin. Drug. Discov. Devel. (2003) **6** 648–657.
38 Ali M., Jha S.K., Kaur S., Mallick B.N. Role of GABA-A receptor in the preoptic area in the regulation of sleep- wakefulness and rapid eye movement sleep. Neurosci. Res. (1999) **33** 245–250.
39 Osaka T., Matsumara B. Noradrenaline inhibits preoptic sleep-active neurons through alpha-2-receptors in the rat. Neurosci. Res. (1995) **21** 323–330.
40 Crossland J. Lewis's pharmacology, Churchill Livingstone, Edinburgh, 1980.
41 Peng W.H., Wu C.R., Chen C.S., Chen C.F., Leu Z.C., Hsieh M.T. Anxiolytic effect of berberine on exploratory activity of the mouse in two experimental anxiety models: interaction with drug acting at 5-HT receptors. Life Sci. (2004) **75** 2451–2462.
42 Hensley M.S., Palmiter K.D. Altered sleep latency and arousal regulation in mice lacking norepinephrine. Pharmacol. Biochem. Behav. (2004) **78** 765–773.
43 Cryan J.F., Dalvi A., Jin S.H. et al. Use of Dopamine-β-hydroxylase- deficient mice to determine the role of norepinephrine in the mechanism of action of antidepressant drugs. J. Pharmacol. Exp. Ther. (2001) **298** 651–657.
44 Gavend M.M., Serre F., Gavend M.R., Ragoucy C., Caron P. Effect of acute administration of cyclazocine on the metabolism of biogenic amines in different regions of rat brain. Psychopharmacology (1981) **75** 79–83.
45 Commissiong J.W., Karoum F., Reiffenstein R.J., Neff N.H. Cyclobenzaprine: a possible mechanism of action for its muscle relaxant effect. Can. J. Physiol. Pharmacol. (1981) **59** 37–44.

Journal of Ethnopharmacology 120 (2008) 7–12

Contents lists available at ScienceDirect

Journal of Ethnopharmacology

journal homepage: www.elsevier.com/locate/jethpharm

Anti-inflammatory activity of *Acanthus ilicifolius*

K.T. Mani Senthil Kumar[a], Bapi Gorain[a], Dilip K. Roy[a], Zothanpuia[a], Samir K. Samanta[a], Mintu Pal[a], Prova Biswas[a], Amrita Roy[a], Dipan Adhikari[a], Sanmoy Karmakar[a,b], Tuhinadri Sen[a,b,*]

[a] *School of Natural Product Studies, Department of Pharmaceutical Technology, Jadavpur University, Kolkata 700 032, West Bengal, India*
[b] *Division of Pharmacology, Department of Pharmaceutical Technology, Jadavpur University, Kolkata 700 032, West Bengal, India*

ARTICLE INFO

Article history:
Received 2 April 2007
Received in revised form 7 July 2008
Accepted 16 July 2008
Available online 25 July 2008

Keywords:
Mangrove
Acanthus ilicifolius
Inflammation
COX–LOX inhibitor
Cytokines

ABSTRACT

Acanthus ilicifolius Linn, is a perennial herb (Acanthaceae) widely found in the Sundarban mangroves and is popularly used for its wound healing effects. In the present study an attempt was made to evaluate the anti-inflammatory activity of the *Acanthus ilicifolius* leaves. The methanolic fraction of *Acanthus ilicifolius* leaf extract produced significant inhibition of rat paw oedema, when administered both prior to and after carrageenan administration, in a manner similar to BW755C a synthetic cyclooxygenase (COX) and lipoxygenase (LOX) inhibitor. The extract decreased protein exudation and leukocyte migration in the peritoneal fluid, thereby indicating its effectiveness towards inhibiting peritoneal inflammation. It also produced significant inhibition of COX (1 and 2) and 5-LOX activity. Preincubation of the extract inhibited the production of proinflammatory cytokines (TNFα and IL-6) in lipopolysaccharide (LPS)-stimulated peripheral blood mononuclear cells (PBMCs). The methanolic fraction of the extract was also found to possess significant free radical (DPPH, ABTS, superoxide and hydroxyl radical) scavenging activity. The extract on intraperitoneal administration augmented the endogenous antioxidant status, as evident from the significant increase of ferric reducing ability of plasma (FRAP) and total peroxyl radical trapping activity of plasma (TRAP).

1. Introduction

Mangroves are salt tolerant vegetations, widely found in the tropical and subtropical intertidal regions. The ecosystems comprises of heterogeneous habitats with the flora and fauna adapted to the difficult environmental conditions. The Sundarban ecosystem is one of the most biologically productive and taxonomically diverse ecosystems of the South-east Asia (Mann, 2000).

Acanthus ilicifolius Linn. (Acanthaceae) is an evergreen spinus herb, widely found in the Sunderban region, popularly used for its wound healing ability by the coastal inhabitants of West Bengal. On survey of ethnomedical literature it was found that the leaves of *Acanthus ilicifolius* are used for the treatment of rheumatism, snakebite, paralysis and asthma in different parts of the world (Babu et al., 2001). The whole plant extract has been reported to possess analgesic and anti-inflammatory activities (Agshikar et al., 1979), while no such report has been published in reference to the leaves of *Acanthus ilicifolius*. Methanolic extract of the leaves has been reported to exhibit hepatoprotective (Babu et al., 2001) and tumor reducing activities (Babu et al., 2002). Leishmanicidal activity of 2-benzoxazolinone, isolated from the leaves of this plant has also been documented (Kapil et al., 1994). Phytochemical studies with the plant revealed the presence of lignans (Kanchapoom et al., 2001) and megastigmane glycosides (Wu et al., 2003).

According to various medical literatures, several adverse reactions are known to be associated with the conventional non-steroidal anti-inflammatory drugs (NSAIDs), thereby limiting the widespread application of these agents. Development of newer anti-inflammatory compounds possessing fewer side effects still remains a challenge to the scientific community. Accordingly, our laboratory had been actively engaged in studies related to screening of Indian medicinal plants, both mangrove and also local varieties, for novel anti-inflammatory molecules. During the course of such investigations we had been able to identify some local plants like *Pluchea indica* (coastal mangrove region) (Sen et al., 1993), *Bryophyllum pinatum* (Pal and Nag Chaudhuri, 1991) and *Calotropis procera* (Sen et al., 1998), possessing simultaneous anti-inflammatory and antiulcer activity, attributed to probable blockade of COX and LOX enzyme systems.

In the present study an attempt has been made to evaluate the anti-inflammatory profile of *Acanthus ilicifolius* with a view towards

* Corresponding author at: Department of Pharmaceutical Technology, Jadavpur University, Kolkata 700 032, West Bengal, India. Tel.: +91 33 24146666.
E-mail address: tssen@hotmail.com (T. Sen).

0378-8741/$ – see front matter © 2008 Elsevier Ireland Ltd. All rights reserved.
doi:10.1016/j.jep.2008.07.024

elucidation of the probable mechanism of action, using various in vitro and in vivo experimental models.

2. Materials and methods

2.1. Plant material and preparation of the methanolic fraction

The leaves of *Acanthus ilicifolius* (Acanthaceae) were from the Canning region of West Bengal. The plant material was taxonomically identified and authenticated by the Botanical Survey of India and a voucher specimen (AC/2004/1) has been preserved for further utilization. The leaves were shade dried, sliced and pulverized using a mechanical grinder. The powdered leaves (3.5 kg) were defatted by maceration with petroleum ether (at room temperature; 48 h). This process was repeated (three times) for complete removal of the fatty materials. It was then dried in air and subsequently subjected to extraction with chloroform as above. Thereafter, the extraction was carried out with methanol. After exhaustive extraction, the methanolic extract was collected and concentrated under reduced pressure at 45–50 °C. A greenish brown concentrated methanolic extract (AC-M) was obtained (yield 0.45%, w/w with respect to the dried starting material). The final product was then stored at 4 °C.

2.2. Animals used

Adult male Charles Foster rats (weighing 120–150 g), and male Swiss albino mice (weighing 20–25 g) were used for the study. The animals were housed in polypropylene cages at 25 ± 2 °C (with 12 h light and dark cycle). All the animals were acclimatized to laboratory environment for a week before the experiment. The animals were provided free access to standard pellet diet and water ad libitum. The care and use of laboratory animals were strictly in accordance to the guidelines prescribed by the Institutional Ethical Committee (constituted under the guidelines Committee for the Purpose of Control and Supervision of Experiments on Animals, India).

2.3. Drugs and chemicals

Carrageenan (κ 80% and λ 20%); 1,1-diphenyl-2-picryl hydrazyl hydrate (DPPH) and lipopolysaccharide (LPS, E.coli: B4) were purchased from Sigma–Aldrich (St. Louis, MO, USA). Tripyridyltriazine (TPTZ) was purchased from Fluka chemical company (Buchs, Switzerland). All other unlabelled chemicals and reagents were of analytical grade (SRL Mumbai, E.Merck India).

2.4. Determination of total phenolic compounds

The content of phenolic compounds was determined according to the method of Singleton and Rossi (1965). Samples (150 μl) were mixed with 750 μl of Folin–Ciocalteu's reagent and 600 μl of sodium carbonate (7.5%). The tubes were then incubated at 50 °C for 10 min and the absorption was measured at 760 nm. The total phenolic content was expressed as quercetin equivalents (QE).

2.5. Carrageenan induced rat paw oedema (pre- and post-treatment)

The control vehicle (isotonic saline 0.9%, w/v), test and standard drugs were administered 30 min prior to the administration of carrageenan (Sigma Type I; 0.1 ml of 1%, w/v solution) in the subplantar tissue of the hind paw. The paw volumes were measured using Plethysmometer (Model No 7141; UGO Basile, Italy), immediately and thereafter at hourly intervals, for 5 h, following administration of carrageenan (Chattopadhyay et al., 2004; Nag Chaudhuri et al., 2005).

In the post-treatment study, the same procedure was repeated where the test drugs were administered (intraperitoneally), 2 h after the administration of carrageenan (Boughton-Smith et al., 1993).

2.6. Exudative inflammation

Acanthus ilicifolius (200 and 400 mg/kg; i.p.), acetylsalicylic acid (100 mg/kg; i.p.) and the control vehicle (normal saline; i.p.) were administered to different groups of animal. The leukocyte count and the protein content (using Bradford reagent) in the peritoneal exudate was determined 3 h following the intraperitoneal administration of 0.05N acetic acid (Nag Chaudhuri et al., 2005).

2.7. Effect on PGE_2 production by COX-2 (whole blood assay)

Freshly collected blood (heparinised) was incubated with acetylsalicylic acid (12 μg/ml) for 6 h, followed by incubation at 37 °C for 1 h with different concentrations of *Acanthus ilicifolius* or the standard drug. Thereafter, 10 μl of LPS was added to the reaction mixture, and then the tubes were again incubated at 37 °C for 24 h. Finally, the plasma was separated by centrifugation (at 2000 rpm for 10 min) and was used for the determination of PGE_2 content (ELISA kit; GE Healthcare).

2.8. Effect on cyclooxygenase (COX-1 and 2) using Amplex red-based fluorimetric assay

The assay was performed using COX assay kit (ELISA). Briefly, the test and the standard drugs were incubated with the appropriate COX enzymes (COX-1, 1.5 U/well and COX-2, 2.5 U/well), in a reaction buffer (0.1 M Tris–HCl buffer, pH 8.0; 5 mM EDTA; 2 mM phenol and 2.5 mM hematin) for a period of 15 min at 37 °C. Then 50 μM amplex red was added to the mixture followed by addition of arachidonic acid (100 μM/well), thereafter the fluorescence (excitation 544 nm and emission 590 nm) was measured up to a period of 30 min.

2.9. Effects on production of cytokines [interleukin-6 (IL-6) and tumour necrosis factor-α (TNF-α)]

Human peripheral blood mononuclear cells were prepared according to Yaqoob et al. (1998). The cells were suspended in culture medium (HEPES-buffered RPMI containing 2 mM glutamine and antibiotics) and were incubated with either methanolic fraction of acanthus or the standard drug (6 h at 37 °C) followed by stimulation with bacterial lipopolysaccharide. At the end of the incubation, the medium was collected and cytokines were analysed by ELISA kit according to the manufacturers instruction.

2.10. Effect on 5-lipoxygenase (LOX) enzyme

The assay mixture (3 ml) consisted of 5 nM of 5-LOX enzyme (Soybean; Sigma-type V, 108 KD) in Tris–HCl buffer (pH 9.0). This enzyme mixture was incubated with the test substances for 15 min at room temperature. After the incubation period freshly prepared 90 μM arachidonic acid in 50 mM Tris–HCl buffer (pH 9.0) was added to the mixture. Finally, the enzyme inhibition was measured as decrease in absorbance of the reaction mixture at 234 nm for 180 s using Hitachi U 2000 Spectrophotometer (Kulkarni et al., 1990).

2.11. 2,2-Diphenyl-1-picryl hydrazine hydrate (DPPH) scavenging activity

Different concentrations of the test substances (*Acanthus ilicifolius*, vitamin C and quercetin) were incubated (in darkness) with DPPH (0.3 mM in methanol). After 30 min of incubation at room temperature, the absorbance was measured at 518 nm (Mensor et al., 2001).

2.12. 2,2′-Azinobis-3-ethylbenzothiazoline-6-sulfonic acid (ABTS) radical decolorization assay

ABTS solution (diluted to an absorbance of 0.745) was mixed with different concentrations of the test or standard drugs. The decrease in absorbance of the reaction mixture (incubated in dark for 5 min) was measured at 734 nm (Re et al., 1998).

2.13. Measurements of reductive ability

Samples in 3.5 ml phosphate buffer (0.2 M; pH 6.6) were mixed with $K_3Fe(CN)_6$ (1.0%, w/v) solution and was incubated at 50 °C for 20 min. Thereafter, 2.5 ml of trichloroacetic acid (TCA) was added to the mixture and centrifuged at 3000 rpm (10 min). The supernatant (2.5 ml) was mixed with 0.5 ml of freshly prepared $FeCl_3$ solution (0.1%, w/v) and then the absorbance was recorded at 700 nm (Oyaizu, 1986).

2.14. Superoxide anion scavenging activity

The reaction mixture containing nitro blue tetrazolium (NBT; 0.156 μM) and NADH (468 μM; in 100 mM phosphate buffer pH 7.4) were mixed with different concentrations of the test samples, followed by the addition of phenazine methosulphate (PMS) (60 (M; in 100 mM phosphate buffer, pH 7.4). The reaction mixture was then incubated at 25 °C (5 min) and the absorbance was recorded at 560 nm (Nishimiki and Rao, 1972).

2.15. Hydroxyl radical scavenging

The reaction mixture containing 2-deoxy-D-ribose (1 mM), phenyl hydrazine (0.2 mM), (in phosphate buffer, pH 7.4) and different concentration of the test samples were incubated for 4 h at 37 °C. The reaction was stopped by the addition of 2.8 % (w/v) trichloroacetic acid solution, followed by centrifugation at 5000 rpm (10 min). The supernatant was mixed with aqueous 1% (w/v) thiobarbituric acid (TBA). The TBA reactive product thus formed was directly measured at 532 nm (Halliwell et al., 1987).

2.16. Effect on ferric reducing ability of plasma (FRAP)

Acanthus ilicifolius, quercetin, vitamin C and vitamin E were administered (i.p.) to different groups of animals. After 2 h, blood samples were withdrawn and the plasma was separated for the determination of FRAP. Then 300 μl of freshly prepared FRAP reagent (10 mM tripyridyltriazine, 20 mM ferric chloride and 500 mM acetate buffer) was mixed with 10 μl of plasma and the absorbance was measured at 593 nm (Benzie and Strain, 1996).

2.17. Total peroxyl radical trapping ability: TRAP assay

Acanthus ilicifolius, quercetin and vitamin C were administered (i.p.) to different groups of animals. One hour later, blood samples were withdrawn and the plasma was separated for the determination of TRAP. Ten microliters of plasma was diluted to 1 ml with phosphate buffer saline, followed by addition of

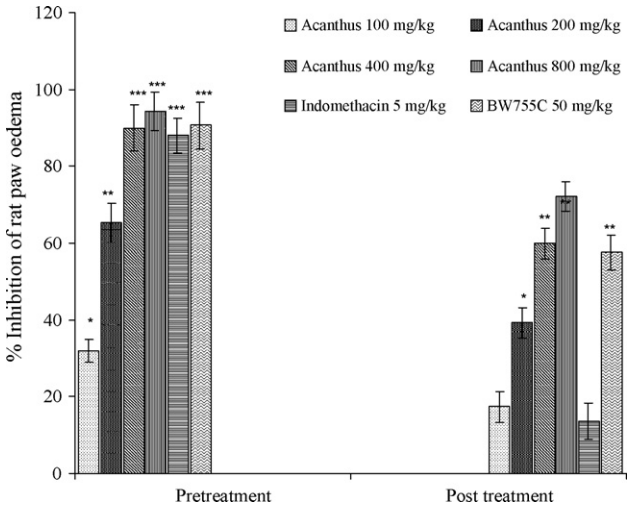

Fig. 1. Effect of *Acanthus ilicifolius*, indomethacin and BW 755C on carrageenan induced paw edema (values are mean ± S.E.; $n = 6$). *P*-value (versus control): $^{*}P < 0.05$, $^{**}P < 0.01$ and $^{***}P < 0.001$.

2′,7′-dichloroflouroscien diacetate (DCFH-DA) in a final concentration of 14 μmol/l. The reaction was initiated by the addition of 2,2′-diazobis (2amidinopropane) dihydrochloride (56 mmol/L). The absorbance was measured at 504 nm using Hitachi U 2000 spectrophotometer (Valkonen and Kuusi, 1997).

2.18. Statistical analysis

Results were expressed as mean ± S.E. ($n = 6$). Statistical analyses were performed with one-way analysis of variance (ANOVA) followed by post hoc Dunnett's test using prism software. "*P*" value less than 0.05 were considered to be statistically significant.

3. Results

3.1. Total polyphenol composition

The amount of total phenolic compounds present in the methanolic fraction of *Acanthus ilicifolius* leaf extract was found to be 310 ± 3 mg (expressed as quercetin equivalents per g of extract).

3.2. Carrageenan-induced rat paw oedema

Methanolic fraction of *Acanthus ilicifolius* significantly inhibited (ED_{50} = 146.2 mg/kg; 95% CL = 69.38–286.2), both the early and late phases of carrageenan-induced paw oedema (Fig. 1). In the post-treatment model (drug administration after 2 h), the extract (ED_{50} = 194.1 mg/kg; 95% CL = 135.8–301.4) and BW 755C (COX–LOX inhibitor) significantly decreased the carrageenan induced rat paw oedema, however, indomethacin was found to produce no significant inhibitory activity (Fig. 1).

3.3. Exudative inflammation

Pretreatment with the test drug (200 and 400 mg/kg; i.p.) produced significant inhibition of peritoneal protein exudation (Table 1) and also caused significant reduction of total leukocyte count in the peritoneal exudate when compared with the control group of animals.

Table 1
Effect of the methanolic fraction of *Acanthus ilicifolius* and acetyl salicylic acid on peritoneal inflammation (values are mean ± S.E.; $n = 6$)

Drug	Dose (mg/kg)	Acetic acid induced peritoneal inflammation			
		Leukocytes/ml of exudate	Inhibition (%)	Protein (mg/ml)	Inhibition (%)
Saline control	–	2780 ± 24	–	14.30 ± 0.27	–
Acanthus ilicifolius	200	1440 ± 21	48*	10.20 ± 0.24	29*
Acanthus ilicifolius	400	640 ± 36	77*	7.37 ± 0.53	49*
Acetylsalicylic acid	200	487 ± 11	83*	5.83 ± 0.29	59*

Animals were pre-treated with the drugs and peritoneal inflammation was produced by administration of acetic acid. *P* value (versus control)
* $p < 0.01$

3.4. Effect on PGE_2 release

The methanolic fraction of *Acanthus ilicifolius* leaf extract (1 μg/ml, 11%; 10 μg/ml, 46%) and the standard drug etoricoxib (1 μg/ml, 47%; 10 μg/ml, 98%) significantly inhibited COX 2 dependent PGE_2 generation in LPS-stimulated whole blood assay.

3.5. Effect of Acanthus ilicifolius on in vitro COX assay

The methanolic fraction of *Acanthus ilicifolius* significantly inhibited both COX 1(1 (g/ml; 99%) and COX 2 (1 (g/ml; 87%) enzymes. However, acetylsalicylic acid (18 (g/ml) produced 97% inhibition of COX 1 and that of rofecoxib (3.14 (g/ml) was found to be 95% for COX 2.

3.6. Effect on pro-inflammatory cytokines (IL-6 and TNFα)

The methanolic fraction of *Acanthus ilicifolius* significantly inhibited the secretion of the pro-inflammatory cytokines in LPS-stimulated mononuclear cells. *Acanthus ilicifolius* exhibited an IC_{50} of 88.64 ± 6.3 (g/ml (IL-6) and 1.24 ± 0.28 (g/ml (TNFα), respectively. As evident from the IC_{50} values, dexamethasone was found to be more effective (IL-6, 39.41 ± 2.8 (g/ml; TNFα, 0.18 ± 0.02 (g/ml).

3.7. Effect of Acanthus ilicifolius on soybean 5-lipoxygenase

The methanolic fraction of *Acanthus ilicifolius* (1 (g/ml) demonstrated 79% inhibition of enzyme activity, which was found to be higher in case of BW 755C (91%) and quercetin (84%), at identical concentration.

3.8. Free radical scavenging activity of Acanthus ilicifolius

Significant DPPH free radical scavenging activity was observed with the test drug (Table 2). However, the IC_{50} values of quercetin (5.82 (g/ml) and vitamin C (6.62 (g/ml) were moderately less than that of the *Acanthus ilicifolius* (8.4 (g/ml).

The methanolic fraction of *Acanthus ilicifolius* leaf extract produced a concentration dependent scavenging of $ABTS^{\cdot+}$ radical (IC_{50} of 10.34 (g/ml). Quercetin (IC_{50} 3.6 (g/ml) and vitamin C (IC_{50} 4.86 (g/ml) were found to be more effective in comparison to the test drug (Table 2). The methanolic fraction and the standard antioxidants significantly scavenged both superoxide and hydroxyl radicals (Table 2).

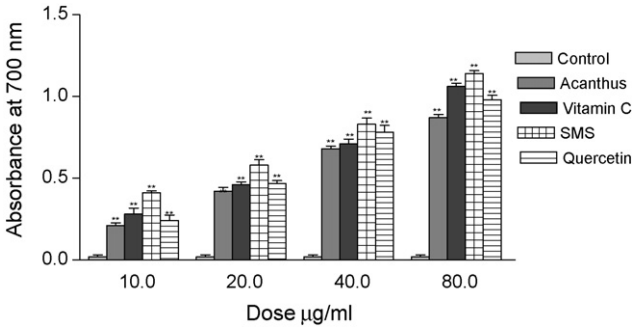

Fig. 2. Reductive ability of the methanolic fraction of *Acanthus ilicifolius* (values are mean ± S.E.; $n = 4$). *P*-value (versus control): $^{**}P < 0.01$.

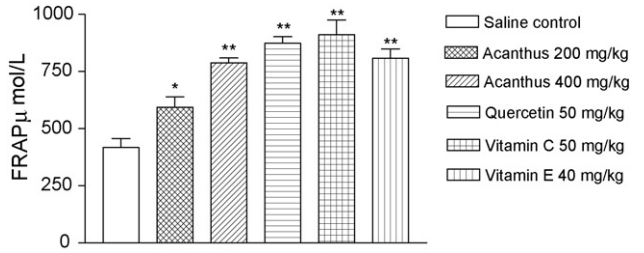

Fig. 3. Effect of *Acanthus ilicifolius* (methanolic fraction) and the standard antioxidants on the ferric reducing ability of the plasma (FRAP) following single intraperitoneal administration (values are mean ± S.E.; $n = 6$). *P*-value (versus control): $^{*}P < 0.05$, and $^{**}P < 0.01$.

3.9. Reductive ability

The methanolic fraction of *Acanthus ilicifolius* leaf extract demonstrated significant reductive ability, which was also found to be concentration dependent (Fig. 2).

3.10. Effect on FRAP

Ferric reducing ability of the plasma (FRAP) was significantly elevated following intraperitoneal administration of *Acanthus ilicifolius* (Fig. 3).

Table 2
Scavenging activity of *Acanthus ilicifolius* against DPPH, ABTS, superoxide and hydroxyl radicals (values are expressed as mean ± S.E.; $n = 4$)

Drugs	Inhibitory concentration (IC_{50}) (g/ml			
	DPPH radical	ABTS radical	Superoxide radical	Hydroxyl radical
Acanthus	8.40 ± 0.06	10.34 ± 0.02	78.12 ± 2.51	24.60 ± 1.10
Quercetin	5.28 ± 0.08	3.60 ± 0.03	30.19 ± 1.32	14.32 ± 0.52
Vitamin C	6.62 ± 0.05	4.86 ± 0.03	52.18 ± 3.14	21.08 ± 0.34
Sodium metabisulphite	–	–	–	11.3 ± 0.22

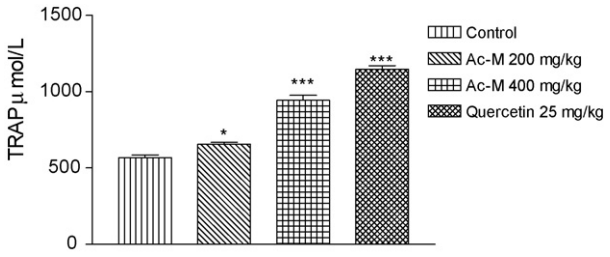

Fig. 4. Effect of *Acanthus ilicifolius* (methanolic fraction) and quercetin on total peroxyl radical trapping ability (TRAP) (values are mean ± S.E.; $n = 6$). *P*-value (versus control): $^{*}P < 0.05$, $^{**}P < 0.01$, and $^{***}P < 0.001$.

3.11. Effect on TRAP

Pretreatment with *Acanthus ilicifolius* produced significant as well as dose dependent elevation of the total peroxyl radical trapping ability of plasma (Fig. 4).

4. Discussion

Conventional NSAIDs are the most commonly prescribed agents used for the management of inflammation and pain, however, toxic manifestation associated with these agents is a matter of concern. As a result, several new approaches are now considered for design and development of superior anti-inflammatory compounds, showing fewer side effects. In the present study, we have evaluated the anti-inflammatory activity of *Acanthus ilicifolius*. The methanolic fraction of the *Acanthus ilicifolius* when administered up to a dose of 1200 mg/kg, produced no visible side effects or death, and the dose range was found to be well tolerated in the treated groups.

Carrageenan induced rat paw oedema, is a well-accepted and popular model for evaluating anti-inflammatory activity. Carrageenan is known to produce a biphasic response (Vinegar et al., 1969), where the early phase is related to the production of histamine, leukotrienes', PAF and possibly cyclooxygenase products, while the delayed phase is linked to the neutrophil infiltration, eicosanoid release, production of free radicals and also release of other neutrophil derived mediators (Cuzzocrea et al., 1998). Interestingly NSAIDs may not be effective in reducing the inflammation in the later phase of such oedema formation, (Boughton-Smith et al., 1993). In the present study, *Acanthus ilicifolius* leaf extract produced significant and also dose dependent inhibition of carrageenan induced paw oedema. Moreover, during post-treatment (i.e., drug administered after 2 h following carrageenan injection), the methanolic fraction was again found to be effective against carrageenan induced paw oedema. Our findings were found to be similar to that of BW755C (a COX and LOX inhibitor), which was also found to be highly effective, particularly in the post-treatment studies (administered after the induction of oedema), when compared to the popular NSAIDs (Boughton-Smith et al., 1993).

Intraperitoneal administration of acetic acid produces a sustained increase in capillary permeability, thereby leading to increased cellular infiltration coupled with protein exudation, ultimately leading to severe inflammatory conditions. The present findings indicate the effectiveness of the methanolic fraction of *Acanthus ilicifolius* leaf extract against acetic acid induced peritoneal inflammation in a manner similar to that of the NSAIDs (Northover, 1963; Whittle, 1964). It was also observed that the methanolic fraction (at 1 μg/ml) produced significant inhibition of cyclooxygenase (1 and 2), however, the extract did not produce such equivalent effectiveness (46% at 10 μg/ml) towards LPS induced PGE_2 release in peripheral blood mononuclear cells. Moreover, the methanolic fraction was also found to possess significant 5-LOX inhibitory activities, comparable to that of phenidone and BW 755C.

During inflammation, the leukocytes and macrophages migrating to the site of injury are known to produce the superoxide radical O_2^-, which in turn lead to the generation of hydrogen peroxide. Furthermore, in the presence of suitable transitional elements, hydrogen peroxide may be transformed to the highly reactive hydroxyl radical. These radicals can also act as second messengers, thereby activating the production of other inflammatory mediators (Garcia et al., 1996).

Antioxidant activity of various test compounds can be rapidly evaluated with in vitro test systems employing DPPH, $ABTS^+$ radicals. In the present study the methanolic fraction of *Acanthus ilicifolius* and standard drug quercetin significantly scavenged both DPPH and ABTS radicals in a concentration dependent manner and also demonstrated significant reductive ability. Moreover, the methanolic fraction of *Acanthus ilicifolius* significantly scavenged both superoxide (generated from the PMS-NADH system) and hydroxyl radicals (derived from deoxy-D-ribose and phenyl hydrazine).

Acanthus ilicifolius leaf extract also improved the endogenous antioxidant status as was evident from the increased levels of FRAP, a sensitive index for understanding the reducing capacity of biological fluid during oxidative stress (Benzie and Strain, 1996). Intraperitoneal administration of *Acanthus ilicifolius* produced a significant (concentration dependent) elevation of TRAP.

According to reports, anti-inflammatory agents like synthetic pyrazoline derivatives (phenidone, BW 755C; inhibitor of COX and LOX) and some plant polyphenolics are also potent antioxidants, and such antioxidant activity probably contribute towards their COX–LOX inhibitory effects (Charlier and Michaux, 2003).

Reactive oxygen species are known to activate a number of intracellular signaling pathways such as NFκB, which in turn activates the transcription of various pro-inflammatory cytokines (interleukins and TNFα), cell adhesion molecules and also COX 2 (Pavlick et al., 2002). It has also been observed that TNFα production in the LPS-stimulated cells is dependent on 5-LOX activity, which has been confirmed with the use of 5-LOX inhibitors like L656, 224 but not with acetylsalicylic acid (MacIntyre and Pope, 1991). In conformity with these findings, our study with *Acanthus ilicifolius* revealed significant inhibition of IL-6 and TNFα in human PBMC (stimulated with LPS), and the IC_{50} value were found to be 88.64 ± 6.3 and 39.41 ± 2.84, respectively.

Thus on the basis of the present findings we can suggest that the observed anti-inflammatory activity of *Acanthus ilicifolius* may be attributed to its inhibitory effect on the COX–LOX enzymes, probably influenced in turn by the superior free radical trapping activity of the components present in the extract. Further, studies are being conducted to identify and characterize the compound(s) responsible for the observed inhibition of COX and LOX.

Acknowledgements

We thankfully acknowledge the active support of Prof. S. Hazra, Director, School of Oceanographic Studies, Jadavpur University. We are also immensely thankful to the University Grants Commission (U.G.C., New Delhi, India) for the financial assistance, in the form of a research project. We would also like to thank Dr. J.R. Vedasiromoni, Mr. Rajib Barik and Dr. L. Manikandan for their expert advice and support.

References

Agshikar, N.V., Naik, V.R., Abraham, G.J., Reddy, C.V., Naqvo, S.W., Mittal, P.K., 1979. Analgesic and anti-inflammatory activity of *Acanthus ilicifolius* Linn. Indian Journal of Experimental Biology 17, 1257–1258.

Babu, B.H., Shylesh, B.S., Padikkala, J., 2001. Antioxidant and hepato protective effect of *Acanthus ilicifolius*. Fitoterapia 72, 272–277.
Babu, B.H., Shylesh, B.S., Padikkala, J., 2002. Tumor reducing and anti-carcinogenic activity of *Acanthus ilicifolius* in mice. Journal of Ethnopharmacology 79, 27–33.
Benzie, F.F., Strain, J.J., 1996. The ferric reducing ability of plasma (FRAP) as a measure of "Antioxidant Power". Analytical Biochemistry 239, 70–76.
Boughton-Smith, N.K., Deakin, A.M., Follenfant, R.L., Whittle, B.J., Garland, L.G., 1993. Role of oxygen radicals and arachidonic acid metabolites in the reverse passive Arthus reaction and carrageenan paw oedema in rats. British Journal of Pharmacology 110, 896–902.
Charlier, C., Michaux, C., 2003. Dual inhibition of cyclooxygenase-2 (COX-2) and 5-lipoxygenase (5-LOX) as a new strategy to provide safer non-steroidal anti-inflammatory drugs. European Journal of Medicinal Chemistry 38, 645–659.
Chattopadhyay, P., Besra, S.E., Gomes, A., Das, M., Sur, P., Mitra, S., Vedashiromoni, J.R., 2004. Anti-inflammatory activity of tea (*Camellia sinensis*) root extract. Life Science 74, 1839–1849.
Cuzzocrea, S., Zingarelli, B., Hake, P., Salzman, A.L., Szabo, C., 1998. Anti-inflammatory effects of mercaptoethylguanidine, a combined inhibitor of nitric oxide synthase and peroxynitrite scavenger in carrageenan induced models of inflammation. Free Radical Biology and Medicine 24, 450–459.
Garcia, F.P., Marin, E., Canigueral, S., Adzet, T., 1996. Anti-inflammatory action of *Pluchea sagitalis*: involvement of an antioxidant mechanism. Life Science 59, 2033–2040.
Halliwell, B., Gutteridge, J.M., Aruoma, O.I., 1987. The deoxyribose method: a simple 'test tube' assay for determination of rate constants for reaction of hydroxyl radicals. Analytical Biochemistry 165, 215–219.
Kanchapoom, T., Kamel, M.S., Kasal, R., Yamasaki, K., Picheasoonthon, C., Hiraga, Y., 2001. Lignan glycosides from *Acanthus ilicifolius*. Phytochemistry 56, 369–372.
Kapil, A., Sharma, S., Wahidulla, S., 1994. Leishmanicidal activity of 2-benzoxazolinone from *Acanthus ilicifolius* in vitro. Planta Medica 60, 187–188.
Kulkarni, A.P., Mitra, A., Chaudhuri, J., Byczkowski, J., Richards, I., 1990. Hydrogen peroxide: a potent activator of dioxygenase activity of soybean lipoxygenase. Biochemical Biophysical Research Communication 166, 417–423.
MacIntyre, J.P., Pope, B.L., 1991. The involvement of protein kinase C, calcium, and 5-LOX in the production of tumor necrosis factor by a cloned interleukin-3 dependent cell line with natural cytotoxic activity. International Journal of Immunopharmacology 13, 175–184.
Mann, K.H., 2000. Ecology of Coastal Waters: With Implication for Management, 2nd ed. Blackwell Science, Inc., Massachusetts.
Mensor, L.L., Menezes, F.S., Leitão, G.G., Reis, A.S., Santos, T.C., Coube, C.S., Leitão, S.G., 2001. Screening of Brazilian plant extracts for antioxidant activity by the use of DPPH free radical method. Phytotherapy Research 5, 127–130.
Nag Chaudhuri, A.K., Karmakar, S., Roy, D., Pal, S., Pal, M., Sen, T., 2005. Anti-inflammatory activity of Indian black tea (Sikkim variety). Pharmacological Research 51, 169–175.
Nishimiki, M., Rao, N.A., 1972. The occurance of superoxide anion in the reaction of reduced phenazine methosulphate and molecular oxygen. Biochemical and Biophysical Research Communication 46, 849–854.
Northover, B.J., 1963. The permeability to plasma proteins of the peritoneal blood vessels of the mouse, and the effect of substances that alter permeability. Journal of Pathology and Bacteriology 85, 361–370.
Oyaizu, M., 1986. Studies on product of browning reaction prepared from glucose amine. Japanese Journal of Nutrition 44, 307–315.
Pal, S., Nag Chaudhuri, A.K., 1991. The anti-ulceractivity of *Bryophylum pinnatum* leaf extract in experimental animal. Journal of Ethnopharmacology 33, 97–102.
Pavlick, K.P., Laroux, F.S., Fuseler, J., Wolf, R.E., Gray, L., Hoffman, J., Grisham, M.B., 2002. Role of reactive metabolites of oxygen and nitrogen in inflammatory bowel disease. Free Radical Biology and Medicine 33, 311–322.
Re, R., Pellegrini, N., Proteggente, A., Pannala, A., Yang, M., Rice-Evans, C., 1998. Antioxidant activity applying an improved ABTS radical cation decolorization assay. Free Radical Biology and Medicine 72, 1231–1237.
Sen, T., Ghosh, T.K., NagChaudhuri, A.K., 1993. Studies on the mechanism of anti-inflammatory and anti-ulcer activities of *Pluchea indica*—probable involvement of 5-LOX pathway. Life Science 52, 737–743.
Sen, T., Basu, A., NagChaudhuri, A.K., 1998. Studies on the possible mechanism of the gastric mucosal protection by *C. procera*-involvement of 5-LOX pathways. Fundamental and Clinical Pharmacology 12, 82–87.
Singleton, V.L., Rossi, J.A., 1965. Colorimetry of total phenolics with phosphomolybdic–phosphotungstic acid reagents. American Journal of Entomology and Viticulture 16, 144–158.
Valkonen, M., Kuusi, T., 1997. Spectrophotometric assay for total peroxyl radical-trapping antioxidant potential in human serum. Journal of Lipid Research 38, 823–833.
Vinegar, R., Scheriber, W., Hugo, R.J., 1969. Biphasic development of carrageenan edema in rats. Journal of Pharmacology and Experimental Therapeutics 166, 96–103.
Whittle, B.A., 1964. The use of changes in capillary permeability in mice to distinguish between narcotic and non-narcotic analgesics. British Journal of Pharmacology 22, 246–253.
Wu, J., Zhang, S., Huang, J., Xiao, Q., Li, Q., Long, L., Huang, L., 2003. Megastigmane and flavone glycosides from *Acanthus ilicifolius*. Pharmazie 58, 363–364.
Yaqoob, P., Knapper, J.A., Webb, D.H., Williams, C.M., Newsholme, E.A., Calder, P.C., 1998. Effect of olive oil on immune function in middle aged men. American Journal of Clinical Nutrition 67, 129–135.